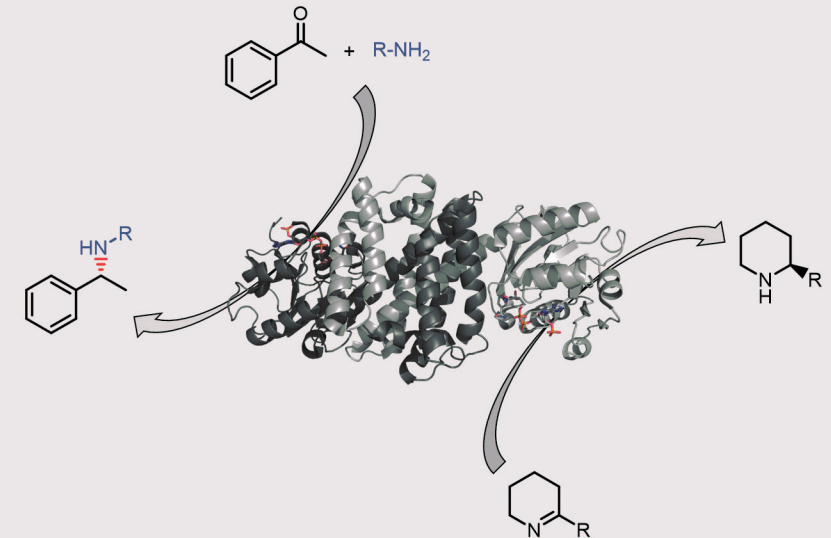
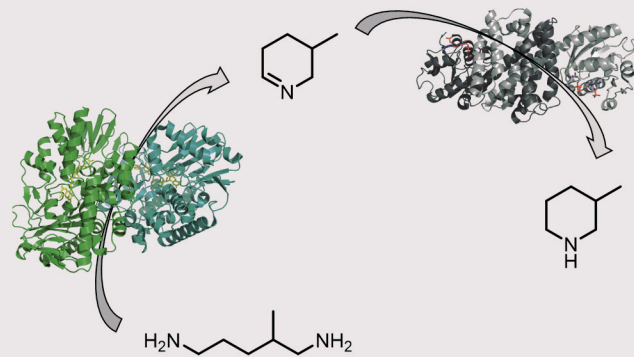


- Discovery, selection and characterization of novel imine reductases
- Reduction of cyclic and exocyclic imines
- Application of imine reductases for reductive aminations
- Evolution of an amine oxidase and combination with imine reductases for the generation of *N*-heterocyclic amines

Universität Stuttgart 2016

CHARACTERIZATION AND APPLICATION OF NOVEL IMINE REDUCTASES

CHARAKTERISIERUNG UND ANWENDUNG NEUER IMINREDUKTASEN



Philipp Scheller

PHILIPP SCHELLER

Institut für Technische Biochemie – Universität Stuttgart

Characterization and application of novel imine reductases

Charakterisierung und Anwendung neuer Iminreduktasen

Von der Fakultät 4: Energie-, Verfahrens- und Biotechnik der Universität Stuttgart
zur Erlangung der Würde eines Doktors der Naturwissenschaften (Dr. rer. nat.)
genehmigte Abhandlung.

Vorgelegt von
Philipp Scheller
aus
Biberach an der Riß

Hauptberichter: Prof. Dr. Bernhard Hauer
Mitberichter: Prof. Dr. Ralf Takors
Vorsitzender: Prof. Dr. Karl-Heinrich Engesser

Tag der Verteidigung: 23.05.2016

Institut für Technische Biochemie der Universität Stuttgart

2016

*“The reasonable man adapts himself to the world;
the unreasonable one persists in trying to adapt the world to himself.
Therefore all progress depends on the unreasonable man.”*

- George Bernard Shaw, *Man and Superman*, 1903

COVER

FRONT:

The front cover shows the application of an imine reductase for the reduction of cyclic imines and for the reductive amination of a ketone to generate primary or secondary chiral amines.

BACK:

The back cover illustrates the combination of an amine oxidase and an imine reductase in cascade reactions to transform polyamines into heterocyclic amines. In the first reaction the polyamine is transformed into an aminoaldehyde by the amine oxidase, thereby triggering its spontaneous cyclization to a cyclic imine which is in the second step reduced by the imine reductase.

I DECLARATION OF AUTHORSHIP

Declaration of Authorship:

I hereby declare that the present thesis entitled "Characterization and application of novel imine reductases" is the result of my own work, that all sources used or quoted have been indicated, and that I have not used any illegitimate means. I further declare that I have not submitted this thesis for a degree in some form or another.

Erklärung über die Eigenständigkeit der Dissertation:

Ich versichere, dass ich die vorliegende Arbeit mit dem Titel „Charakterisierung und Anwendung neuer Iminreduktasen“ selbständig verfasst und keine anderen als die angegebenen Quellen und Hilfsmittel benutzt habe. Aus fremden Quellen entnommene Passagen und Gedanken sind als solche kenntlich gemacht. Des Weiteren bestätige ich ausdrücklich, dass die hier vorgelegte Dissertation nicht in gleicher oder ähnlicher Form bei einer anderen Institution zur Erlangung eines akademischen Grades eingereicht wurde

Stuttgart, 15.1.2016

Philipp Scheller

II AUTHOR CONTRIBUTIONS

The present thesis was prepared under the supervision of Prof. Dr. Bernhard Hauer in the period of February 2012 to March 2015 at the Institute of Technical Biochemistry at the University of Stuttgart, Germany.

Some data of the present thesis was already published or submitted for publication. Contributions to the individual manuscripts made by the author of this work are summarized in this chapter.

List of publications:

- Scheller, P. N. & Nestl, B. M. The biochemical characterization of three imine reducing enzymes from *Streptosporangium roseum* DSM43021, *Streptomyces turgidiscabies* and *Paenibacillus elgii*. *Appl. Microbiol. Biotechnol*, manuscript submitted

The author designed and performed all experiments of this work. The author was further involved in the data analysis, data interpretation and the preparation of the manuscript.

- Lenz, M., Scheller, P. N., Richter, S. M., Hauer, B. & Nestl, B. M. Cultivation and purification of two stereoselective imine reductases from *Streptosporangium roseum* and *Paenibacillus elgii*. *Protein Expr. Purif.* (2016), DOI: 10.1016/j.pep.2016.05.003

The author established the expression of IRED genes and developed the purification methods, as well as the analytical SEC-HPLC method to determine the protein purity. The author was further involved in the data interpretation and the preparation of the manuscript.

- Fademrecht, S., Scheller, P. N., Nestl, B. M., Hauer, B. & Pleiss, J. Identification of imine reductase-specific sequence motifs. *Proteins* 84, 600–610 (2016)

The author contributed experimental indications for differences in the cofactor binding of (*R*)- and (*S*)- type IREDs. The author was further involved in the data interpretation and the preparation of the manuscript.

- Scheller, P. N., Lenz, M., Hammer, S. C., Hauer, B. & Nestl, B. M. Imine Reductase-Catalyzed Intermolecular Reductive Amination of Aldehydes and Ketones. *ChemCatChem* 7, 3239–3242 (2015)

The author designed and performed all experiments of this work except for the reductive aminations of cyclohexylmethylketone with ammonia as substrate and the ¹H-NMR analyses to monitor imine formation. The author was further involved in the data analysis, data interpretation and the preparation of the manuscript.

- Scheller, P. N., Fademrecht, S., Hofelzer, S., Pleiss, J., Leipold, F., Turner, N. J., Nestl, B. M. & Hauer, B. Enzyme Toolbox: Novel Enantiocomplementary Imine Reductases. *ChemBioChem* 15, 2201–2204 (2014)

The author designed and performed all experiments of this work except for the bioinformatic analyses and the experiments to check for dehydrogenase activity with substrates indicated by the predicted GenBank names of the novel IREDs. The author was further involved in the selection process of the novel IREDs, the data analysis, data interpretation and the preparation of the manuscript.

III DANKSAGUNGEN

An dieser Stelle möchte ich mich gerne bei den vielen Leuten bedanken die direkt oder indirekt die Anfertigung dieser Arbeit ermöglicht haben, sei es durch die Mitarbeit an diesem Projekt, hilfreiche Ratschläge und Diskussionen zum Thema oder dadurch, dass sie mich persönlich unterstützt haben.

An erster Stelle möchte ich mich bei Herrn Prof. Dr. Bernhard Hauer dafür bedanken, dass er es mir ermöglicht hat meine Promotion am Institut für Technische Biochemie durchzuführen. Für die Überlassung dieses spannenden Projektes, das in mich gesetzte Vertrauen, Ihre Unterstützung und die Ermutigung eigene Ideen zu verfolgen und auch umzusetzen möchte ich mich ganz herzlich bedanken. Ebenso möchte ich für die Möglichkeit danken zahlreiche internationale Konferenzen und Projekttreffen besuchen zu können.

Bedanken möchte ich mich auch bei Herrn Prof. Dr. Ralf Takors für die freundliche Übernahme des Zweitgutachtens meiner Arbeit und bei Herrn Prof. Dr. Karl-Heinrich Engesser für die freundliche Übernahme des Prüfungsvorsitzes.

Ganz besonders bedanken möchte ich mich bei Dr. Bettina Nestl für die hervorragende Betreuung während meiner Promotion. Zahlreiche hilfreiche und inspirierende Diskussionen über Iminreduktasen, die kritische Korrektur verschiedener Manuskripte und dieser Arbeit haben die gesamte Entwicklung dieses Projektes erst möglich gemacht und werden sicher auch in Zukunft zu weiteren spannenden Erkenntnissen führen.

Bei Dr. Janosch Klebensberger möchte ich mich dafür bedanken ins S2 Labor aufgenommen worden zu sein und dort den besten Benchplatz des gesamten Instituts belegen zu dürfen. Außerdem möchte ich für die zahlreichen Hilfestellungen bei molekular- und mikrobiologischen Fragen danken. Zudem sollten die zahllosen mehr oder weniger ernsten, aber immer inspirierenden, wissenschaftlichen Diskussionen nicht unerwähnt bleiben.

Bedanken möchte ich mich ebenso bei Dr. Sandra Facey für Ihre Hilfe in molekular- und mikrobiologischen Angelegenheiten, für das Überlassen mehrerer Materialien (Plasmide, Stämme...), die Zusammenarbeit bei der jährlichen Betreuung des TBC I Praktikums und ihre Bereitschaft als „native speaker“ zu helfen.

Ebenso möchte ich mich bei Dr. Bernd Nebel bedanken für die vielen Hilfen in analytischen Fragestellungen und die Instandhaltung und Pflege der HPLCs und GCs.

Bei Sven Richter möchte ich mich dafür bedanken, dass er mir bei der Aufreinigung verschiedener Proteine, beim Packen von Säulen, Benutzung der Äkta, usw. stets geholfen hat.

II DANKSAGUNGEN

Prof. Dr. Jürgen Pleiss und insbesondere Silvia Fademrecht möchte ich für die erfolgreiche Kooperation die zur Erstellung der „Iminreduktase Engineering Database“ geführt hat und die bioinformatischen Arbeiten zu den Iminreduktasen danken.

Darüber hinaus möchte ich allen derzeitigen und ehemaligen Mitarbeitern des ITBs für die freundliche und entspannte Atmosphäre danken. Die gemeinsame Zeit im Institut, auf Konferenzen, Projekttreffen und bei allen anderen Gelegenheiten (Bad Boll, Schwarzenberg, wandern, grillen, Kaffeekrone, bad taste...) wären ohne euch, Jenny, Silke, Sandra V., Thorsten, Mirko, Andy, Jörg, Jule, Lisa, Chris (Schneck), Sebastian, Sara, Jan, Matthias, Philipp T., Maïke, Leonie, Sandra N., Domme, Mihaela, Silvi, Conny, Rebecca, Chris (Katze), Stephan, Konrad, Martin, Tobi, Björn, Mina, Melli, Daniel, Sumire, Miri, Wouter, Franzi und Per-Olof, nur halb so schön gewesen.

Bedanken möchte ich mich auch bei den Studenten Sascha Siebenhaller, Sebastian Hofelzer, Julia Mörk, Thomas Zubiks, Lea Kolb, Konrad Krämer, Sylvie Reves dos Santos und Tea Pajan die an verschiedenen Teilen dieses Projektes mitgearbeitet haben und von mir betreut wurden.

Der europäischen Union und unseren Kooperationspartner möchte ich für die Finanzierung dieses Projektes im Rahmen von „Chem21“ danken. Ganz herzlich sei an dieser Stelle auch noch unseren Kooperationspartner von GSK und Orion Pharma, gedankt für ihr Interesse an und ihre Zusammenarbeit auf diesem Projekt. Besonders danken möchte ich noch Dr. Josef Messinger von Orion Pharma für das Überlassen von verschiedenen Substraten die während dieser Arbeit getestet wurden.

Zum Schluss möchte ich mich noch bei Christine, meinen Eltern und meinen Schwestern bedanken. Ihr wart während der letzten Jahre meines Studiums und meiner Promotion stets für mich da und habt mich in jeder Hinsicht bedingungslos unterstützt – vielen Dank dafür.

IV TABLE OF CONTENTS

I	DECLARATION OF AUTHORSHIP	5
II	AUTHOR CONTRIBUTIONS	6
III	DANKSAGUNGEN	7
IV	TABLE OF CONTENTS	9
V	ABBREVIATIONS	13
VI	ABSTRACT	14
VII	ZUSAMMENFASSUNG	16
1	INTRODUCTION.....	18
1.1	The importance of chiral amines in natural products and pharmaceuticals.....	18
1.2	Chemical and biocatalytic methods for the preparation of chiral amines	19
1.2.1	Chemical methods for the resolution of racemic amines and asymmetric synthesis for the stereoselective formation of amines	19
1.2.2	Strategies and challenges for the biocatalytic generation of chiral amines	22
1.2.3	Enzymes and enzymatic cascade reactions for the preparation of primary α -chiral amines.....	23
1.2.4	Enzymes and enzymatic cascade reactions for the preparation of secondary and tertiary α -chiral amines.....	26
1.2.5	Imine reductases – a novel class of enzymes with the ability to generate primary, secondary and tertiary amines.....	28
1.2.6	The integration of IREDs in cascade reactions to prepare chiral amines	30
1.2.7	The enzymatic generation of cyclic imines by polyamine oxidases and their combination with IREDs.....	30
1.3	Aims of this work and experimental strategy	31
2	METHODS AND MATERIALS	33
2.1	Materials	33
2.1.1	Chemicals.....	33
2.1.2	Enzymes	33
2.1.3	Kits	33
2.1.4	DNA Sequences	33
2.1.5	Primers.....	36
2.1.6	Plasmids.....	37
2.1.7	<i>E. coli</i> strains	38
2.2	Cultivation media and growth of bacterial cells	39
2.3	Preparation of competent cells and transformation of <i>E. coli</i>	39
2.4	PCR for amplification of DNA	40
2.5	Restriction enzyme based gene cloning	40
2.6	Gibson assembly for molecular cloning	40
2.7	Methods to generate mutants and mutant libraries	41
2.7.1	Site directed mutagenesis – QuikChange [®] method.....	41
2.7.2	Random mutagenesis by epPCR.....	41
2.7.3	Site saturation mutagenesis with degenerated codons	42
2.8	Gene expression in shake flasks and deep well plates	42
2.9	Cell lysis and purification of proteins.....	43
2.9.1	Immobilized Metal Affinity Chromatography (IMAC) for purification of His ₆ -tagged IREDs.....	43
2.9.2	Ion exchange chromatography with a MonoQ column as second IRED purification step.....	44
2.9.3	Ion exchange chromatography with a Q-sepharose HP column for purification of PuO- <i>Re</i> wt and mutants	44

IV TABLE OF CONTENTS

2.10	Protein quantification by BCA assay	44
2.11	Solid phase assay and activity assays with cell lysate for HTS of PuO- <i>Re</i> mutant libraries.....	44
2.11.1	Solid phase assay	44
2.11.2	Activity assays with cell lysates.....	45
2.12	Liquid phase assays to determine the specific activities of purified proteins.....	45
2.12.1	Spectrophotometric detection of NADPH consumption to determine the IRED activity	45
2.12.2	Detection of H ₂ O ₂ formation by PuO- <i>Re</i>	47
2.13	Whole cell biotransformations with IREDs	48
2.14	Biotransformations with purified proteins	48
2.14.1	IRED biotransformations with cyclic imine substrates	48
2.14.2	IRED biotransformations with exocyclic imine substrates.....	48
2.14.3	Reductive amination reactions with <i>R</i> -IRED- <i>Sr</i>	49
2.15	Reaction cascade with purified IREDs and PuO- <i>Re</i>	49
2.16	Reaction cascade with whole cells expressing IREDs and PuO- <i>Re</i>	49
2.17	Preparation of samples for GC and HPLC analytics and derivatizations	50
2.18	GC-FID and GC-MS analytics	50
2.19	HPLC analytics.....	52
2.20	SEC analysis on HPLC to determine the protein purity	53
2.21	Synthesis of substrates and products and NMR analysis.....	53
2.21.1	Synthesis of 2-methylpiperideine (imine 3a).....	53
2.21.2	Synthesis of 2-phenylpiperideine (imine 3b)	54
2.21.3	Synthesis of 2- <i>p</i> -fluorophenylpiperideine (imine 3c).....	54
2.21.4	Synthesis of 1-methyl-1,2,3,4-tetrahydroisoquinoline (amine 6b).....	55
2.21.5	Synthesis of 1,4-diaminopentane and 1,5-diaminohexane (polyamines 32 and 33)	55
3	RESULTS	56
3.1	Imine reductases – novel biocatalysts	56
3.1.1	Identification and selection of novel IREDs	56
3.1.2	Imine reducing activity of the novel IREDs	60
3.2	Biochemical characterization of the novel IREDs.....	63
3.2.1	pH Profile of the IREDs.....	63
3.2.2	Thermostability of the IREDs	65
3.2.3	Oligomerization of the IREDs.....	66
3.2.4	Effect of organic solvents on the activity of the IREDs	67
3.3	Whole cell biotransformations to investigate the substrate spectrum and the selectivity of the IREDs.....	69
3.4	Determination of IRED kinetic parameters to investigate the substrate preference	72
3.5	Biotransformations with purified IREDs.....	74
3.5.1	Establishing biotransformations with purified IREDs and 2-methylpyrroline 1	74
3.5.2	The reduction of exocyclic imine substrates and the optimization of biotransformations with purified IREDs	75
3.5.3	Biotransformations of further exocyclic imine substrates	80
3.6	The reductive amination of aldehydes and ketones with IREDs	81
3.6.1	The reductive amination of aldehydes.....	82
3.6.2	The reductive amination of ketones to generate chiral amines	83
3.6.3	Kinetic characterization of the reductive amination reaction	84
3.7	Production of <i>N</i> -heterocycles by enzymatic cascade reactions with IREDs – the enzymatic generation of cyclic imines with PuO- <i>Re</i>	86

3.8	Directed evolution of PuO- <i>Re</i> to expand the substrate scope	88
3.8.1	Random mutagenesis by epPCR.....	88
3.8.2	Semi-rational design by site-saturation mutagenesis	91
3.9	Cascade reactions to transform polyamines into cyclic amines.....	94
3.9.1	The combination of purified PuO- <i>Re</i> and IREDs	94
3.9.2	Cascade reaction with whole cells expressing PuO- <i>Re</i> and the IREDs.....	96
4	DISCUSSION	98
4.1	Identification, selection and definition of enzymes of the IRED family	98
4.1.1	The importance of IREDs as novel biocatalysts for the generation of chiral amines	98
4.1.2	Defining and expanding the known sequence space of IREDs.....	98
4.1.3	Cofactor binding of IREDs and mechanistic aspects for the enzymatic imine reduction	99
4.2	Biochemical characterization of novel IREDs.....	101
4.3	Exploration of the substrate spectrum of the IREDs.....	102
4.3.1	Reduction of cyclic and exocyclic imines	102
4.3.2	Enantioselectivities for the reduction of imines.....	104
4.3.3	Reduction of carbonyls	105
4.3.4	Reduction of activated C=C bonds and others	106
4.3.5	Investigation of the substrate preference of IREDs and considerations for the search of natural substrates	106
4.4	Application of IREDs as whole cell biocatalysts	107
4.5	Applications with purified IREDs	108
4.5.1	Reduction of exocyclic imine substrates and analytical challenges for their detection	108
4.5.2	Reductive amination reactions – the potential of IREDs.....	110
4.5.3	Optimizations for enzymatic reductive amination reactions	111
4.5.4	Kinetic characterization of the reductive amination reaction	112
4.6	Establishing cascade reactions with IREDs	113
4.6.1	The selection of an amine oxidase and the investigation of its substrate scope	113
4.6.2	Mutagenesis of PuO- <i>Re</i> to enhance the activity for non-natural polyamines.....	114
4.6.3	Application of IREDs in cascade reactions.....	116
5	CONCLUSION AND OUTLOOK	118
6	REFERENCES.....	119
7	SUPPORTING INFORMATION	137
7.1	Michaelis-Menten plots of IREDs and mutants with substrate 2-methylpyrroline 1	137
7.2	Biotransformations with IREDs	139
7.2.1	IRED catalyzed whole cell biotransformations and chiral GC/HPLC-traces for determination of product formations and determination of the enantiomeric excess in these biotransformations.....	139
7.2.2	Biotransformations with purified IREDs and GC/HPLC-traces for determination of product formations and determination of the enantiomeric excess in these biotransformations.....	145
7.3	Characterization of the IREDs	152
7.3.1	Thermostability	152
7.3.2	Specific activities of the IREDs in the presence of different water miscible organic solvents	154
7.3.3	HPLC-SEC runs for determination of the IRED purity	155
7.4	Michaelis-Menten plots of IREDs with cyclic imine substrates 3a to 3c and 5a to 5b	158
7.5	The reductive amination of aldehydes and ketones	163
7.6	Michaelis-Menten plots of <i>R</i> -IRED- <i>Sr</i> for the kinetic characterization of the reductive amination of 11 with 22	170

IV TABLE OF CONTENTS

7.7	NMR experiments to determine the actual imine fraction and estimation of a "true" K_M value.....	173
7.8	Oxidation of polyamines by PuO- <i>Re</i>	173
7.8.1	Analysis of PuO- <i>Re</i> reaction products by GC-MS headspace.....	173
7.8.2	Activity of purified PuO- <i>Re</i> E324D.....	174
7.8.3	Purification of PuO- <i>Re</i> wt and mutants by ion exchange chromatography.....	174
7.8.4	Activity of purified PuO- <i>Re</i> wt and PuO- <i>Re</i> mutants with polyamine substrates 28 to 38	175
7.9	Michaelis-Menten plots of putrescine oxidase wild type and mutants.....	176
7.10	GC-traces of the cascade reaction with purified proteins to transform polyamines into <i>N</i> -heterocycles.....	181
7.11	GC-traces of whole cell biotransformations with <i>E. coli</i> strains expressing PuO- <i>Re</i> and an IRED simultaneously to transform polyamines into <i>N</i> -heterocycles.....	185
7.12	NMR spectra.....	186
8	CURRICULUM VITAE.....	196

V ABBREVIATIONS

°C	degree Celsius	K_{eq}	equilibrium constant
Å	Ångström	K_i	inhibition constant
ABC	ammonium bicarbonate buffer	K_M	Michaelis constant
ACN	acetonitrile	$K_{M\ app}$	apparent Michaelis constant
ADH	alcohol dehydrogenase	KRED	ketoreductase
Amp	ampicillin	l	liter
Ara	L-arabinose	LB	lysogeny broth
β-HAD	β-hydroxyacid dehydrogenase	MAO-N	monoamine oxidase from <i>Aspergillus niger</i>
BLAST	Basic Local Alignment Search Tool	mbar	millibar
BSA	bovine serum albumin	mg	milligram
CAST	combinatorial active-site saturation test	MeOH	methanol
Cm	chloramphenicol	min	minute
cm	centimeter	μl	microliter
cv	column volume	ml	milliliter
cww	cell wet weight	μM	micromolar
DAD	diode array detector	mM	millimolar
DBU	diazobicyclo-[5.4.0]-undec-7-ene	MS	molecular sieve
DCM	dichloromethane	MTBE	methyl <i>tert</i> -butyl ether
DEA	diethylamine	Mw	molecular weight
DHFR	dihydrofolate reductase	NAD(P)H	nicotinamide adenine dinucleotide (phosphate)
DMSO	dimethyl sulfoxide	NaOH	sodium hydroxide
DNA	deoxyribonucleic acid	NCS	<i>N</i> -Chlorosuccinimide
DTT	DL-dithiothreitol	Ni	nickel
<i>E. coli</i>	<i>Escherichia coli</i>	nm	nanometer
EDTA	ethylenediaminetetraacetic acid	NMR	nuclear magnetic resonance
ee	enantiomeric excess	n.a.	not available
epPCR	error prone PCR	n.d.	not determined
eq	equivalents	OD	optical density
ERED	ene reductase	PCR	polymerase chain reaction
eV	electron Volt	pdb	Protein Data Bank
EtOH	ethanol	PMSF	phenylmethanesulfonyl fluoride
g	gram	ppm	parts per million
GC	gas chromatography	PuO	putrescine oxidase
GC-FID	gas chromatography coupled to flame ionization detector	Rh	rhodium
GC-MS	gas chromatography coupled to mass spectrometry	RNA	ribonucleic acid
h	hour	Ru	ruthenium
H ₂ O ₂	hydrogen peroxide	RT	room temperature
HEH	Hantzsch ester	s	second
HPLC	high-performance liquid chromatography	SDS-PAGE	sodium dodecyl sulfate polyacrylamide gel electrophoresis
HRP	horseradish peroxidase	SEC	size exclusion chromatography
HTS	high throughput screening	SOC	super optimal broth with catabolite repression
IBCF	isobutyl chloroformate	TB	terrific broth
iProp	isopropyl alcohol	<i>t</i> -BuOH	<i>tert</i> -butyl alcohol
IPTG	isopropyl-β-D-1-thiogalactopyranoside	TLC	thin layer chromatography
Ir	iridium	TRIS	Tris-(hydroxymethyl)-aminomethane
IRED	imine reductase	U	units
IS	internal standard	UV	ultraviolet
k	kilo	v/v	volume/volume
k_{cat}	turnover number	wt	wild type
$k_{cat\ app}$	apparent turnover number	ω-TA	ω-transaminase
k_{cat}/K_M	catalytic efficiency	X-Gal	5-bromo-4-chloro-3-indolyl-β-galactopyranoside
kDa	kilo Dalton		

VI ABSTRACT

Chiral amines are an ubiquitously distributed class of bioactive compounds, what turns them into preferred scaffolds for pharmaceuticals. The high chemical and enantiomeric purities required for such an application are ideally suited for biocatalysis as enzymatic methods routinely display high specificities. The established methods for chiral amine synthesis with lipases, ω -transaminases and amine oxidases, however have considerable limitations regarding their access to pharmaceutically relevant chiral secondary and tertiary amines. Recently the new enzyme class of imine reductases (IREDs) was described, offering an attractive extension to the currently used techniques as the preparation of imines by chemical methods in organic solvents is a well established and widely applicable method.

As the number of IREDs known initially was limited to only three enzymes, this project started with a database search for the discovery of novel enzymes. For the first time it was shown that the IRED family is much larger than assumed and over 350 novel, putative IREDs were identified. A sequence analysis of the database members revealed (*R*)- type and (*S*)- type superfamilies and led after an update to the identification of IRED specific sequence motifs. These criteria allowed to define this new enzyme family on a sequence level and discriminate them from the closest related homologues.

Based on the biochemical information about the three published IREDs and a conservation analysis of the database members, three new enzymes from *Streptosporangium roseum* DSM43021, *Streptomyces turgidiscabies* and *Paenibacillus elgii* were selected for characterization. The enzymes were shown to encode for functional IREDs with much higher activity than the previously known IREDs. By site directed mutagenesis the mechanism of the IREDs was probed and the importance of a conserved Tyr for catalysis of an (*S*)- type IRED shown, while the crucial role of the proposed Asp residue for catalysis in the (*R*)- type IREDs was questioned. The characterization of the new IREDs revealed their pH optima and confirmed the suspected dimerization. The thermostability of the IREDs was investigated and the selected (*S*)- type IRED identified as the most stable enzyme known to date. Further the activity in the presence of water miscible organic solvents was tested and high tolerance *versus* MeOH found. In biotransformations all IREDs showed high activity and a broad panel of cyclic imines was fully converted to piperidines and tetrahydroisoquinolines with enantioselectivities up to 99% *ee*. With purified IREDs kinetic constants for these substrates were recorded and their substrate preference investigated. This indicated a preference of the (*S*)- type IRED for more bulky substrates, compared to the (*R*)- type IREDs. After optimization of the reaction conditions, with purified IREDs also high activities and chemo- as well as enantioselectivities for very labile exocyclic imines were detected. The possibility to effectively reduce already low levels of such imines led to the application of one (*R*)- type IRED for the generation of novel C-N bonds by reductive aminations. The established methodology revealed the crucial influence, conditions that favor imine formation (high molar excess of the amine nucleophile and high pH) display on the conversion rates. Under optimized conditions, different carbonyls could efficiently be transformed with a variety of amines in the aqueous buffer system with moderate to good conversions into primary and secondary (chiral) amines with very high selectivities (*ee* up to 98%).

Finally, an application of IREDs in cascade reactions to produce saturated *N*-heterocyclic compounds was envisioned. A microbial putrescine oxidase (PuO) was chosen to selectively oxidize polyamines to

aminoaldehydes, thereby triggering their spontaneous cyclization to an imine. To target a broad range of heterocycles, PuO was characterized with a range of unnatural polyamines. The results indicated a narrow substrate scope and low activity for these compounds. To enhance the activity for such substrates directed evolution of PuO with epPCR was performed and led to the identification of a Glu residue, representing a hotspot for mutagenesis. This residue aligns to one of the multiple channels that lead into the deeply buried active site of PuO and it is located in the second shell around the active site. By site-saturation mutagenesis further mutants in the active site and this channel were generated and many mutants with smaller amino acids demonstrated the influence of this hotspot position to increase the activity of the enzyme. The best mutant exhibited considerably increased activities (up to 25-fold) for unnatural polyamines and also for natural polyamines the substrate spectrum was strongly shifted from putrescine towards longer polyamines like spermidine which is now transformed with a 10-fold increased catalytic efficiency (k_{cat}/K_M).

The combination of both enzymes in purified form as well as in whole cells enabled the production of heterocyclic amines relying on the consecutive transformation of the substrate by both enzymes. While with the whole cell system only low amounts of the *N*-heterocyclic compounds were produced, the utilization of purified enzymes led in case of all three IREDs to high conversions of different polyamines into pyrrolines and piperidines.

VII ZUSAMMENFASSUNG

Chirale Amine stellen eine allgegenwärtige Klasse an bioaktiven Verbindungen dar, weshalb sie auch bevorzugte Leitstrukturen für Pharmazeutika ausmachen. Die sehr hohen chemischen- und enantiomeren Reinheiten die für einen solchen Einsatz erforderlich sind, stellen ideale Voraussetzungen für biokatalytische Herstellungsmethoden dar, da enzymatische Methoden oft hohe Spezifitäten aufweisen. Jedoch besitzen die derzeit etablierten Methoden die zur Synthese chiraler Amine eingesetzt werden können und auf Lipasen, ω -Transaminasen und Aminoxidasen basieren, beträchtliche Limitierungen was ihren Einsatz zur Darstellung pharmazeutisch relevanter chiraler sekundärer und tertiärer Amine betrifft. Kürzlich wurde mit den Iminreduktasen (IREDs) eine neue Enzymklasse beschrieben die eine attraktive Erweiterung zu den derzeit verwendeten Biokatalysatoren darstellt, da die chemische Synthese von Iminen in organischen Lösemitteln eine etablierte und breit anwendbare Methode repräsentiert.

Da die Anzahl bekannter IREDs mit nur drei beschriebenen Enzymen zunächst sehr gering war, startete dieses Projekt mit einer Datenbankanalyse zur Entdeckung neuer Enzyme. Zum ersten Mal wurde hierbei gezeigt, dass die IRED Familie wesentlich größer ist als angenommen und über 350 neue, putative IREDs wurden identifiziert. Über eine Sequenzanalyse wurden die Datenbankvertreter in (*R*)-Typ und (*S*)-Typ Familien eingeteilt und nach einem Datenbankupdate wurden IRED spezifische Sequenzmotive identifiziert. Diese Kriterien ermöglichten die Definition von IREDs auf Sequenzebene und ihre Unterscheidung von den nächstverwandten Enzymen.

Basierend auf publizierten biochemischen Daten der drei bekannten Enzyme und einer Konservierungsanalyse der Datenbankvertreter wurden drei neue Enzyme aus *Streptosporangium roseum* DSM43021, *Streptomyces turgidiscabies* und *Paenibacillus elgii* zur Charakterisierung ausgewählt. Es wurde gezeigt, dass diese Sequenzen für funktionale IREDs kodieren welche wesentlich höhere Aktivitäten besitzen als die bisher bekannten IREDs. Über ortsgerichtete Mutagenese wurde der Mechanismus der IREDs untersucht und der Einfluss eines konservierten Tyr auf die Aktivität der (*S*)-Typ IRED gezeigt, während gleichzeitig die essentielle Rolle des Asp Restes, welcher für die (*R*)-Typ IREDs als katalytisch wichtig vorgeschlagen wurde, hinterfragt wurde. Zur Charakterisierung der drei IREDs wurden deren pH Optima untersucht und die vermutete Dimerisierung bestätigt. Die Thermostabilität wurde untersucht und die ausgewählte (*S*)-Typ IRED als die stabilste der derzeit bekannten IREDs ausgemacht. Weiterhin wurde die Aktivität der IREDs in Gegenwart Wasser mischbarer organischer Lösemittel untersucht und eine hohe Toleranz gegenüber MeOH festgestellt. In Biotransformationen zeigten alle IREDs hohe Aktivitäten und eine breite Auswahl an zyklischen Iminen wurde vollständig umgesetzt und sowohl Piperidine als auch Tetrahydroisochinoline wurden mit sehr hohen Enantioselektivitäten von bis zu 99% ee erhalten. Mit den aufgereinigten IREDs wurden die kinetischen Konstanten für diese Substrate bestimmt und die Substratpräferenz der IREDs untersucht. Dies deutete auf ein breiteres Substratspektrum der (*S*)-Typ IRED hinsichtlich sperriger Substrate hin im Vergleich zu den (*R*)-Typ IREDs.

Nach Optimierung der Reaktionsbedingungen mit aufgereinigten IREDs wurden zudem hohe Aktivitäten und sowohl Chemo- als auch Enantioselektivitäten für den Umsatz von sehr labilen exozyklischen Iminen gezeigt. Die Möglichkeit auch sehr geringe Mengen solcher Imine effektiv umsetzen zu können

fürte zur Anwendung einer (*R*)- Typ IRED für die Generierung neuer Kohlenstoff-Stickstoff Bindungen durch reduktive Aminierung. Die entwickelte Methodik enthüllte den elementaren Einfluss welchen Reaktionsbedingungen die die Iminbildung begünstigen (hoher molarer Überschuss an Aminnukleophil und hohe pH Werte) auf die Umsatzraten besitzen. Unter optimierten Bedingungen konnte die effiziente Umsetzung verschiedener Carbonyle mit einer Auswahl an unterschiedlichen Aminen im wässrigen Puffersystem mit moderaten bis guten Umsetzungen und sehr hohen Selektivitäten (bis zu 98% ee) in primäre und sekundäre (chirale) Amine gezeigt werden.

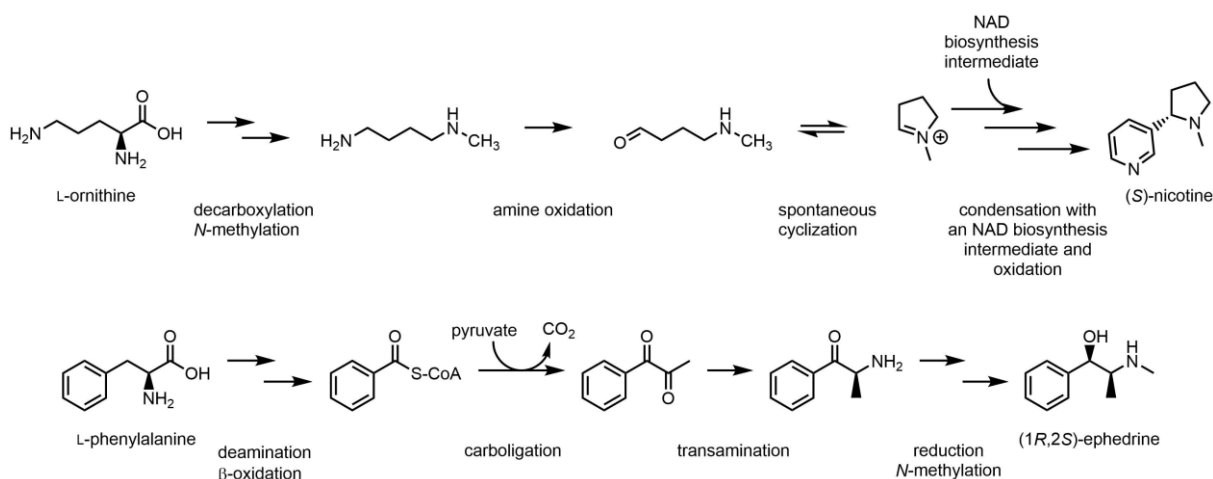
Des Weiteren wurde eine Anwendung der IREDs in Kaskadenreaktionen untersucht, die die Produktion von gesättigten, stickstoffhaltigen Heterozyklen ermöglicht. Eine mikrobielle Putrescinoxidase (PuO) wurde für die selektive Oxidation von Polyaminen zu Aminoaldehyden ausgewählt um deren spontane Zyklisierung zu einem Imin zu induzieren. Um dies auf ein breites Spektrum an Heterozyklen anwenden zu können, wurde die Aktivität der PuO mit einer Auswahl an nicht-natürlichen Polyaminen untersucht. Die Ergebnisse deuteten auf ein beschränktes Substratspektrum mit geringen Aktivitäten für diese Verbindungen hin. Zur Verbesserung der Aktivitäten für solche Substrate, wurde durch gerichtete Evolution über epPCR ein Glu Aminosäurerest identifiziert, welcher ein Hotspot für die Mutagenese darstellt. Die Seitenkette dieser Aminosäure befindet sich in einem der zahlreichen Kanäle die in die tief im Inneren des Enzyms liegende aktive Tasche führen, zudem befindet sich diese Aminosäure in der sogenannten zweiten Schale um das aktive Zentrum. Über ortsgerichtete Sättigungsmutagenese wurden weitere Mutanten im aktiven Zentrum des Enzyms und in diesem Kanal generiert; hierbei verdeutlichten mehrere Mutanten mit kleinere Aminosäureseitenketten den Einfluss der Hotspot Position darauf, die Aktivität des Enzyms zu erhöhen. Die beste Mutante wies beträchtlich gestiegene Aktivitäten (bis zu einer 25-fachen Erhöhung) für nicht-natürliche Polyamine auf und zeigte auch für natürliche Polyaminsubstrate eine starke Veränderung im Substratspektrum des Enzyms von Putrescin hin zu längeren Polyaminen wie Spermidin, die jetzt mit einer über 10-fach höheren katalytischen Effizienz (k_{cat}/K_M) umgesetzt wurden.

Die Kombination aus beiden Enzymen sowohl in aufgereinigter Form, als auch in ganzen Zellen ermöglichte dann die Produktion von heterozyklischen Aminen welche auf die aufeinanderfolgende Transformation des Substrates durch beide Enzyme angewiesen war. Während mit dem Ganzzellsystem nur geringe Mengen der stickstoffhaltigen Heterozyklen gebildet wurden, resultierte die Verwendung von aufgereinigten Enzymen im Fall aller drei IREDs in hohen Umsätzen von verschiedenen Polyaminen zu Pyrrolinen und Piperidinen.

1 INTRODUCTION

1.1 The importance of chiral amines in natural products and pharmaceuticals

Optically active amines and amino acids play central roles in all living systems and the general importance these molecules and thereof derived heterocycles have for all organisms is directly reflected by their ubiquitous distribution in nature.¹⁻⁴ As an example amino acids are the universal element of proteins and next to this they also function as precursors for DNA and RNA bases, so they are directly involved in the biosynthesis of all of the most important biological macromolecules.⁵ In addition, they also play crucial roles in the signaling in metabolic pathways and are part of many secondary metabolites like alkaloids.⁵⁻⁷ Following terpenes, alkaloids like nicotine represent the second largest class of natural products and most of them are also derived from amino acids (Scheme 1).⁶⁻⁸



Scheme 1: Chiral amines in natural products derived from amino acids.

The top row shows the proposed biosynthetic pathway for (S)-nicotine, the main alkaloid of tobacco plants.⁷ (S)-nicotine binds to acetylcholine receptors, making it a powerful stimulating drug that can lead to addiction.⁷ In contrast, (R)-nicotine is not active.⁷ Decarboxylation of L-ornithine leads to diaminobutane, which is in the next step methylated at one of the amine moieties.^{6,7} Oxidation of the other amine group to an aldehyde triggers the spontaneous cyclization.^{6,7} The cyclic imine is proposed to further react with an intermediate of the NAD biosynthesis, thereby introducing the dihydropyridine ring.^{6,7} The final step represents the oxidation to the pyridine.^{6,7}

Bottom row: One of the potential ephedrine biosynthesis pathways is shown. Ephedrine and other substituted amphetamines have various applications as precursors for pharmaceuticals.⁸ The biosynthesis of ephedrine starts from L-phenylalanine, but depending on the organism different metabolic routes are possible.⁸ In the one shown above after deamination, cinnamic acid is coupled to Coenzyme A by a cinnamyl-CoA ligase.⁸ In a biosynthetic route similar to the β-oxidation the carbon chain is shortened and later by a thiamine diphosphate-dependent enzyme with pyruvate again elongated, introducing the diketone motif.⁸ One of the carbonyl groups is transformed into the chiral amine by a ω-transaminase (ω-TA) and the other one is reduced.⁸ The last step represents the further modification by N-methylation.⁸

The high biological activity provoked by many of these compounds is thought to be based on the structural information that is introduced by the ability of the chiral amines to build up numerous hydrogen bonds with adjacent (macro-) molecules.^{4,9} Hence, it is not surprising that such amines are prominent scaffolds for the synthesis of natural products including their analogs, pharmaceuticals and agrochemicals.^{3,4,9} Their leading role is underlined by the estimation that over 40% of all current pharmaceuticals contain chiral amines.² The different biological activity chiral molecules display was already known for long but this importance tragically recollected during the early 1960's with the insomnia drug thalidomide.^{2,10,11} Whereas the (R)- enantiomer of the drug had the desired effect, the (S)- enantiomer showed teratogenic outcomes (Figure 1), but the drug can also easily racemize

in vivo.^{2,11} Another example for the different effects the individual enantiomers of a drug can display are the two isomers of ethambutol (Figure 1). The (*S,S*)- enantiomer is an effective antituberculosis agent but the (*R,R*)- enantiomer causes blindness.^{3,10}

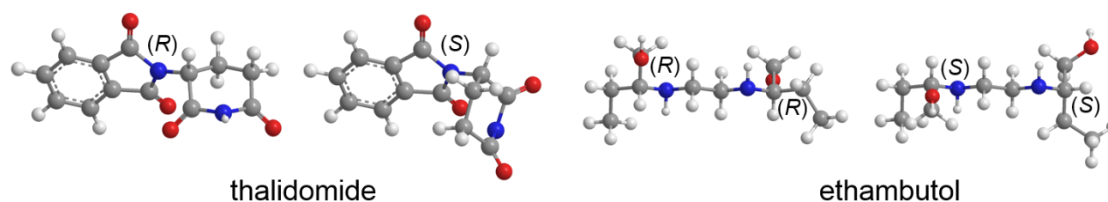


Figure 1: (*R*)- and (*S*)- enantiomers of thalidomide (left) and the (*R,R*)- and the (*S,S*)- forms of ethambutol (right). In both cases each enantiomer of the drug has very different effects. For thalidomide the (*R*)- enantiomer is the active drug, whereas the (*S*)- enantiomer showed teratogenic effects^{2,10,11} and in case of ethambutol the (*S,S*)- form is effective against tuberculosis, but the (*R,R*)- form can lead to blindness.^{3,10}

Following the thalidomide scandal, the American Food and Drug Administration and its European counterpart set strict rules for the approval of new pharmaceuticals and by 1992 toxicological tests for each single enantiomer of a racemic drug were required.^{2,3} Also for already licensed pharmaceuticals the reapproval in their enantiopure form resulted in attractive concessions, speeding up the chiral switch and leading to a boost of chiral chemistry in the pharmaceutical industry.^{3,11} The agrochemical industry followed up this trend as thereby also the economic effect is improved and the environmental impact reduced.³ In a study from the pharmaceutical industry by Carey *et al.* the importance of amines in the synthesis of pharmaceuticals was illuminated.¹² More than 90% of all heterocyclic small molecule pharmaceuticals contain nitrogen atoms and the numbers for protections and deprotections of amino groups exceed by far the ones for hydroxyl-, carboxyl- and thiol groups.¹² Chirality is often supplied in form of chiral building blocks and in these synthesis routes introduced as early as possible to maintain flexibility and reduce the number of steps.^{3,12} For compounds to serve as enantiopure building blocks however optical purities of > 99.5% ee are required.¹² As it allows to approach higher yields asymmetric synthesis would be the desired strategy for the production of such building blocks, but on an industrial scale also the resolution of racemic materials is still a profitable process.^{3,10} Next to their direct use as building blocks chiral amines also have additional important roles for the synthesis of other enantiopure compounds. They are frequently used as chiral auxiliaries for stereoselective organic synthesis and can be used as resolving agents for the preparation of chiral carboxylic acids.^{3,13}

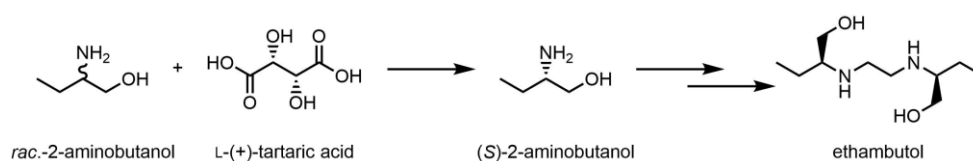
1.2 Chemical and biocatalytic methods for the preparation of chiral amines

1.2.1 Chemical methods for the resolution of racemic amines and asymmetric synthesis for the stereoselective formation of amines

Due to their prominent roles and many applications the demand for chiral amines is steadily increasing.^{2,3} Synthetic organic chemistry has harnessed much progress in every decade, but especially the above mentioned chiral switch resulted in the fast development of novel enantioselective synthesis routes for the production of chiral amines.¹⁴ The diastereomeric crystallization of chiral amines or carboxylic acids with amines and the use of chiral amines as auxiliaries seems therefore somehow outdated compared to sophisticated methods in asymmetric synthesis and although their impact is

1 INTRODUCTION

decreasing in latest years, these methods still have some validation today.¹⁵ Frequently both methods lead to a rapid, reliable and highly selective way for production of the target molecule.^{3,13,16} The application of chiral auxiliaries often is straightforward and the setting of selectivity by such a strategy is relatively universal.^{13,16} Additionally, even for an imperfect selective outcome, the diastereomeric character of the intermediate allows an easy separation.^{13,16} Due to its simplicity and the ease of use the diastereomeric crystallization of amines was also on an industrial scale a popular method some time ago.^{3,10,15} In the last years however, the trend was rather to use this method as a second step for enantioenrichment in case asymmetric synthesis did not result in the desired purity, than for the crystallization of racemic mixtures.^{9,15} Nevertheless established processes are still running and for example the resolution of (*S*)-2-aminobutanol, which is the key chiral intermediate for one of the most important tuberculosis drugs (ethambutol), is still performed by resolution with L-(+)-tartaric acid.^{3,10,17}



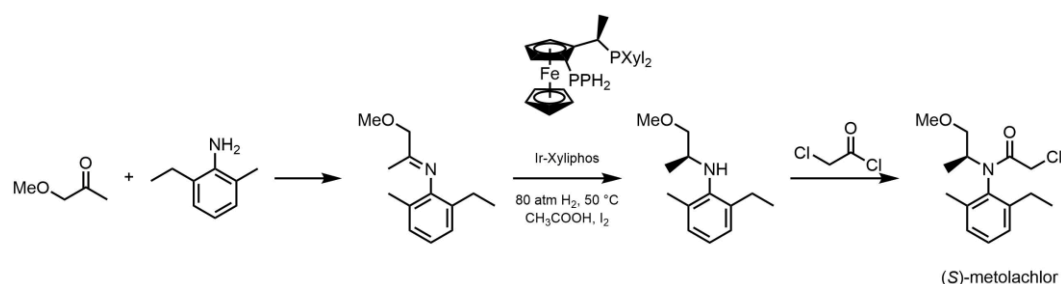
Scheme 2: Diastereomeric crystallization of (*S*)-2-aminobutanol with L-(+)-tartaric acid to produce the chiral precursor for the tuberculosis drug ethambutol.

Nevertheless asymmetric synthesis has made tremendous improvements for the preparation of chiral amines driven by the recent progress in organocatalysis and by the development of chiral ligands for transition metal catalysts.¹⁴ The enantioselective hydrogenation of enamides and enamines is a way to generate chiral amines and radical- and nucleophilic addition reactions to (activated) imines, catalyzed by metals or chiral phosphoric acids, are also intensively investigated.^{1,9,16,18} In contrast, the metallonitrene catalyzed C-H amination and the asymmetric hydroamination of unsaturated carbon-carbon bonds are a rather new fields of research.^{1,16} However, the broad availability of alkynes, allenes and dienes and the high atom economy of the latter process render it an attractive target, albeit especially the amination of alkenes remains challenging due to the high energetic activation barrier that has to be overcome.^{1,16} The detailed reviewing of all of these methods is beyond the scope of this introduction and therefore only the (asymmetric) reductive amination, which is regarded as the most popular and broadly applicable method for the enantioselective synthesis of chiral amines will be introduced.^{9,14,19,20}

The basic principle for the reductive amination is the condensation of a carbonyl and an amine. This versatile and widely applicable coupling reaction directly leads to the imine intermediate of the reaction, which is in the next step reduced to the amine.⁹ A strict definition of this process would be the direct one pot transformation of a ketone or aldehyde into an amine, without the isolation of the imine intermediate which is sometimes described as an indirect reductive amination.⁹ Two-step processes that involve previous imine formation (but not isolation), before the reducing agent is applied are however covered.^{1,9} Challenges that are arising for such direct reductive amination procedures are related to the choices of suitable and highly selective catalysts and reducing reagents.^{9,14} Chemoselectivity is crucial, as the undesired reduction of the starting carbonyl to an alcohol has to be avoided, but the imine must efficiently be targeted.^{9,14} Further, other reducible intermediates like hemiaminals and enamines that are arising during imine formation or from isomerizations should also not be reduced.^{9,14} To achieve a highly

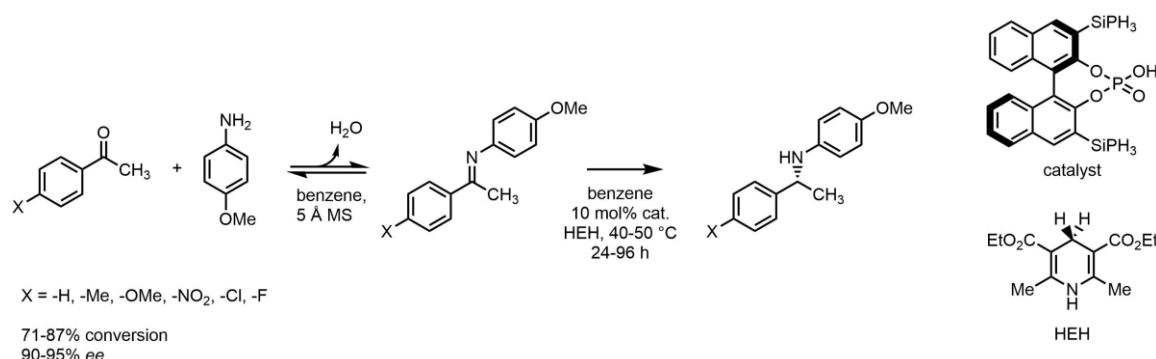
enantioselective outcome in this reaction is also difficult and sets special requirements to the catalysts. Acyclic imines form mixtures of *E/Z* intermediates, complicating the stereoselective reduction.^{9,14} Finally, the elimination of water is an essential step to shift the equilibrium of the carbonyl and amine condensation towards the side of the imine.^{1,9,14,16,20}

For reductive aminations, the asymmetric hydrogenation of the imine intermediate with stoichiometric amounts of H₂ gas is particularly attractive.^{1,16,21} Unfortunately the high pressure required and the leaching of the expensive metals (in most cases Ru, Rh and Ir are employed) hampers large scale applications.^{1,16,21} Nevertheless such methods are viable for industrial production and one of the world's largest enantioselective catalytic processes is the chiral Ir-Xyliphos catalyzed imine hydrogenation to produce the herbicide (*S*)-metolachlor (Scheme 3).^{1,16,22,23}



Scheme 3: Ir-catalyzed enantioselective hydrogenation to produce the chiral intermediate for the synthesis of the herbicide (*S*)-metolachlor.²³ This process is performed on an industrial scale and with > 10 000 t per year one of the largest enantioselective catalytic processes.²³

Inspired by the fact that the majority of chiral molecules is not produced by organometallic catalysis but by nature, the groups of List and MacMillan, amongst others, have pioneered organocatalytic methods with Hantzsch esters (HEH) as hydrogen source for enantioselective imine reduction.^{24–26} Hantzsch esters can be seen as an organocatalytic mimic to the biological reducing agents NAD(P)H and the use of chiral phosphoric acids results in the coordination and activation of the HEH and the imine.^{24,25} By this method the direct reductive amination of a broad range of (aromatic) ketones and aromatic amines was shown with quite high selectivities (Scheme 4).^{24–27}



Scheme 4: Overview about some of the reductive aminations performed by Storer *et al.*²⁵ Various acetophenone derivatives were reacted with *p*-anisidine to form the imine intermediates.²⁵ The addition of the molecular sieve (MS) was critical to shift the equilibrium.²⁵ An example for one of the chiral phosphoric acid catalysts that were investigated is shown on the right side.²⁵ Also shown is the Hantzsch ester (HEH) that was employed as reducing agent.

Heterocyclic amines like pyridines, piperidines and pyrrolidines have important roles as solvents, but especially the chiral derivatives of the saturated heterocyclic compounds find also numerous

applications as building blocks for pharmaceuticals.^{28,29} They are usually obtained by hydrogenation of pyridines at elevated temperatures and pressure in the presence of metal catalysts like nickel, palladium or ruthenium.^{28,30} In combination with chiral auxiliaries this can be used for an asymmetric hydrogenation, directly leading to enantioenriched products.³¹ In other cases crystallizations or kinetic resolution were investigated^{32,33} and in some cases also asymmetric reductive amination reactions have been developed.³⁴ Nevertheless, their preparation in high yields with high enantiomeric excess amounts remains challenging.²⁹ For example, for the rather simple (*R*)-2-methylpyrrolidine, which finds applications in histamine H₃-receptor antagonistic drugs^{35,36} or as part of HIV reverse transcriptase inhibitors,³⁷ Merck has published an optimized synthesis route.²⁹ It starts from the readily available *N*-Boc-protected L-proline and within 4 steps the product is obtained in about 80% yield with > 99% ee.²⁹ This represented a tremendous improvement to the previously reported crystallization process of racemic 2-methylpyrrolidine that required several recrystallizations, diminishing the yield to only 28%²⁹ and at the same time reveals the potential the asymmetric reduction of cyclic imines has to improve the synthesis for such important pharma precursors.

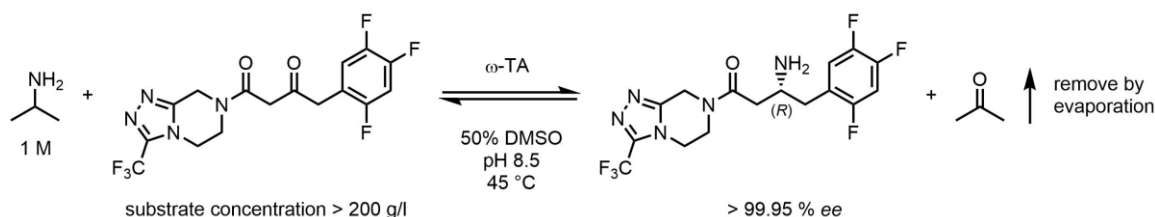
1.2.2 Strategies and challenges for the biocatalytic generation of chiral amines

The importance of biocatalysis to solve synthetic challenges is steadily increasing as it becomes more and more a facile usable technology.^{38–40} Biocatalysis is therefore regarded as an important extension to currently established techniques in the chemical industry.^{38–40} These changes are driven by the immense technological progress in biochemistry and molecular biology.^{38–41} The vast availability of genetic information, combined with high throughput screening methods and novel bioinformatics tools have considerably facilitated the identification and production of novel enzymes.^{38–41} These combinations have led to numerous examples for novel enzymes and their application for the generation of chiral intermediates.^{2,38,41–45} The high chemo-, regio- and enantioselectivities enzymes often display are one of the driving forces for this development.^{3,38–40} Next to that biocatalysis benefits also from mild reaction conditions and is generally regarded as “green”.^{3,38–40}

Maybe less focused are some of the still remaining drawbacks of biocatalysis. Current chemistry focuses mainly on rather unpolar aliphatic hydrocarbons that display in contrast to the natural sugar based feedstock only limited solubility in aqueous solvents.^{40,46,47} Under a space-time yield perspective however the low concentrations that are accessible represent a significant challenge, further do they complicate the downstream processing of the final products.⁴⁷ Yet, the shift to unphysiological conditions to overcome these limitations by increasing the temperature or the addition of organic solvents often results in low stability of the biocatalyst.^{48,49} The engineering of enzyme stability is therefore an important task next to increasing the activity and selectivity.^{48,49} Another drawback for biocatalysis is that many reactions that are performed in synthetic chemistry are not available to enzymes.⁵⁰ The discovery of novel enzymes and the improvements in computational enzyme design and engineering, however also resulted in first noticeable advances for non-natural reactions catalyzed by protein scaffolds.^{38,41,51–56}

A recently published and highly respectable example illustrating many of the above mentioned tremendous proceedings is the engineering of a (*R*)-selective ω -transaminase (ω -TA), performed by Codexis Inc. and Merck for the preparation of the anti-diabetic drug sitagliptin (Scheme 5).⁵⁷ Structure

guided and random approaches were combined and in 11 rounds of mutagenesis the final biocatalyst acquired 27 mutations, showing now enhanced activity (~ 40000-fold) and stability under conditions applicable for an industrial process.^{38,57} Compared to the chemical Rh-catalyzed process the yields would be over 10% increased, the productivity over 50% increased and at the same time the produced waste reduced by about 19%.^{38,57}



Scheme 5: Highly selective ω -TA-catalyzed amination of pro-sitagliptin to produce the chiral amine of the drug. Over 11 rounds of mutagenesis the activity and stability of the biocatalysts was optimized.⁵⁷ The evolved enzyme is stable and active in 50% DMSO at 45 °C and tolerates high substrate loadings.⁵⁷ To shift the reaction equilibrium towards the amination, isopropylamine is used as amine donor and the coproduct acetone removed by evaporation at the elevated temperatures and reduced pressure.⁵⁷

1.2.3 Enzymes and enzymatic cascade reactions for the preparation of primary α -chiral amines

The possibility to use ω -TAs for the preparation of chiral amines was already shown above at the example of the drug sitagliptin, however also other enzymatic methods for the production of chiral primary amines are available and have been commercialized. In Figure 2 an overview about some of the most widely applicable enzymatic methods for the generation of primary α -chiral amines is given and these enzymes might hence be summarized as an enzymatic toolbox for chiral amine synthesis.

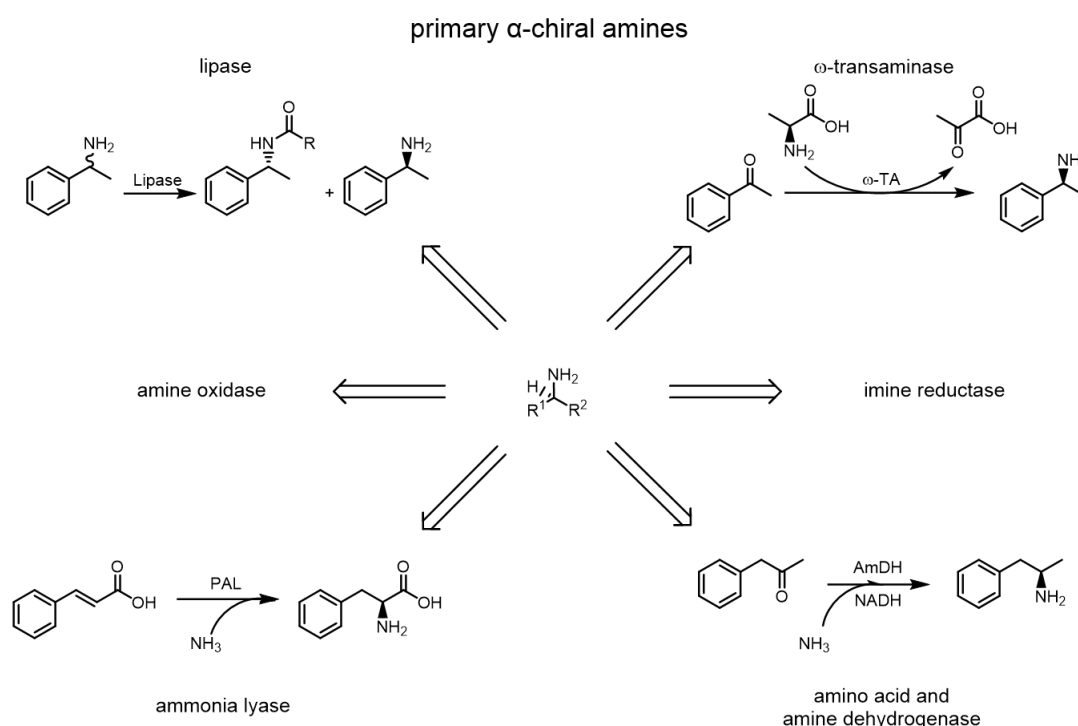
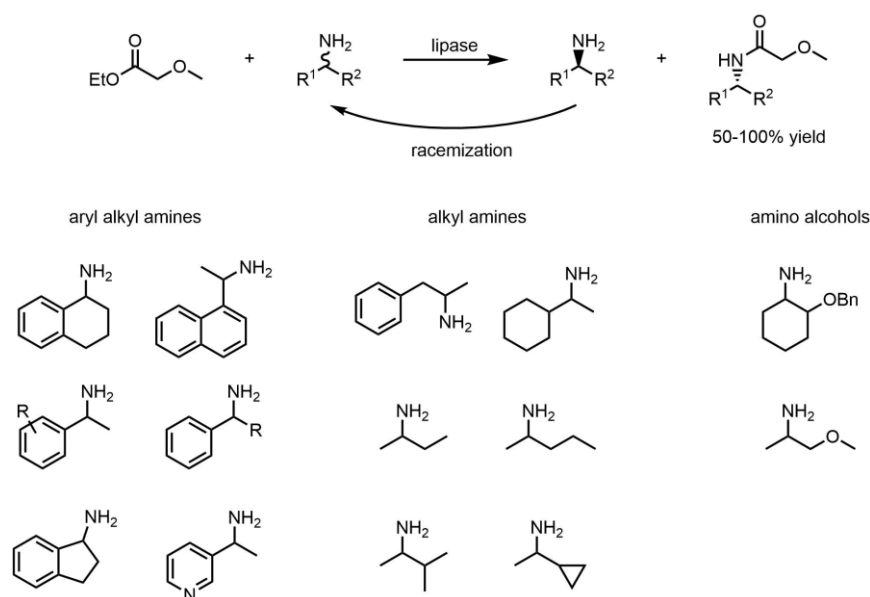


Figure 2: Biocatalyst toolbox comprising the most popular enzymes for the production of primary chiral amines by kinetic resolution or asymmetric synthesis.

1 INTRODUCTION

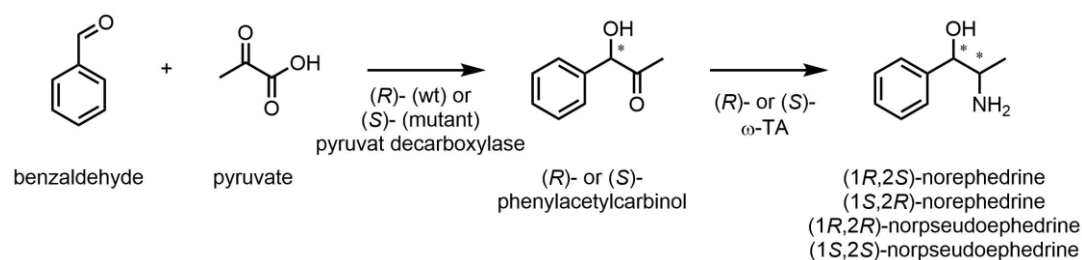
The kinetic resolution of racemic starting material is possible with lipases and ω -transaminase and the ChiPros[®] process of BASF is able to supply enantiopure (*R*)- and (*S*)- amines on a ton scale (Scheme 6).^{2,3,46,58–61} Amongst others, the lipase from *Burkholderia plantarii* and *Candida antarctica* lipase B are employed for the acetylation of the (*R*)- amine, yielding the (*S*)- enantiomer in almost pure form.^{3,58} After separation by distillation or extraction, the (*R*)- amide is cleaved under basic conditions, giving also access to this product in enantiopure form.³ Alternatively, if only one of the enantiomers is required, the process can sometimes be transformed into a dynamic kinetic resolution to approach more than 50% yield, but the inclusion of such a racemization step typically requires harsh conditions (Scheme 6).⁵⁹



Scheme 6: Lipase catalyzed dynamic kinetic resolution by methoxyacetylation of racemic amines to produce enantiomerically enriched amines.^{58,59} By the racemization of the unreacted enantiomer the yields can be increased above 50%, but this typically requires harsh conditions.⁵⁹ The bottom row shows some of the products that are accessible on a ton scale by the ChiPros[®] process of BASF.^{1,61}

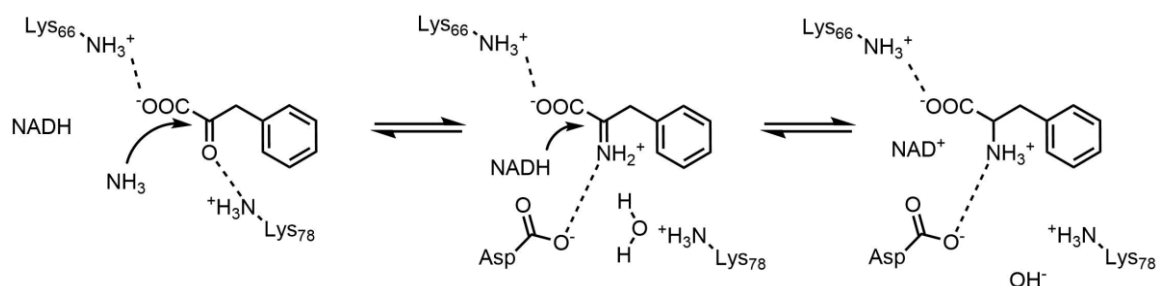
By employing the deamination reaction, ω -TAs can also be used for a kinetic resolution, but the more interesting alternative is to use them for asymmetric synthesis by performing the amination reaction and approaching higher yields than 50% under suitable reaction conditions.^{62,63} Such a reaction formally represents a reductive amination as the prochiral starting ketone is transformed into an amine.^{62,64} Difficulties for such a process are the unfavorable reaction equilibrium for reductive aminations, requiring the amine donor to be present in high excess and/or the removal of the formed co-product.⁶⁵ The sitagliptin process for example uses isopropylamine as amine donor and the formed co-product acetone is removed at higher temperatures and low pressure.⁵⁷ As ω -TAs are frequently inhibited by higher concentrations of these co-substrates and co-products also cascade reactions to recycle the amine donor and shift the equilibrium have been envisioned.^{59,64–70} These parameters still set a burden for large scale applications of ω -TAs and might require extensive protein engineering. In contrast, other problems that have encountered ω -TAs a couple of years ago are solved. Initially most of the described enzymes showed (*S*)- selectivity, but in a study by Höhne *et al.* 17 novel (*R*)- selective transaminases were identified.⁷¹ Additionally many mutants with a broadened substrate scope and high throughput

screening (HTS) methods for these enzymes have been reported.^{57,66,68,72} Their increased popularity also promoted the exploitation of ω -TAs for reaction cascades. The bioamination of alkenes after oxyfunctionalization⁷³ and the amination of alcohols by combining alcohol dehydrogenases (ADHs) and ω -TAs was described.⁷⁴ Additionally, these enzymes were employed for the production of aminoalcohols. In a work published by Sehl *et al.* the combination of thiamin diphosphate-dependent lyases and ω -TAs with different selectivities allowed to produce all different isomers of norephedrine (1*R*,2*S* and 1*S*,2*R*) and norpseudoephedrine (1*R*,2*R* and 1*S*,2*S*) (Scheme 7).^{75,76}



Scheme 7: Enzymatic cascade reaction to generate different ephedrine isomers, published by Sehl *et al.*^{75,76} By using two enantiocomplementary pyruvate decarboxylases first the carbon skeleton is assembled and the stereocenter of the hydroxyl group is set.^{75,76} By a combination with enantiocomplementary ω -TAs then the second stereocenter was introduced with the chiral amine.^{75,76}

In contrast to ω -TAs amino acid dehydrogenases and thereof derived amine dehydrogenases perform a “true” reductive amination (Scheme 8). Amino acid dehydrogenases are known for long time and the reductive amination of α -ketoacids with these enzymes is performed on an industrial scale to produce natural and unnatural amino acids.^{44,62,77} The power to assimilate free ammonia makes them potent enzymes for the generation of chiral amines distinguishing them also from most other enzymes in the above shown summary (Figure 2). In this way alanine dehydrogenase is also frequently used for the “real” reductive amination part in cascades that involve ω -TAs by recycling the generated pyruvate to alanine, which serves as the amine donor.^{64,65} Several crystal structures of these enzymes are available and the mechanism was investigated in detail.^{78–80} As most enzymes are specific for natural amino acids, the first D-amino acid dehydrogenase that has a broad substrate specificity was obtained by protein engineering⁸¹ and this technique was also used to expand the substrate scope to unnatural homo-amino acids^{82,83} or to β -keto acids for production of unnatural β -amino acids.⁸⁴ An even more aspirational engineering approach was performed for the first time in the group of Bommarius. By saturation mutagenesis of amino acids in the carboxyl binding pocket of the active site, the enzymes were relieved from their dependency on α -ketoacids.⁸⁵ These newly generated amine dehydrogenases were evolved from a leucine dehydrogenase⁸⁵ and phenylalanine dehydrogenase scaffold⁸⁶ and are able to perform the reductive amination of different ketone substrates with ammonia.^{85,86} Due to the great potential such “reductive aminases” have to produce chiral amines they were further evolved⁸⁷ and also other groups have generated such enzymes.^{88,89} During the writing of this thesis also two articles covering the amination of alcohols by the combined action of ADHs and an amine dehydrogenase in a cascade reaction were published.^{89,90} Yet, as these enzymes depend on the parent amino acid dehydrogenase scaffold, showing L-selectivity, it seems logical that they only allow access to one of the two enantiomers and still depend on ammonia as nitrogen source, leading to primary amines.



Scheme 8: Reductive amination of α -keto-acids (phenylpyruvate is shown here) with ammonia by phenylalanine dehydrogenase and NADH as reducing agent.^{79,80} Lys₇₈ is an essential amino acid for activation of the α -keto group to facilitate the nucleophilic attack of ammonia.^{78–80} The imine intermediate is stabilized by an Asp residue and reduced by a hydride transfer from NADH.^{79,80} Lys₆₆ constitutes the carboxyl binding pocket and was the first amino acid to be mutated in the studies by Abrahamson *et al.* to generate amine dehydrogenases.^{78–80,85}

Next to amino acid dehydrogenases ammonia lyases are able to assimilate a source of free nitrogen and form novel carbon-nitrogen bonds. Under suitable conditions (high ammonia concentrations) the hydroamination reaction of these enzymes can be exploited for the asymmetric synthesis of various natural and unnatural amino acids and derivatives thereof.^{50,91–97} These enzymes also have been engineered and coupled with L-amino acid oxidases or D-amino acid oxidases in cascades to produce enantiomerically pure L- and D-phenylalanine derivatives by deracemizations, starting for both with cinnamic acids.⁹⁵

1.2.4 Enzymes and enzymatic cascade reactions for the preparation of secondary and tertiary α -chiral amines

As it was described above in detail, most enzymatic methods only allow access to primary amines and the number of enzymes that can additionally be used for asymmetric synthesis of secondary and tertiary amines is rather small (Figure 3).

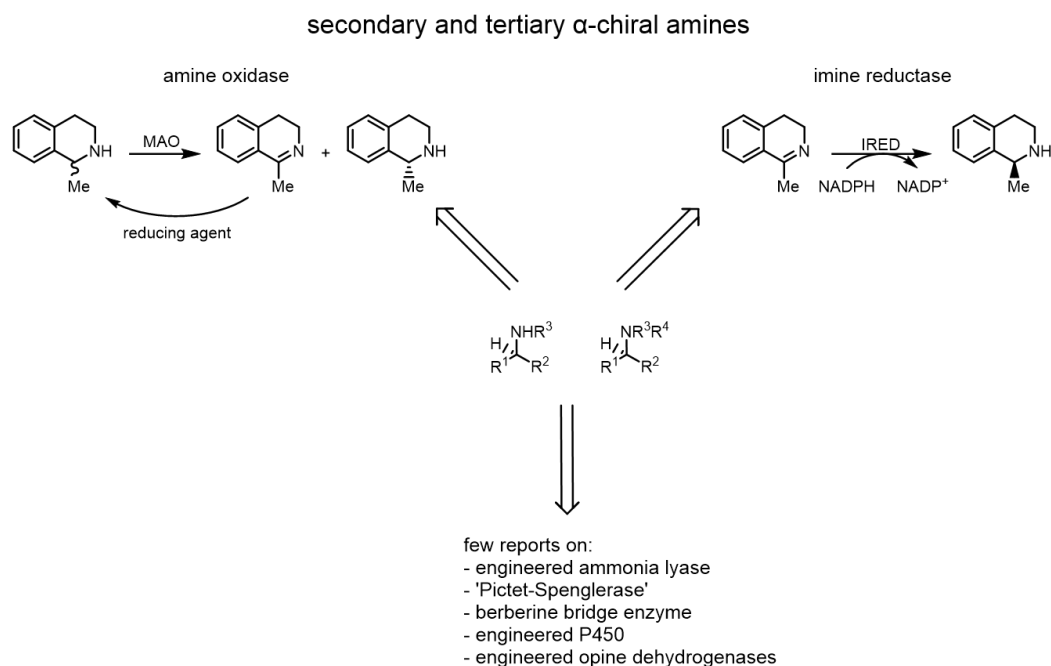
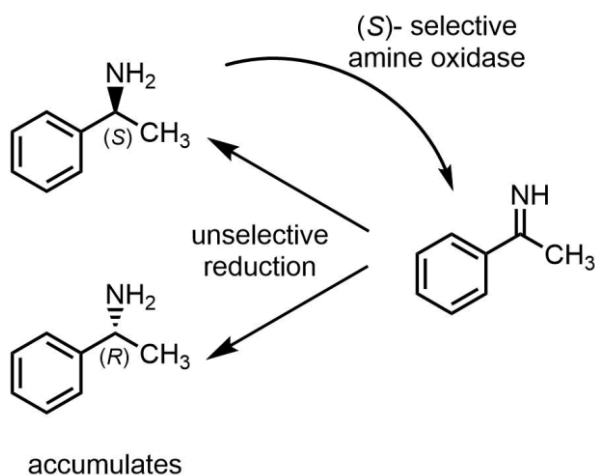


Figure 3: Biocatalyst toolbox comprising an overview about enzymatic methods that were reported for the generation of secondary- and tertiary chiral amines. In addition to this application, amine oxidases and imine reductases can also be used to generate primary amines.

A noticeable engineering approach of ammonia lyases broadened the substrate scope of methylaspartate ammonia lyase.⁹⁸ Next to ammonia now also a few other amine nucleophiles are accepted and the electrophile acceptor scope was enlarged to some fumarate derivatives.⁹⁸ These mutations enabled methylaspartate ammonia lyase now also to be applied for the production of amino acid derivatives with secondary amines.⁹⁸ Since amino acid lyases are considered as one of the most selective enzymes,⁵⁰ despite these first improvements their substrate spectrum is still considered as very limited. Next to this enzyme also some more “exotic” enzymes catalyzing transformations that result in the selective establishment of carbon-nitrogen bonds for secondary and tertiary amines have recently been described or engineered (Figure 3). Derived from alkaloid biosynthesis the oxidative carbon-carbon bond forming reaction of the berberine bridge enzyme also results in chiral amines^{99–101} as do the “Pictet-Spenglerases” norcoclaurine synthase and strictosidine synthase.^{102–105} The group of Frances Arnold has recently published their engineering of P450_{BM3} (better P411 as the most active variants had the Cys ligand of the heme replaced by Ser) for CH amination.⁵⁵ Finally, Codexis Inc. has patented engineered opine dehydrogenase variants with up to 29 mutations, acquired over 11 rounds of directed evolution, that are able to perform reductive aminations and produce chiral secondary and tertiary amines under industrial relevant conditions (see also 4.5.2).^{106,107}

The above described enzymatic transformations are all excellent examples for the discovery and engineering of new enzymes and enzymatic activities that in the future might play important roles for chiral amine synthesis, however currently they lack general applicability. Hence, the most popular enzymatic methods published in literature that are applicable for secondary and tertiary amines are deracemizations employing monoamine oxidase from *Aspergillus niger* (MAO-N).² In the initial discovery of this flavin containing enzyme from the fungi *Aspergillus niger* by Schilling and Lerch it showed mainly activity with a few primary aliphatic monoamines.^{108,109} Directed evolution performed in the group of Turner over about 15 years led to numerous enzyme variants with broadened substrate scope, activity and improved selectivity.^{110–115} The first mutants allowed the deracemization of primary amines (mainly α -methylbenzylamine and derivatives thereof, Scheme 9),^{110,111} but soon also variants with activity for secondary^{111,112,116} and tertiary amines^{113,115} were generated. By solving the crystal structures of several mutants also the effects for (some of) the mutations could be rationally assigned and more focused libraries were generated.^{115,117} For deracemizations the strict (*S*)-selectivity of MAO-N is used and combined with a nonselective reducing agent (Scheme 9).^{2,118} In such a procedure the unreacted (*R*)-enantiomer accumulates and the product can be obtained in (theoretically) 100% yield.^{2,118}

For the preparation of the other enantiomer, (*R*)-selective amine oxidases have been developed by protein engineering from a D-amino acid oxidase and a D-nicotine oxidase, enabling now access to (*S*)-amines.^{119,120} Next to the group of Turner also industry has evolved MAO-N¹²¹ for its application in deracemizations on production scale.^{38,121} Deracemizations with MAO-N are however not restricted to these one step transformations. The combination with ω -TAs was explored in several examples^{122,123} and for non-chiral amines with ω -TAs also dealkylation reactions have been envisioned.¹²³ Further, the combination with artificial metalloenzymes capable of imine reduction was investigated (see also below).¹²⁴



Scheme 9: Deracemization of α -methylbenzylamine with the (S)- selective MAO-N.³⁹ The unreacted (R)- enantiomer accumulates as the reduction of the imine is not selective.^{39,118}

1.2.5 Imine reductases – a novel class of enzymes with the ability to generate primary, secondary and tertiary amines

Clearly, although much progress was made, there is still a lack of generally applicable enzymatic methods for the generation of secondary- and tertiary amines, especially regarding at the same time the formation of novel carbon-nitrogen bonds. Actually such a reaction would exactly represent an enzymatic counterpart for the reductive amination procedure in organic chemistry, the most widely applicable and popular chemical method for the generation of chiral amines.^{9,19} Unfortunately only limited numbers of imine reducing enzymes were described, although imines represent crucial intermediates in metabolic pathways.^{125–128} Especially their hydrolytic sensitive nature for long hindered a more detailed investigation of their potential as precursors for the generation of a broad range of chiral amines. Li *et al.* were the first ones to report the screening of a dynamic combinatorial library for the generation of various amines over imine intermediates, using caffeate induced whole cells of *Acetobacterium woodii*.¹²⁹ The responsible enzyme however was not reported so far. Also other groups have reported the reduction of imines by different strains, including *Saccharomyces cerevisiae*,¹³⁰ *Candida parapsilosis* ATCC 7330,¹³¹ *Saccharomyces bayanus*¹³² and cell free extracts of *Eisenia foetida*.¹³³ However in none of these reports the responsible enzyme was identified. The lack of enzymes suitable for the reduction of synthetically useful imines promoted the group of Thomas Ward to develop artificial metalloenzymes by the incorporation of biotinylated aminosulfonamide ligands with Rh, Ru and Ir in a protein (streptavidin) scaffold able to stereoselectively reduce imines.^{124,134–136}

The identification of the now designated class of imine reductases (IREDs) was then accomplished by Mitsukura *et al.*^{137–139} In their work, published 2010, imine reducing activity was detected after screening a large range of microorganisms (688 in total) for the reduction of the cyclic imine 2-methylpyrroline **1**.¹³⁷ Bacterial strains of the genus *Streptomyces* that resulted in the formation of the (R)- and (S)- amine products (a secondary amine) were identified and for the first time the following identification of the enzymes was also successfully achieved.^{137,139–141} Shortly thereafter, in 2011 the identification and purification of the (R)- selective IRED was published¹³⁸ and in 2013 also the cloning of the (S)- selective enzyme.¹³⁹ Meanwhile also the first crystal structure of a third IRED (an (R)- selective enzyme from

Streptomyces kanamyceticus (*R*-IRED-*Sk*) was solved and a mechanism proposed.¹⁴² An Asp residue in the assumed active site was suggested to be catalytically important for protonation of the imine substrate and its crucial role verified by site directed mutagenesis (Figure 4).¹⁴²

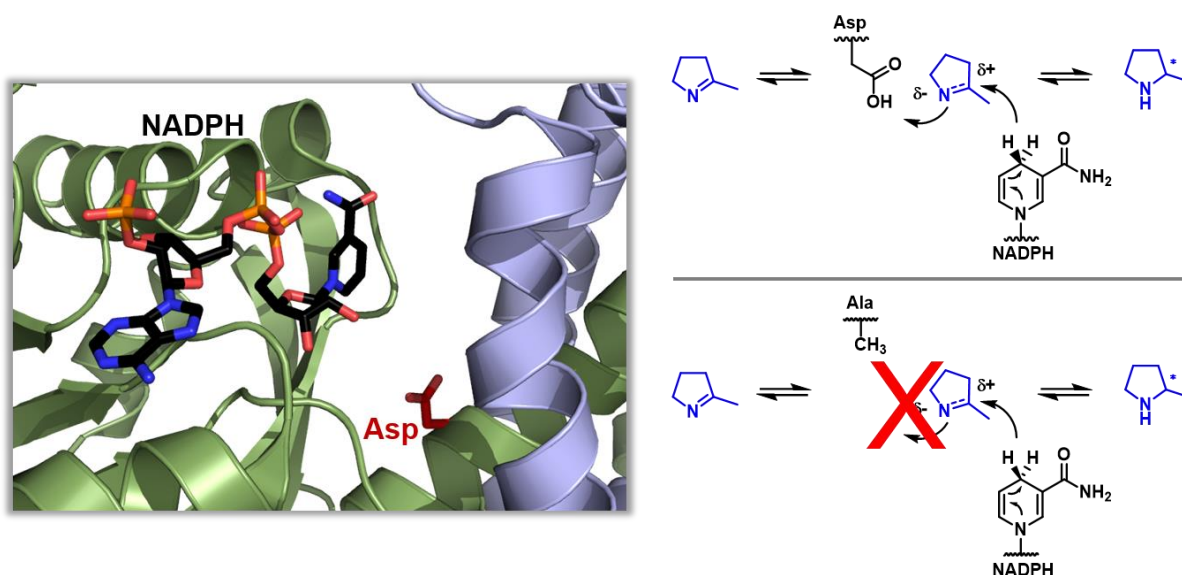


Figure 4: Left: Active site cleft of *R*-IRED-*Sk* with the NADPH cofactor in black and the proposed catalytic Asp residue in red (pdb code *R*-IRED-*Sk*: 3zgy¹⁴²). Subunit A of the IRED is shown in green and subunit B in blue. Right: Proposed mechanism for the enzymatic imine reduction by the Asp containing IRED.¹⁴² Protonation of the imine substrate by the active site amino acids to an iminium ion is followed by the hydride transfer from NADPH.¹⁴² This mechanism was suggested by Rodríguez-Mata *et al.* for an Asp containing IRED.¹⁴² Replacement of Asp by either Asn or Ala rendered the enzyme inactive (bottom right).¹⁴²

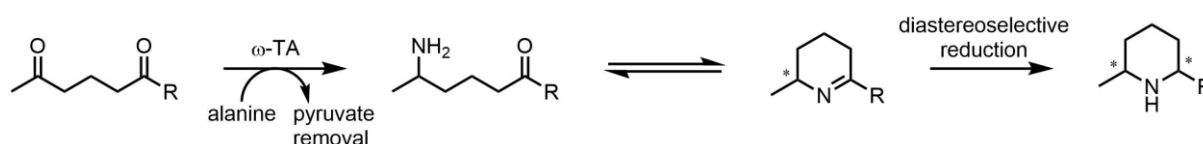
In the initial report on the newly discovered *R*-IRED a small set of imines, ketones and heterocyclic compounds (furanes, imidazoles, thiazoles, pyrimidines and pyrazines) was investigated for reduction, but activity was only found for imine **1**.¹³⁸ Also the substrate spectrum of the *S*-IRED was reported to be narrow and restricted to a few imines.¹³⁹ The very restricted substrate spectrum of the (*S*)-selective enzyme described by Mitsukura *et al.*¹³⁹ was in a following work published 2013 by Leipold *et al.* however revised¹⁴³ and broad activities and very high selectivities demonstrated for this enzyme.^{139,143} The investigated substrates comprised many cyclic imines and iminiums (pyrrolidines, piperidine, isoquinolines and others) and led to the formation of chiral secondary and tertiary amines by using the wild type (wt) enzyme.¹⁴³ The enormous potential for the preparation of chiral amines with IREDs that was suggested by the study of Leipold *et al.*¹⁴³ led to a rapid increase of published new IREDs and applications of them since 2014.^{144–153} A new enzyme from *Streptomyces aurantiacus* was described by the group of Prof. Dr. Müller and its crystal structure solved in cooperation with the group of Prof. Dr. Einsle.¹⁴⁴ In addition, the crystal structure of the (*S*)-selective IRED, which was initially described by Mitsukura *et al.*¹³⁹ was solved and the potential of these IREDs investigated for the reductive amination of ketone substrates.¹⁴⁴ The IREDs proved to be functional for this reaction, however the conversions were very low (from 0.1% to maximum 8.8% with 76% ee).¹⁴⁴ A few weeks later our group published their investigations on the discovery of novel IREDs.¹⁴⁵ By a database analysis it was for the first time shown, that the IRED family is much larger than assumed: hundreds of putative enzymes were identified and by characterization of three selected members, these enzymes were shown to encode for functional IREDs, with much higher activities than the previously described IREDs.¹⁴⁵ In this study also catalytically important residues were identified and verified by site-directed mutagenesis.¹⁴⁵ To not anticipate these

findings, details about this discovery and the characterization of these enzymes, as well as the investigations on their substrate spectrum and the comparison with other IREDs that were published in the last two years during this work was ongoing will be presented and discussed in the following chapters.

1.2.6 The integration of IREDs in cascade reactions to prepare chiral amines

A first publication of a reaction cascade that included the use of an IRED to prepare chiral amines was published during the writing of this thesis.¹⁵³ In this work, performed in the group of Turner, an IRED was combined with the (*R*)-selective amine oxidase 6-HDNO¹²⁰ for deracemizations.¹⁵³ As in contrast to the nonselective reduction with ammonia borane the reduction with the IRED is selective, higher enantiomeric excess values can be approached in fewer cycles of the deracemization procedure (see also Scheme 9 for the deracemization with a nonselective reducing agent).¹⁵³ Likewise also the use of enantiocomplementary IREDs and the (*S*)-selective MAO-N might be envisioned.

In addition one application of ω -TAs is described that led to chiral saturated heterocyclic amines over an imine intermediate. This noticeable exception, in which the use of a ω -TAs resulted in secondary amines was published by the group of Kroutil.¹⁵⁴ In their work, the monoamination of a diketone triggered its spontaneous cyclization to a cyclic imine.¹⁵⁴ The use of different ω -TAs in combination with a diastereoselective chemical reduction enabled the access to all possible diastereomers of the generated 2,6-disubstituted piperidine, in this way representing a chemical/biological reaction cascade (Scheme 10).^{154–156} This reaction cascade was later extended by O'Reilly *et al.* and an enzymatic cascade combining ω -TAs and MAO-N for deracemization with a nonselective reducing agent set up,¹²² however the reducing agent might now also be substituted by an IRED.



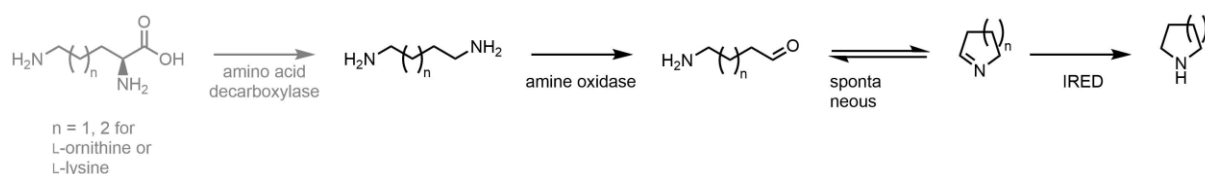
R = propyl, isopropyl, phenyl, etc.

Scheme 10: Chemical/biological reaction cascade to generate secondary amines with ω -TAs.¹⁵⁴ The monoamination of a diketone triggers the spontaneous cyclization to the piperidine ring which is chemically reduced.¹⁵⁴ Most ω -TAs showed high specificity for the sterically less demanding ketone and depending on their selectivity the (*R*)- or (*S*)-aminoketone was accessed.¹⁵⁴ By the combination with different chemical reducing agents all diastereomers could be obtained.^{154,155}

1.2.7 The enzymatic generation of cyclic imines by polyamine oxidases and their combination with IREDs

The use of the (*S*)-selective MAO-N and the engineering of (*R*)-selective amine oxidases to generate cyclic imines for deracemizations was already described above and another path to such compounds was shown with ω -TAs that were applied for the monoamination of diketones.^{2,118–120,122,154,155} In addition, the enzymatic generation of such imines might also be accomplished by polyamine oxidases with substrates that already contain the required number of carbon atoms and nitrogen. The selective oxidation of one of the amine moieties should then trigger their spontaneous cyclization as it was

described in the ω -TA procedure.^{122,154,155} With these compounds also a renewable resource of the substrates is accessible.^{157,158} Polyamine oxidases are yet in contrast to MAO-N not thoroughly investigated for biocatalytic purposes. In nature, these enzymes are involved in the degradation of polyamines and amino acids into intermediates of the tricarboxylic acid cycle^{159–161} and the described applications of them mainly include their use as biosensors for biogenic amines to monitor food and beverage freshness.^{162–164} The two best characterized members of this enzyme family are the putrescine oxidases from *Kocuria rosea*^{165–169} and *Rhodococcus erythropolis*.^{161,170–173} While the first enzyme was described already decades ago, the latter one was identified and characterized in 2008.¹⁶¹ It is well suited for heterologous expression in *E. coli*,¹⁶¹ shows high activity with its natural substrate 1,4-diaminobutane and activity was also reported with a range of related natural polyamines.¹⁶¹ In further works also the nature of the flavin binding was investigated^{170,171} and the crystal structure of the enzyme solved.¹⁷¹ Due to this full characterization and its high activity with the natural substrate,¹⁶¹ the putrescine oxidase from *Rhodococcus erythropolis* (PuO-Re) represents a promising candidate for a combination with IREDs to allow the *de novo* production of (chiral) saturated heterocyclic amines from renewable resources (Scheme 11).



Scheme 11: Enzymatic generation of cyclic imines by the regioselective oxidation of a polyamine with an amine oxidase. The products of these enzymatic reactions spontaneously cyclize to cyclic imines and in aqueous systems exist in an equilibrium of both forms, however compared to ω -TAs the amine oxidase performs a practically irreversible reaction to the aminoaldehyde. The reduction to the saturated heterocyclic compound could now be performed by an IRED.

1.3 Aims of this work and experimental strategy

Considering the current limitations with respect to the biocatalytic preparation of chiral secondary and tertiary amines, IREDs are regarded as a promising extension to the available methods. However as these enzymes were just recently described for the first time only very few enzymes are known and many of their properties remain to be discovered. This work will therefore focus on the identification and characterization of novel IREDs.

For the identification of the novel IREDs a database analysis will be performed in cooperation with the bioinformatics group of the Institute of Technical Biochemistry. With the acquired data this novel protein family will have to be analyzed on a sequence level to establish guidelines for the definition and classification of IREDs. For the experimental confirmation of these analyses, three putative IREDs will be selected and characterized with respect to parameters that might enable their use as biocatalysts. The pH-activity profiles of these enzymes, their thermostabilities and the activities in presence of organic solvents were chosen for investigation. To be able to compare the new enzymes to the three (at this time) in literature described IREDs, kinetic constants with a set of model substrates will be determined. As such analyses require purified proteins, the expression and purification of these new enzymes will have to be established in advance.

Having the enzymes available and assessed their biochemical properties, potential applications to generate chiral amines by the use of IREDs will be approached. The substrate spectrum and the scope of reactions that can be catalyzed by the IREDs will be investigated in whole cell biotransformations and with purified enzymes using a panel of cyclic and exocyclic imines and carbonyl substrates. The targeted reactions include the reduction of the preformed imines to (chiral) amines and the direct reductive amination of the carbonyl compounds with a variety of different amines.

Finally, the use of IREDs in multistep biocatalysis was envisioned. Such a reaction cascade could enable the *de novo* synthesis of *N*-heterocyclic compounds from renewable resources. The second enzyme required for the reaction cascade, a putrescine oxidase, was known from literature, but described to display a narrow substrate spectrum. To approach a broad applicability in terms of the generated *N*-heterocyclic compounds, protein engineering strategies by combining random methods (epPCR) and semi-rational strategies (site-saturation mutagenesis) were pursued to enhance the activity of the enzyme for unnatural polyamine substrates. The generated mutants were to be screened with previously established HTS systems and characterized to verify crucial positions that influence oxidation activity. Finally, this putrescine oxidase and the IREDs were to be combined and *in vitro* and an *in vivo* systems were investigated for their formation of *N*-heterocyclic compounds by the consecutive transformation of polyamines by both enzymes.

2 METHODS AND MATERIALS

2.1 Materials

2.1.1 Chemicals

Except otherwise noted, all solvents, buffer components and chemicals were obtained from Sigma-Aldrich and Fluka (Steinheim, Germany), Carl Roth GmbH (Karlsruhe, Germany), Acros Organics (Geel, Belgium), VWR (Darmstadt, Germany), Alfa Aesar (Karlsruhe, Germany), TCI Deutschland GmbH (Eschborn, Germany) and abcr GmbH (Karlsruhe, Germany).

Polyamine substrates Bis(3-aminopropyl)amine **35**, 3-(3-Aminopropoxy)propylamine **37** and 2-(2-Aminoethoxy)ethylamine **38** were kindly provided by Orion Pharma (Espoo, Finland). Acetophenone was sourced from Riedel-de-Haën AG (Seelze, Germany) and acrylamide from Serva (Heidelberg, Germany). Nylon membranes for solid phase HTS were from GE Healthcare (Hybond-N; GE-Healthcare Europe GmbH; Freiburg, Germany) or Carl Roth GmbH (Roti®-Nylon 0.2; Karlsruhe, Germany) and BugBuster lysis reagent from MerckMillipore (Merck KGaA, Darmstadt, Germany). DNA and Protein Markers for agarose and SDS gel electrophoresis were from peqlab (peqlab Biotechnologie GmbH, Erlangen, Germany) or Fermentas (Thermo Fisher Scientific Germany, Braunschweig, Germany).

2.1.2 Enzymes

Horseradish Peroxidase was obtained from AppliChem (Darmstadt, Germany), Catalase, DNase I and lysozyme were sourced from Sigma Aldrich (Steinheim, Germany), glucose-6-phosphate dehydrogenase from *Leuconostoc mesenteroides* (NH₄)₂SO₄ precipitated was purchased from Roche Diagnostics (Mannheim, Germany) and lyophilized from Alfa Aesar (Karlsruhe, Germany). Restriction enzymes, T4 DNA ligase and alkaline phosphatase were from Thermo Fisher Scientific (Braunschweig, Germany), *Pfu* polymerase from GeneOn (Ludwigshafen, Germany) and enzymes for Gibson Assembly from NEB (Frankfurt am Main, Germany).

2.1.3 Kits

Kits for purification of PCR products, gel extraction of DNA and minipreparations were from Zymo Research (Freiburg, Germany). The BCA Assay Kit for determination of protein concentrations was from Pierce (Thermo Fisher Scientific Germany, Braunschweig, Germany).

2.1.4 DNA Sequences

The genes for the IREDs contained an N-terminal His₆ tag and a 3CV protease cleavage site, resulting in 21 additional amino acids. The synthesized DNA also contained additional homologous regions and a ribosome binding site (AGGAGG) for the plasmid pBAD33, allowing the DNA to be used for Gibson Assembly with this plasmid. In case of the putrescine oxidase the synthetic DNA also contained a

2 METHODS AND MATERIALS

ribosome binding site (the same as above) and restriction enzyme recognition sites for cloning in pBAD18 plasmid DNA. Further the start codon was modified from Val (GTG) to Met (ATG) and an Ala as second amino acid inserted, resulting in an additional *Nco*I restriction endonuclease site (CCATGG). Gene synthesis was done by GeneArt™ (Life Technologies GmbH, Darmstadt, Germany) and DNA sequencing was performed by GATC Biotech (Konstanz, Germany).

Table 1: Synthesized genes and their corresponding GenBank entries. Genes encoding for IREDs were synthesized in codon optimized form for expression in *E. coli*. The gene encoding for PuO-*Re* was not codon optimized.

Name	abbreviation	GenBank entry	codon optimized
(<i>R</i>)- imine reductase <i>Streptosporangium roseum</i> DSM 43021	<i>R</i> -IRED- <i>Sr</i>	YP_003336672.1	yes
(<i>R</i>)- imine reductase <i>Streptomyces turgidiscabies</i>	<i>R</i> -IRED- <i>St</i>	WP_006374254.1	yes
(<i>S</i>)- imine reductase <i>Paenibacillus elgii</i>	<i>S</i> -IRED- <i>Pe</i>	WP_010497949.1	yes
Putrescine oxidase <i>Rhodococcus erythropolis</i> NCIMB 11540	PuO- <i>Re</i>	EU240877.1	no

The introduced amino acid sequence to encode for the His₆-tag and the 3CV protease cleavage site in case of the IREDs was (new Met start codon in green and His₆ tag in blue):

“MGSSHHHHHHSSGLEVLFGQPA“ encoded by the following DNA sequence:

“ATGGGTAGCAGCCATCATCACCACCATCATAGCAGCGGTCTGGAAGTTCTGTTTCAGGGTCCGGCA”

Sequence of the synthetic DNA for *R*-IRED-*St* (Met start codon in green, His₆ tag in blue and stop codons in red):

CTACTGTTTCTCCATACCCGTTTTTTTTGGGCTAGCGAATTCGAGCTCTTTTTTGGTACCAGGAGGA
TTACATATGGGTAGCAGCCATCATCATCACCACCATCATAGCAGCGGTCTGGAAGTTCTGTTTCAGGG
TCCGGCAGGCGATAATCATACCAGCGTTAGCGTTATTGGTCTGGGTCTGATGGGTCAGGCACTG
GCAGCAGCATTCTGAAAGCAGGTCATGCAACCACCGTTTGGAAATCGTAGCGCAGATAAAGCAG
ATGGTGTGTTGCAAATGGTGCAGTTCTGGCAGCCGCACCGGCAGATGCAGTTGCAGCAAGCGA
TCTGGTTGTTGTTTGTGTTAGCACCTATGATGTTGTGCATGATGTTATTGGTAGCCTGGGTGATGC
ACTGCGTGGTAAAACCGTTGTTAATCTGACCAGCGGTAGCAGCGAACAGGCAAGTGCAGACCGCA
GAATGGGCAGAAAAAATGGTGCCCGTTATCTGGATGGTGCCATTATGATTACCCCTCCGGGTAT
TGGCACCGAAACCGCAGTGCTGTTTTATGCCGGTGATCAGGCAGTTTTTATGATGCACATGAACCGG
TGCTGAAACTGCTGGGTGCAGGCACCACCTATCTGGGCACCGATCATGGTAAACCGGCACTGTT
TGATGTGAGCCTGCTGGGCCTGATGTGGGGTGCAGTGAATAGCTTTCTGCATGGTGTGCAATTG
TTGAAACCGGTGGTGTAAAGCACAGGATTTTCTGCCGTGGGCTCATATGTGGCTGGATGCCATT
AAAATGTTTACCGCAGATTATGCAGCACAGATTGATGCGGGTATGAAAAATTTCCGGCAAATGA
TGCAACCCTGAAACCCATCTGGGTGCGCTGAAACATCTGGTTGAAGAAAGCGAAGCACTGGGT
GTTGATACCGAACTGCCGAAATATAGCGAAGCCCTGATGGAAGGTATTATTGCACAGGGTCATGC
CAAAAATTCATATGCCAGCGTTGTTAAAGCCTATCGTCGTCCGGCACGTTAATAATCTAGACTGCA
GAAGCTTGGCTGTTTTGGCGGATGAGAGAAGATTTTCAGCCTGATACAGA

Native protein sequence of *R*-IRED-*St*

MGDNHTSVSVIGLGLMGQALAAFLKAGHATTVWNRSADKADGVVANGAVLAAAPADAVAASDLVV
VCVSTYDVVHVDVIGSLGDALRGKTVVNLTSGSSEQARQTAEWAENKNGARYLDGAIMITPPGIGTETAV
LFYAGDQAVFDAHEPVLKLLGAGTTLGTDHKGKPALFDVSLGLMWGALNSFLHGVAIIVETGGVKAQ
DFLPWAHMLDLAIKMFADYAAQIDAGDEKFPANDATLETHLGALKHLVEESEALGVDELTPKYSEAL
MEGIIAQGHAKNSYASVVKAYRRPAR

Sequence of the synthetic DNA for *R*-IRED-*Sr* (Met start codon in green, His₆ tag in blue and stop codons in red):

```
CTACTGTTTCTCCATACCCGTTTTTTTTGGGCTAGCGAATTCGAGCTCTTTTTTGGTACCAGGAGGA
TTACATATGGGTAGCAGCCATCATCATCACCATCATAGCAGCGGTCTGGAAGTTCTGTTTCAGGG
TCCGGCACGTGATACCGATGTTACCGTTCTGGGTCTGGGCCTGATGGGTTCAGGCACTGGCAGGC
GCATTTCTGAAAGATGGTCATGCAACCACCGTTTGGAAATCGTAGCGAAGGTAAAGCAGGTCAGCT
GGCAGAACAGGGTGCAGTTCTGGCAAGCAGCGCACGTGATGCAGCAGAAGCAAGTCCGCTGGT
TGTTGTTTGTGTTAGCGATCATGCAGCAGTTCGTGCCGTTCTGGATCCGCTGGGTGATGTTCTGG
CAGGTCGTGTTCTGGTTAATCTGACCAGCGGCACCAGCGAACAGGCACGTGCAACCGCAGAATG
GGCAGCAGAACGTGGTATTACCTATCTGGATGGTGAATTATGGCAATTCGCGAGGTTGTGGGC
ACCGCAGATGCATTTCTGCTGTATAGCGGTCCGGAAGCAGCATATGAAGCACATGAACCGACCC
TCCGTAGCCTGGGTGCAGGCACCACATATCTGGGTGCCGATCATGGTCTGAGCAGCCTGTATGA
TGTTGCACTGCTGGGTATTATGTGGGGCACCCCTGAATAGCTTTCTGCATGGTGCAGCCCTGCTG
GGCACAGCAAAGTTGAAGCCACCACCTTTGCACCGTTTCAAATCGTTGGATTGAAGCAGTTAC
CGGTTTTGTTAGCGCATATGCCGGTTCAGGTTGATCAGGGTGCATATCCGGCACTGGATGCAACC
ATTGATACCCATGTTGCAACCGTTGATCATCTGATTCATGAAAGCGAAGCAGCCGGTGTAAATAC
CGAACTGCCTCGTCTGGTTCGTACCCTGGCAGATCGTGCCCTGGCTGGCGGTTCAGGGTGGTCT
GGGTTATGCAGCAATGATTGAACAGTTTCGTAGCCCGAGCGCATATAATACTAGACTGCAGAAGC
TTGGCTGTTTTGGCGGATGAGAGAAGATTTTCAGCCTGATACAGA
```

Native protein sequence of *R*-IRED-*Sr*:

```
MRD TDVTVLGLGLMGQALAGAF LKDG HATTVWNRSE GKAGQLAEQ GAVLASSARDAEASPLVVVC
VSDHAAVRAVL DPLGDVLAGRVLVNL TSGTSEQARATAEWAER GITYLDGAIMAIPQVVTADAFLL
YSGPEAA YE AHEPTLRSLGAGT TYLGADHGLSSLYDVALLGIMWGLNSFLHGAALLGTAKVEATTF A
PFANRWIEAVTGFVSAYAGQVDQGAYPALDATIDTHVATVDHLIHESEAAGVNTELPRLVRTLADRAL
AGGQGG LGYAAMIEQFRSPSA
```

Sequence of the synthetic DNA for *S*-IRED-*Pe* (Met start codon in green, His₆ tag in blue and stop codons in red):

```
CTACTGTTTCTCCATACCCGTTTTTTTTGGGCTAGCGAATTCGAGCTCTTTTTTGGTACCAGGAGGA
TTACATATGGGTAGCAGCCATCATCATCACCATCATAGCAGCGGTCTGGAAGTTCTGTTTCAGGG
TCCGGCAAATAGCAGCAATCCGAAAGATAACATTAGCGTTGGTAGCGCAAGCACCGCAACCAATC
GTAAAAGCGTTACCGTTATGGGTCTGGGTCCGATGGGTTCAGGCAATGGCAGGCGTTTTTCTGGA
AAGCGGTTATGAAGTTACCGTTTGAATCGTACCGCAAGCAAAGCAGATGAACTGGTTGCAAAAAG
GTGCAATTCGTGCCAGCACCGTTGATGAAGCACTGGCAGCAAACGAACTGGTTATTCTGAGCCT
GACCGATTATGATGCAATGTATGCAATTCTGGAACCGAGCAGCGCAAATCTGAGCGGTAAGTTC
TGGTGAATCTGAGCAGCGATACACCGGAAAAAGTTCGTGAAGCAGCAAATGGCTGGCAGATCG
TGGTGCACGTCATGTTACCGGTGGTGTTCAGGTTCCGCCTAGCGGTATTGGTAAACCGGAAAGC
TATACCTATTATAGCGGTCCGCGTGAAGTTTTTGAAGCACATCGTGAAAGCCTGGAATTCTGAC
CGGTACAGATTATCGTGGTGAAGATCCGGGTCTGGCAATGCTGTATTATCAGATTTCAGATGGATA
TCTTCTGGACCAGTATGCTGAGCTATCTGCATGCACTGGCCGTTGCCAAAGCAAATGGTATTACC
GCAAACAGTTTTCTGCCGTATGCAAGCGCAACCCCTGAGCAGCCTGCCGAGTTTGTGAATTCTA
TACACCGCGTCTGGATGAAGGTAACATCCGGGTGATGTTGATCGTCTGGCCATGGGCCTGGCA
AGCGTTGAACATATTGTTTCATACCACCGAAGATGCAGGTATTGATACCACCCCTGCCTGCAGCAGT
TCTGAAATCTTTAAACGTGGCATGGAATAATGGTCATGCCGGTGTAGCTTTACCAGCCTGATTG
AAATTTTCAAATCCGGTGCGCAGCTATAATACTAGACTGCAGAAGCTTGGCTGTTTTGGCGGA
TGAGAGAAGATTTTCAGCCTGATACAGA
```

Native protein sequence of *S*-IRED-*Pe*:

```
MNSSNPKDNISVGSASTATNRKSVTVMGLGPMGQAMAGVFLESGYEVTVWNRRTASKADELVAKGAI
RASTVDEALANELVILSLTDYDAMYAILEPSSANLSGKVLVNLSSDTPEKVVREAAKWLADRGRARHVT
GGVQVPPSGIGKPESYTYYS GPREVFEAHRESLEILTGTDIRGEDPGLAMLYYQIQMDIFWTSMLSYL
HALAVAKANGITAKQFLPYASATLSSLPQFVEFYTPRLDEGKHPGDVDRLAMGLASVEHIVHTTEDAGI
DITLPAAVLEIFKRMENGHAGDSFTSLIEIFKNPVR
```


2 METHODS AND MATERIALS

Sequence of the synthetic DNA for PuO-*Re* (Met start codon in green, stop codons in red and introduced *Nco*I restriction site underlined):

```
CACTATAGGGCGAATTGAAGGAAGGCCGTCAAGGCCGCATGAATTCTTTTTTGGGCTAGCAGGA
GGATTAACCATGGGCCCTACTCTCCAGAGAGATGTTGCAATCGTCGGCGCCGGCCCTCTGGCC
TGGCAGCGGCAACCGCGCTGCGCAAGGCCGGCTTGTCCGTCGCCGTGATCGAAGCACGCGATC
GTGTCCGAGGCCGCACGTGGACCGACACCATCGACGGCGCAGTCTGGAGATCGGCGGCCAGT
GGGTCTCCCCGACCAGACTGCTCTGATCTCCTTGCTCGACGAACCTCGGCCTGAAGACTTTTCA
GCGCTACCGCGAGGGGCGAGTCCGTCTACATCTCGTCAGCAGGCGAGCGGACTCGATACACGGG
CGATTCCTTCCCCACGAACGAGACCACCAAGAAGGAGATGGACCGTCTCATCGACGAGATGGAC
GATCTCGCAGCGCAGATCGGCGCCGAGGAGCCGTGGGCACATCCCCTCGCCCGGATCTCGAC
ACAGTCTCCTTCAAGCAGTGGGTGATCAATCAGTCCGACGACGCCGAGGCCCGTGACAACATCG
GCCTCTTCATCGGGGTGGTATGCTCACCAAGCCCGCCACTCGTTCTCCGCCCTACAGGCCGT
ACTCATGGCCGCTTCCGCGAGGCTCGTTCTCCACCTCGTGGACGAGGACTTCATCCTCGACAAG
CGAGTGATCGGCGGAATGCAGCAGGTATCTATCCGCATGGCGGAGGCCCTCGGTGACGACGTC
TTCCTCAACGCACCCGTGCGTACGGTGAAGTGAACGAATCCGGTGCAACGGTGTGGCGGAC
GGCGACATTCGCGTCGAGGCAAGCCGAGTGATCCTGGCCGTACCACCCAACCTCTACTCCCGGA
TCTCCTACGATCCCCCGCTGCCGCGTCTGTCAGCACCAGATGCATCAGCATCAGTCTCTCGGCCT
CGTCATCAAGGTGCACGCCGTGTACGAGACGCCTTTCTGGCGCGAAGACGGCCTCTCCGGCAC
CGGCTTCCGCGCGTCCGAGGTAGTGCAGGAGGTGTACGACAACACCAACCACGAGGACGATCG
CGGCACCCTGGTCGCTTTTGTCTCCGACGAGAAGGCCGACGCGATGTTTCGAGCTTTCCGCCGAG
GAGCGTAAGGCCACGATTCTGGCCTCACTCGCCCGCTACCTGGGCCCGAAGGCCGAAGAGCCG
GTTGTGTACTACGAATCCGACTGGGGCTCGGAGGAATGGACCCGCGGTGCGTACGCGGCGAGC
TTCGATCTCGGCGGCCTGCACCGCTACGGCGCGGATTCCCGCACGCCCGTCGGACCGATCCAC
TTCTCGTGCTCCGACATCGCAGCCGAGGGATACCAGCACGTGGACGGTGCCGTTCCGGATGGGT
CAGCGCACCGCCGCCGACATCATCGCCGCGAGCAAGGCCTGATAACCCGGGTCTAGAGTCCGAC
AAGCTTCTGGGCCTCATGGGCCTTCTTTCCTACTGCCCGCTTTCCAG
```

Native protein sequence of PuO-*Re*:

```
VPTLQRDVAIVGAGPSGLAAATALRKAGLSVAVIEARDRVGGRTWTDITDGA VLEIGGQWVSPDQ TAL
ISLLDELGLKTFERYREGESVYISSAGERTRYTGDSFPTNETTKEMDRLIDEMDDLAAQIGAE EEPWAH
PLARDLDTVSFKQWLINQSDDAEARDNIGLFIAGGMLTKPAHSFSALQAVLMAASAGSFSHLVDEDFIL
DKRVIGGMQQVSIRMAEALGDDVFLNAPVRTVKWNESGATVLADGDIRVEASRVILAVPPNLYSRISY
DPPLPRRQHQMHQHQSLGLVIKVHAVYETPFWREDGLSGTGFGASEVQEVYDNTNHEDDRGTLVA
FVSDEKADAMFELSAEERKATILASLARYLGPKEEPPVYYESDWGSEEWTRGAYAASF DLGGLHRY
GADSRTPVGPPIHFSCSDIAAEGYQHVDGAVRMGQR TAADIARSKA
```

2.1.5 Primers

The following primers were used in this work to amplify DNA, generate mutants and for sequencing purposes. All primers were synthesized by metabion International AG (Martinsried, Germany)

Table 2: Summary of primers used in this study. Primers were used for PCR to generate fragments for Gibson Assembly (GA), for (site directed) mutagenesis and for sequencing. The numbering for the mutations corresponds not to the native protein sequence, but starts with the Met start codon of the corresponding expression construct. For example *R*-IRED-*Sr* D191A refers to amino acid number 170 of the native protein sequence.

Primer name	direction	sequence
pBAD_GA	forward	5'-CTACTGTTTCTCCATACCCG-3'
	reverse	5'-CTGTATCAGGCTGAAAATCTTCTC-3'
<i>R</i> -IRED- <i>Sr</i> D191A	forward	5'-GCAGCCTGTATGCTGTTGCACTGCTG-3'
	reverse	5'-CTGTATCAGGCTGAAAATCTTCTC-3'
<i>R</i> -IRED- <i>St</i> D193A	forward	5'-CGGCACTGTTTGCTGTGAGCCTGCTG-3'
	reverse	5'-CAGCAGGCTCACAGCAAACAGTGCCG-3'
<i>S</i> -IRED- <i>Pe</i> Y208D	forward	5'-CTGGCAATGCTGTATGATCAGATTCAGATGG-3'
	reverse	5'-CCATCTGAATCTGATCATACAGCATTGCCAG-3'
pBAD	forward	5'-CCATAAGATTAGCGGATCCTACCTG-3'
	reverse	5'-CACTTCTGAGTTCGGCATGGGG-3'

Table 2: continued.

Primer name	direction	sequence
PuO- <i>Re</i> _E324D	forward	5'-GTCCGAGGTAGTGCAGGACGTGTACGACAACACCAACC-3'
	reverse	5'-GGTTGGTGTTCGTACACGTCTGCACTACCTCGGAC-3'
PuO- <i>Re</i> _L168F169	forward	5'-GAGGCCCGTGACAACATCGGCNNKNNKATCGCGGGTGGTATGCTACC-3'
	reverse	5'-GGTGAGCATACCACCCGCGATMNNMNNNGCCGATGTTGTACGGGCCTC-3'
PuO- <i>Re</i> _V201E203	forward	5'-GGCTCGTTCTCCACCTCDNKGACNNKGACTTCATCCTCGACAAG-3'
	reverse	5'-CTTGTGCGAGGATGAAGTCMNNGTGCMNHGAGGTGGGAGAACGAGCC-3'
PuO- <i>Re</i> _M174	forward	5'-CTCTTCATCGCGGGTGGTNHKCTCACCAAGCCCGCCCAC-3'
	reverse	5'-GTGGCGGGCTTGGTGAGMDNACCACCCGCGATGAAGAG-3'
PuO- <i>Re</i> _L207	forward	5'-GTGGACGAGGACTTCATCNYGACAAGCGAGTGATCGGC-3'
	reverse	5'-GCCGATCACTCGCTTGTCTRNNGATGAAGTCCTCGTCCAC-3'
PuO- <i>Re</i> _D104	forward	5'-CGGACTCGATACAGGGCANNKTCCTTCCCCACGAACGAG-3'
	reverse	5'-CTCGTTCTGGGGGAAGGAMNNGCCCGTGTATCGAGTCCG-3'
PuO- <i>Re</i> _SE_ libraryA ^[a]	forward	5'-GCAGGCTCGTTCTCCACNDTGTGGACNHKGACTTCNDTCTCGACAAGCGAGTGATC-3'
	reverse	5'-GATCACTCGCTTGTGCGAGAHNGAAGTCMDNGTCCCAHNGTGGGAGAACGAGCCTGC-3'
PuO- <i>Re</i> _SE_ libraryB ^[a]	forward	5'-GGCTCGTTCTCCACCTCNDTGTGACGAGNDTTTCATCCTCGACAAGCGA-3'
	reverse	5'-TCGCTTGTGCGAGGATGAAAHNCTCGTCAHNGAGGTGGGAGAACGAGCC-3'
PuO- <i>Re</i> _SE_ libraryC ^[a]	forward	5'-CTCGTTCTCCACCTCGTGNDTGAGGACNDTATCCTCGACAAGCGAGTG-3'
	reverse	5'-CACTCGCTTGTGCGAGGATAHNGTCTCAHNCACGAGGTGGGAGAACGAG-3'

^[a]: The libraries were generated and screened by solid phase assay but no further analysis was done during this project. The lysate screening, purification and characterization of these mutants is ongoing work of another PhD project at the Institute of Technical Biochemistry.

2.1.6 Plasmids

Plasmids used in this study were pBAD18 (pBR322 ori, ampicillin resistance, arabinose inducible expression) and pBAD33 (pACYC184 ori, chloramphenicol resistance, arabinose inducible expression).¹⁷⁴ Maps for pBAD33 and pBAD18 are shown in Figure 5 and Figure 6.

Table 3: Plasmids used and generated in this study. The numbering for the mutations corresponds not to the native protein sequence, but starts with the Met start codon of the corresponding expression construct. For example *R*-IRED-*Sr* D191A refers to amino acid number 170 of the native protein sequence.

plasmid	insert	ITB #	source/generated by
pBAD33	-		Dr. Sandra Facey, ITB Stuttgart
pBAD18	-		Dr. Sandra Facey, ITB Stuttgart
pBAD33	<i>R</i> -IRED- <i>Sr</i>	pITB1236	this work
pBAD33	<i>R</i> -IRED- <i>St</i>	pITB1237	this work
pBAD33	<i>S</i> -IRED- <i>Pe</i>	pITB1238	this work
pBAD33	<i>R</i> -IRED- <i>Sr</i> D191A	pITB1239	this work
pBAD33	<i>R</i> -IRED- <i>St</i> D193A	pITB1240	this work
pBAD33	<i>S</i> -IRED- <i>Pe</i> Y208A	pITB1241	this work
pBAD18	<i>PuO-<i>Re</i></i>	pITB1242	this work
pBAD18	<i>PuO-<i>Re</i></i> E324D	pITB1243	this work
pBAD18	<i>PuO-<i>Re</i></i> E203G	pITB1244	epPCR
pBAD18	<i>PuO-<i>Re</i></i> I154V E203V	-	epPCR
pBAD18	<i>PuO-<i>Re</i></i> E203S	pITB1245	saturation mutagenesis
pBAD18	<i>PuO-<i>Re</i></i> V201S E203G	pITB1246	saturation mutagenesis
pBAD18	<i>PuO-<i>Re</i></i> L207V	pITB1247	saturation mutagenesis
pBAD18	<i>PuO-<i>Re</i></i> V201A E203P	pITB1248	saturation mutagenesis
pBAD18	<i>PuO-<i>Re</i></i> D104L	pITB1249	saturation mutagenesis
pBAD18	<i>PuO-<i>Re</i></i> L168S F169Q	pITB1250	saturation mutagenesis
pBAD18	<i>PuO-<i>Re</i></i> V201A E203G	pITB1251	saturation mutagenesis
pBAD18	<i>PuO-<i>Re</i></i> A24T V201A E203M	pITB1252	saturation mutagenesis

2 METHODS AND MATERIALS

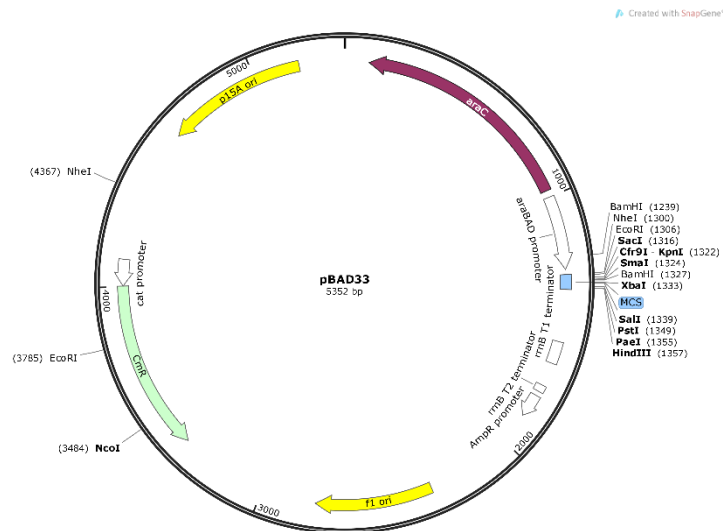


Figure 5: Vector map of pBAD33. The map was generated with Snapgene.



Figure 6: Vector map of pBAD18. The map was generated with Snapgene.

2.1.7 *E. coli* strains

The following *E. coli* strains were used in this work:

E. coli XL1-Blue for cloning and molecular biological applications (plasmid production, etc.) and *E. coli* JW5510¹⁷⁵ for protein expression and biotransformations.

Genotype *E. coli* XL1-Blue:

endA1 gyrA96(nal^R) thi-1 recA1 glnV44 relA1 hsdR17(r_K m_K⁺) lac [F' proAB⁺ lac^M Δ(lacZ)M15::Tn10]

Genotype *E. coli* JW5510:

F⁻ Δ(araD-araB)567 ΔlacZ4787(::rrnB-3) λ⁻ ΔyggJG763::kan rph-1 Δ(rhaD-rhaB)568 hsdR514

2.2 Cultivation media and growth of bacterial cells

For growth of bacteria lysogeny broth (LB) medium (yeast extract 5 g/l, tryptone 10 g/l and NaCl 10 g/l) or terrific broth (TB) medium (tryptone 12 g/l, yeast extract 24 g/l, glycerol 4 ml/l and 1 x TB buffer: 72 mM K₂HPO₄ and 17 mM KH₂PO₄) was used.

To prepare competent cells and after transformations cells were cultivated in SOC medium (yeast extract 5 g/l, tryptone 20 g/l, NaCl 0.584 g/l, KCl 0.186 g/l, MgSO₄ 20 mM, glucose 20 mM) at 37 °C and 180 rpm.

LB agar plates contained 1.5% agar and the respective antibiotics.

Cells were generally grown at 37 °C and 180 rpm.

Protein expression was always performed in TB medium and for protein expression the temperature was lowered to 25 °C. Cells were grown in Infors HT Multitron Shakers (Infors AG, Bottmingen, Switzerland).

For long term storage of *E. coli* cultures glycerol stocks were prepared and stored at - 80 °C. Glycerol stocks were generated by the addition of final 15% sterile glycerol to LB grown overnight cultures.

The following antibiotics and inducers were used:

Ampicillin at a final concentration of 100 µg/ml and chloramphenicol (dissolved in EtOH) at a final concentration of 34 µg/ml. L-arabinose was used at a final concentration of 0.02% for induction of protein expression

2.3 Preparation of competent cells and transformation of *E. coli*

Chemically competent cells of *E. coli* for transformations were prepared according to the RbCl method as described in literature.¹⁷⁶

For screening of PuO-*Re* libraries electrocompetent cells were used. Preparation of them was done as described in literature.¹⁷⁷

E. coli cells that were used for the preparation of competent cells were grown in SOC media as described above.

Transformation of chemically competent cells was done by heat shock at 42 °C for 30 s after incubating cells and DNA for 30 min on ice. Afterwards cells were incubated with SOC media for 1 h at 37 °C and 180 rpm.

For the transformation of mutant libraries in electrocompetent cells they were mixed with the salt free DNA in a previously chilled electroporation cuvette with 0.2 cm electrode gap (Bio-Rad Laboratories GmbH, Munich, Germany). Electroporation was then done with 2 kV in a GenePulser from Bio-Rad (Bio-Rad Laboratories GmbH, Munich, Germany). After the transformation the cells were immediately

recovered in 1 ml pre-warmed SOC medium and grown for 20 min at 37 °C and 180 rpm. After this time cells were plated on nylon membranes for screening. Nylon membranes were previously placed on LB-Amp-Ara plates and pre-warmed to 25 °C. In preliminary tests the transformation efficiency and plating volume was estimated to obtain ~ 1500 colonies per membrane.

2.4 PCR for amplification of DNA

Standard PCR protocols were used for the amplification of the DNA obtained from GeneArt™ with the synthetic DNA encoding for the IREDs. Due to its high GC content (~ 65%) touchdown PCR was used for the amplification of the putrescine oxidase gene.¹⁷⁸

Successful amplification of the targets was verified by illumination of the peqGREEN (peqlab Biotechnologie GmbH, Erlangen, Germany) stained DNA with UV light after agarose gel electrophoresis. After PCR the amplification products were purified with the PCR purification kit from ZymoResearch (Freiburg, Germany).

2.5 Restriction enzyme based gene cloning

The synthetic gene encoding for PuO-*Re* was amplified by PCR, purified and afterwards digested with *EcoRI* and *HindIII* for 2 h. pBAD18 plasmid DNA was obtained by minipreparation from XL1-Blue cells and also digested with *EcoRI* and *HindIII* for 4 h. The digested plasmid DNA was dephosphorylated with FastAP (alkaline phosphatase) for 1 h and purified by agarose gel electrophoresis.

The PuO-*Re* insert DNA and the digested plasmid DNA were mixed in a ratio of 5:1 and ligated with T4 DNA ligase overnight at 18 °C. Next day, the ligase was heat inactivated and 2.5 µl of the ligation mixture transformed in chemically competent *E. coli* XL1-Blue cells. Cells that grew overnight were used to inoculate fresh cultures for minipreparations to confirm the correct ligation by DNA sequencing.

Cloning of the epPCR PuO-*Re* libraries was done as for the wild type gene, but the libraries directly transformed in electrocompetent *E. coli* JW5510 cells for screening.

2.6 Gibson assembly for molecular cloning

Gibson Assembly was used for generation of IRED expression constructs. Therefore the synthetic DNA with the IRED genes (already containing homology regions to the pBAD33 plasmid) was amplified by PCR. The PCR products were purified and mixed with digested and purified pBAD33 plasmid DNA. Isothermal Gibson assembly was performed with an equimolar ratio of the DNA fragments according to literature for 1 h in a PCR machine at 50 °C.^{179–181} After cooling down to 8 °C, assembly products were transformed in chemically competent *E. coli* XL1-Blue cells. Cells were plated on LB-Cm agar plates and grown overnight at 37 °C. Some of these colonies were picked and grown for a minipreparation. DNA Sequencing of the plasmid then confirmed the correct assembly.

2.7 Methods to generate mutants and mutant libraries

2.7.1 Site directed mutagenesis – QuikChange® method

Site directed mutagenesis was performed according to the QuikChange® procedure of the commercial available kit from Agilent.¹⁸²

2.7.2 Random mutagenesis by epPCR

epPCR was performed to generate random mutant libraries of PuO-*Re*. epPCR was done as described by Cirino *et al.*¹⁸³

Conditions for an epPCR were modified compared to usual PCR in a way that an epPCR dNTP mix consisting of final 0.2 mM dGTP, 0.2 mM dATP, 1 mM dCTP and 1 mM dTTP was used. Further, MgCl₂ was increased and MnCl₂ was included (1-10 µM). The DNA template was reduced to 10 ng and the amplification performed with *Taq* polymerase. The setup and the amplification program for the epPCR are shown in Table 4 and Table 5.

Table 4: Setup for the epPCR.

component	volume [µl]	final concentration
<i>Taq</i> Buffer with KCl 10 X	5	1x
ep-dNTP mix 10 X	5	see above
forward Primer 5 µM	3	0.3 µM
revers Primer 5 µM	3	0.3 µM
MgCl ₂ 25 mM	14	7 mM
MnCl ₂ (x µM)	5	variable (1-10 µM)
template DNA	1	0.2 ng/µl
<i>Taq</i> 1 U/µl	5	0.1 U/µl
H ₂ O	9	-
final volume	50	

Table 5: PCR program for the epPCR.

temperature	time	cycles
95 °C	2 min	1
95 °C	15 s	
57 °C	15 s	30
72 °C	2 min	
72 °C	10 min	1
8 °C	∞	1

After the epPCR the template DNA was digested with *DpnI* and the individual libraries (variations in the MnCl₂ concentration) cloned into a TOPO-TA cloning vector (Life Technologies, Darmstadt, Germany) according to the manufacturer's instructions for estimation of the library diversity. After transformation in *E. coli* XL1-Blue, the cells were grown on LB-Kan-XGal (50 µg/ml kanamycin and 20 µg/ml XGal) plates and white colonies picked for sequencing. To estimate the mutation load from each library 10 randomly picked colonies were sequenced.

Libraries having an average mutation load of about 4 changed nucleotides corresponding to 1-2 amino acid exchanges were used for screening.

For screening, epPCR mutant libraries of PuO-*Re* were cloned with *EcoRI* and *HindIII* into pBAD18 and then transformed in electrocompetent cells of *E. coli* JW5510 (see 2.3) for screening. Library screening was done as described in 2.11.

2.7.3 Site saturation mutagenesis with degenerated codons

Saturation mutagenesis of PuO-*Re* was done with QuikChange style primers containing degenerated codons, but to achieve adequate efficiencies during amplification and transformation a modified Gibson Assembly protocol was used.^{179–181}

PCR was therefore performed with the pBAD sequencing primers and one QuikChange primer, resulting in an exponential amplification of the DNA and incorporation of the degenerated codon. Afterwards the upstream and downstream fragments containing the mutations were assembled with the plasmid backbone (3 fragments, ratio 1:1:1) and the libraries transformed in *E. coli* JW5510 for screening. From one of the grown plates a whole plate resuspension and minipreparation thereof was done for sequencing as library quality control.¹⁸⁴

2.8 Gene expression in shake flasks and deep well plates

Expression of IRED and PuO-*Re* genes was done in the same way, but the antibiotic was different. For cells with PuO-*Re* in pBAD18 ampicillin (100 µg/ml) was used and for pBAD33 with the IRED genes chloramphenicol (34 µg/ml) was used. For the cells with both plasmids that were tested in the reaction cascade, Amp and Cm as antibiotics were used.

Protein production was performed in the arabinose deficient *E. coli* host JW5510. Expression was performed in TB media with antibiotics and the cells were grown after inoculation with the overnight culture at 37 °C and 180 rpm. After about 2.5 h the cells reached an OD₆₀₀ of ~ 0.7 and gene expression was induced with 0.02% L-Arabinose. The cells were shifted to 25 °C and 180 rpm and expression performed overnight.

Next day the cells were harvested by centrifugation at 4 °C and 9000 g for 30 min (centrifuge Avanti J 26S XP, Beckman Coulter, Krefeld, Germany; rotor JLA 8.1).

The cells were then used for biotransformations (see 2.13) or for purification of the expressed protein (see 2.9).

Generation of small amounts of cell lysate for screening of PuO-*Re* mutant libraries was done by expression in 96 well plates.

Therefore a preculture was grown over night in 800 µl LB media in a 96 deep well plate (MASTERBLOCK®, Greiner Bio-One, Frickenhausen, Germany). Each well was inoculated with a single colony from an agar plate of the mutant libraries using a sterile tooth pick.

The plates were sealed with BREATHSeal™ (Greiner Bio-One, Frickenhausen, Germany) and incubated over night at 37 °C and 180 rpm. On the next day, the plate was replicated to a new plate

using a 96 well plate replicator stamp and afterwards 200 µl sterile 60% glycerol added to store the plate at - 80 °C.

The new deep well plates contained 800 µl TB media with Amp (100 µg/ml) and 0.02% L-Ara for expression. The plates were incubated at 25 °C overnight for growth and expression of the mutant libraries.

After expression, the cells were centrifuged at 4 °C in the plate for 1 h at 4000 rpm (Eppendorf centrifuge 5810R, swing out rotor A-4-62). For cell lysis the pellet was resuspended in 200 µl BugBuster solution (1 x Bug Buster from a 10 x stock, DTT 1 mM, EDTA 0.5 mM, DNase 0.1 µg/ml, PMSF 1 mM, Tris buffer final 50 mM pH 8.0 and glycerol 5 % final) per well. Lysis was performed for 15 min at 25 °C and subsequently the lysate cleared by centrifugation at 4 °C (90 min, 4000 rpm). The cleared lysate was then transferred to a new 96 well plate and stored at - 80 °C until further screening.

2.9 Cell lysis and purification of proteins

2.9.1 Immobilized Metal Affinity Chromatography (IMAC) for purification of His₆-tagged IREDs

For His₆-tag purification of IREDs the cell pellets from the expression were resuspended in 1.5 ml/g buffer A (sodium phosphate 50 mM pH 7.0 with 300 mM KCl, 5 % glycerol, 1 mM β-mercaptoethanol and 5 mM imidazole), combined and frozen at - 80 °C. After thawing of the cell suspension, DNase I (1 µl/ml from a 5 mg/ml stock) and lysozyme (1 µl/ml from a 5 mg/ml stock) were added. Cell disruption was performed by high-pressure homogenization (3 cycles, 750-1000 bar) with an EmulsiFlex C-5 (Avestin, Canada).

The cell lysate was cleared by centrifugation for 45 min at 4 °C and 38800 g (centrifuge RC 6 Plus, Sorvall) and afterwards filtered using 0.2 µm filters (PES membrane, VWR, Darmstadt, Germany).

The lysate could be stored at - 80 °C or was used immediately for purification.

Protein purification was done at 8 °C using an ÄktaExplorer (GE Healthcare Europe, Freiburg, Germany) equipped with up to three serial 5 ml HiTrap Chelating Sepharose HP columns charged with Ni²⁺ (GE Healthcare Europe, Freiburg, Germany). Unbound and weakly bound proteins were washed off from the column with 5 column volumes (cv) of a 4% mixture of buffer A and B (buffer A + 500 mM imidazole). For elution of His₆-tagged IREDs the concentration of buffer B was raised to 40% for 8 cv, followed by a cleaning step for 5 cv with 100% buffer B. Fractions with highly purified IREDs were pooled and concentrated by ultrafiltration using a Vivaspin ultrafiltration spin column (10 kDa Mw cut off, PES membrane, Sartorius, Goettingen, Germany). Desalting was done with PD10-columns (Sephadex G 25 Medium, 85-260 µm, GE Healthcare, Freiburg, Germany). For storage, NADPH was added and the IREDs frozen in small aliquots at - 80 °C. Analysis of IRED purity was done by SDS-PAGE using 15% gels and size exclusion chromatography on HPLC (see 2.20).

2.9.2 Ion exchange chromatography with a MonoQ column as second IRED purification step

For further purification of *R*-IRED-*Sr* by ion exchange chromatography using a MonoQ column, the buffer was exchanged to MonoQ Buffer A (20 mM BisTris pH 7.0, 5% glycerol). The column was then washed with two steps (6% and 15%) MonoQ Buffer B (20 mM BisTris pH 7.0, 5 % glycerol, 1 M KCl) and the IRED eluted with 45% buffer B.

Fractions containing *R*-IRED-*Sr* were individually concentrated and the buffer exchanged to 20 mM BisTris with 5 % glycerol by washing them in Vivaspin ultrafiltration spin column. Prior to storage at – 80 °C NADPH was added.

2.9.3 Ion exchange chromatography with a Q-sepharose HP column for purification of PuO-*Re* wt and mutants

Lysis of cells expressing PuO-*Re* was done as described above for cells expressing IREDs. Purification of PuO-*Re* or the respective mutant was then done by ion exchange chromatography with a Q-Sepharose HP column as described by van Hellemond *et al.*¹⁶¹ Purified proteins were analyzed by SDS-PAGE (Figure S67).

2.10 Protein quantification by BCA assay

Quantification of purified proteins was done with the BCA kit from Pierce (Thermo Fisher Scientific Germany, Braunschweig, Germany) according to the manufacturer's instruction.

2.11 Solid phase assay and activity assays with cell lysate for HTS of PuO-*Re* mutant libraries

2.11.1 Solid phase assay

Solid phase assay screening for amine oxidase activity was done as described in literature with slight modifications.

After transformation a sufficient amount of cells was plated on the nylon membrane. The volume was estimated that about 1500 cells were growing on one plate. Cells were then grown over night at 25 °C on LB-Amp-Ara plates for expression of the PuO-*Re* mutants.

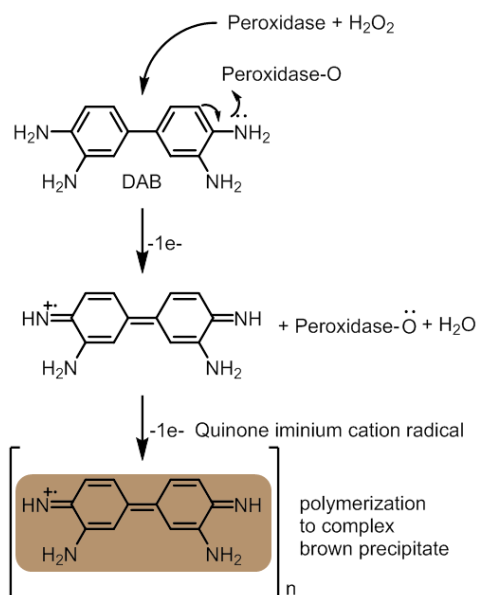
Next day, the membranes were frozen at - 20 °C for at least 1 h. After thawing of the membranes they were placed on a 90 mm diameter filter paper in a glass petri dish (SCHOTT AG, Mainz, Germany) soaked with 1.8 ml Tris buffer 50 mM pH 8.0 with 0.1 mg/ml HRP for background reduction.

After 1 h background reduction the membranes were transformed into a new petri dish with a filter paper soaked with the assay solution (Tris buffer 50 mM pH 8.0, 0.01 mg/ml HRP, 0.5 mg/ml diaminobenzidine and 10 mM substrate). The membranes were incubated at room temperature until the active colonies developed an intense dark brown color (Scheme 12 and Figure 27). These colonies were transformed

with a sterile tooth pick to a new membrane and subjected a second screening round after overnight grow to eliminate false positives and refine the screening procedure. Active colonies in the second screening round were transferred to LB-Amp plates and then grown in 96 well plates as described above (2.8).

From the epPCR library about 60000 - 70000 colonies were screened.

For saturation mutagenesis, the library size was calculated and screened to a completeness of > 95% to > 99% (depending on the library size, calculated with GLUE).¹⁸⁵



Scheme 12: Polymerization of 3,3-diaminobenzidine to a complex brown dye precipitate with HRP and H₂O₂.¹⁸⁶

2.11.2 Activity assays with cell lysates

Expression of mutant libraries in 96 well plates and generation of cell lysates was done as described above. Lysates were used for activity assays with 4-aminoantipyrine and vanillic acid as described in paragraph 2.12.2.¹⁸⁷ Depending on the activity with the screened substrate 5-25 μ l of the lysate were used.

Active mutants were then reassessed in triplicates with 5-20 μ g total protein from individual small scale (50 ml) expressions.

2.12 Liquid phase assays to determine the specific activities of purified proteins

2.12.1 Spectrophotometric detection of NADPH consumption to determine the IRED activity

To determine the pH profile of IREDs, the thermostability, the activity in presence of organic solvents and record kinetic parameters the specific activities of the IREDs were determined by monitoring the consumption of the co-substrate NADPH photometrically in a PolarStar Omega 96 well plate reader (BMG Labtech GmbH, Ortenberg, Germany) at 340 nm or 370 nm. One unit of IRED activity was defined as the amount of protein that oxidizes 1 μ mol NADPH per minute.

2 METHODS AND MATERIALS

Typically reactions were performed in 96 well plates (Greiner Bio-One GmbH, Frickenhausen, Germany) at 30 °C with an appropriate amount of enzyme in a final volume of 300 µl sodium phosphate buffer 50 mM pH 7.0. 0.3 µM of NADPH were used for recordings with substrates 2-methylpyrroline **1** and 2-methylpiperideine **3a** performed at 340 nm and 0.3 - 0.6 µM NADPH were used for recordings at 370 nm, done for substrates possessing an aromatic ring (2-phenylpiperideine **3b**, 2-*p*-fluorophenylpiperideine **3c**, 3,4-dihydroisoquinoline **5a** and 1-methyl-3,4-dihydroisoquinoline **5b**). The extinction coefficients were for each experiment determined experimentally as some of the substrates exhibited slightly brown color or overlapped partially with the NADPH spectrum.

For 340 nm a typical ϵ of 5.136 mM⁻¹ cm⁻¹ was determined and for 370 nm ϵ was 2.066 mM⁻¹ cm⁻¹.

To determine the pH profile of the IREDs the following buffers were used: sodium citrate buffer (pH 4.0 - 6.5; prepared according to McIlvaine),¹⁸⁸ sodium phosphate buffer (pH 6.0 - 8.0), Tris HCl buffer (pH 7.5 - 9.0) and glycine NaOH buffer (pH 8.5 - 10.0). In these assays 5 mM of substrate **1** was used.

The activity in presence of organic solvents was determined in sodium phosphate buffer pH 7.0 with 5% to 25% organic solvent and 5 mM of substrate **1**.

To determine the half life time of the IREDs at 30 °C and 50 °C samples were incubated at the respective temperature and regularly samples taken. The residual specific activity with 10 mM of substrate **1** was then plotted against the time and a nonlinear regression with the Solver plugin of Microsoft Excel performed to an exponential decay function of the form: $A=A_0 \cdot e^{-\lambda t}$ with A_0 representing the specific activity at $t = 0$ h to calculate the half-life times.

Determination of the T_{50}^{15} [°C] was done as described in literature with slight modifications.¹⁸⁹ Small samples of the enzymes were incubated in a PCR machine for 15 min at the respective temperatures following a relaxation time of 15 min at 8 °C. The residual specific activity with 10 mM of substrate **1** was then determined and plotted against the temperature. The curve was fitted by nonlinear regression with the Solver plugin of Microsoft Excel to a sigmoidal dose response curve of the following form:

$$A = A_{\min} + \frac{(A_{\max} - A_{\min})}{1 + \left(\frac{X}{C}\right)^B}$$

of the middle part (Hill Slope) and C representing the inflection point (X_{50})¹⁹⁰ to calculate the T_{50}^{15} [°C] with the reference value for maximum (100%) activity after incubation on ice.

For investigation of the temperature dependency of the reaction rate of *S*-IRED-*Pe* the specific activity with 10 mM of substrate **1** was determined at different temperatures. Therefore an Ultrospec 3000 photometer (Pharmacia Biotech, now part of GE HealthCare) with a temperature controlled cuvette holder (Fisons B3 Heating Circulator Bath, Haake) was used. The temperature of the buffer in the cuvette was extra controlled in a reference cuvette with a thermometer and after staying constant for at least 2 min, the reactions were started by the addition of IRED, NADPH and substrate. The total volume

added was less than 5%. To avoid substrate evaporation at increased temperatures the cuvettes were sealed (Figure 7).



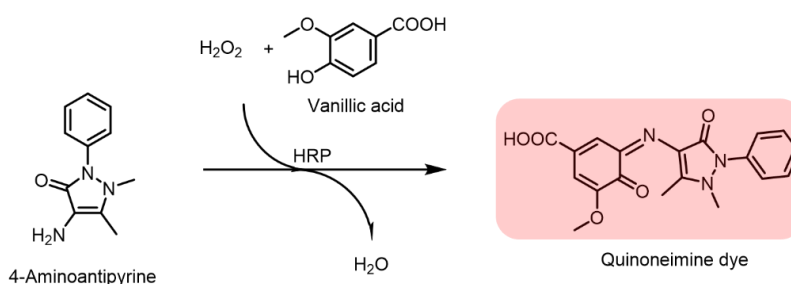
Figure 7: Experimental setup to determine the temperature dependence of the reaction rate of S-IRED-Pe.

Kinetic constants of the IREDs were calculated by determining the specific activity of the enzymes with varying concentrations of the different substrates (see x-axis of Figure S1 to Figure S5 and Figure S34 to Figure S48). Substrates were either dissolved in H₂O or DMSO, with the organic solvent being present from 1-5% maximum, depending on the solubility of the respective substrate. Nonlinear regression of the measured activities to the Michaelis-Menten equation was then performed with the Solver plugin of Microsoft Excel using "XL_Kinetics" or self-written spreadsheets.^{191,192} With some substrates, the IREDs showed lower activities at higher concentrations. In these cases the Michaelis-Menten equation was adapted to substrate inhibition kinetics using the following formula: " $v = (v_{max} \times [S]) / (K_M + [S] \times (1 + ([S]/K_I)))$ ".

To determine the kinetics for the reductive amination reaction, the same setup was used as described above. The substrate solution consisted of varying concentrations of aldehyde **11** premixed with the respective excess amount (equimolar, 10-fold and 50-fold) of amine **22** adjusted to pH 8.0 or pH 9.0 in buffer.

2.12.2 Detection of H₂O₂ formation by PuO-Re

Amine oxidase activity was determined by monitoring the formation of the co-product H₂O₂ in a coupled spectrophotometric assay with HRP and 4-aminoantipyrine plus vanillic acid as dye according to Holt *et al.*¹⁸⁷ In combination with HRP and H₂O₂ they are converted into a red quinoneimine dye (Scheme 13).



Scheme 13: Formation of a red quinoneimine dye by HRP from 4-aminoantipyrine and vanillic acid with H₂O₂.¹⁸⁷

This assay was also used to determine the activity with lysates from the PuO-*Re* mutant libraries and to determine the kinetic constants for purified PuO-*Re* by measuring the specific activities of the enzyme at different substrate concentrations. Calculation was done as described above for the IREDs.

The absorbance coefficient of the dye was determined with a H₂O₂ calibration curve to be 6.212 mM⁻¹ cm⁻¹ (literature 6.234 mM⁻¹ cm⁻¹).¹⁸⁷

2.13 Whole cell biotransformations with IREDs

Whole cell biotransformations with IREDs were performed with fresh cells directly after an overnight expression. After cell harvest, the pellet was washed once with 50 ml sodium phosphate buffer 50 mM pH 7.0. Biotransformation samples consisted of OD=30 cells (~ 50 mg/ml cww), 10 mM of the imine substrates (dissolved either in H₂O or DMSO) and 50 mM glucose for cofactor recycling. Reactions were performed in 50 mM sodium phosphate buffer pH 7.0 with a final DMSO concentration of maximum 5%. Biotransformations were done in screwed capped glass vials at 25 °C and 180 rpm. Regularly (usually 0 h, 0.5 h, 1 h, 3 h, 5 h, 8 h, and 24 h) samples were taken, mixed with internal standard, the cells centrifuged and the supernatant analyzed by GC or HPLC as described below (2.18 and 2.19). As negative control cells harboring an empty pBAD33 plasmid were used.

2.14 Biotransformations with purified proteins

2.14.1 IRED biotransformations with cyclic imine substrates

Biotransformation using purified IREDs were done according to literature¹⁴² with slight modifications. The IRED concentration in the reactions was 250 µg/ml and 10 mM of the imine substrate from a H₂O, DMSO or MeOH stock were used. The maximum concentration of organic solvent was 5%. For cofactor recycling 5 mM NADPH, 20 mM glucose-6-phosphate and 5 U/ml glucose-6-phosphate dehydrogenase were used. In a later stage of the project the NADPH was scaled down to 2.5 mM and 25 mM glucose-6-phosphate was used. This change did not result in alterations of the conversions and conversion rates.

Reactions were performed in 50 mM sodium phosphate buffer pH 7.0. Samples were incubated in screwed capped glass vials at 25 °C and 180 rpm. As negative control the IREDs were heat inactivated at 95 °C for 10 min.

For GC analytics, regularly samples were taken and mixed with an internal standard. Preparation of the sample for GC or HPLC analytics was done as described below (2.18 and 2.19).

2.14.2 IRED biotransformations with exocyclic imine substrates

Biotransformations with exocyclic imine substrates were done as with cyclic imines but Tris buffer (50 mM) with a pH of 8.0 was used and the IRED scaled up to 2.5 mg/ml. In addition glucose-6-phosphate dehydrogenase from *Leuconostoc mesenteroides* was used in its lyophilized powder form. Reconstitution of the lyophilized powder was done in small aliquots at 1 kU/ml with the

following buffer: 5 mM glycine buffer pH 8.0 with 0.1% bovine serum albumin (BSA). Each aliquot was used maximum twice as advised by the manufacturer.

The substrate was added from a DMSO or MeOH stock and the final concentration of the organic solvent was maximum 5%.

2.14.3 Reductive amination reactions with *R*-IRED-*Sr*

Reductive amination reactions with IREDs were performed with a final protein concentration of 2.5 mg/ml or 10 mg/ml. As negative controls reactions were done in which the IRED was substituted by heat inactivated enzyme (10 min at 95 °C) or by BSA. The other components of the control biotransformations were identical to the ones with active IRED.

Reactions for reductive aminations consisted of 10 mM carbonyl substrate (benzaldehyde **11** or acetophenone **20**, dissolved in DMSO) and the amine substrate (ammonia **21**, methylamine **22** and aniline **12** dissolved either in H₂O or DMSO) at equimolar, 10-fold and 50-fold excess of the amine to the carbonyl substrate. For recycling of the NADPH cofactor (2.5 mM in reactions) 25 mM glucose-6-phosphate and 5 U/ml of the reconstituted lyophilized glucose-6-phosphate dehydrogenase were used. Reactions were performed in Tris-HCl buffer at a pH of 8.0, 8.5 and 9.0 with a final DMSO concentration of 5% in all samples. The reactions were incubated in 5 ml screwed capped glass vials at 25 °C and 180 rpm and regularly samples were taken.

Preparation of samples for GC or HPLC analysis was done as described below.

2.15 Reaction cascade with purified IREDs and PuO-*Re*

For the reaction cascade with purified proteins IREDs and PuO-*Re* were used in equimolar ratio (10 μM each enzyme). Samples were incubated in 100 mM Tris buffer pH 8.0 with 2.5 mM NADPH, 20 mM glucose-6-phosphate, 5 U/ml glucose-6-phosphate dehydrogenase, catalase (2000 U/ml) and 10 mM amine substrate (dissolved in H₂O). Samples were incubated for 3 h at 25 °C and 180 rpm and afterwards quenched by the addition of 50 μl 5 M NaOH, followed by derivatization as described in 2.17.

2.16 Reaction cascade with whole cells expressing IREDs and PuO-*Re*

For coexpression of IREDs and PuO-*Re* wt chemically competent cells of *E. coli* strain JW5510 were transformed with both plasmids simultaneously. Cells were plated on LB-Amp-Cm and a single colony of the grown transformants used for overnight expression of both proteins as described above for strains having only one plasmid.

Biotransformations were then set up as described in 2.13 for IRED biotransformations, but Tris buffer pH 8.0 was used. Biotransformations were performed at 25 °C and 180 rpm in screwed capped glass vials and regularly samples were taken.

For analysis, cells were centrifuged down and the supernatant used for extraction and derivatization as described below (2.17).

2.17 Preparation of samples for GC and HPLC analytics and derivatizations

Samples of IRED biotransformations with substrates **1** and **3a** were derivatized and extracted with acetic anhydride and dichloromethane as solvent as described by Dobos *et al.*¹⁹³

IRED biotransformations with the residual substrates (**3b**, **3c**, **5a** to **5c**, benzylidenemethylamine **7**, benzylideneaniline **9**, benzophenoneimine **15** and phenylethylideneaniline **18**) and reductive amination reactions were extracted twice with MTBE after the addition of 50 μ l 5 M NaOH to the supernatant. Extractions of reactions with substrate cinnamaldehyde **45** were done twice with MTBE without the addition of NaOH.

Derivatization of 2-phenylpiperidine **4b**, α -methylbenzylamine **26** and *N*- α -dimethylbenzylamine **27** for chiral GC was done with acetic anhydride. 200 μ l of the extracted sample were used and mixed with 20 μ l acetic anhydride and 20 μ l pyridine, incubated for 1 h at 70 °C followed by quenching with 200 μ l 2% aqueous methylamine solution. The organic phase was then analyzed by GC-FID.

Derivatization of polyamines and biotransformation products from polyamines in the reaction cascade with purified proteins and whole cells was done with isobutylchloroformate (IBCF) as described by Cunha *et al.*¹⁹⁴

2.18 GC-FID and GC-MS analytics

Results of the biotransformations with substrates **1**, **3a** to **3c** and their corresponding products were analyzed by GC. Reductive amination reactions with amine nucleophiles ammonia **21** and methylamine **22** were also analyzed by GC, as well as reactions with polyamine substrates 1,4-diaminobutane **28**, 1,5-diaminopentane **29** and 1,5-diamino-2-methylpentane **31**. GC-FID analyses were carried out on a Shimadzu GC-2010 equipped with an AOC-20i auto injector. Identification of compounds was done by detection *via* flame ionization detector (FID) and comparison of the retention times to commercial available reference materials. For quantification of biotransformations, calibration curves with the authentic standards were prepared. GC conditions and programs are given in Table 6. The GC-FID was operated with H₂ as carrier gas (linear velocity 30 cm/s) and samples were injected in split mode. In addition product analyses were done by GC-MS on a Shimadzu GCMS-QP2010 system equipped with an AOC-5000 auto injector and He as carrier gas. Mass spectra were determined by electron impact (EI) ionization with 70 eV, an ion source temperature of 200 °C and an interface temperature of 250 °C. Mass detection was performed in scan mode from 35 m/z to 500 m/z. Columns and oven temperature programs were the same as for GC-FID analysis.

For GC-MS headspace the CombiPal sampler was operated in headspace mode with a 2.5 ml heated headspace syringe. Biotransformation samples were filled in 20 ml headspace vials and heated to 150 °C. 250 μ l of the gas phase were injected for analysis.

2 METHODS AND MATERIALS

Table 6: GC-FID and GC-MS conditions used for analysis and quantification. The column "compounds" lists only the substrates of the biotransformations in case of the achiral methods. Products and byproducts could be detected with the same method. For the chiral methods only the detected products are listed in this column. The basis for the assignment of the enantiomers and comments are given in the last column.

compounds	column	chiral	injector temperature [°C]	detector temperature [°C]	column oven temperature program	comment/ assignments of enantiomers
1-acetylated	DB5	no	250	330	100 °C hold 2 min, 30 °C/min to 130 °C, 5 °C/min to 150 °C hold 1 min, 50 °C/min to 310 °C hold 3 min	
2-acetylated	β-Dex 225	yes	250	255	100 °C hold for 2 min, 50 °C/min to 130 °C, 1.5 °C/min to 150 °C, 50 °C/min to 210 hold 1 min	authentic reference material of (<i>R</i>)- and (<i>S</i>)- enantiomers; (<i>R</i>)- before (<i>S</i>)-; Figure S6.
3a-acetylated	DB5	no	250	330	100 °C hold for 2 min, 35 °C/min to 140 °C, 5 °C/min to 170 °C, 75 °C/min to 310 hold 3 min	
4a-acetylated	β-Dex 225	yes	250	255	100 °C hold for 2 min, 50 °C/min to 130 °C, 1.5 °C/min to 150 °C, 75 °C/min to 230 hold 3 min	authentic reference material of (<i>S</i>)- enantiomer; analogy to 2; (<i>R</i>)- before (<i>S</i>)-; Figure S7.
3b and 3c	ZB-5	no	250	330	100 °C hold for 2 min, 30 °C/min to 150 °C, 5 °C/min to 185 °C, 75 °C/min to 320 °C hold 3 min	
4b-acetylated	CP-Chirasil Dex-CB	yes	210	250	90 °C, 4 °C/min to 200 °C hold 3 min	Figure S7; (<i>S</i>)- before (<i>R</i>)-. ¹⁴⁷
7, 11, 20	ZB-5	no	250	330	65 °C hold for 3 min, 30 °C/min to 109 °C, 1 °C/min to 117 °C, 50 °C/min to 325 °C hold 3 min	given are the imines and carbonyl substrates for the reductive amination reaction.
26-acetylated and 27-acetylated	CP-Chirasil Dex-CB	yes	225	225	90 °C, 10 °C/min to 140 °C, 1.5 °C/min to 158 °C, 75 °C/min to 220 °C hold 3 min	authentic reference material of (<i>R</i>)- and (<i>S</i>)- enantiomers; (<i>S</i>)- before (<i>R</i>)-; Figure S55 and Figure S57.
45	DB5	no	250	330	70 °C hold for 2 min, 30 °C/min to 130 °C, 2 °C/min to 145 °C, 50 °C/min to 300 hold 2 min	
28, 29 and 31	DB-5	no	250	200 / 250	50 °C hold for 2 min, 15 °C/min to 90 °C, 20 °C/min to 220 °C hold 1 min, 25 °C/min to 320 °C hold 4 min	reaction cascade with purified proteins and whole cells.
28 and 29	DB-5	no		200 / 250	80 °C hold for 3 min, 8 °C/min to 120 °C, 50 °C/min to 310 °C hold 2 min	GC-MS headspace.

columns:

ZB-5 (Phenomenex, Aschaffenburg, Germany): length; 30 m x 0.25 mm x 0.25 μm

CP-Chirasil Dex-CB (Agilent, Waldbronn, Germany): length: 25 m x 0.25 mm x 0.25 μm

Supelco β-Dex 225 (Sigma Aldrich, Steinheim, Germany): length 30 m x 0.25 mm x 0.25 μm

DB5 (Agilent, Waldbronn, Germany): length 30 m x 0.25 mm x 0.25 μm

2 METHODS AND MATERIALS

2.19 HPLC analytics

Substrate conversions and product formations in biotransformations with **5a** to **5c**, **9**, **15**, **18** and **11** with **12** were analyzed by reversed-phase HPLC on an Agilent 1200 series system equipped with a diode array detector (G1315D), degasser (G1322A), quaternary pump (G1311A), temperature controlled column compartment (G1316A) and a standard autosampler unit (G1329A) from Agilent Technologies (Waldbronn, Germany). Chiral analysis of biotransformations products was done with chiral stationary phases by normal phase HPLC using an identical HPLC device. Detection of analytes was done by monitoring their UV signals. Identification of compounds was performed by comparison with reference materials and by comparing their absorbance spectra from 200-310 nm. Quantification of compounds was done using calibration curves with the authentic standards at their maximum specific absorbance wavelengths. The applied methods and parameters for detection are summarized in Table 7.

Table 7: HPLC methods and settings used for analysis and quantification. The column "compounds" lists only the substrates of the biotransformations in case of the achiral methods. Products and byproducts could be detected with the same method. For the chiral methods only the detected products are listed in this column. The basis for the assignment of the enantiomers and comments are given in the last column. Mobile phases: ABC = ammonium bicarbonate buffer, ACN = acetonitrile, iProp = isopropyl alcohol, DEA = diethylamine.

compounds	column	chiral	mobile phase	flow rate [ml/min]	injection volume [μl]	temperature [°C]	DAD settings (wavelength/bandwidth and reference)	comment/ assignments of enantiomers
5a and 5b	XBridge C8	no	isocratic 10 mM ABC pH 9.0 / ACN 67.5/32.5	0.6	0.5	25	216/4; 248/4; 264/4 Ref: 360/100	
6b	Chiralpak IC	yes	isocratic heptane/iProp/DEA 98:2:0.1	1	5	20	248/4; 264/4 Ref: 360/100	Figure S11; (S)- before (R)-. ¹⁴³
5c	XBridge C8	no	isocratic 10 mM ABC pH 9.0 / ACN 67.5/32.5	0.6	1	25	226/8; 248/4; 276/4; 284/4 Ref 360/100	
4c	Chiralpak IC	yes	isocratic hexane/ iProp:DEA (99.5/0.5) 98/2	1	5	25	220/4; 248/4; 264/4 Ref 360/100	Figure S8; (R)- before (S)-. ¹⁴⁷
9 , 15 and 18	XBridge C8	no	isocratic 10 mM ABC pH 9.0 / ACN 55/45	0.6	0.5	30	22/10; 240/4; 256/4; 284/4 Ref 360/100	
18	Chiralpak IB	yes	isocratic hexane/iProp 95/5	0.4	2.5	20	220/10; 244/10; 292/10 Ref 360/10	Figure S19; (S)- before (R)-. ¹⁹⁵⁻¹⁹⁷

columns:

XBridge C8 3 x 100 mm, 3.5 μm particle size (Waters, Eschborn, Germany)

Chiralpak IC 250 x 4.6 mm ID (Chiral Technologies Europe, Illkirch, France)

Chiralpak IB 150 x 4.6 mm ID (Chiral Technologies Europe, Illkirch, France)

2.20 SEC analysis on HPLC to determine the protein purity

Analysis of His₆-tagged IRED purity by size exclusion chromatography on HPLC was performed as described in literature.¹⁵¹ A Phenomenex Yarra 3 μ SEC-2000 column (Aschaffenburg, Germany) was used with an Agilent 1200 HPLC system equipped with a diode array detector (G1315D), degasser (G1322A), quaternary pump (G1311A), temperature controlled column compartment (G1316A) and a temperature controlled high performance autosampler unit (G1367B). Analytes were separated in runs performed for 25 min using a mobile phase of 50 mM sodium phosphate buffer pH 6.5 with 100 mM NaCl at a flow rate of 0.2 ml/min and 30 °C. Until injection, the samples in the autosampler unit were kept at 8 °C. 5 μ l of the purified protein solution diluted to a concentration of 2 μ g/ μ l in the mobile phase were injected and the UV signal at 280 nm recorded. Estimation of the IRED purity was then done by calculating the fraction of the A₂₈₀ signal corresponding to the IRED compared to the total UV₂₈₀ signal. For calibration of the size exclusion column a gel filtration standard from BioRad was used (#151-1901, Bio-Rad Laboratories GmbH, Munich, Germany).

2.21 Synthesis of substrates and products and NMR analysis

The following compounds were not commercially available and hence synthesized to be used as substrates for IREDs, PuO-*Re* or as product standards for identification and quantification of biotransformation results.

Synthesized compounds were characterized by ¹H- and ¹³C- nuclear magnetic resonance (NMR) spectroscopy on a Bruker Avance 500 spectrometer operating at 125.76 MHz or 500.15 MHz at 23 °C in deuterated solvents with tetramethylsilane as internal standard. Chemical shifts are expressed in ppm relative to tetramethylsilane.

2.21.1 Synthesis of 2-methylpiperideine (imine **3a**)

Synthesis of imine substrate **3a** was done as described in literature.^{144,198}



Scheme 14: Synthesis of imine **3a** from amine **4a** with NCS and DBU.

7.5 g (56 mmol) *N*-Chlorosuccinimide (NCS) were dissolved in 250 ml dry diethyl ether and under N₂ atmosphere on ice slowly 6 ml (51 mmol) **4a** were added over 30 min. The reaction was then stirred overnight at room temperature. The complete conversion of the amine was confirmed by TLC staining and by GC-MS. The organic phase was washed with water (3 x 50 ml), dried over MgSO₄ and the solvent completely removed by rotary evaporation until a slightly yellow oily liquid was obtained (6.64 g, 49.7 mmol, 97.4%). The oil was dissolved in 50 ml dry DCM and over 25 min slowly 9.8 ml

diazobicyclo-[5.4.0]-undec-7-ene (DBU, 65.7 mmol, 1.3 equivalents) were added. The solution was stirred for 6 h at room temperature. During this time the color changed from pale yellow to dark brown and by GC the conversion to the imine was confirmed.

Purification of the imine was done by distillation at reduced pressure (800 to 400 mbar) and precipitation of the product as its hydrochloride salt by the addition of 2 M HCl in diethyl ether afforded imine **3a** as slightly yellow ionic liquid (0.7 g, 7.1 mmol, 14% yield). NMR spectra (Figure S92 and Figure S93) were in accordance with literature results.^{144,147,199}

¹H-NMR (500 MHz, CD₃OD) δ (ppm): 1.80 – 1.95 (m, 4 H), 2.40 (s, 3 H), 2.77 – 2.85 (m, 2 H), 3.60 – 3.68 (m, 2 H).

¹³C-NMR (500 MHz, CD₃OD) δ (ppm): 18.0, 20.2, 24.8, 32.1, 45.8, 191.9.

2.21.2 Synthesis of 2-phenylpiperideine (imine **3b**)

Synthesis of imine substrate **3b** was performed during the supervision of a chemist internship according to literature.^{34,143,147} Imine **3b** hydrochloride was obtained as brown crystals with about 50% yield (4.7 mmol, 0.92 g). NMR spectra (Figure S94 and Figure S95) were in accordance with literature results.¹⁴⁷

¹H-NMR (500 MHz, CD₃OD) δ (ppm): 2.06 – 2.02 (m, 4 H), 3.31 – 3.35 (m, 2 H), 3.81 – 3.89 (m, 2 H), 7.61 – 7.70 (m, 2 H), 7.75 – 7.82 (m, 1 H), 7.86 - 7.94 (m, 2 H).

¹³C-NMR (500 MHz, CD₃OD) δ (ppm): 18.4, 20.4, 29.9, 46.5, 129.0, 130.8, 133.2, 136.2, 185.3.

2.21.3 Synthesis of 2-*p*-fluorophenylpiperideine (imine **3c**)

Synthesis of imine substrate **3c** was performed during the supervision of a chemist internship analogously to the synthesis route for **3a** with NCS and DBU as described above. The imine was obtained as a mixture of a green-yellow oil and yellow needles of DBU after evaporation of the solvent. Purification of the crude product was done by flash column chromatography during this work.

For flash column chromatography the silica was deactivated with 1% trimethylamine. Purification with cyclohexane:ethyl acetate (70:30) with 0.5% trimethylamine afforded the product as clear yellow liquid in 46% yield (0.36 g, 2 mmol) with > 95% purity after evaporation of the solvent. NMR spectra (Figure S96 and Figure S97) were in accordance with literature results.¹⁴⁷

¹H-NMR (500 MHz, CDCl₃) δ (ppm): 1.63 – 1.71 (m, 2H), 1.79 – 1.87 (m, 2 H), 2.57 – 2.63 (m, 2 H), 3.78 – 3.85 (m, 2 H), 7.0 – 7.10 (m, 2 H), 7.73 – 7.79 (m, 2 H).

¹³C-NMR (500 MHz, CDCl₃) δ (ppm): 19.7, 21.8, 27.0, 49.8, 115.0 (d, J = 21.8 Hz), 127.8 (d, J = 8.2 Hz), 136.3 (d, J = 3.0 Hz), 163.7 (d, J = 248.8 Hz), 164.5.

2.21.4 Synthesis of 1-methyl-1,2,3,4-tetrahydroisoquinoline (amine **6b**)

Amine **6b** was synthesized by reduction with NaBH₄ from imine **5b** as described in literature by Huber *et al.*¹⁴⁴

1 mmol (0.182 g) imine hydrochloride were dissolved in 5 ml ice cold MeOH. 2 mmol NaBH₄ (75.7 mg) were dissolved in dry ice cold MeOH and added under N₂ atmosphere to the imine.

After stirring for 2 h on ice the imine was fully reduced as indicated by HPLC analysis and TLC staining with Ninhydrin solution (1.5 g Ninhydrin dissolved in 100 ml *n*-butanol with 3 ml acetic acid). The reaction was stopped by the addition of 5 ml 5 M NaOH. The amine product was extracted twice with 20 ml DCM, washed with H₂O and the organic phase dried by the addition of MgSO₄. The organic phase was filtered and concentrated by rotary evaporation. 0.126 g of amine **6b** was obtained as slightly yellow oil in about 87% yield. NMR spectra (Figure S98 and Figure S99) were in accordance with literature results.^{143,144}

¹H-NMR (500 MHz, D₂O) δ (ppm): 1.52 (d, *J* = 6.8 Hz, 3 H), 2.84 – 2.92 (m, 1 H), 2.94 – 3.02 (m, 1 H), 3.06 – 3.14 (m, 1 H), 3.34 (dt, *J* = 12.5, 5.5 Hz, 1 H), 4.28 (q, *J* = 6.7 Hz, 1 H), 7.20 – 7.30 (m, 4 H).

¹³C-NMR (500 MHz, D₂O) δ (ppm): 20.1, 26.9, 39.8, 50.8, 126.1, 126.5, 127.0, 129.1, 133.3, 137.2.

2.21.5 Synthesis of 1,4-diaminopentane and 1,5-diaminohexane (polyamines **32** and **33**)

Polyamine substrates no. **32** and **33** were synthesized at the Institute of Technical Biochemistry during the supervision of a chemist internship according to literature.²⁰⁰

NMR spectrum 1,4-diaminopentane (polyamine **32**) (Figure S100):

¹H-NMR (125 MHz, CDCl₃) δ (ppm): 1.28 (d, *J* = 6.3 Hz, 3 H), 1.41 – 2.17 (m, 8 H), 2.82 – 3.11 (m, 2 H), 3.40 – 3.59 (m, 1 H).

NMR spectrum 1,5-diaminohexane (polyamine **33**) (Figure S101):

¹H-NMR (125 MHz, CDCl₃) δ (ppm): 1.06 (d, *J* = 6.3 Hz, 3 H), 1.26 – 1.37 (m, 4 H), 1.38 – 1.49 (m, 6 H), 2.64 – 2.74 (m, 2 H), 2.83 – 2.96 (m, 1 H).

3 RESULTS

3.1 Imine reductases – novel biocatalysts

3.1.1 Identification and selection of novel IREDs

IREDs were just recently described and have emerged as promising biocatalysts for chiral amine synthesis.^{107,201} These enzymes can be applied either for the asymmetric reduction of imines, in reductive amination reactions or as part of enzymatic cascade reactions. This work will deal with examples for all of these different applications. At the time this work started, only three IREDs were described in total in the public available literature^{137–142} and an additional one in a Japanese patent.²⁰² These first IREDs were discovered by Mitsukura *et al.* using traditional screening of microorganisms, purification of the responsible proteins and the identification of the genes.^{139–141} With the availability of the sequences by BLAST²⁰³ homologous genes can be found in GenBank,²⁰⁴ which stores an increasing number of genetic information obtained from whole genome sequencing projects and thereby provides sequences for a wealth of uncharacterized biocatalysts. After a BLAST search with the sequences of the two initially by Mitsukura *et al.* described IREDs (the (*R*)- selective IRED from *Streptomyces sp.* GF3587 (*R*-IRED-Ss) and the (*S*)- selective IRED from *Streptomyces sp.* GF3546 (*S*-IRED-Ss))¹²⁷⁻¹²⁹ indeed about 350 putative novel IREDs were identified. Interestingly, at the time of the first BLAST search many of the obtained entries were designated as new sequences. They were often stored for less than three months in GenBank, again underlining the novelty of the IRED superfamily and the importance of expanding the known sequence space for the discovery of novel enzymes.

In cooperation with Silvia Fademrecht[†] the identified sequences were used to set up a database for identification and selection of novel IREDs. The bioinformatic works including the establishment of the database and the analysis of the sequences were done by Silvia Fademrecht.

All sequences that were selected for storage in the in house established database system²⁰⁵ had an expectation threshold (*E* value) of 10^{-30} to ensure a high global sequence identity to already confirmed IRED sequences. This stringent threshold was chosen as due to the limited information available about characterized IREDs no further criteria could be applied to refine and reduce the number of sequences. The average sequence identity of all database members was 36%. The final version of this database was named “Imine Reductase Engineering Database” and made publically available online under: <https://ired.biocatnet.de/>.¹⁴⁵

A network analysis of the sequences stored in the database, that was based on sequence similarity revealed a clear separation into two superfamilies above a sequence identity threshold of 49% (Figure 8).¹⁴⁵ They can be traced back to the (*R*)- selective IRED (*R*-IRED-Ss) and the (*S*)- selective IRED (*S*-IRED-Ss) that were used as seed sequences.^{139–141} Therefore, the superfamilies were further dedicated as an (*R*)- type IRED and an (*S*)- type IRED superfamily. The assignment into these two superfamilies and the thereof derived classification at the very early stage of IRED discovery is inherently restricted to the limited number and information available for the few characterized enzymes. During the ongoing work on this project, many more novel IREDs were characterized and information about them published in literature.^{142–150} To include the growing information available about IREDs, the

[†]: Bioinformatics group, Institute of Technical Biochemistry, University of Stuttgart.

database was updated and contains at the current version > 1400 entries encoding for more than 1100 proteins, divided into 14 superfamilies.¹⁵² Nevertheless for most of the superfamilies no enzymes are characterized. Hence, it is difficult to make general predictions about novel IREDs stored in the database with respect to their activity and selectivity. In contrast, for the characterized members of the (*R*)- type IRED and (*S*)- type IRED superfamilies (in the actual database, version 3, they were renamed as superfamily 1 and superfamily 2)¹⁵² a few exceptions from the suggested selectivity pattern are now described.^{148,149} Nevertheless as the overall majority of the IRED superfamily members tend to show the dedicated selectivity pattern, the initially suggested predictions based on global sequence identity greatly facilitate the selection and the characterization of novel IREDs. With further clarifications about the mechanism of the enzymatic imine reduction, as well as the resolution of more structures it is expected that a refinement of the IRED classification will allow more precise predictions.

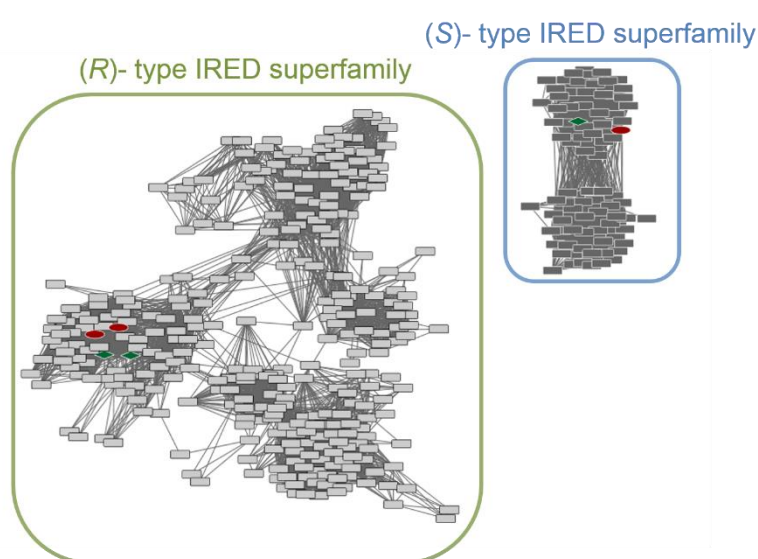


Figure 8: Assignment of the (*R*)- type IRED superfamily (circled in green) and the (*S*)- type IRED superfamily (circled in blue) in the first version of the "Imine Reductase Engineering Database".¹⁴⁵ The (*R*)- type superfamily contains 282 proteins whereas the (*S*)- type superfamily is considerably smaller with only 74 members. Superfamilies were further divided into three homologous families for the (*R*)- type IREDs and two homologous families for the (*S*)- type IREDs. IREDs that were at the time of publication described in literature (*R*-IRED-Ss, *R*-IRED-Sk and *S*-IRED-Ss) are colored as green diamonds. Novel IREDs that were selected for characterization in this work are colored as red ellipses. This figure was provided by Silvia Fademrecht.¹⁴⁵

To prove that the putative IRED sequences, stored in the database indeed encode for functional enzymes, capable of imine reduction some of the database members were selected for biochemical characterization. For the selection of these enzymes the bioinformatic database analyses and the information about the biochemical properties of the published IREDs were combined to estimate the importance of conserved residues that might be responsible for the imine reducing activity.

In the initial characterization performed by Mitsukura *et al.* several potential enzyme inhibiting compounds were tested and the results indicated a hydroxy- and thiol- sensitive nature of *R*-IRED-Ss.¹³⁸ In contrast, chelating agents like EDTA did not result in decreased activity, making metal assisted catalysis unlikely.¹³⁸ During this time a third IRED was published in the public literature.¹⁴² An (*R*)-selective enzyme from *Streptomyces kanamyceticus* (*R*-IRED-Sk) was cloned, its crystal structure resolved and a mechanism proposed (see also 1.2.5).¹⁴² Based on its sequence similarity, the enzyme clustered in the (*R*)- type IRED superfamily, thereby also further indicating the established selectivity pattern. The sequence of this enzyme was therefore used as an additional seed sequence for the

3 RESULTS

database.¹⁴⁵ By combining the biochemical- and the new mechanistic information with the conservation analysis, novel IREDs were now selected. An alignment of these three characterized enzymes with their closest related homologous was performed (Figure 9). As highlighted in this alignment (Figure 9), IREDs possess many overall conserved residues (yellow), superfamily specific conserved residues (blue and green), but also major deviations in the conserved positions could be identified from the consensus sequence (red). The selection of the novel IREDs for characterization was done based on the highest sequence identity, but disregarding the sequences that showed major deviations in the conserved residues (colored in red in Figure 9). The selected enzymes for characterization were derived from *Streptosporangium roseum* DSM 43021 (highest sequence identity to *R*-IRED-*Sk*¹⁴²), *Streptomyces turgidiscabies* (highest sequence identity to *R*-IRED-*Ss*^{138,141}) and *Paenibacillus elgii* (highest sequence identity to *S*-IRED-*Ss*^{139,140}; see also Table 8).

Table 8: Novel IREDs that were selected for characterization and their relation to the three already characterized IREDs.

origin of novel IRED	abbreviation	homology to	sequence identity	superfamily
<i>Streptosporangium roseum</i> DSM 43021	<i>R</i> -IRED- <i>Sr</i>	<i>R</i> -IRED- <i>Sk</i>	60.8%	1 ((<i>R</i>)- type)
<i>Streptomyces turgidiscabies</i>	<i>R</i> -IRED- <i>St</i>	<i>R</i> -IRED- <i>Ss</i>	80.7%	1 ((<i>R</i>)- type)
<i>Paenibacillus elgii</i>	<i>S</i> -IRED- <i>Pe</i>	<i>S</i> -IRED- <i>Ss</i>	60.5%	2 ((<i>S</i>)- type)

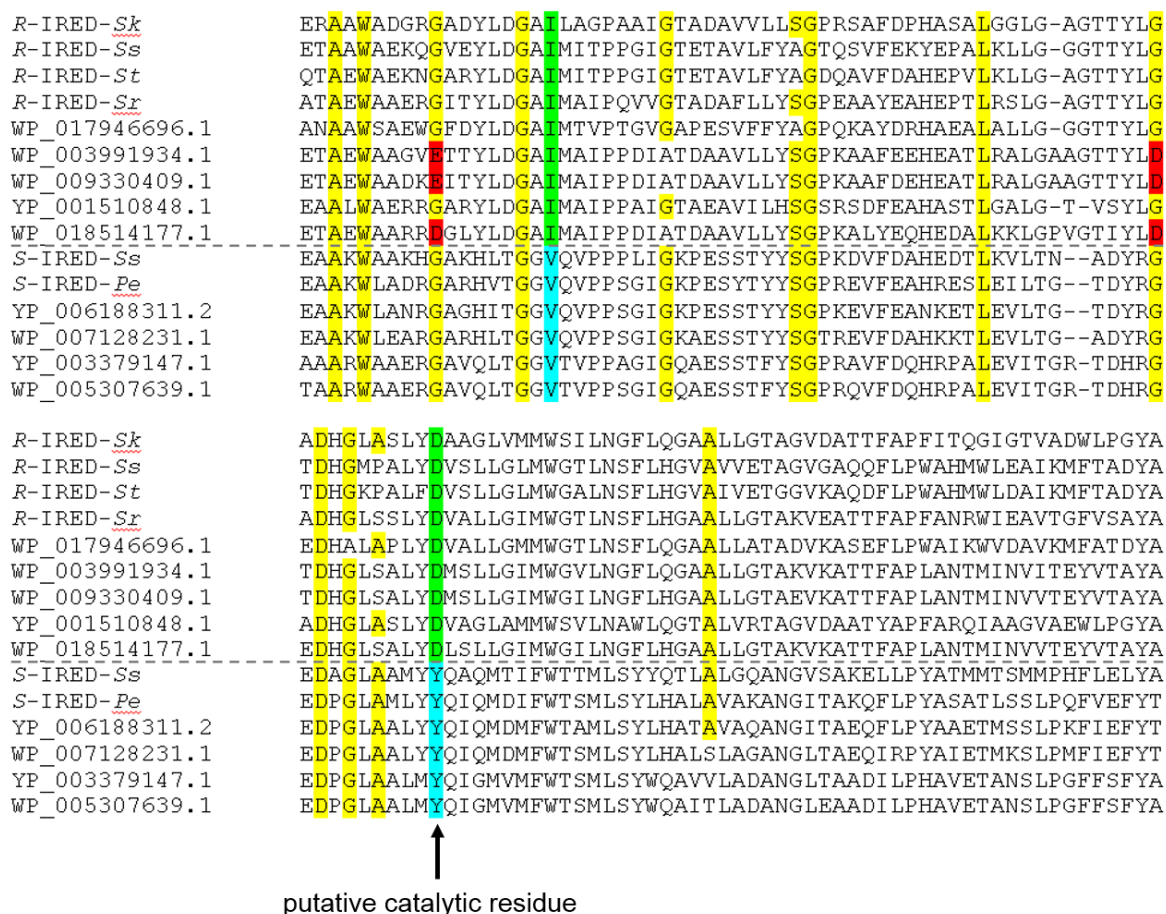


Figure 9: Excerpt of an alignment of the closest homologous sequences (next to others, they include *R*-IRED-*Sr*, *R*-IRED-*St* and *S*-IRED-*Pe*) to the three characterized IREDs from *Streptomyces kanamyceticus* (*R*-IRED-*Sk*),¹⁴² *Streptomyces* sp. GF3587 (*R*-IRED-*Ss*)¹⁴⁰ and *Streptomyces* sp. GF3546 (*S*-IRED-*Ss*)¹³⁹. Residues colored in yellow are conserved in both IRED superfamilies, green/blue colored residues are superfamily specific conserved and red residues indicate a deviation from the consensus sequence. The details about the selection of *R*-IRED-*Sr*, *R*-IRED-*St* and *S*-IRED-*Pe* for characterization are given in the main text.

For production of the three IREDs, the corresponding genes were ordered from GeneArt™ in codon-optimized form for expression in *E. coli*. As expression system the arabinose inducible pBAD33 plasmid (Figure 5) was chosen as the pET/IPTG based expression system was meanwhile described to result in large amounts of insoluble protein.¹⁴³ Furthermore plasmids of the pBAD series can be combined as they possess compatible origins of replication and different selection markers.¹⁷⁴ This might facilitate the combinatorial use of different expression plasmids and the establishment of enzymatic cascade reactions. Plasmids from the pBAD33 series, however do not have a ribosome binding site, hence in the ordered DNA a synthetic one (AGGAGG) was included seven bases in front of the ATG start codon. Design of this ribosome binding site was done considering criteria published in literature for high level expression.^{206–209} In addition an N-terminal His₆-tag for purification and a 3CV protease cleavage site for tag removal was included.^{210–212} The detailed sequence of the synthetic DNA ordered for each IRED is given in section 2.1.4.

The expression of the three IREDs was tested and optimized during the supervision of the diploma thesis of Sebastian Hofelzer.²¹³ Of the tested conditions, the highest levels of protein were obtained after expression over night at 25 °C in TB media. At higher temperatures IREDs tend to form insoluble inclusion bodies. The purification of the IREDs was established by Ni²⁺ affinity chromatography on an Äkta Explorer system. The result of a typical IRED purification and the purity estimated by size exclusion chromatography (SEC) in HPLC is shown in Figure 10 and Table 9.

In literature IREDs are often described to be well expressed, but insoluble. During these investigations it seemed however that the solubility of the IREDs was mainly affected by the lysis method, something that was also described for other proteins.^{214,215} By using high pressure homogenization the yields of purified protein were usually > 250 mg per liter of *E. coli* culture for each IRED. In contrast, in the beginning cell disruption was performed by ultrasonication and in these cases for the purified proteins often less than 50 mg per liter culture were obtained. However next to an influence on solubility, with high pressure homogenization also a more effective lysis might contribute to the higher yields. On the denaturing SDS gel, IREDs migrated according to their molecular weight around 33 kDa (Figure 10). To visualize also minor contaminants 20 µg total protein were loaded on the gel. According to the SDS gel and based on the SEC analysis in HPLC (Table 9), the purity of the IREDs reached after optimization ~ 90% (the calculation is based on the fraction of the total UV₂₈₀ signal in the HPLC SEC analysis).

Table 9: Purity of IREDs determined by SEC analysis in HPLC.

IRED	purity [%] based on A ₂₈₀ in HPLC SEC analysis	HPLC run
R-IRED-Sr	90.3	Figure S26
R-IRED-St	87.0	Figure S27
S-IRED-Pe	91.6	Figure S28

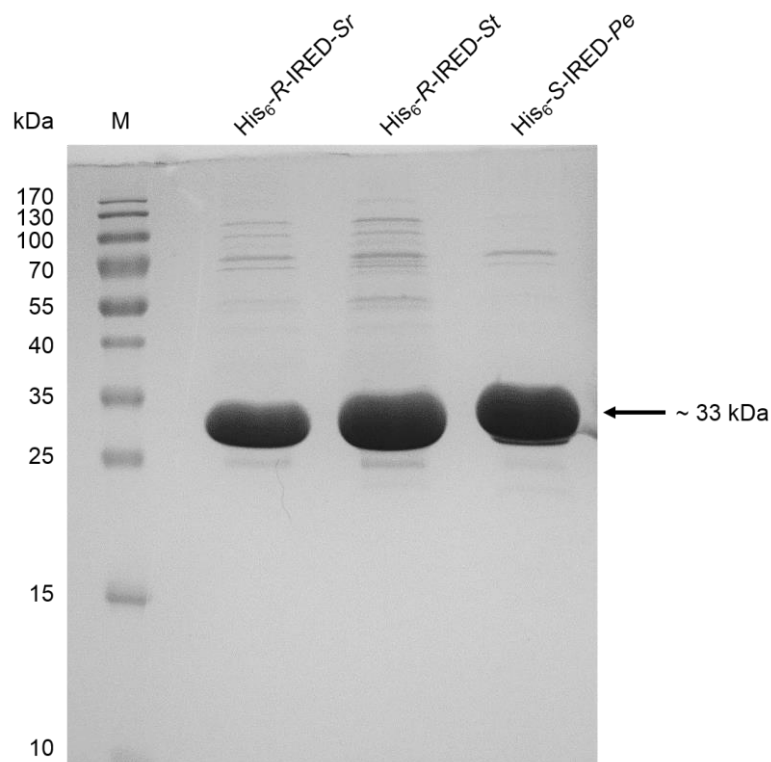


Figure 10: 15% SDS-PAGE of a typical Ni^{2+} affinity chromatography purification of *R*-IRED-*Sr*, *R*-IRED-*St* and *S*-IRED-*Pe*. To compare the purity of the IREDs and visualize minor contaminants 20 μg total protein were loaded.

After purification of the IREDs, the buffer was exchanged and the proteins concentrated. IREDs were found to be very soluble proteins and concentration of them to > 70 mg/ml did not result in precipitation. Interestingly the (*R*)-selective IREDs displayed a bright yellow color after purification, whereas the (*S*)-selective IRED was colorless (Figure 11). This color was also stable during dialysis, but lost after heat denaturation of the enzyme. A spectral analysis of the two proteins indicated a maximum of the absorbance around 340 nm.

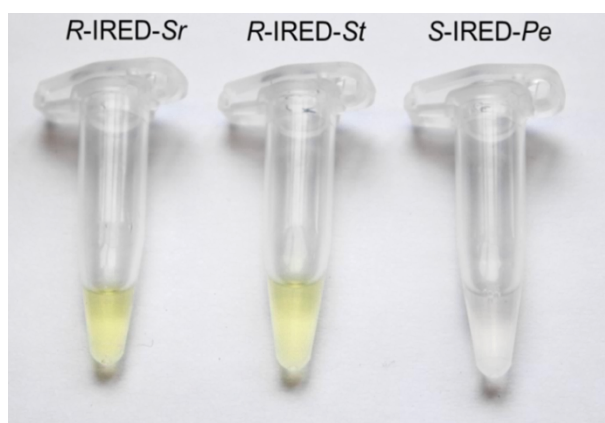


Figure 11: Color of purified IREDs. *R*-IRED-*Sr*: 86 mg/ml; *R*-IRED-*St*: 81 mg/ml; *S*-IRED-*Pe*: 74 mg/ml.

3.1.2 Imine reducing activity of the novel IREDs

To verify and determine the activity of these newly selected putative IREDs the reduction of the previously described substrate 2-methylpyrroline **1** was tested with whole cells having the IREDs

expressed as well as with purified proteins. As controls in whole cell biotransformations, cells with an empty pBAD33 plasmid were used, whereas for the reduction with purified proteins, the enzymes were heat inactivated (95 °C, 10 min).

Biotransformations employing whole cells with this substrate resulted in a rapid conversion of the substrate, in contrast to the cells with an empty vector that did not show any conversion. Both of the *R*-IREDs fully converted the substrate within 3 hours to the amine product 2-methylpyrrolidine **2**, whereas the (*S*)-selective IRED showed conversions of around 95% in 24 h (Table 10, Figure 12 and Table S1). By chiral GC-FID also the expected selectivity could be confirmed. The *R*-IREDs performed the transformations with an excellent enantiomeric excess of 98.3% and 99.0% for *R*-IRED-*Sr* and *R*-IRED-*St*, respectively, whereas the product of the *S*-IRED-*Pe* catalyzed biotransformation was obtained in 94.9% ee (Table 10, Figure S6).

Also in biotransformations with purified proteins excellent conversion rates could be obtained (summarized in detail in section 3.5).

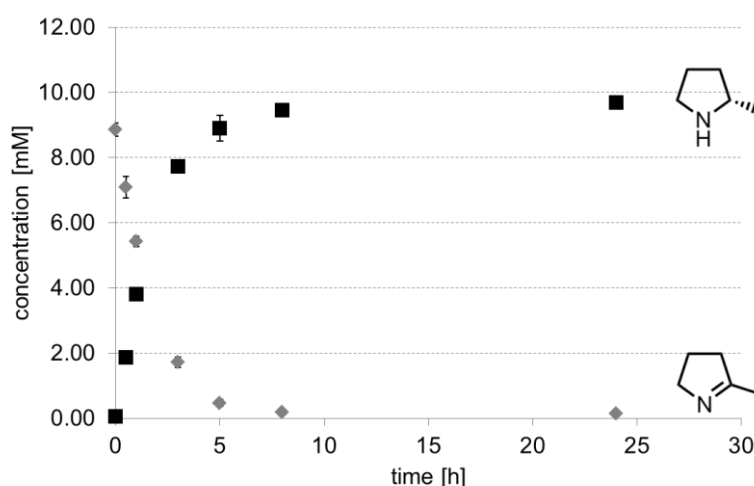


Figure 12: Time course of the reduction of 10 mM 2-methylpyrroline **1** to 2-methylpyrrolidine **2** by whole cells expressing the gene encoding for *S*-IRED-*Pe*. The measured points are the average of a triplicate and the error bars show the standard deviation.

To compare these three novel IREDs to the ones that were at that time described in literature, the kinetic constants were determined for the imine substrate **1**. In a spectrophotometric assay the initial decrease of the NADPH absorbance at 340 nm was monitored and the specific activities plotted *versus* the different employed substrate concentrations. As all three IREDs showed decreased activities at higher substrate loadings, the Michaelis-Menten equation was adapted to substrate inhibition kinetics. For all three enzymes the affinities for **1** were in the low mM range, but the turnover numbers showed greater variations. *R*-IRED-*Sr* is one of the most active IREDs for the turnover of this substrate, having a k_{cat} of approximately 1 s^{-1} . In contrast, the (*S*)-selective IRED showed comparably lower turnover numbers of only about 0.03 s^{-1} . The kinetic constants for this substrate for the three IREDs are summarized in Table 11.

After solving the first crystal structure of an IRED (the (*R*)-selective IRED from *Streptomyces kanamyceticus* (*R*-IRED-*Sk*)) a catalytic mechanism was proposed for this enzyme based on analogy with the structurally closely related enzyme family of the β -hydroxyacid dehydrogenases (β -HADs).^{142,216,217} It involves the protonation of the imine substrate by an Asp (position 187) in the active

3 RESULTS

site of the enzyme, followed by the reduction *via* the hydride transfer from NADPH.¹⁴² This Asp residue represents one of the highest conserved residues of IREDs and almost all of the (*R*)- type IREDs possess this amino acid (86% Asp and 11% Glu) at standard position 187.¹⁴⁵ However, it is a superfamily specific conserved amino acid (see also Figure 9) and with one exception all of the members of the (*S*)- type IREDs have a Tyr residue at this position.¹⁴⁵ These residues are located in the assumed active site cleft of the enzymes within a distance of 5-7 Å from the NADPH. To underline the importance of the Asp residue, the group of Prof. Dr. Gideon Grogan at University of York has performed mutagenesis at this position and the substitution with either Ala or Asn rendered *R*-IRED-*Sk* inactive (see also Figure 4).¹⁴² In order to confirm the crucial role of this residue and at the same time investigate whether the Tyr at the same position in the (*S*)- type superfamily could adopt the role of the proposed catalytic Asp, site directed mutagenesis with these three novel IREDs was performed. By mutating the respective residues to Ala, the proposed catalytic function of the enzymes should be abolished or at least diminished. The mutants were generated by QuikChange® PCR and indeed in biotransformations an effect was observed. The expression level of all three mutants (*R*-IRED-*Sr* D191A, *R*-IRED-*St* D193A and *S*-IRED-*Pe* Y208A) was about equal compared to the wt enzymes, based on SDS-PAGE analysis with the lysate of the soluble protein fraction. Yet, the (*R*)- selective IREDs showed decreased conversion rates to about 15% and 5%, for *R*-IRED-*Sr* and *R*-IRED-*St*, respectively, but not a complete inactivation (Table 10). Due to the full conversion of substrate **1** with the wild type enzymes, the comparison of the conversion rates was done with the initial measuring points 0.5 h and 1 h (Table 10). In contrast, the (*S*)- selective IRED hardly showed any conversion in 24 h (total product formation < 1%; Table 10). In addition to the decreased conversion rates, also the enantioselectivities for the enzymatic reduction decreased. Again the effect was more pronounced for *S*-IRED-*Pe*, for which a drop from about 95% ee to about 65% ee was observed (Table 10).

Table 10: Product formations and enantiomeric excess values in [%] for the reduction of 10 mM **1** with whole cells expressing IREDs and mutants thereof. All biotransformations were done in triplicates and the error represents the standard deviation. -: not detected.

IRED	product formation [%]				ee [%]
	0.5 h	1 h	8 h	24 h	
<i>R</i> -IRED- <i>Sr</i>	46.29 ± 0.42	89.79 ± 2.89	> 99	> 99	98.3 ± 0.0 (<i>R</i>)
<i>R</i> -IRED- <i>St</i>	29.58 ± 1.49	64.59 ± 4.19	> 99	> 99	99.0 ± 0.0 (<i>R</i>)
<i>S</i> -IRED- <i>Pe</i>	18.66 ± 0.12	38.07 ± 0.38	94.54 ± 1.33	96.84 ± 1.01	94.9 ± 0.0 (<i>S</i>)
<i>R</i> -IRED- <i>Sr</i> D191A	7.22 ± 0.14	14.89 ± 0.32	58.32 ± 4.21	63.73 ± 3.81	91.4 ± 0.1 (<i>R</i>)
<i>R</i> -IRED- <i>St</i> D193A	1.11 ± 0.23	2.17 ± 0.06	13.40 ± 0.35	17.42 ± 2.40	94.1 ± 0.0 (<i>R</i>)
<i>S</i> -IRED- <i>Pe</i> Y208A	-	-	0.37 ± 0.18	0.88 ± 0.21	65.7 ± 0.3 (<i>S</i>)

After purification of the *R*-IRED mutants, also their catalytic constants were determined, analogously to the wt enzymes. Both mutant enzymes showed decreased affinities and turnover numbers for imine substrate **1**. Overall the catalytic efficiency (k_{cat}/K_M) decreased by a factor of about 100 for *R*-IRED-*Sr* D191A and 400-fold for *R*-IRED-*St* D193A, respectively. In addition, both mutant enzymes showed enhanced substrate inhibition. The kinetic constants for the mutant enzymes are also summarized in

Table 11. Due to the low activity in whole cell biotransformations with *S*-IRED-*Pe* Y208A this enzyme was not purified for further analysis.

Table 11: Kinetic constants for the reduction of **1** with purified IREDs and mutants. All specific activities were determined in triplicates for varying concentrations of the substrate. To calculate k_{cat} , K_{M} and K_{i} the data was then fitted by nonlinear regression to the Michaelis-Menten equation.

enzyme	K_{M} [mM]	k_{cat} [s ⁻¹]	$k_{\text{cat}}/K_{\text{M}}$ [s ⁻¹ mM ⁻¹]	K_{i} [mM]	Michaelis-Menten plot
<i>R</i> -IRED- <i>Sr</i>	1.08 ± 0.13	0.96 ± 0.02	0.89 ± 0.11	28.40 ± 3.01	Figure S1
<i>R</i> -IRED- <i>St</i>	1.81 ± 0.07	0.45 ± 0.02	0.25 ± 0.02	21.07 ± 1.48	Figure S2
<i>S</i> -IRED- <i>Pe</i>	1.29 ± 0.15	26.32 × 10 ⁻³ ± 1.53 × 10 ⁻³	20.40 × 10 ⁻³ ± 2.61 × 10 ⁻³	33.28 ± 8.02	Figure S3
<i>R</i> -IRED- <i>Sr</i> D191A	11.19 ± 1.34	0.10 ± 0.01	8.98 × 10 ⁻³ ± 1.29 × 10 ⁻³	4.69 ± 0.41	Figure S4
<i>R</i> -IRED- <i>St</i> D193A	5.41 ± 0.80	3.04 × 10 ⁻³ ± 0.06 × 10 ⁻³	0.56 × 10 ⁻³ ± 0.08 × 10 ⁻³	17.16 ± 1.50	Figure S5

3.2 Biochemical characterization of the novel IREDs

As the available literature for characterized IREDs is still rather poor and many properties of these enzymes are unknown, in the following a biochemical characterization of the three newly selected enzymes was performed. This included the determination of the pH optima, the thermal stability of the enzymes and their activity in the presence of different organic solvents. As IREDs were described to form dimers in solution and the resolved crystal structures also indicate that this might be required for activity, the oligomerization state of these enzymes was determined by SEC in HPLC. The substrate profile and selectivity of *R*-IRED-*Sr*, *R*-IRED-*St* and *S*-IRED-*Pe* as well as the reactions they can catalyze will be discussed in the following chapters (3.3, 3.4, 3.5 and 3.6).

3.2.1 pH Profile of the IREDs

To optimize the use of IREDs in *in vitro* systems, the pH profile of the three novel IREDs was elucidated. To determine the optimal pH for the enzymatic reduction, the specific activity of the purified enzymes was recorded with substrate **1** using different buffer conditions. The stock solutions of the enzymes were prepared in highly concentrated form (30-50 mg/ml) and for the activity assays the IREDs had to be diluted by a factor of 50-1000. Hence, residual buffer components from the storage and purification could be neglected. The tested buffers involved a pH range from pH 4.0 to pH 10.0, always with two overlapping data points after switching to the next buffer systems. The overlapping data points allowed to check for effects provoked by the different buffer ions. For the pH range from 4.0 to 6.5 sodium citrate buffer according to McIlvaine¹⁸⁸ was used, from pH 6.0 to pH 8.0 sodium phosphate buffer was used, from pH 7.5 to pH 9.0 Tris HCl buffer was used and from pH 8.5 to pH 10.0 glycine/NaOH buffer was employed.

All three IREDs displayed a relatively broad pH profile, with their maximal specific activity determined at a neutral pH of 7.0 in sodium phosphate buffer. Above pH 9.0 and below pH 5.5 the activity rapidly decreased (Figure 13, Figure 14 and Figure 15). In contrast to a recent report in literature,¹⁴⁸ the pH profile of the Tyr containing *S*-IRED-*Pe* is comparable to the pH profiles of the (*R*)-selective IREDs that possess Asp in their active sites (see also 4.2).

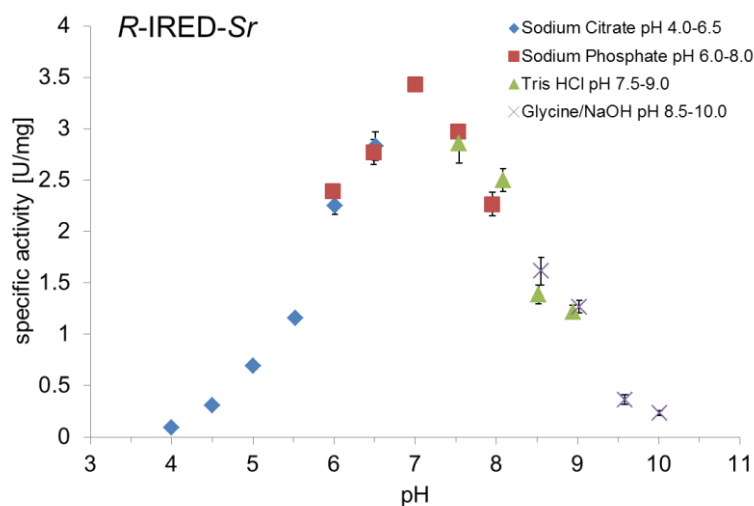


Figure 13: pH profile of *R-IRED-Sr* for the reduction of **1** in sodium citrate buffer (pH 4.0 - 6.5), sodium phosphate buffer (pH 6.0 - 8.0), Tris HCl buffer (pH 7.5 - 9.0) and glycine/NaOH buffer (pH 8.5 - 10.0). Specific activities were determined in triplicates with 5 mM of **1** at 30 °C and the error bars show the standard deviation.

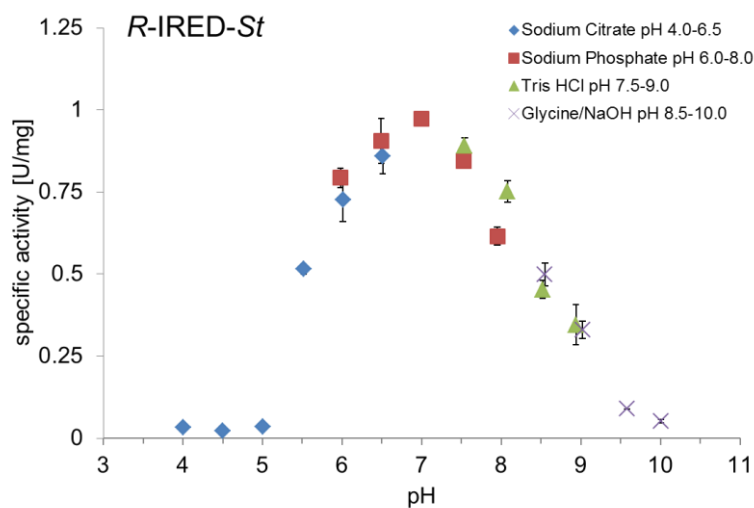


Figure 14: pH profile of *R-IRED-St* for the reduction of **1** in sodium citrate buffer (pH 4.0 - 6.5), sodium phosphate buffer (pH 6.0 - 8.0), Tris HCl buffer (pH 7.5 - 9.0) and glycine/NaOH buffer (pH 8.5 - 10.0). Specific activities were determined in triplicates with 5 mM of **1** at 30 °C and the error bars show the standard deviation.

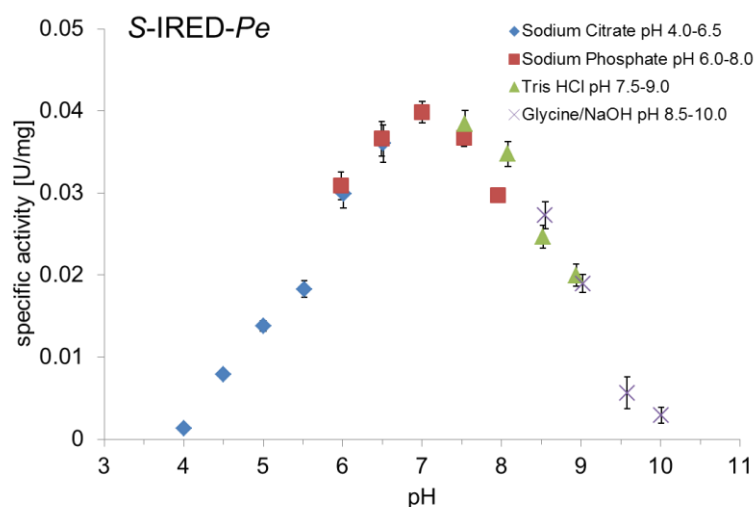


Figure 15: pH profile of *S-IRED-Pe* for the reduction of **1** in sodium citrate buffer (pH 4.0 - 6.5), sodium phosphate buffer (pH 6.0 - 8.0), Tris HCl buffer (pH 7.5 - 9.0) and glycine/NaOH buffer (pH 8.5 - 10.0). Specific activities were determined in triplicates with 5 mM of **1** at 30 °C and the error bars show the standard deviation.

3.2.2 Thermostability of the IREDs

Next to their pH dependency, the thermal stabilities of the three IREDs were investigated. In initial thermostability tests *S*-IRED-*Pe* showed enhanced resistance against inactivation at 30 °C and 40 °C, but the (*R*)- selective IREDs rapidly lost their activity at the higher temperature. For the determination of the half-life times the (*R*)- selective IREDs were therefore incubated at 30 °C and *S*-IRED-*Pe* at 50 °C. Regularly samples were taken and an activity assay with **1** as substrate performed. The declining residual specific activity was then fitted to an exponential decay function and the half-life time calculated. At 30 °C, the (*R*)- selective IREDs lost most of their activity within one day, resulting in half-life times of about 9 h and about 18 h for *R*-IRED-*Sr* and *R*-IRED-*St*, respectively (Figure 16 and Table 12). In contrast *S*-IRED-*Pe* was much more stable and after 7 days at 50 °C more than 70% of the residual activity could be detected. Based on this data, the calculated half-life time is > 400 h (Table 12).

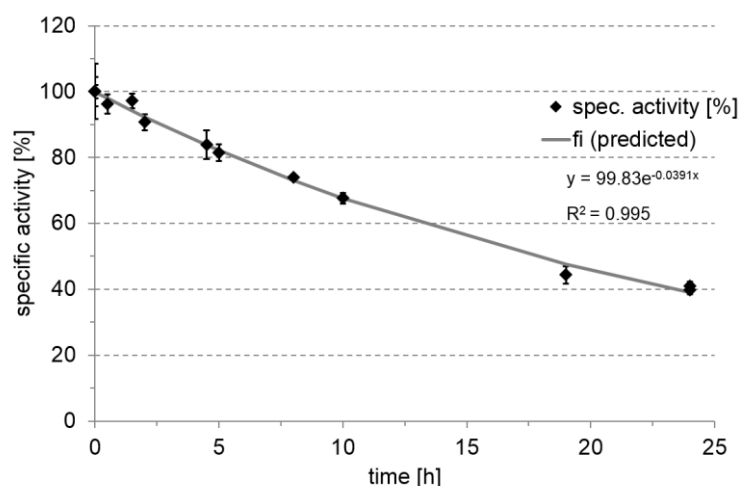


Figure 16: Residual specific activities in [%] for the reduction of 10 mM **1** to determine the half-life time of *R*-IRED-*St* after incubation at 30 °C. The decreasing activities were fitted to an exponential decay function of the formula $A=A_0 \cdot e^{-\lambda t}$ with A_0 representing the specific activity at $t = 0$ h (set as 100%). All activities were determined in triplicates and the error bars give the standard deviation.

Table 12: Half-life times of *R*-IRED-*Sr* and *R*-IRED-*St* at 30 °C and half-life time of *S*-IRED-*Pe* at 50 °C.

IRED	temperature [°C]	half-life time [h]	plot
<i>R</i> -IRED- <i>Sr</i>	30	9.2	Figure S21
<i>R</i> -IRED- <i>St</i>	30	17.8	Figure 16
<i>S</i> -IRED- <i>Pe</i>	50	> 400	Figure S22

In addition for all three IREDs temperatures were determined at which the enzymes retain 50% residual activity after incubation for a certain time (T_{50}). In literature, these T_{50} values are frequently used to quantify and compare thermostability.^{49,189} The time frame set in these experiments was 15 min and the resulting T_{50}^{15} [°C] values are summarized in Table 13. To determine the data, small samples of the IREDs were incubated for 15 min in a PCR cycler spanning a gradient from 25 °C to 70 °C. To ensure comparability of all samples the PCR cycler started at 8 °C, heated then for 15 min to the desired temperatures, followed again by a cooling step to 8 °C for 15 min. After that relaxation time, the residual specific activity with substrate **1** was determined and the data fitted to a four parameter dose-response

3 RESULTS

curve using nonlinear regression. From the fitting function the T_{50}^{15} [°C] was calculated. Close to 40 °C, the (*R*)- selective IREDs rapidly lost activity and the calculated T_{50}^{15} were about 39 °C and 38 °C for *R*-IRED-*Sr* and *R*-IRED-*St*, respectively (Table 13). As expected from the greater half-life time *S*-IRED-*Pe* had to be incubated at around 65 °C to reach the T_{50}^{15} (Table 13).

Table 13: Calculated temperatures at that the IREDs retain 50% activity after a 15 min incubation time (T_{50}^{15} [°C]).

IRED	T_{50}^{15} [°C]	plot
<i>R</i> -IRED- <i>Sr</i>	38.8	Figure S23
<i>R</i> -IRED- <i>St</i>	38.2	Figure S24
<i>S</i> -IRED- <i>Pe</i>	65.0	Figure 17

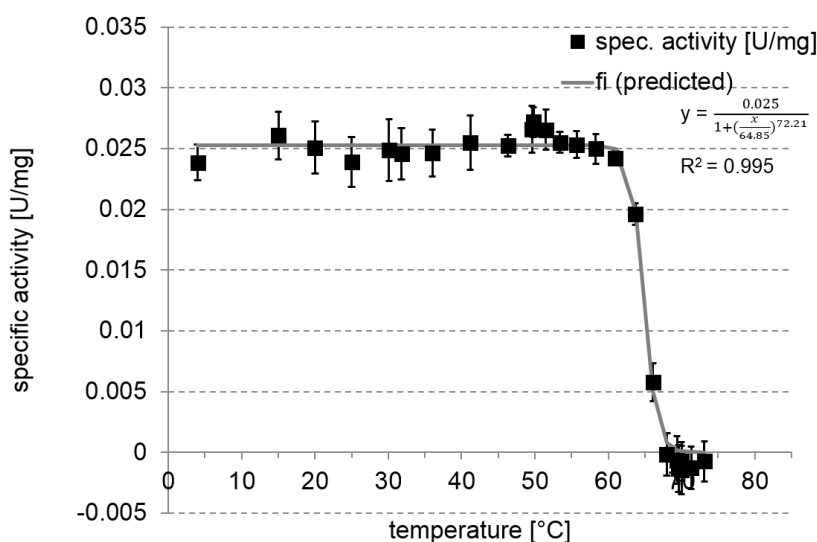


Figure 17: Specific activities for the reduction of 10 mM **1** in [U/mg] with *S*-IRED-*Pe* after incubation at different temperatures for 15 min. Activities were fitted to a sigmoidal dose-response curve to determine the T_{50}^{15} . Using the above shown data *S*-IRED-*Pe* displayed 50% residual activity when incubated at 65.0 °C for a period of 15 min. All activities were determined in triplicates and the error bars give the standard deviation.

Due to the higher thermal stability for *S*-IRED-*Pe* also the temperature-activity profile was recorded. The holder for the cuvette with the buffer was heated with a temperature-controlled water bath and in a second reference cuvette the temperature in the cuvette measured (see also Figure 7 for the experimental setup). After the desired reaction temperature stayed constant for some time, the reaction was started by the addition of *S*-IRED-*Pe*, substrate and NADPH. The specific activities were then calculated and plotted against the temperature. As it is generally agreed a temperature increase of about 10 °C resulted in the doubling of the reaction rates. The maximum activity was reported at ~ 65 °C, followed by a strong drop, due to the rapid inactivation of the enzyme (Figure S25).

3.2.3 Oligomerization of the IREDs

Dimerization was described for IREDs^{138,139} and most IRED crystal structures were also resolved as dimers (or dimers of dimers).^{142,144,148} Considering the three dimensional structure of IREDs, in which both subunits arrange by a so called reciprocal domain swapping,¹⁴² dimerization seems to be essential for the proper function of the enzyme. To check the oligomerization state of these three novel IREDs,

the purified proteins were analyzed by SEC in HPLC. Thereby also the degree of purity from the purification could be estimated more quantitatively than by SDS-PAGE. The calibration of the SEC column was performed with a gel filtration standard containing proteins and vitamins of known molecular weight. All IREDs eluted after around 13.8 min, a retention time that indicates that these proteins form dimers in solution (Figure 18).

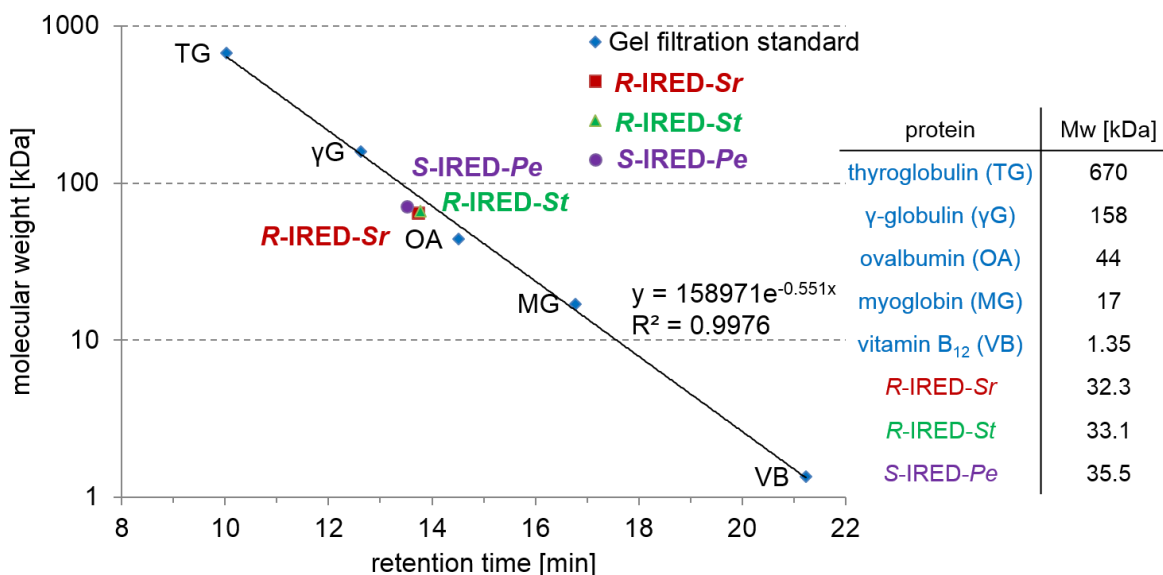


Figure 18: Calibration of the Yarra 3µ SEC-2000 column with a gel filtration standard from BioRad (blue diamonds) TG: thyroglobulin (670 kDa), γG: γ-globulin (158 kDa), OA: ovalbumin (44 kDa), MG: myoglobin (17 kDa), VB: vitamin B₁₂ (1.35 kDa). SEC analysis in HPLC was used for purity analysis of the IREDs and to examine their oligomerization state. According to the retention time of around 13.8 min, all three IREDs form dimers in solution.

3.2.4 Effect of organic solvents on the activity of the IREDs

In general amines are regarded as rather polar compounds, however some of the higher molecular weight imine substrates and amine products that were chosen for investigation display only limited solubility in aqueous buffer systems. In addition the preparation of sufficiently concentrated substrate stock solutions facilitates the experimental setup and enhances reproducibility. By the addition of small amounts of co-solvents also insufficient mixing might be avoided and the stability of hydrolytically unstable exocyclic imines enhanced. To avoid damaging the enzyme, the effect of different water miscible solvents on the IRED activity was investigated. The solvents selected for investigation were methanol (MeOH), ethanol (EtOH), dimethyl sulfoxide (DMSO), acetonitrile (ACN), glycerol, *tert*-butyl alcohol (*t*-BuOH), isopropyl alcohol (iProp) and acetone. All solvents were tested in concentrations from 5% to 25% (% v/v) and the specific activities of the IREDs with substrate **1** determined.

All three IREDs showed a similar trend with MeOH, glycerol and DMSO being well tolerated solvents (60% to 80% residual activity), whereas the other solvents often led in already low concentrations to strongly decreased activities (Figure 19, Figure 20 and Figure 21). Again, as already observed for the pH and the temperature profile, the (*S*)-selective IRED from *Paenibacillus elgii* showed the broadest tolerance *versus* non physiological conditions. Even in the presence of 25% MeOH around 60% of the initial activity is left. In addition to Figure 19, Figure 20 and Figure 21, all specific activities for the three IREDs at all concentrations of the eight solvents are summarized in Table S9.

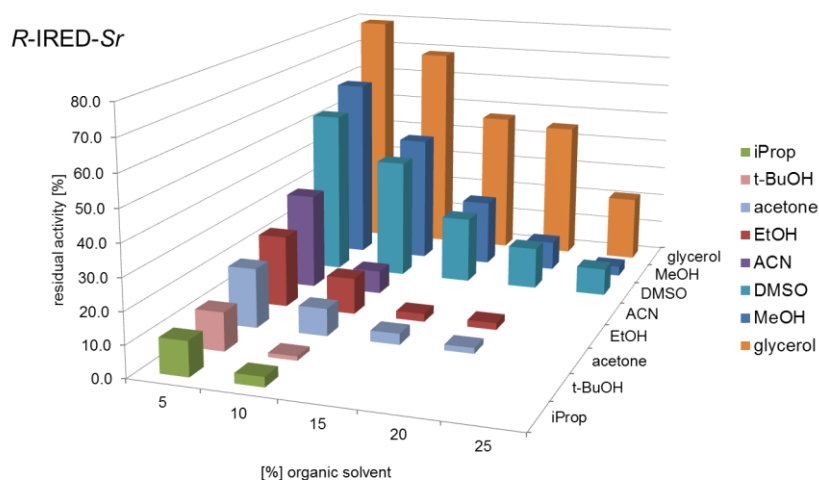


Figure 19: Effect of different water miscible organic solvents on the activity of *R-IRD-Sr*. All solvents were tested in concentrations from 5%-25%. The specific activity was recorded in triplicates with 5 mM of **1** as substrate. The reference value for 100% activity was determined for a solvent free system (sodium phosphate buffer 50 mM pH 7.0). Activities < 1% are not shown in Figure 19.

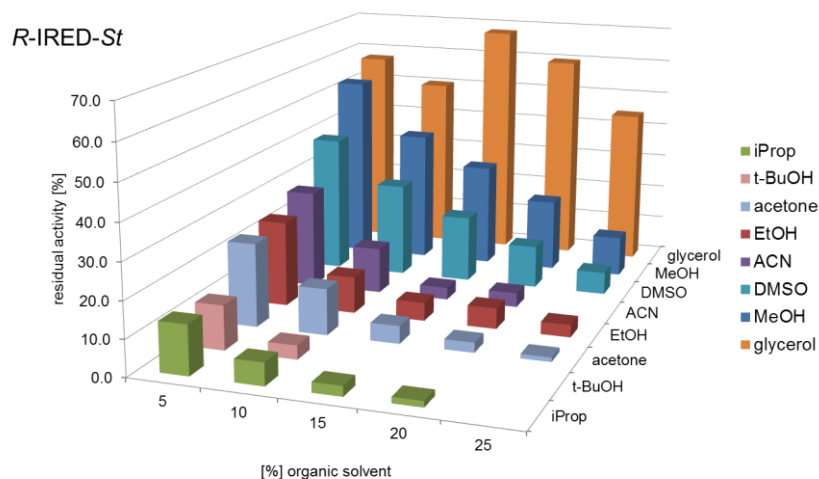


Figure 20: Effect of different water miscible organic solvents on the activity of *R-IRD-St*. All solvents were tested in concentrations from 5%-25%. The specific activity was recorded in triplicates with 5 mM of **1** as substrate. The reference value for 100% activity was determined for a solvent free system (sodium phosphate buffer 50 mM pH 7.0). Activities < 1% are not shown in Figure 20.

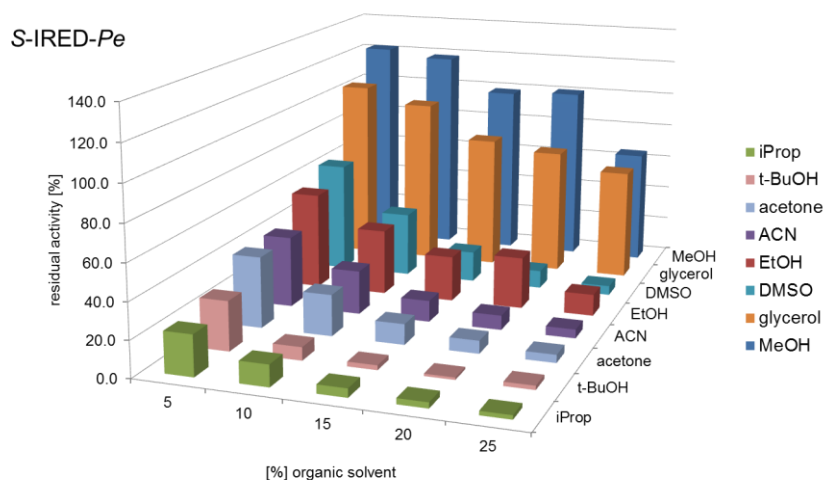


Figure 21 Effect of different water miscible organic solvents on the activity of *S-IRD-Pe*. All solvents were tested in concentrations from 5%-25%. The specific activity was recorded in triplicates with 5 mM of **1** as substrate. The reference value for 100% activity was determined for a solvent free system (sodium phosphate buffer 50 mM pH 7.0).

3.3 Whole cell biotransformations to investigate the substrate spectrum and the selectivity of the IREDs

The natural role of IREDs and the substrates that are converted by them in the host organisms are unknown, instead they were discovered by screening for microorganisms that were able to catalyze the stereoselective reduction of imine **1**.¹³⁷ To further explore the substrate scope and the selectivity of these three novel IREDs, whole cell biotransformations were performed with a panel of cyclic imine substrates, bearing different substituents next to the C=N double bond. In addition several isoquinoline derivatives were investigated for their activity and selectivity. As negative controls, cells with an empty pBAD33 plasmid were employed. For whole cell biotransformations always fresh cells had to be used, as after storage and freezing the cells lost considerable amounts of activity. Cells for biotransformations were used after expression over night at 25 °C. Prior to use cells were washed once with buffer.

To investigate the influence different ring sizes and other substituents next to the C=N double bond display on the activity and selectivity of the IREDs several cyclic piperideine substrates, analogously to the already tested five-membered cyclic imine substrate 2-methylpyrroline **1**, were selected for reduction. The chosen substrates 2-methylpiperideine **3a**, 2-phenylpiperideine **3b** and 2-*p*-fluorophenylpiperideine **3c** were not commercially available and had to be synthesized. Details about the synthesis of them, their purification and the NMR spectra are summarized in 2.21 and 7.12. The selected isoquinoline substrates included 3,4-dihydroisoquinoline **5a**, 1-methyl-3,4-dihydroisoquinoline **5b** and 6,7-dimethoxy-1-methyl-3,4-dihydroisoquinoline **5c**.

Biotransformations were done with a final OD₆₀₀ of 30 (~ 50 mg/ml cell wet weight) of IRED expressing cells and glucose for *in situ* cofactor regeneration. Regularly samples of the biotransformation were taken and the conversions for all of these substrates determined by GC or HPLC analysis using calibration curves with authentic standards of the substrates and products. The selectivities of the products were determined by chiral GC or chiral HPLC analysis. Assignment of the produced enantiomers was done by comparison with authentic enantiopure standards or by comparison with the available literature. Details therefore are given in the sections 2.18 and 2.19 and in Figure S6, Figure S7, Figure S8 and Figure S11.

Except for substrate **5c** all three IREDs converted this panel of model compounds. Often conversion rates were high and led to full substrate consumption in 24 h (Table 14). By increasing the ring size from a pyrroline to a piperideine scaffold, conversion rates strongly increased. Substrate **3a** was fully converted in less than 1 h with cells expressing an *R*-IRED. Also for cells with *S*-IRED-*Pe* full conversion was obtained and within < 5 h this required considerably less time than for imine **1**. However, although the substrate was completely converted with all three IREDs, only about 65% of the product could be recovered in all of these biotransformations (Table 14). In contrast, cells with an empty pBAD33 plasmid did not show any conversion. By chiral GC the enantiomeric excess for product **4a** was determined and found to be > 99% for all three IREDs, with no traces from the opposite enantiomer detectable (Figure S7). In contrast, with the phenyl substituted substrate **3b** conversion rates strongly dropped and for *S*-IRED-*Pe* after 24 h only 14% of the product was detected. Using cells expressing an *R*-IRED within 8 h about 50% of the product could be obtained (Table 14), although the substrate was fully consumed by the cells (exemplarily shown in Figure S9 for *R*-IRED-*Sf*). Along with the decreased conversion rates

3 RESULTS

also the selectivity for product **4b**, that was obtained in these biotransformations, decreased. The highest enantiomeric excess of about 68% ee for (*R*)-**4b** was obtained with *S*-IRED-*Pe* (Table 14 and Figure S7)^{II}. Interestingly with a *p*-fluorophenyl modification, substrate **3c** was converted much better by all three IREDs. In already 1 h reaction time cells with *R*-IRED-*St* produced > 80% of the product and the use of cells with *R*-IRED-*Sr* resulted in > 90% conversion to the amine in 24 h (Figure S10). Transformation by *S*-IRED-*Pe* was slightly lower, but still led to 63% product formation in 24 h (Table 14). The selectivities for this product (**4c**) were determined by chiral HPLC and in the biotransformations excellent enantiomeric excess values of up to 90% were obtained for all three IREDs (Table 14 and Figure S8). The full dataset containing all samples and the ee values measured at different times is given in Table S2.

Table 14: Product formations and enantiomeric excess values in [%] obtained in whole cell biotransformations with 10 mM of piperidine substrates **3a**, **3b** and **3c** performed with *E. coli* JW5510 expressing *R*-IRED-*Sr*, *R*-IRED-*St* or *S*-IRED-*Pe*. The values in Table 14 are the average of a triplicate and the error gives the standard deviation. The change in the selectivity from the (*R*)- to the (*S*)- product for *R*-IRED-*Sr* and *R*-IRED-*St* and *vice versa* in the case of *S*-IRED-*Pe* is caused by a change in the priority of the substituents for the Cahn-Ingold-Prelog assignment.

		3a: R = methyl 3b: R = phenyl 3c: R = <i>p</i> -fluorophenyl		4a: R = methyl 4b: R = phenyl 4c: R = <i>p</i> -fluorophenyl	
substrate	IRED	product formation [%]			ee [%]
		1 h	8 h	24 h	
3a	<i>R</i> -IRED- <i>Sr</i>	64.38 ± 1.48	64.22 ± 2.21	64.35 ± 8.15	> 99 (<i>R</i>)
	<i>R</i> -IRED- <i>St</i>	66.99 ± 2.72	69.86 ± 7.11	64.81 ± 2.02	> 99 (<i>R</i>)
	<i>S</i> -IRED- <i>Pe</i>	58.95 ± 4.00	74.18 ± 6.89	69.00 ± 1.04	> 99 (<i>S</i>)
3b	<i>R</i> -IRED- <i>Sr</i>	20.88 ± 0.31	43.62 ± 1.26	48.02 ± 1.83	23.2 ± 0.4 (<i>S</i>)
	<i>R</i> -IRED- <i>St</i>	26.69 ± 0.84	50.05 ± 2.09	47.79 ± 1.20	56.0 ± 0.3 (<i>S</i>)
	<i>S</i> -IRED- <i>Pe</i>	1.06 ± 0.11	9.54 ± 0.30	14.22 ± 0.19	67.9 ± 0.5 (<i>R</i>)
3c	<i>R</i> -IRED- <i>Sr</i>	46.67 ± 2.34	89.79 ± 8.17	94.06 ± 4.37	86.5 ± 0.0 (<i>S</i>)
	<i>R</i> -IRED- <i>St</i>	82.26 ± 4.96	96.11 ± 3.42	94.39 ± 5.22	90.0 ± 0.0 (<i>S</i>)
	<i>S</i> -IRED- <i>Pe</i>	8.17 ± 1.05	49.95 ± 1.39	63.00 ± 0.41	87.0 ± 0.0 (<i>R</i>)

Except from substrate **5c**, isoquinolines were well accepted by all three IREDs. The simplest member of them **5a**, was fully converted with all three IREDs in less than 8 h (Table 15 and complete dataset in Table S3). Using the methyl substituted analog **5b** it was shown that these transformations also proceed selectively (Figure S11). Conversions for substrate **5b** reached > 95% using the (*R*)- selective IREDs, with the better enantioselectivity for the (*R*)- product displayed by *R*-IRED-*Sr* (93% ee). Although *R*-IRED-*Sr* and *R*-IRED-*St* are closely related (> 54% sequence identity^{III}), the selectivity for the product in this biotransformation differed considerably and with *R*-IRED-*St* it was obtained with an ee of only around 50%. *S*-IRED-*Pe* produced the opposite enantiomer in about 95% ee with 80% conversion in 24 h (Table 15). In contrast, the bulkier substrate **5c** was only accepted by *S*-IRED-*Pe*. In 24 h

^{II}: The opposite stereoselectivity for products **4b** and **4c**, compared to **4a** is not caused by a different optical orientation, but is due to the change in the priority numbering of the substituents for the Cahn-Ingold-Prelog assignment.²⁹¹

^{III}: Pairwise sequence alignments were performed using the European Molecular Biology Open Software Suite (EMBOSS) applying the Needleman-Wunsch algorithm to the native IRED sequence.²⁹²⁻²⁹⁴

around 15% of the product was formed and this increased to about 30% in 48 h (Table S3). By chiral HPLC the formation of the (*S*)- enantiomer of the product could be confirmed, but no sufficient resolution from the residual substrate was obtained to be able to calculate an *ee* value^{IV}. Both (*R*)- selective enzymes did not lead to any product formed (Table 15). These results were meanwhile also confirmed by data published in literature, indicating a broader range of substrates accepted by *S*-IREDS.^{143,147} Interestingly for this substrate also cells with an empty pBAD33 plasmid showed some substrate consumption (~ 20% in 24 h, Figure S12), but no product formation could be detected. The full dataset for the whole cell biotransformations with isoquinolines **5a** to **5c** with all values is given in Table S3. A summary of the conversions and selectivities for all of the whole cell biotransformation after 24 h is also given in Figure 37.

Table 15: Product formations and enantiomeric excess values in [%] obtained in whole cell biotransformations with 10 mM of isoquinoline substrates **5a**, **5b** and **5c** performed with *E. coli* JW5510 expressing *R*-IRED-*Sr*, *R*-IRED-*St* or *S*-IRED-*Pe*. The values in Table 15 are the average of a triplicate and the error gives the standard deviation. -: not detected; n.a.: not available; n.d.: not determined.

substrate	IRED	product formation [%]			<i>ee</i> [%]
		1 h	8 h	24 h	
5a	<i>R</i> -IRED- <i>Sr</i>	75.52 ± 4.18	> 99	> 99	n.a.
	<i>R</i> -IRED- <i>St</i>	83.75 ± 2.91	> 99	> 99	n.a.
	<i>S</i> -IRED- <i>Pe</i>	67.14 ± 0.91	> 99	> 99	n.a.
5b	<i>R</i> -IRED- <i>Sr</i>	51.59 ± 3.32	99.32 ± 6.35	91.51 ± 6.71	93.0 ± 0.2 (<i>R</i>)
	<i>R</i> -IRED- <i>St</i>	37.14 ± 0.93	98.06 ± 3.63	94.18 ± 4.14	50.7 ± 0.1 (<i>R</i>)
	<i>S</i> -IRED- <i>Pe</i>	9.25 ± 0.31	54.75 ± 2.45	79.42 ± 4.75	94.9 ± 0.1 (<i>S</i>)
5c	<i>R</i> -IRED- <i>Sr</i>	-	-	-	-
	<i>R</i> -IRED- <i>St</i>	-	-	-	-
	<i>S</i> -IRED- <i>Pe</i>	-	9.62 ± 0.85	14.82 ± 0.75	n.d. (<i>S</i>)

^{IV}: The separation of the enantiomers of product **6c** was described with different chiral HPLC methods by Leipold *et al.*¹⁴³ and Heath *et al.*¹²⁰ using a Chiralcel OD-H column and by Quinto *et al.*,²⁹⁵ Dürrenberger *et al.*¹³⁴ and Muñoz Robles *et al.*¹³⁶ with a Chiralpak IC column. The columns Chiralpak IB (equivalent to Chiralcel OD-H)²⁹⁶ and Chiralpak IC were available and all of the described methods tested, however none of them resulted in a sufficient separation of the reaction products. In all cases one of the enantiomers co-eluted with the residual substrate and method optimization also did not lead to a satisfactory separation. With Chiralpak IB the (*R*)- enantiomer of the product eluted first but overlapped with the peak of substrate **5c**. In these runs the formed product (*S*)-**6c** could be detected. With Chiralpak IC the (*S*)- enantiomer of the product eluted first but no separation of the residual imine substrate was possible. With this method nothing of (*R*)-**6c** could be detected and therefore it was concluded that the enzyme is (*S*)- selective.

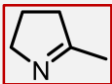
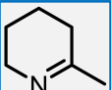
3.4 Determination of IRED kinetic parameters to investigate the substrate preference

To determine not only the conversions and the selectivities for whole cell biotransformations, but also get insights into the substrate preference of the three novel IREDs, kinetic constants were determined for the set of cyclic imine model substrates (substrates **1**, **3a** to **3c** and **5a** to **5b**).

Kinetic constants were determined by spectrophotometrically monitoring the decrease of the NADPH absorbance and calculation of the initial specific activities with different substrate concentrations. The kinetics of the three enzymes with substrate **3a** were determined as described above for **1**, using a wavelength of 340 nm. Due to their strong absorbance at 340 nm for substrates **3b**, **3c**, **5a** and **5b** a wavelength of 370 nm was used.

In general the kinetic constants reflect the conversion rates from the biotransformation employing whole cells expressing the IREDs (see 3.3). For the substrates **1**, **3a** and **5a** higher turnover numbers were measured compared to their substituted analogs **3b** to **3c** and **5b** (Table 17 for *R*-IRED-*Sr*, Table 18 for *R*-IRED-*St* and Table 19 for *S*-IRED-*Pe*). In the biotransformations this is reflected by higher conversion rates. For isoquinoline substrates **5a** and **5b** higher affinities were measured for all IREDs, compared to the pyrroline and piperidine substrates. The determined K_M values for **5a** and **5b** are in the low μM range, compared to affinities in the mid μM to the mM range for substrates **1** and **3a** to **3c** (Table 17, Table 18 and Table 19). By directly comparing substrates **1** and **3a** it becomes obvious that all IREDs prefer six-membered rings as substrates, compared to pyrrolines. The Michaelis-Menten plots for these two substrates recorded with *S*-IRED-*Pe* are shown in Figure 22. The catalytic efficiency (k_{cat}/K_M) of this enzyme for substrate **3a** is approximately four times higher than for **1** (Table 16), meaning that if both substrates would be present to the enzyme at the same time, it would discriminate them in favor of **3a**. The same tendency was much more pronounced, for the *R*-IREDs that showed about 60- and 160-times higher catalytic efficiency (*R*-IRED-*Sr* and *R*-IRED-*St*, respectively) comparing these two substrates (Table 16). Indeed, the use of substrate **3a** with *R*-IRED-*Sr* resulted in one of the highest observed k_{cat}/K_M value for all IRED substrates.^{107,147,148,150} As observed for substrates **1** and **3a** (see for example in Figure 22), IREDs tend to be inhibited by some of the substrates at higher concentrations. The inhibition was however less pronounced for *S*-IRED-*Pe* and often inhibition constants were in the range of 100 mM.

Table 16: Comparison of the catalytic efficiency (k_{cat}/K_M) of *R*-IRED-*Sr*, *R*-IRED-*St* and *S*-IRED-*Pe* with substrates **1** and **3a**. All three enzymes prefer the piperidine substrate **3a**.

k_{cat}/K_M [s ⁻¹ mM ⁻¹]	 1	 3a
<i>R</i> -IRED- <i>Sr</i>	0.89 ± 0.11	54.81 ± 4.28
<i>R</i> -IRED- <i>St</i>	0.25 ± 0.02	35.65 ± 2.65
<i>S</i> -IRED- <i>Pe</i>	20.40 × 10 ⁻³ ± 2.61 × 10 ⁻³	84.36 × 10 ⁻³ ± 4.91 × 10 ⁻³

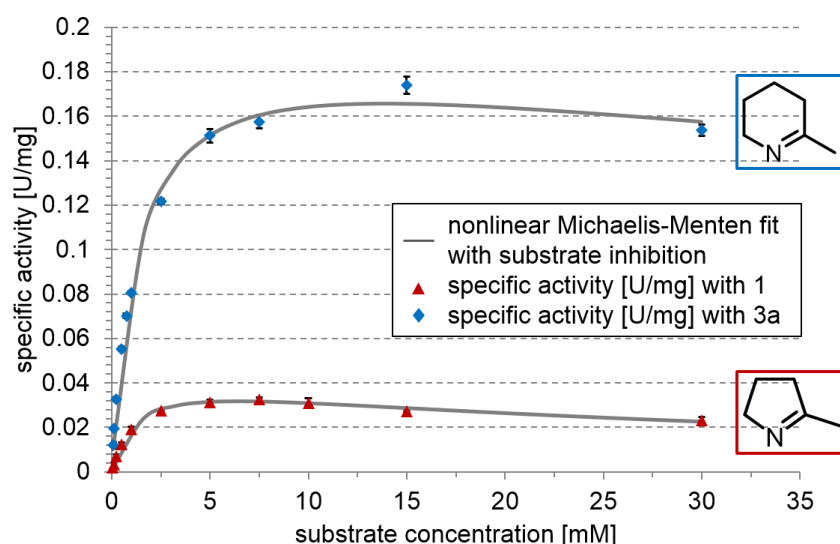


Figure 22: Michaelis-Menten plots for *S*-IRED-*Pe* with substrates **1** and **3a**. The six-membered piperidine substrate is reduced with an about four times higher catalytic efficiency. The enzyme was inhibited by both substrates at higher concentrations.

Table 17: Summary of the kinetic constants recorded for *R*-IRED-*Sr* with the panel of cyclic imine model substrates **1**, **3a** - **3c** and **5a** - **5b**. All specific activities were determined in triplicates for varying concentrations of the substrate. To calculate k_{cat} , K_{M} and K_{I} the data was then fitted by nonlinear regression to the Michaelis-Menten equation.

imine	K_{M} [μM]	k_{cat} [s^{-1}]	$k_{\text{cat}}/K_{\text{M}}$ [$\text{s}^{-1} \text{mM}^{-1}$]	K_{I} [mM]	Michaelis-Menten plot
1	$1.08 \times 10^3 \pm 0.13 \times 10^3$	0.96 ± 0.02	0.89 ± 0.11	28.40 ± 3.01	Figure S1
3a	195.84 ± 15.09	10.74 ± 0.14	54.81 ± 4.28	10.78 ± 1.60	Figure S34
3b	450.25 ± 10.27	$43.13 \times 10^{-3} \pm 0.64 \times 10^{-3}$	$98.78 \times 10^{-3} \pm 2.60 \times 10^{-3}$	16.27 ± 1.64	Figure S37
3c	376.37 ± 38.42	$44.41 \times 10^{-3} \pm 1.21 \times 10^{-3}$	0.12 ± 0.01	-	Figure S40
5a	50.43 ± 5.80	0.42 ± 0.01	8.36 ± 0.98	5.95 ± 1.41	Figure S43
5b	78.17 ± 16.21	0.22 ± 0.01	2.84 ± 0.61	23.89 ± 0.78	Figure S46

Table 18: Summary of the kinetic constants recorded for *R*-IRED-*St* with the panel of cyclic imine model substrates **1**, **3a** - **3c** and **5a** - **5b**. All specific activities were determined in triplicates for varying concentrations of the substrate. To calculate k_{cat} , K_{M} and K_{I} the data was then fitted by nonlinear regression to the Michaelis-Menten equation.

imine	K_{M} [μM]	k_{cat} [s^{-1}]	$k_{\text{cat}}/K_{\text{M}}$ [$\text{s}^{-1} \text{mM}^{-1}$]	K_{I} [mM]	Michaelis-Menten plot
1	$1.81 \times 10^3 \pm 0.07 \times 10^3$	0.45 ± 0.02	0.25 ± 0.02	21.07 ± 1.48	Figure S2
3a	229.59 ± 16.24	8.18 ± 0.19	35.65 ± 2.65	31.22 ± 3.66	Figure S35
3b	265.67 ± 15.01	$119.41 \times 10^{-3} \pm 4.04 \times 10^{-3}$	0.45 ± 0.03	6.55 ± 0.83	Figure S38
3c	319.00 ± 14.46	0.20 ± 0.00	0.61 ± 0.03	10.68 ± 0.39	Figure S41
5a	57.67 ± 9.88	0.33 ± 0.02	5.79 ± 1.08	3.62 ± 0.74	Figure S44
5b	26.41 ± 3.38	$101.03 \times 10^{-3} \pm 1.78 \times 10^{-3}$	3.83 ± 0.49	14.52 ± 2.02	Figure S47

3 RESULTS

Table 19: Summary of the kinetic constants recorded for *S*-IRED-*Pe* with the panel of cyclic imine model substrates **1**, **3a** - **3c** and **5a** - **5b**. All specific activities were determined in triplicates for varying concentrations of the substrate. To calculate k_{cat} , K_M and K_I the data was then fitted by nonlinear regression to the Michaelis-Menten equation.

imine	K_M [μM]	k_{cat} [s^{-1}]	k_{cat}/K_M [$\text{s}^{-1}\text{mM}^{-1}$]	K_I [mM]	Michaelis-Menten plot
1	$1.29 \times 10^3 \pm 0.15 \times 10^3$	$26.32 \times 10^{-3} \pm 1.53 \times 10^{-3}$	$20.40 \times 10^{-3} \pm 2.61 \times 10^{-3}$	33.28 ± 8.02	Figure S3
3a	$1.95 \times 10^3 \pm 0.43 \times 10^3$	$117.78 \times 10^{-3} \pm 3.27 \times 10^{-3}$	$84.36 \times 10^{-3} \pm 4.91 \times 10^{-3}$	140.38 ± 20.54	Figure S36
3b	$1.42 \times 10^3 \pm 0.05 \times 10^3$	$2.74 \times 10^{-3} \pm 0.09 \times 10^{-3}$	$1.93 \times 10^{-3} \pm 0.10 \times 10^{-3}$	7.72 ± 0.23	Figure S39
3c	$2.82 \times 10^3 \pm 0.08 \times 10^3$	$10.31 \times 10^{-3} \pm 0.05 \times 10^{-3}$	$3.66 \times 10^{-3} \pm 0.11 \times 10^{-3}$	-	Figure S42
5a	126.21 ± 4.33	$109.40 \times 10^{-3} \pm 2.23 \times 10^{-3}$	0.87 ± 0.04	91.26 ± 9.74	Figure S45
5b	137.79 ± 9.83	$11.16 \times 10^{-3} \pm 0.37 \times 10^{-3}$	$81.03 \times 10^{-3} \pm 6.38 \times 10^{-3}$	-	Figure S48

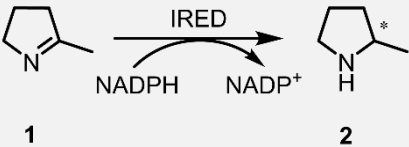
3.5 Biotransformations with purified IREDs

3.5.1 Establishing biotransformations with purified IREDs and 2-methylpyrroline **1**

Next to their application as whole cell biocatalysts, the use of IREDs was also tested in purified form. Although the required purification of the enzymes and the need for a cofactor regeneration system, initially represents an increased effort, it could become of advantage for an overall process as the use of isolated enzymes might facilitate product recovery and downstream processing or might eliminate competing side reactions.^{38,45,46,62} Ketoreductases (KREDs) for examples are nowadays usually employed in purified form.⁴⁵

To establish a setup for biotransformations with isolated IREDs, the reduction of **1** was investigated. For regeneration of the NADPH cofactor glucose-6-phosphate and glucose-6-phosphate dehydrogenase were chosen. Using 250 $\mu\text{g}/\text{ml}$ of the enzyme, with *R*-IRED-*Sr* and *R*-IRED-*St* the substrate could be fully converted within 1 h as shown in Table 20 and Figure 23. As already observed in whole cell biotransformations and confirmed by determining the kinetic constants, the use of *S*-IRED-*Pe* resulted in a slower conversion rate but after 24 h > 99% of substrate **1** were reduced to the amine by the enzyme (Table 20). As control for these biotransformations and all of the following that were performed with purified proteins, the respective IREDs were heat inactivated (95 °C for 10 min) and in none of these control reactions any product formation could be observed.

Table 20: Conversion of 10 mM substrate **1** to product **2** in [%] with purified IREDs. The biotransformations were performed in triplicates and the errors give the standard deviation.

					
substrate	IRED	product formation [%]			
		0.5 h	1 h	8 h	24 h
1	<i>R</i> -IRED- <i>Sr</i>	97.45 ± 3.69	> 99	> 99	> 99
	<i>R</i> -IRED- <i>St</i>	68.53 ± 0.82	99.11 ± 0.65	> 99	> 99
	<i>S</i> -IRED- <i>Pe</i>	6.07 ± 0.00	14.49 ± 0.06	81.91 ± 1.64	> 99

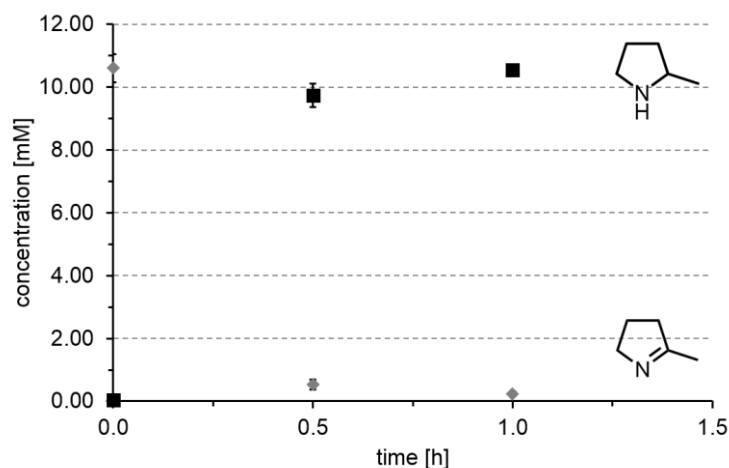


Figure 23: Time course for the reduction of 10 mM imine **1** to amine **2** with purified *R*-IRED-*Sr*. All measured points are the average of a triplicate and the error bars show the standard deviation.

3.5.2 The reduction of exocyclic imine substrates and the optimization of biotransformations with purified IREDs

To explore the substrate scope and the reactions that can be catalyzed by IREDs, their activity was tested with some more challenging exocyclic imines, representing a new class of substrates for these enzymes. Due to the hydrolytic sensitive nature of the C=N double bond these substrates are generally expected to be less stable.^{218,219} The use of isolated enzymes might therefore be preferable compared to whole cell biocatalysts as in such a system no transport barrier across the cell membrane exists.

In a first test the conversions of two exocyclic imine substrates were tested with the IREDs. The selected substrates were benzylidenemethylamine **7** and benzylideneaniline **9**. By GC analysis low activity for all three IREDs with **7** could be detected and **9** was converted in low amounts with the (*R*)-selective IREDs. As an initial optimizing step, the enzyme amount used for the biotransformation was increased to 2.5 mg/ml and the reaction examined at different pH values. Whereas at pH 7.0 and below mainly the hydrolysis products of the imines (benzaldehyde **11** and aniline **12**) were detected, at pH 8.0 using the increased amount of enzymes for all three IREDs with substrate **7** conversions to the amine product **8** well above the background could be obtained (14% with *S*-IRED-*Pe* and > 50% with *R*-IRED-*St*; Table 21, full dataset shown in Table S4). In addition for imine substrate **9** increased formation of the amine product could be detected. The best conversions were observed by the use of *R*-IRED-*St* (about 67%), whereas it remained low for *R*-IRED-*Sr* (< 10% product formation, Table 22, full dataset shown in Table S5) and with *S*-IRED-*Pe* only traces of the product could be detected. Next to the amine products, in both biotransformations (**7** and **9** as substrate) two byproducts could be detected in relatively high quantities (depending on the enzyme and substrate from 3% to > 50%). These two byproducts were identified as benzylalcohol **13** and benzylamine **14**.

The further optimization of the setup for the reduction of exocyclic imines aimed for a deeper understanding of the formation of the two reaction byproducts benzylalcohol **13** and benzylamine **14**. The formation of imines by the condensation of carbonyls and amines, as well as their hydrolysis is a spontaneous process. In an aqueous buffer system however it is expected not to be on the side of the

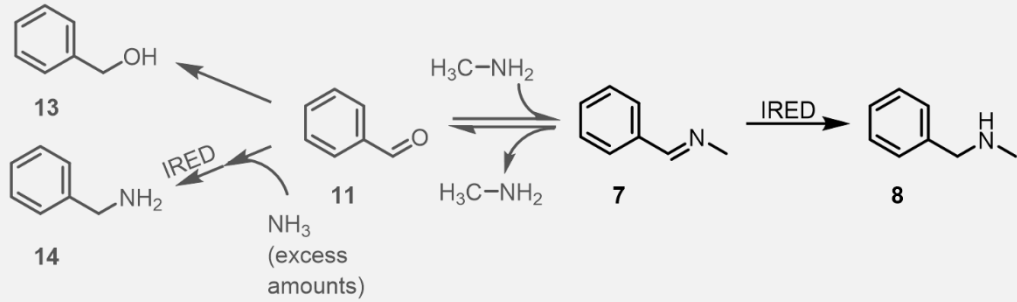
3 RESULTS

imine. The reactions leading to these two byproducts are therefore assumed to be due to the rapid hydrolysis of the imine substrate in the aqueous buffer system.

The reduction to the alcohol could theoretically be due to several issues. As neither the natural substrate nor the mechanisms of the IREDs is fully understood, yet, it should be taken into account that these enzymes might also be able to reduce carbonyl compounds nevertheless, in literature all attempts to catalyze the reduction of others than C=N double bonds failed.^{138,146,147} Another possibility for the reduction of the C=O double bond could be the contamination of the enzyme preparation with co-purified KREDs. In the initial purifications of the IREDs it was attempted to maximize the yields of the enzymes and therefore the enzymes used in the biotransformations described above had purities of less than 85% as determined by SEC in HPLC (Table 23, Figure 24 and Figure S31).

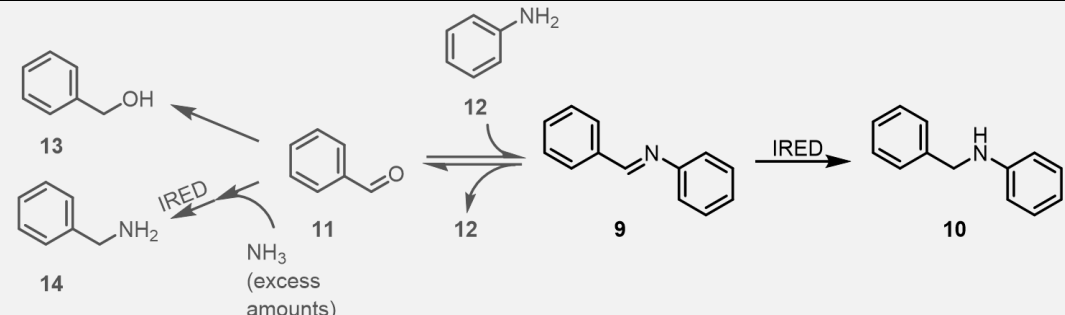
As described above the formation of imines is in an equilibrium with their hydrolysis. Although their formation in the aqueous system is assumed to be unfavored, small amounts of the imine are present. Thus, the second byproduct benzylamine was formed by a reductive amination reaction of benzaldehyde **11** with ammonia. This means, that IREDs represent very effective catalysts in withdrawing already small amounts of imines from this equilibrium. A possible source for the ammonia that led to the reductive amination reaction might be provided by the cofactor regeneration system. The employed glucose-6-phosphate dehydrogenase was supplied as ammonium sulfate precipitation and by its application considerable amounts of ammonia (final concentration ~ 30 mM) are transferred to the reaction system.

Table 21: Formation of product **8** in [%] by reduction of 10 mM of the exocyclic imine substrate **7** with all three IREDs. Experiments were done in triplicates and errors give the standard deviation. Due to the instability of the imine bond in the aqueous buffer system, substrate **7** hydrolyzed to benzaldehyde **11** and methylamine. The formation of two new byproducts by the further conversion of **11** is also given in [%]. Reduction of **11** is assumed to be caused by contaminating KREDs in the purified enzyme preparation. The reductive amination of **11** is assumed to be catalyzed by the IREDs with the cofactor regeneration system (supplied as ammonium sulphate precipitation) as the nitrogen source. -: not detected.



time [h]	product formation [%]								
	R-IRED-Sr			R-IRED-St			S-IRED-Pe		
	8	13	14	8	13	14	8	13	14
1	9.81 ± 0.26	4.44 ± 0.16	-	8.26 ± 0.29	-	-	-	-	-
3	22.77 ± 0.84	12.73 ± 0.86	-	15.26 ± 0.09	2.43 ± 0.39	-	4.22 ± 0.37	-	-
24	42.01 ± 0.92	46.22 ± 1.95	11.77 ± 0.15	56.67 ± 0.36	4.35 ± 0.23	-	13.92 ± 0.51	3.83 ± 0.55	-

Table 22: Formation of product **10** in [%] by reduction of 10 mM of the exocyclic imine substrate **9** with the (*R*)-selective IREDs. Experiments were done in triplicates and errors give the standard deviation. Due to the instability of the imine bond in the aqueous buffer system, substrate **9** hydrolyzed to benzaldehyde **11** and aniline **12**. The formation of two new byproducts by the further conversion of **11** is also given in [%]. Reduction of **11** is assumed to be caused by contaminating KREDs in the purified enzyme preparation. The reductive amination of **11** is assumed to be catalyzed by the IREDs with the cofactor regeneration system (supplied as ammonium sulphate precipitation) as the nitrogen source.



time [h]	product formation [%]					
	<i>R</i> -IRED- <i>Sr</i>			<i>R</i> -IRED- <i>St</i>		
	10	13	14	10	13	14
1	0.91 ± 0.11	9.07 ± 0.60	2.61 ± 0.20	11.89 ± 0.42	1.68 ± 0.04	1.96 ± 0.07
3	3.58 ± 0.64	19.93 ± 1.08	3.21 ± 0.19	33.90 ± 1.63	2.73 ± 0.10	1.83 ± 0.05
24	6.49 ± 2.65	64.14 ± 2.77	7.59 ± 0.46	67.00 ± 13.99	10.49 ± 0.82	4.30 ± 0.39

To proof the above mentioned considerations for byproduct formation and further optimize the setup to suppress their formation, biotransformations with imine **7** were repeated under modified conditions. First, to confirm that the cofactor regeneration system supplied the ammonia for the reductive amination reaction, this glucose-6-phosphate dehydrogenase preparation was substituted by a lyophilized formulation from a different vendor. The use of this salt free version should prevent the amination reaction (formation of benzylamine **14**).

To check for contaminating KREDs in the enzyme preparation, one of the applied IREDs (*R*-IRED-*Sr*, approx. 84% purity, Table 23, Figure 24 and Figure S31) was subjected to a further purification step by ion exchange chromatography with a MonoQ column. After the ion exchange chromatography an increase in purity could be observed by SDS-PAGE and in HPLC analysis (Table 23, Figure 24 and Figure S32). The purity of the peak fractions from the MonoQ purification was determined to be > 95% (Table 23). The fractions B12 and B11 of this enzyme preparation (Figure 24) were now combined and used for the biotransformation with modified conditions (lyophilized glucose-6-phosphate dehydrogenase) and **7** as substrate. Another control experiment to check for alcohol **13** formation, was performed by using the *R*-IRED-*Sr* mutant D191A in a biotransformation. As described in the first chapters (Table 11 in 3.1.2) this enzyme exhibits ~ 100-fold decreased activity (k_{cat}/K_M) for the reduction of the cyclic imine substrate **1**. With about 89% purity after Ni²⁺ affinity chromatography (Table 23, Figure S29), the IRED mutant *R*-IRED-*Sr* D191A displayed slightly higher purity than the wt enzyme (approx. 84%, Table 23).

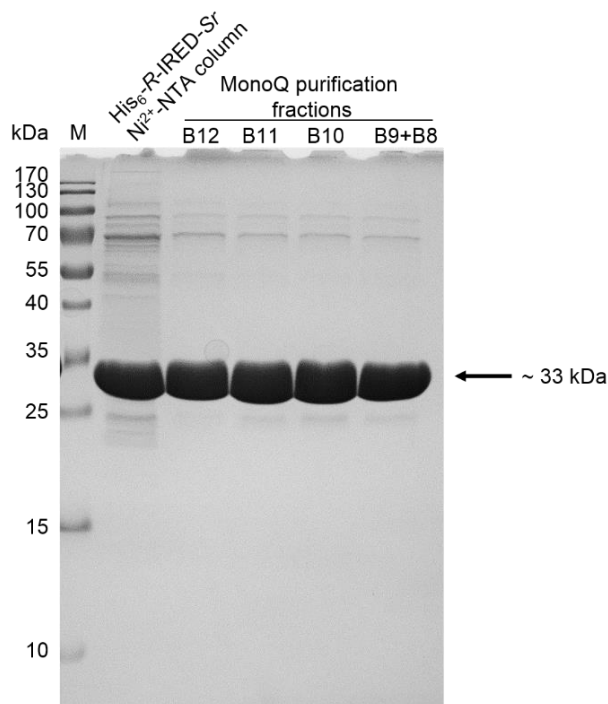


Figure 24: SDS-PAGE to compare the purity of *R-IRED-Sr* purified by Ni^{2+} affinity chromatography with the fractions of the *R-IRED-Sr* preparation of the further purification by ion exchange chromatography. To compare the purity and to visualize also minor contaminants, 20 μg total protein were loaded for all samples.

Table 23: HPLC SEC analysis to determine the purity of Ni^{2+} affinity chromatography and MonoQ purified *R-IRED-Sr*. In addition the purity of the IRED mutant *R-IRED-Sr* D191A is given. This protein was purified only by Ni^{2+} affinity chromatography. As in this purification only the fractions containing the highest IRED content were taken and combined, the yields decreased but the protein reached a higher degree of purity than the wt enzyme that was purified by the same technique.

IRED and purification step			purity [%]	HPLC run
<i>R-IRED-Sr</i>	wt	Ni^{2+} -NTA column	84.0%	Figure S31
<i>R-IRED-Sr</i>	wt	MonoQ fraction B12	> 95%	Figure S32
<i>R-IRED-Sr</i>	wt	MonoQ fraction B11	> 95%	data not shown
<i>R-IRED-Sr</i>	wt	MonoQ fraction B10	> 95%	data not shown
<i>R-IRED-Sr</i>	wt	MonoQ fraction B9+B8	94.9%	data not shown
<i>R-IRED-Sr</i>	D191A	Ni^{2+} -NTA column	89.0%	Figure S29

By increasing the enzyme purity from about 84% to > 95% (Table 23) the fraction of the amine product **8** raised from about 40% to ~ 80% in 24 h (Table 21, Table 24 and Figure 25). At the same time, the formation of alcohol **13** was reduced from > 45% to only ~ 6% (Table 21, Table 24 and Figure 25). In addition by the substitution of the glucose-6-phosphate dehydrogenase with its lyophilized version no formation of benzylamine **14** could be detected. This indicates that the ammonia for the reductive amination was indeed supplied by the cofactor regeneration system.

In reactions catalyzed by the IRED mutant *R-IRED-Sr* D191A after 24 h, no amine product **8** was detected and although the purity was also higher than in case of the wt enzyme still about 3% benzylalcohol **13** were formed (Table 24). This underlines that IREDs definitively prefer the reduction of C=N double bonds and it seems likely that the majority of the carbonyl reduction of benzaldehyde **11** is caused by contaminations with co-purified KREDs. A weak promiscuous activity of IREDs towards carbonyls can at the moment however also not fully be excluded. As the purity of about 89% obtained with the mutant *R-IRED-Sr* D191A seemed to be sufficient to have tolerable levels of carbonyl reduction

activity, care was taken that this level of purity was obtained in all further purification by IMAC by combining only the peak fractions of the eluting IRED.

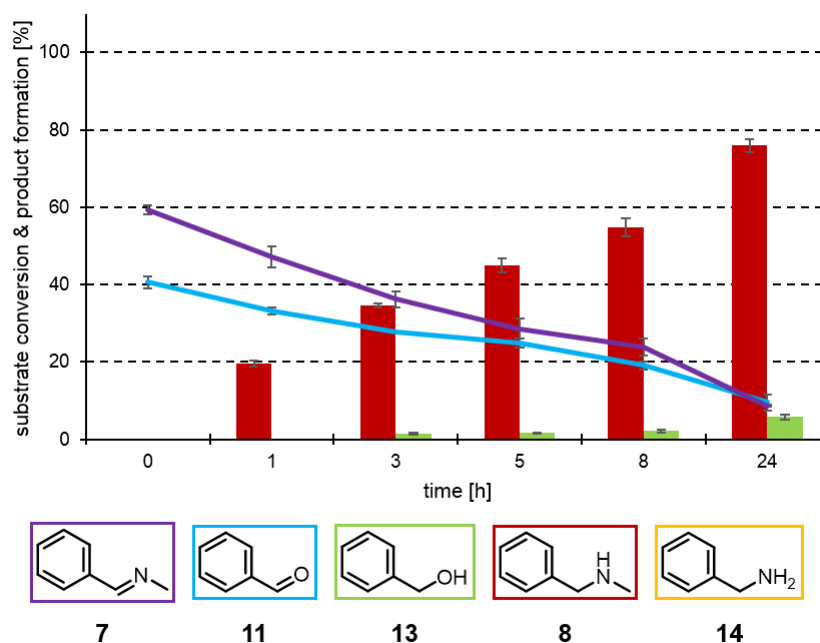


Figure 25: Time course showing the substrate conversion and product formation in [%] for the reduction of 10 mM imine substrate **7** to the amine product **8** with MonoQ purified *R*-IRED-Sr (fractions B12+B11 were combined, > 95% purity, see Table 23). The biotransformation was done in triplicates and the error bars give the standard deviation. By increasing the purity of the IRED, the formation of the alcohol byproduct was reduced. The use of lyophilized glucose-6-phosphate dehydrogenase for cofactor regeneration suppressed the reductive amination reaction that resulted in the formation of benzylamine **14** in the biotransformations above, as no ammonia is present in this enzyme preparation.

Table 24: Formation of product **8** in [%] by reduction of 10 mM of the exocyclic imine substrate **7** with MonoQ purified *R*-IRED-Sr (fractions B12+B11 were combined, > 95% purity, see Table 23) and the IRED mutant *R*-IRED-Sr D191A (~ 89% purity, see Table 23). The biotransformations were done in triplicates and the errors give the standard deviation. The increase in IRED purity decreased the formation of the alcohol **13** byproduct. As intended, the formation of the amination product **14** was prevented by the use of lyophilized glucose-6-phosphate dehydrogenase, thus confirming the ammonium sulphate precipitated version of it as the ammonia source for the reductive amination reaction. In biotransformations with the mutant *R*-IRED-Sr D191A no amine product was formed, but the alcohol byproduct. -: not detected.

		product formation [%]									
		<i>R</i> -IRED-Sr MonoQ purification (> 95% purity)					<i>R</i> -IRED-Sr D191A				
time [h]		7	8	11	13	14	7	8	11	13	14
0		59.43 ± 0.92	-	40.57 ± 1.20	-	-	59.01 ± 2.31	-	40.99 ± 2.81	-	-
1		47.11 ± 2.02	19.62 ± 0.51	33.27 ± 0.65	-	-	60.94 ± 1.75	-	39.06 ± 1.79	-	-
3		36.16 ± 1.62	34.62 ± 0.38	27.76 ± 0.16	1.46 ± 0.22	-	60.96 ± 2.04	-	39.04 ± 1.86	-	-
5		28.61 ± 1.99	44.98 ± 1.38	24.79 ± 0.88	1.63 ± 0.09	-	60.81 ± 2.75	-	39.19 ± 1.86	-	-
8		23.84 ± 1.65	54.81 ± 1.87	19.12 ± 0.74	2.23 ± 0.31	-	62.91 ± 3.33	-	37.09 ± 1.54	-	-
24		8.71 ± 0.27	75.88 ± 1.37	9.58 ± 1.64	5.83 ± 0.51	-	53.18 ± 2.58	-	44.29 ± 1.24	2.53 ± 0.44	-

3.5.3 Biotransformations of further exocyclic imine substrates

With this optimized reaction setup two more exocyclic imine substrates were investigated for their reduction by IREDs. Benzophenoneimine **15** with an electron rich di-arylic structure and phenylethylideneaniline **18** were tested as additional substrates. The latter one is structurally closely related to **9**, but due to the additional methyl group allows determining the selectivity for the reduction of exocyclic imine substrates, as during the reduction a stereocenter is formed.

In the negative control for the biotransformation with imine **15**, performed with heat inactivated enzyme, the hydrolysis of the substrate could be followed for about 5-8 h and after this time only the hydrolyzed byproduct (ketone **17**) could be detected (Figure S17). This indicates a slightly higher hydrolytic stability in direct comparison with imine **7**, which instantly after the reaction setup hydrolyzed and resulted in a detectable ratio of approximately 40/60 benzaldehyde **11** and benzylidenemethylamine **7** by GC analysis ($t = 0$ h in Figure 25 in 3.5.2). With the active enzyme (*R*-IRED-*Sr*) the reduction of imine **15** to the amine product benzhydrylamine **16** could be detected and after about 3 h close to 50% of it was formed (Table 25). At this time in the biotransformations also most of the residual imine substrate was hydrolyzed, thus further product formation was also limited (Figure S16). The other two IREDs, *R*-IRED-*St* and *S*-IRED-*Pe*, showed in preliminary tests only very low conversion of **15** and were therefore not further investigated. The HPLC peak areas in these initial investigation were only ~ 1.3% and about 10% for *R*-IRED-*St* and *S*-IRED-*Pe* compared to the area of *R*-IRED-*Sr*.

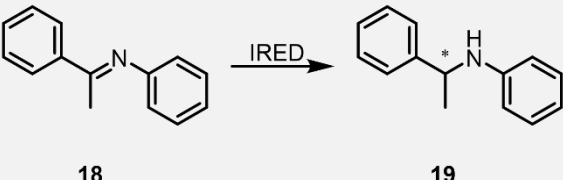
Table 25: Formation of benzhydrylamine **16** and the hydrolytic byproduct benzophenone **17** in [%] in a biotransformation with purified *R*-IRED-*Sr* and 10 mM of imine **15** as substrate. For the negative control, the IRED was heat inactivated by treatment at 95 °C for 10 min. Both reactions were done in triplicates and the errors give the standard deviation. Further reduction of **17** to the alcohol was not observed in all cases. The full dataset with all measured points is given in Table S6 and Figure S16. -: not detected.

product formation [%]				
time [h]	<i>R</i> -IRED- <i>Sr</i>		negative control	
	16	17	16	17
1	34.22 ± 0.98	30.91 ± 0.42	-	45.32 ± 0.19
3	47.56 ± 0.37	40.75 ± 1.78	-	76.90 ± 2.35
24	52.55 ± 2.94	45.84 ± 1.55	-	88.48 ± 2.64

To determine the stereoselectivity of the *R*-IREDs for the reduction of exocyclic substrates, imine **18** was selected. As *S*-IRED-*Pe* showed only low activity with **9** (see 3.5.2), it was not tested with imine **18**. Analogously to imine **9** *R*-IRED-*St* was more active with substrate **18** and the amine product **19** was obtained with about 80% conversion in 24 h. In contrast, *R*-IRED-*Sr* only produced about 10% of **19** (Table 26). By chiral HPLC the selectivity was determined and both enzymes found to be (*R*)-selective, producing **19** with a very high ee of 88% and 94%, respectively (Table 26 and Figure S19). Again, as also seen in the case of imine **15**, the hydrolysis of this electron rich substrate took slightly longer than

for substrates like **7**. In the negative controls with the heat inactivated enzymes it took about 5-8 h until a potential equilibrium of the ketone/amine (acetophenone **20** and aniline **12**) and imine (phenylethylideneaniline **18**) was reached.

Table 26: Product formations and stereoselectivities in [%] for the reduction of 10 mM **18** by (*R*)-selective IREDs. Both biotransformations were performed in triplicates and the errors give the standard deviation. For a better overview in Table 26 only the desired product **19** is shown. Quantification of the hydrolytic products **12** and **20** is shown in the full dataset in Table S7. Reduction of the ketone **20** to 1-phenylethanol **25** was not observed or is below the detection limit. -: not detected; n.d.: not determined.

				
product formation [%]				
time [h]	<i>R</i> -IRED- <i>Sr</i>		<i>R</i> -IRED- <i>St</i>	
	19	ee [%]	19	ee [%]
1	-	n.d.	21.32 ± 1.08	n.d.
3	1.48 ± 0.23	n.d.	47.71 ± 2.57	n.d.
24	10.18 ± 5.65	94.2 ± 0.5 (<i>R</i>)	83.85 ± 20.47	87.8 ± 0.3 (<i>R</i>)

3.6 The reductive amination of aldehydes and ketones with IREDs

The hydrolytically sensitive nature of the imine bond for long term has hindered the discovery of broadly applicable imine reducing enzymes and the existence of imines in nature was believed to be restricted to transient intermediates in specialized metabolic pathways or during enzyme catalysis.^{39,53,58,113-117,176-178} The full exploitation of this reversible imine formation for the subsequent reduction by an IRED to result in novel C-N bonds therefore represents a synthetically highly desirable goal. First indications for such a reductive amination were already observed as a formed byproduct with ammonia **21** and benzaldehyde **11** during the reduction of exocyclic imines (Table 21 and Table 22). In these experiments already very low levels of the imine intermediate (they were below the detection limit) led to considerable amounts of the reductive amination product (approximately 5-10%, see Table 21 and Table 22). As this bimolecular reaction represent a very attractive extension for potential applications of IREDs, an efficient process for this reductive amination was to be developed. The parameters affecting the individual steps of the reaction were taken into account and their influence investigated. As *R*-IRED-*Sr* showed for most substrates the highest activities (Table 14, Table 15, Table 17 and Table 21) and proved in initial tests superior to the other two IREDs, this enzyme was selected for the optimization process. During the purification process care was taken to reach a level of about 90% purity (determined by SEC analysis in HPLC, see also Figure 10) to avoid too high byproduct formations (as discussed in 3.5.2).

3.6.1 The reductive amination of aldehydes

First the reductive amination of aldehydes was investigated. Benzaldehyde **11** served as the model carbonyl acceptor and three different amine nucleophiles were used (ammonia **21**, methylamine **22** and aniline **12**). These three amine nucleophiles differ in their nucleophilicity with **21** being the weakest one.²²³ In an attempt to shift the equilibrium from the carbonyl/amine to the condensation (imine) side also the use of different excess amounts of the amine donors were investigated. Amines were used in equimolar concentrations, as well as in 10-fold and 50-fold molar excess amounts (except for **12**, which was not used at this concentration due to solubility limitations). To be able to compare the conversion rates and judge byproduct formation, all reactions were done with the same batch of purified protein and each IRED aliquot was used only once. As negative controls, reactions were performed under identical conditions with heat inactivated *R*-IRED-*Sr* (95 °C for 10 min) and with BSA substituting the IRED. In none of these control reactions however any product formation was observed.

In general in these biotransformations, the conversion rates increased along with the excess amount of the amine nucleophile and also led to higher overall product formations. By using **21** as nucleophile the concentration of the product (benzylamine **14**) after 24 h raised from 7% to 51% and final 61% with the increasing amount of the nucleophile (equimolar, 10-fold and 50-fold, Table 27). With the more potent nucleophile **22** also the conversion rates increased and after 1 h at equimolar concentration 6% of the amination product **8** were formed, whereas at the higher excess amounts (10-fold and 50-fold) 33% and 58% of **8**, respectively, were formed in 1 h (Table 27). Amine **12** was also an effective nucleophile and a final conversion to the amination product **10** of 25% after 24 h was obtained (Table 27). In contrast, the use of higher excess amounts of **12** (10-fold molar excess) was not advisable and the final conversions in 24 h dropped to less than 5%. It might be possible that the use of this nucleophile at the high concentrations caused inhibitory effects on the applied IRED.

Next to the amination product the reduction of the carbonyl compound to benzylalcohol **13** was observed. With about 7% alcohol formation this side reaction was most pronounced for the reaction conditions with the lowest amounts of amine nucleophile and decreased at higher excess amounts or when stronger nucleophiles like **22** were used (Table S10, Table S11 and Table S12). Another potential byproduct arises when performing reductive aminations with ammonia as nucleophile. The product that is generated in this case, benzylamine **14**, is also a potent nucleophile. Indeed the low levels of this product that are initially formed are deceptive as **14** instantly reacted with **11**, forming a new imine intermediate **23**. During the proceeding reaction, this intermediate vanished again completely (Figure S49 and Table S10) as **11** was completely converted to **14** and in addition small amounts of the dialkylation product dibenzylamine **24** were found. A full reaction scheme for the formation of the dialkylation product is shown in Scheme S1 and the full dataset can be found in Table S10. Such a highly selective monoamination with only tiny amounts of dialkylation product formed represents a significant advancement over chemical reductive amination methodologies.²²⁴ In these procedures, often two-step processes are required to avoid the formation of extensive amounts of dialkylation products.²²⁴ In addition, at the moment this dialkylation represents an undesired side product, but on the other hand it also highlights the versatility of enzymatic reductive aminations that could be further

developed into reaction cascades to assemble more complex molecules by the repeated (selective) reductive amination of simple precursors.

Table 27: Conversion of 10 mM benzaldehyde **11** into the amination products **14**, **8** and **10** by purified *R*-IRED-Sr using three different amine nucleophiles (**21**, **22** and **12**) at varying molar excess amounts. As negative controls reactions with heat inactivated *R*-IRED-Sr and reactions with BSA substituting the IRED were performed. In none of these control reactions any product formation was observed. All biotransformations were performed in triplicates and the errors give the standard deviation. The full dataset with all measured points is shown in detail in Table S10, Table S11 and Table S12. -: not detected.

11	21: R = H 22: R = methyl 12: R = phenyl	R = H 7: R = methyl 9: R = phenyl	14: R = H 8: R = methyl 10: R = phenyl		
carbonyl acceptor	amine nucleophile	equivalents of nucleophile	product formation [%]		
			1 h	8 h	24 h
11	21	1 ^[a]	< 1 (14) - (24) ^[a]	1.25 ± 0.13 (14) < 1 (24) ^[a]	6.60 ± 0.25 (14) 2.18 ± 0.06 (24) ^[a]
11	21	10 ^[a]	< 1 (14) - (24) ^[a]	21.43 ± 0.28 (14) < 1 (24) ^[a]	51.22 ± 2.13 (14) 3.15 ± 0.03 (24) ^[a]
11	21	50 ^[a]	< 1 (14) - (24) ^[a]	48.03 ± 0.76 (14) < 1 (24) ^[a]	60.66 ± 1.12 (14) < 1 (24) ^[a]
11	22	1	5.54 ± 0.22	34.64 ± 1.29	51.18 ± 2.75
11	22	10	32.82 ± 0.56	71.56 ± 3.31	66.19 ± 0.48
11	22	50	57.95 ± 3.28	73.33 ± 3.80	68.98 ± 4.08
11	12	1	4.06 ± 0.16	13.44 ± 1.30	24.97 ± 5.28

^[a]: given are the equivalents of nucleophile **21**. As detailed above, product **14** that was formed during the reaction acted as an additional nucleophile. Higher amounts of product **14** were obtained as given in the table, but they are trapped in the new imine intermediate **23** formed by the reaction of **11** with **14**. Reduction of this second imine by the IRED led to the dialkylation product **24**. The amounts of **24** formed are given as the second values in Table 27.

3.6.2 The reductive amination of ketones to generate chiral amines

The reductive amination methodology was then extended and the use of ketones as carbonyl substrates investigated as thereby directly chiral amines can be generated. However, compared to an aldehyde, ketones are far less reactive and especially aromatic unsaturated ketones like acetophenone **20** were described to be challenging substrates.²²⁴

By employing the reductive amination conditions developed for aldehydes with ketone **20** as carbonyl compound, only in the case of the 50-fold molar excess amount of the amine nucleophiles considerable levels of the amination products could be detected. Using nucleophile **21** after 24 h ~ 5% of α -methylbenzylamine **26** was found to be formed, whereas the use of **22** resulted in about 9% of *N*- α -dimethylbenzylamine **27** (top row in Table 28). To further optimize the conversion rates, the equilibrium was again shifted towards to condensation product by changing the pH of the reaction. At higher pH values, the fraction of the reactive amine species capable of the nucleophilic attack on the C α carbon can be enhanced. Indeed, increasing the pH of the reaction from 8.0 to 8.5 and 9.0 boosted the conversion rates. With **21** and **22** as nucleophiles the conversions after 24 h could be doubled to 10%

3 RESULTS

and 19%, respectively (Table 28). Due to the lower conversions observed in the combination of **11** and **12**, this nucleophile was not tested here.

As *R*-IRED-*Sr* displays decreased activities at increased pH values (Figure 13) the reactions were also performed with higher enzyme loadings. Using a fourfold increased amount of the enzyme (10 mg/ml), the overall conversions could again be raised to finally 16% with nucleophile **21** and about 40% for nucleophile **22**. Remarkably, the transformations of the enzyme to form the novel C-N bonds proceeded for both nucleophiles with very high to excellent selectivities. The products **26** and **27** were obtained with an *ee* > 97% for **26** and > 86% in the case of **27** as determined by chiral GC analysis (Table 28, Figure S55 and Figure S57).

Table 28: Conversion of 10 mM acetophenone **20** into the amination products **26** and **27** by purified *R*-IRED-*Sr* using the two amine nucleophiles **21** and **22** at different pH values after 24 h. Nucleophiles **21** and **22** were in all reactions used at 50-fold molar excess. As negative controls reactions with heat inactivated *R*-IRED-*Sr* and reactions with BSA substituting the IRED were performed. In none of these control reactions any product formation was observed. Reduction of ketone **20** to the alcohol **25** was in all cases detected only in traces (< 1%). All biotransformations were performed in triplicates and the errors give the standard deviation. The full dataset with all measured points is shown in detail in Table S13 and Table S14.

20		21: R = H 22: R = methyl	26: R = H 27: R = methyl				
amine nucleophile	pH	product formation after 24 h [%]	<i>ee</i> [%]	amine nucleophile	pH	product formation after 24 h [%]	<i>ee</i> [%]
21	8.0	5.45 ± 0.03	96.6 ± 0.2 (<i>R</i>)	22	8.0	8.57 ± 0.08	86.7 ± 0.4 (<i>R</i>)
21	8.5	7.09 ± 0.07	97.6 ± 0.4 (<i>R</i>)	22	8.5	15.19 ± 0.22	86.3 ± 0.3 (<i>R</i>)
21	9.0	10.12 ± 0.06	97.7 ± 0.2 (<i>R</i>)	22	9.0	18.95 ± 1.02	86.3 ± 0.1 (<i>R</i>)
21	9.0	15.82 ± 0.66 ^[a]	97.1 ± 0.1 (<i>R</i>)	22	9.0	39.18 ± 1.38 ^[a]	86.6 ± 0.0 (<i>R</i>)

^[a]: these reactions were performed with the enzyme concentration 4-fold increased to 10 mg/ml.

3.6.3 Kinetic characterization of the reductive amination reaction

To obtain further information about the reductive amination reaction, kinetic measurements were performed for the reaction of *R*-IRED-*Sr* with **11** and **22** at pH 8.0 and pH 9.0 (the reaction is shown in the heading of Table 27). Assuming steady state conditions, the initial reaction rates with a pre-equilibrated substrate solution (**11** with different molar excess amounts of **22** in buffer at the respective pH) were determined. The data was then fitted to the Michaelis-Menten equation, implying that imine **7** is the single substrate for *R*-IRED-*Sr*. Both parameters, the increasing pH value of the reaction or the increase of the amine nucleophile excess amount, had an effect on the determined apparent K_M ($K_{M, app}$) value. Conditions that are assumed to favor imine formation (higher pH, higher nucleophile excess amount, see Table 27 and Table 28) directly go along with a decrease in $K_{M, app}$. The apparent affinity dropped from > 20 mM at pH 8.0 using equimolar concentrations of **22** to less than 2 mM (50-fold excess of **22** at pH 9.0, Figure 26, Table 29 and Figure S59). It is concluded, that in these measurements the increased imine availability directly reflects the relative amount of substrate the enzyme is exposed to.

These results therefore also confirm the above mentioned intention, to shift the equilibrium towards the imine for the optimization of the biotransformations (3.6.1 and 3.6.2). The concentration of the imine is initially assumed to be in a steady-state equilibrium and as it re-forms after withdrawal by the IRED it is expected to stay constant. In such a situation the higher imine availability directly leads to a higher saturation of the enzyme with its substrate and hereby enhances the reaction rates. The maximal turnover numbers were detected at the 50-fold excess amount of **22** at a pH of 8.0 and are around 0.5 min^{-1} . Although imine availability at pH 8.0 is suspected to be lower than at pH 9.0 (Table 29 and above), it seems possible that the reactions rates might be higher as the enzyme loses activity at the higher pH (Figure 13). The strong increase in the determined turnover numbers at the 50-fold excess amount of **22**, both at pH 8.0 and 9.0 (Table 29), might also indicate that under the conditions with the lower excess amounts of **22**, the imine formation could become the rate limiting step of the reaction. Thus, the determined turnover numbers should in this cases be designated as apparent k_{cat} ($k_{\text{cat app}}$).

Table 29: Steady state kinetic parameters for *R*-IRED-Sr catalyzed reductive amination of **11** with different molar excess amounts of **22** at pH 8.0 and 9.0. All specific activities were determined in triplicates for varying concentrations of the substrate. To calculate k_{cat} , K_{M} and K_{I} the data was then fitted by nonlinear regression to the Michaelis-Menten equation.

pH	equivalents of 22	$K_{\text{M app}}$ [mM]	k_{cat} [s^{-1}]	$k_{\text{cat}}/K_{\text{M app}}$ [$\text{s}^{-1} \text{ mM}^{-1}$]	Michaelis-Menten plot
8.0	1	20.47 ± 5.67	$4.45 \times 10^{-3} \pm 0.66 \times 10^{-3}$	$0.22 \times 10^{-3} \pm 0.07 \times 10^{-3}$	Figure S60
8.0	10	4.15 ± 0.29	$5.68 \times 10^{-3} \pm 0.26 \times 10^{-3}$	$1.37 \times 10^{-3} \pm 0.12 \times 10^{-3}$	Figure S61
8.0	50	2.14 ± 0.07	$11.15 \times 10^{-3} \pm 0.34 \times 10^{-3}$	$5.22 \times 10^{-3} \pm 0.24 \times 10^{-3}$	Figure S62
9.0	1	10.54 ± 2.34	$4.31 \times 10^{-3} \pm 0.38 \times 10^{-3}$	$0.41 \times 10^{-3} \pm 0.10 \times 10^{-3}$	Figure S63
9.0	10	3.91 ± 0.43	$5.21 \times 10^{-3} \pm 0.20 \times 10^{-3}$	$1.33 \times 10^{-3} \pm 0.16 \times 10^{-3}$	Figure S64
9.0	50	1.94 ± 0.23	$9.21 \times 10^{-3} \pm 0.56 \times 10^{-3}$	$4.75 \times 10^{-3} \pm 0.63 \times 10^{-3}$	Figure S65

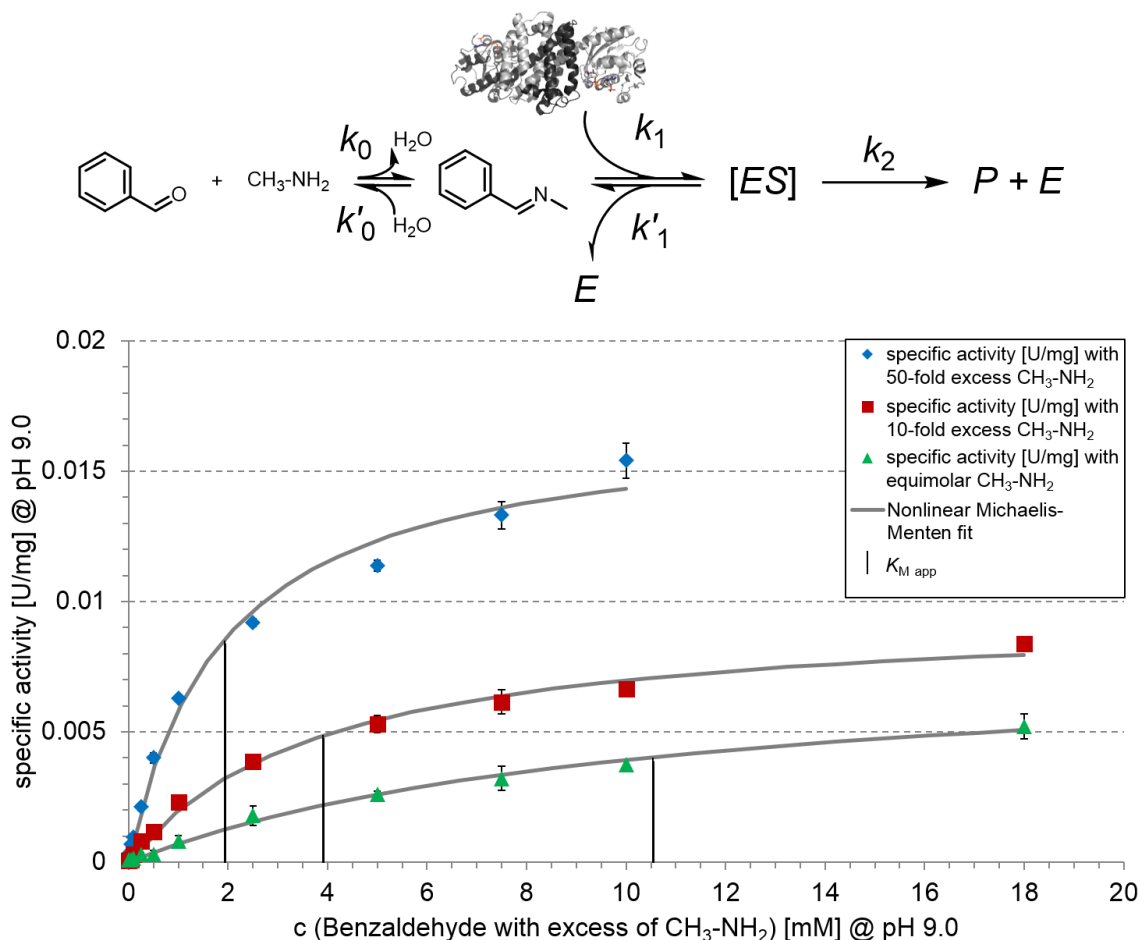


Figure 26: Top: Reaction scheme for the steps of the reductive amination reaction of **11** and **22** with *R*-IREd-Sr (enzyme *E*). As an initial step (k_0) the substrate (S) imine **7** has to form by condensation of benzaldehyde **11** and methylamine **22**. The equilibrium of this reaction then affects the formation (k_1) of the enzyme substrate complex ([ES]). The Michaelis-Menten complex is resolved by the reduction (k_2) to the product (P) **8**.

Bottom: Overlay of the Michaelis-Menten plots for the reductive amination of **11** with different excess amounts of nucleophile **22** at pH 9.0 with *R*-IREd-Sr. Conditions that shift the equilibrium towards imine **7** go along with a decreased $K_{M app}$ value, directly reflecting the relative amount of substrate the enzyme is exposed to.

3.7 Production of *N*-heterocycles by enzymatic cascade reactions with IREDs – the enzymatic generation of cyclic imines with PuO-*Re*

Amine oxidases in combination with IREDs could be used in an enzymatic cascade reaction to establish the *de novo* synthesis of *N*-heterocycles. The irreversible oxidation of a polyamine to an aminoaldehyde triggers its spontaneous cyclization to a cyclic imine, thereby generating the substrate for the second enzyme (IRED) (Scheme 11 in 1.2.3). However in contrast to the widespread use of MAO-N and variants of it,^{2,115,225,226} polyamine oxidases are not thoroughly investigated for biocatalytic purposes. One of the best characterized enzymes in literature is PuO-*Re*.^{161,170–173}

In contrast to the initial characterization of the enzyme, with a range of natural polyamines, amino acids and amino alcohols tested as substrates,¹⁶¹ nothing is known about the activity with non-natural polyamines. The use of such modified polyamines as precursors would directly result in a set of diverse heterocyclic compounds in the reaction cascade. To investigate such polyamines as substrates, a panel composed of linear- and branched polyamines, including symmetric and asymmetric polyamines with oxygen- and nitrogen heteroatoms was investigated. To check for activity with purified PuO-*Re* the

formation of the enzymatic byproduct H_2O_2 was followed in a spectrophotometric assay with horseradish peroxidase (HRP) and a suitable dye system. The substrates were used in excess to ensure the saturation of the enzyme and the specific activities, as well as the relative activities compared to the natural substrate diaminobutane **28** are given in Table 30. By GC-MS headspace it was also confirmed that the aminoaldehydes generated by the oxidation of polyamines **28** and **29** indeed spontaneously cyclize to the cyclic imine (Figure S66).

As it was expected, by far the highest activity was observed with the natural substrate diaminobutane **28**. Although the enzyme was able to oxidize a wide variety of the selected substrates, a general trend was obvious. By increasing the chain length, by using branched polyamines or polyamines with heteroatoms in the middle of the chain, a dramatic loss in activity was observed. The same behavior was also already described for PuO-Re with natural polyamines besides **28**, for example diaminopentane **29** and spermidine **34**.¹⁶¹

Table 30: Specific activities in [U/mg] and the relative activities in [%] compared to the natural substrate **28** for PuO-Re with a range of polyamine substrates. All activities were determined in triplicates by monitoring the formation of the enzymatic byproduct H_2O_2 spectrophotometrically with a suitable dye system and HRP.

structure of polyamine substrate	#	specific activity [U/mg]	relative activity [%]
	28	12.28 ± 0.33	100.00
	29	0.45 ± 0.04	3.69
	30	87.36 x 10 ⁻³ ± 2.64 x 10 ⁻³	0.71
	31	0.33 ± 0.04	2.66
	32	65.62 x 10 ⁻³ ± 3.94 x 10 ⁻³	0.53
	33	3.75 x 10 ⁻³ ± 0.99 x 10 ⁻³	0.03
	34	2.63 ± 0.07	21.40
	35	8.13 x 10 ⁻³ ± 0.28 x 10 ⁻³	0.07
	36	22.59 x 10 ⁻³ ± 1.18 x 10 ⁻³	0.18
	37	9.18 x 10 ⁻³ ± 0.21 x 10 ⁻³	0.07
	38	5.36 x 10 ⁻³ ± 5.22 x 10 ⁻³	0.04

To investigate the molecular basis for the observed strong loss in activity in more detail, kinetic parameters for selected polyamine substrates (**28**, **29**, **31**, **34** and **36**) were determined. By comparing the catalytic efficiency (k_{cat}/K_M) of the enzyme with different substrates, it is possible to evaluate the performance of the enzyme with different substrates.^{227,228} The affinities determined for this set of polyamine substrates were, with the exception of substrate **34**, all in the same order of magnitude. The highest affinity was found for the natural substrate **28** with the K_M value to be around 15 μM . However, although the measured affinities for the other tested substrates increased, it was still feasible to saturate the enzyme with them and all measured K_M values were in the μM range (Table 31). In contrast, the

3 RESULTS

turnover numbers for the non-natural substrates were reduced at least 10-fold and found to be about 1000-fold lower with triamine **36** (Table 31). The reasons for the strongly decreased activities might be due to limitations in the substrate access to the active site, which is deeply buried in the enzyme.¹⁷¹ Also the binding in an unproductive way to the enzyme, not assisting in the formation of a proper enzyme-substrate (ES) complex might contribute to the low turnover numbers.^{229,230}

Table 31: Summary of the kinetic constants recorded for PuO-*Re* with the set of polyamine substrates **28**, **29**, **31**, **34** and **36**. All specific activities were determined in triplicates for varying concentrations of the substrate. To calculate k_{cat} and K_M the data was then fitted by nonlinear regression to the Michaelis-Menten equation.

substrate	K_M [μ M]	k_{cat} [s^{-1}]	k_{cat}/K_M [$s^{-1} mM^{-1}$]	k_{cat}/K_M [%]	Michaelis-Menten plot
28	15.54 \pm 0.64	16.91 \pm 0.19	1088.42 \pm 46.52	100.00	Figure S69
29	22.79 \pm 4.37	1.59 \pm 0.08	69.58 \pm 13.82	6.39	Figure S70
31	31.45 \pm 2.33	1.28 \pm 0.02	40.74 \pm 3.12	3.74	Figure S71
34	131.39 \pm 15.96	1.33 \pm 0.07	10.13 \pm 1.35	0.93	Figure S72
36	42.29 \pm 1.76	14.00 $\times 10^{-3} \pm 0.12 \times 10^{-3}$	0.33 \pm 0.01	0.03	Figure S73

3.8 Directed evolution of PuO-*Re* to expand the substrate scope

3.8.1 Random mutagenesis by epPCR

To alter the efficiency of the enzyme for the oxidation of longer and branched polyamine substrates, mutants were generated. In a first attempt to shift the substrate spectrum of the enzyme, its “anionic point” was modulated.^{166,171} A glutamic acid in the active site is responsible for the correct positioning of the positively charged amine substrate in relation to the flavin cofactor that is in charge of the oxidation (Figure 28).¹⁷¹ By mutation of Glu to Asp, ideally more space should be created and the enhanced substrate binding pocket might accommodate substrates that have longer chain lengths like diaminopentane **29**. This mutant was generated by site directed mutagenesis and purified. Although a shift in the substrate spectrum towards longer polyamines was observed, overall the specific activity of the mutant with all tested substrates was extremely low. It decreased to about 0.3% of the wt activity for 1,4-diaminobutane **28** and to about 2.7% of the wt activity for 1,5-diaminopentane **29** (Table S15). These findings were later also published by Kopacz *et al.* and the effect of the mutation on k_{cat} and K_M analyzed in more detail.¹⁷²

As this rational approach for the optimization of PuO-*Re* proved to be unsuccessful, for further mutagenesis a random mutagenesis strategy based on an error prone PCR (epPCR) for diversity generation was chosen. The required HTS system was based on a solid phase assay adapted from Turner and coworkers.^{110,231} For this assay, the cells were grown on a nylon membrane and after the partial lysis by a freeze thaw cycle, HRP, a suitable dye and the substrates of interest were added. Cells that expressed active enzyme variants produced H_2O_2 and by the action of HRP the dye diaminobenzidine polymerized to a dark brown precipitate (Figure 27). Using this method libraries from directed evolution and metagenome experiments were already screened and led to the identification of improved biocatalysts or novel enzymes, including PuO-*Re* itself.^{110,111,161,231,232}

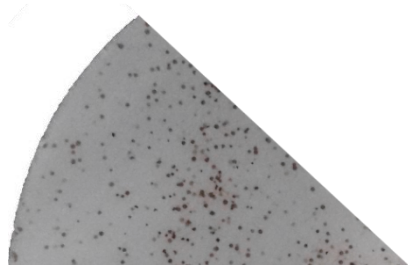


Figure 27: Solid phase assay to screen for oxidase activity. The cells are growing on a nylon membrane and after addition of the substrate of interest and HRP, active cells produce H_2O_2 . The dye diaminobenzidine then polymerizes into a complex brown precipitate, allowing the visual inspection for activity based on differences in color formation.

From an epPCR library about 60000 – 70000 colonies were screened with this solid phase assay towards polyamine substrates **31**, **33**, **36** and **38**. To increase the throughput the substrates screened were clustered according to their activity level and used simultaneously. Colonies that developed a brown color were picked, transferred to a new membrane and subjected to a second screening round to eliminate false positives and refine the screening procedure. Positive mutants after the second screening round were grown in 96 deep well plates for the generation of cell lysate. With the lysates activity assays were performed for the specific substrates and the best mutants thereof were sequenced, purified and characterized in more detail.

In the sequencing results of several of these mutants one residue was identified that was of special interest. Variants that displayed amino acid exchanges at this position also showed the most pronounced effects for oxidizing non-natural substrates. The identified amino acid was a glutamic acid at position 203 of the enzyme which is in the wt enzyme located in the second shell around the active site and its side chain points into one of the 7^V channels that end in the deeply buried cave with the flavin cofactor responsible for the oxidation (Figure 28).¹⁷¹ This position was independently identified in two variants: once it was substituted by a glycine (E203G) and in the second mutant it was replaced by valine (E203V). The second mutant possessed also an additional I154V substitution.

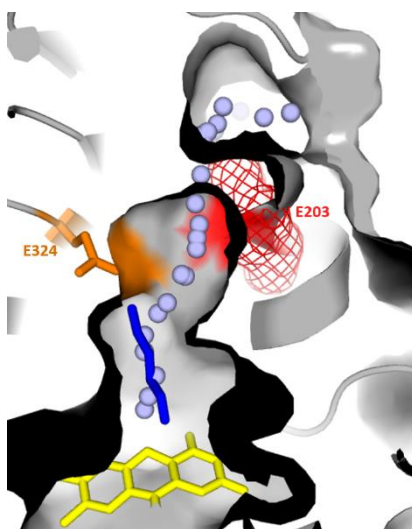


Figure 28: Active site of PuO-Re with the flavin cofactor in yellow sticks and the substrate 1,4-diaminobutane in blue sticks (pdb code: 2YG4).¹⁷¹ The anionic point (E324) responsible for the correct positioning of the substrate in the active site^{166,171} is shown in orange sticks. Position E203 aligning the channel that leads into the active site is highlighted as a red mesh. The identification of the channel (blue dots) was done with the CAVER plugin of HotSpot Wizard.²³³

^V: The 7 channels leading into the active site of the enzyme were identified with the CAVER plugin of HotSpot Wizard.²³³ Except for one channel that aligns to the non-covalently bound flavin cofactor¹⁷⁰ for none of them a function could be deduced.

3 RESULTS

It is likely that by mutations in this channel, substrates can more easily enter the active site for oxidation. Consequently, during the characterization these two mutants (E203G and I154V E203V) displayed much higher activities for most of the substrates (Table 32, Figure 29 and Figure 33). However, not only the turnover numbers were affected. For longer polyamines like spermidine **34** also the affinity determined for the mutant PuO-Re E203G increased (Figure 29). Overall this mutant displayed for polyamine substrate **34** an over 10-fold higher k_{cat}/K_M value compared to the wt enzyme (Table 31 and Table 32). The full characterization of the E203G mutant and the I154V E203V double mutant showed that in both mutants the substrate spectrum of the enzyme was shifted (Table 32 and Figure 30). Diaminobutane **28** is still the substrate that is transformed with the highest catalytic efficiency, however with the mutants the discrimination of polyamine **28** towards longer polyamines is changed and the longer substrates are transformed more efficiently. The relative k_{cat}/K_M for polyamine **29** increased about twofold from 6% to 12% in the I154V E203V double mutant. In case of the E203G mutant the relative k_{cat}/K_M for polyamine **34** compared to the natural substrate is shifted from around 1% for the wt enzyme to about 25% in case of the mutant (Table 31, Table 32 and Figure 30).

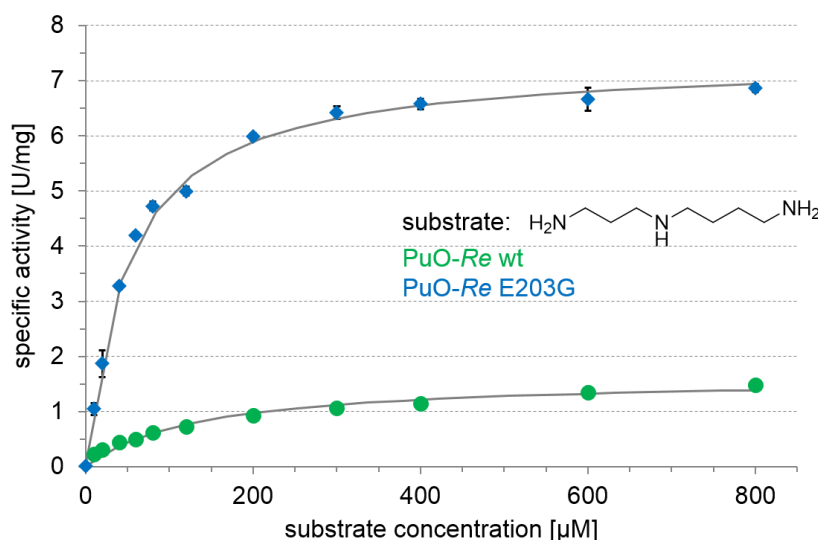


Figure 29: Comparison of the Michaelis-Menten plots for PuO-Re wt (green) and PuO-Re E203G (blue) with polyamine **34**. The mutant shows higher affinity and higher activity with this substrate, resulting in an over 10-fold increased catalytic efficiency (k_{cat}/K_M).

Table 32: Summary of the kinetic constants recorded for PuO-Re mutants E203G and I154V E203V double mutant with the set of polyamine substrates **28**, **29**, **31**, **34** and **36**. By comparing the relative catalytic efficiencies (**28** was always set as 100%) of the mutants to the wt, the shift in the substrate spectrum towards the longer polyamines becomes obvious. All specific activities were determined in triplicates for varying concentrations of the substrate. To calculate k_{cat} and K_M the data was then fitted by nonlinear regression to the Michaelis-Menten equation.

Mutant	substrate	K_M [μM]	k_{cat} [s^{-1}]	k_{cat}/K_M [$\text{s}^{-1} \text{mM}^{-1}$]	k_{cat}/K_M [%]	Michaelis-Menten plot
E203G	28	90.49 \pm 6.01	45.10 \pm 0.63	498.44 \pm 33.86	100.00	Figure S74
	29	199.35 \pm 3.24	4.27 \pm 0.14	21.44 \pm 0.80	4.30	Figure S75
	31	94.11 \pm 8.16	1.55 \pm 0.02	16.44 \pm 1.45	3.30	Figure S76
	34	50.23 \pm 1.45	6.07 \pm 0.04	120.91 \pm 3.61	24.26	Figure S77
	36	119.43 \pm 17.73	11.39 $\times 10^{-3} \pm 0.61 \times 10^{-3}$	0.10 \pm 0.02	0.02	Figure S78
I154V E203V	28	55.00 \pm 4.86	32.98 \pm 1.25	599.58 \pm 57.65	100.00	Figure S79
	29	52.76 \pm 5.63	3.82 \pm 0.10	72.37 \pm 0.48	12.07	Figure S80
	31	48.72 \pm 4.64	1.32 \pm 0.02	27.04 \pm 2.60	4.51	Figure S81

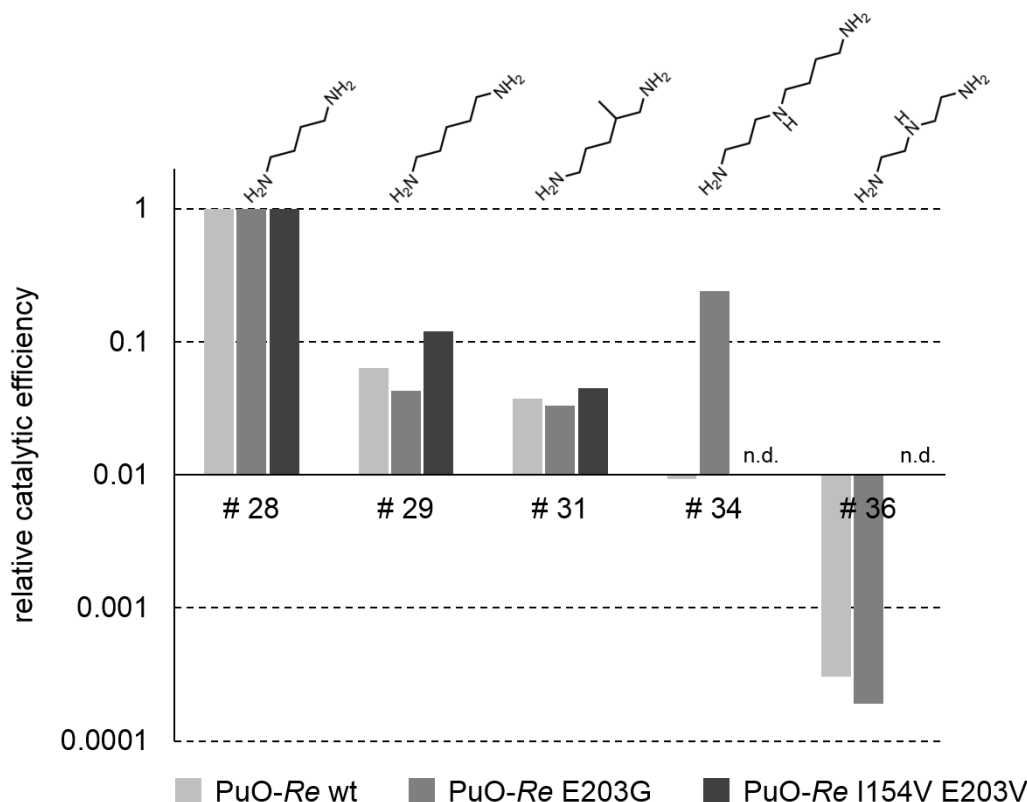


Figure 30: Relative catalytic efficiencies for PuO-Re wt and the mutants E203G and I154V E203V, shown on a logarithmic scale. 1,4-Diaminobutane (**28**) is still the best substrate for all three enzymes (relative $k_{cat}/K_M = 1$), however the substrate spectrum of the mutants is shifted and they show increased activity with longer polyamines like 1,5-diaminopentane (**29**) and 1,5-diamino-2-methylpentane (**31**) for PuO-Re I154V E203V and spermidine (**34**) in case of PuO-Re E203G. The kinetic constants for PuO-Re I154V E203V with polyamines **34** and **36** were not determined (n.d.).

3.8.2 Semi-rational design by site-saturation mutagenesis

Considering the strong impact variations at position E203 had on the activity of PuO-Re, for further mutagenesis a more focused strategy was followed. The selected residues targeted for mutagenesis were all located within the channel that was suggested by position E203, which was also included for the saturation mutagenesis approach. The tertiary structure of the helix around position 203 (shown in red in Figure 31) adopts a U-formed shape (colored in brown in Figure 31, right side) and this element was targeted by several libraries consisting of single-, double- and triple randomizations with different degenerated codons (Table 33). The selection of residues for the simultaneous randomization was done (when possible) considering the CASTing criteria postulated by Reetz.^{189,234,235} Due to this U-shape more degrees of freedom are however available than for a simple α -helix or β -sheet and it was not possible to consider all potential combinations of positions for mutagenesis. The other libraries that were generated targeted the amino acids at position D104 and a double mutant at positions L168 F169 (Figure 31). These amino acids are either located at the surface and the entrance of the channel (D104, colored in purple in Figure 31) or at a turn before the channel approaches the U-shaped helix (L168 F169, colored in cyan in Figure 31). Finally, two active site residues that might directly influence the coordination of the substrate were chosen for mutagenesis (M174 and L207, colored in green in Figure 31). The degenerated codons for the individual libraries (NNK, DNK, NNY, NHK and NDT; for details see Table 33) were selected based on the library sizes that had to be screened and to provide a

3 RESULTS

balanced mix of amino acids but avoiding or minimizing the number of very bulky amino acids in the active site or positively charged amino acids (active site and tunnel) as it is expected that this might lead to some repulsion with the positively charged polyamine substrates. The tools CASTER¹⁸⁹ and AA-Calculator¹⁸⁵ were used for selection of the different degenerated codons.

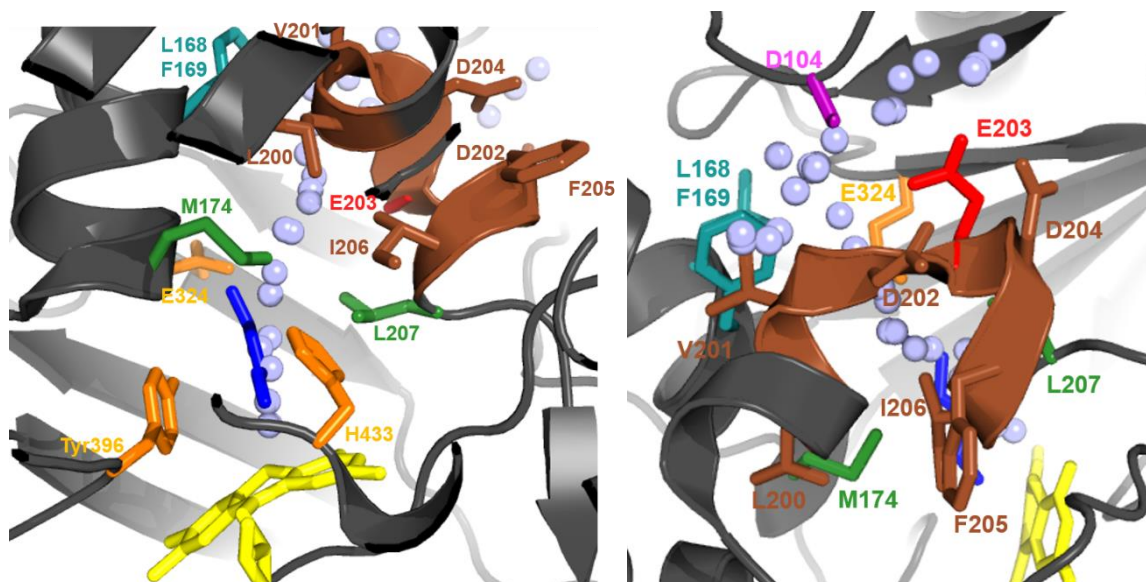


Figure 31: Active site of PuO-Re with the flavin cofactor in yellow sticks and the substrate 1,4-diaminobutane in blue sticks (pdb code: 2YG4).¹⁷¹ The anionic point (E324) responsible for the correct positioning of the substrate in the active site^{166,171} is shown in orange sticks. The identification of the channel (blue dots) was done with the CAVER plugin of HotSpot Wizard.²³³ The left side shows the active site in more detail with amino acids M174 and L207 (green sticks) that were selected for mutagenesis. The other amino acids of the active site (Tyr396 and His433, shown also in orange sticks) constitute the so called aromatic cage of amine oxidases and were excluded from mutagenesis as they are highly conserved.^{161,171,236} The right side shows in more detail the amino acids that were targeted for mutagenesis and which align the potential substrate entrance channel (blue dots). The helix around position E203 (colored in red) adopts a U-shaped shape (highlighted in brown color), resulting in various combinations for simultaneous randomizations at this element. D104 (purple sticks) is at the entrance of this channel and L168 F169 (cyan sticks) are located at a turn before the channel reaches the brown U-shape.

Table 33: Amino acids of PuO-Re targeted for site-saturation mutagenesis with degenerated codons. The location of the targeted position, the degenerated codon and the number of colonies that have to be screened for a library coverage of 95% are given.

targeted residue(s)	location	degenerated codon(s) used for mutagenesis	# colonies for 95% coverage (calculated with CASTER) ¹⁸⁹
D104	channel/surface	NNK	94
L168 F169	channel	NNK NNK	3066
M174	active site	NHK	70
V201 E203	channel	DNK NNK	2299
L207	active site	NNY	94
L200 E203 I206 ^[a]	channel	NDT NHK NDT	10352
V201 D204 ^[a]	channel	NDT NDT	430
D202 F205 ^[a]	channel	NDT NDT	430

degenerated codons:

N = A, C, G, T; K ("Keto") = G, T; H ("not G") = A, C, T; D ("not C") = A, G, T; Y ("pYrimidine") = C, T

amino acids (one letter code, * = stop):

NNK = all 20; NHK = A, N, D, Q, E, H, I, L, K, M, F, P, S, T, Y, V, *; NDT = R, N, D, C, G, H, I, L, F, S, Y, V; DNK = A, R, N, D, C, E, G, I, L, K, M, F, S, T, W, Y, V, *; NNY = A, R, N, D, C, G, H, I, L, F, P, S, T, Y, V

^[a]: The libraries were generated and screened by solid phase assay but no further analysis was done during this project. The lysate screening, purification and characterization of these mutants is ongoing work of another PhD project at the Institute of Technical Biochemistry.

The mutant libraries were generated by a modified Gibson Assembly protocol¹⁷⁹ and, after confirming the homogeneity of the randomized positions by sequencing, screened with the solid phase assay to a coverage of at least 95% as calculated with GLUE.¹⁸⁵ Following this, the mutants were grown in 96 well plates and the screening was continued as described above. For the last three libraries in Table 33 however, the expression in 96 well plates, lysate screening, purification and characterization was continued in another PhD project at the Institute of Technical Biochemistry.

Mutants for which the lysate screening resulted in promising activities were then selected for further characterization. These mutants were purified and their specific activity with the 11 polyamine substrates **28** to **38** determined. A summary of the positions and the activities is shown in Figure 32 and Figure 33. The specific activities for all variants are also given in [U/mg] in Table S16. Overall the previously identified mutation E203G still proved to be the one with the highest influence on activity and it was found several times, also in combinations with other smaller amino acids (serine and alanine) at position V201 (Figure 33). The most impressive result of the mutation at position E203G was found for the oxidation of 1,5-diaminohexane **33**. Whereas this substrate is one of the worst for the wt enzyme and does hardly show any activity, with the mutant it showed an increase in the oxidation rate of about 25-fold (Figure 33 and Figure S68). In contrast, mutations at the entrance of this channel (D104) or another turn of the channel (L168 F169) showed in most cases diminishing effects on activity (Figure 33). Also the library with the mutants for the active site position M174 did not result in any potential candidates for further analysis. Solid phase assay screening still indicated that some of the colonies were active, but after screening their lysates and comparing the activities to the wt enzyme, no candidates remained for follow-up investigation. Interestingly the other position targeted in the active site (L207) turned out to be much more promising. The substitution of it with a valine increased the activity for most substrates and in some cases even higher activities than with E203G were found (Figure 33).

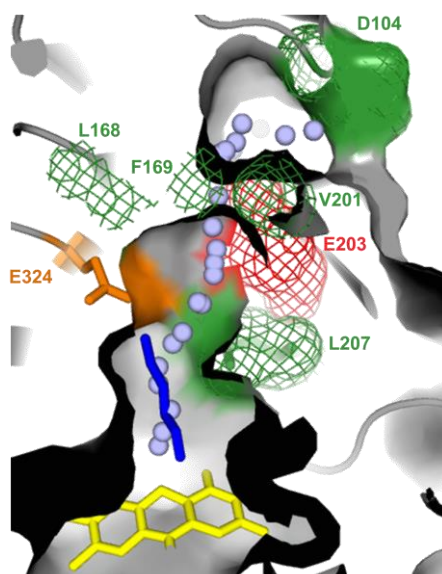


Figure 32: Active site of PuO-*Re* with the flavin cofactor in yellow sticks and the substrate 1,4-diaminobutane in blue sticks (pdb code: 2YG4).¹⁷¹ The mutant at position E203 previously generated by an epPCR is shown as red mesh. Novel positions that were selected for saturation mutagenesis are shown as green meshes. Position E203 was also included in the saturation mutagenesis. Combinations for simultaneous randomizations were done according to the CASTing criteria.^{189,234,235} The anionic point (E324) responsible for the correct positioning of the substrate in the active site^{166,171} is shown as orange sticks. The channel that leads into the active site is depicted as blue dots. Identification of it was done with the CAVER plugin of HotSpot Wizard.²³³

3 RESULTS

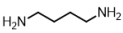
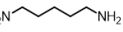
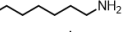
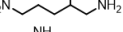
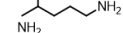
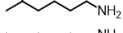
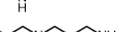
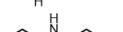
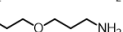
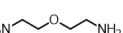

substrate #	wt	E203G	E203S	V201S E203G	L207V	V201A E203P	D104L	L168S F169Q	V201A E203G	A24T V201A E203M	compared to spec. activity of wt in [U/mg]
 28	12.28	275	148	124	116	112	79	30	186	79	< 20%
 29	0.45	733	476	516	456	281	19	186	553	301	< 20%
 30	87.36×10^{-3}	423	335	290	185	213	61	176	372	194	< 20%
 31	0.33	317	202	298	139	145	25	132	223	130	20-80%
 32	65.62×10^{-3}	1548	1495	837	259	622	131	32	1164	980	80-150%
 33	3.75×10^{-3}	2608	1582	1371	180	1420	2		1870	1363	80-150%
 34	2.63	376	193	129	54	4	28	68	182	17	300-1000%
 35	8.13×10^{-3}	349	142	249	604	107	34	53	255	184	300-1000%
 36	22.59×10^{-3}	58	48	35	166	41	68	32	55	38	> 1000%
 37	9.18×10^{-3}	423	186	340	231	182	53	143	460	162	> 1000%
 38	5.36×10^{-3}	142	87	9	724	81	173				> 1000%

Figure 33: Summary of the PuO-*Re* mutants that were generated by epPCR (described above) and saturation mutagenesis. The specific activities of the mutants in relation to the wt activity (in [U/mg]) with the polyamine substrates **28** - **38** are given as numbers in [%]. For a better overview in addition colors show the change in activity in [%]. The value for the best mutant is always shown in bold numbers. In most cases the mutant E203G generated by epPCR proved to be superior. In Table S16 the specific activities in [U/mg] are summarized for all variants.

3.9 Cascade reactions to transform polyamines into cyclic amines

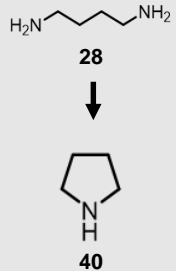
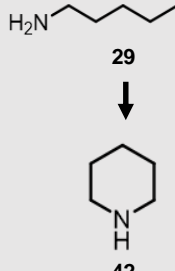
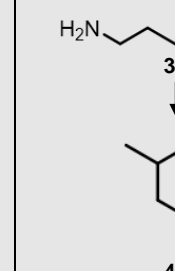
3.9.1 The combination of purified PuO-*Re* and IREDs

The production of *N*-heterocycles by the combined action of PuO-*Re* and IREDs was investigated as a proof of concept with both proteins purified using 10 mM of the polyamine substrates **28**, **29** and **31**. For the cascade reaction, both proteins were used in equimolar ratio. As the turnover numbers for PuO-*Re* wt with polyamines **29** and **31** are in the same range than the turnover numbers for the IREDs with piperidine substrates, the wild type enzyme of PuO-*Re* was used (Table 17, Table 18, Table 19 and Table 31). Thus limitations arising from substrate inhibition of the IREDs or the too high formation of H₂O₂ by PuO-*Re* are intended to be kept to a minimum. Samples were incubated for 3 h at 25 °C and after derivatization analyzed by GC-MS. As controls combinations were done in which always one of the enzymes was inactivated by heat treatment. For an initial analysis and to get an estimation about the performance of the three IREDs, the peak areas corresponding to the polyamines and the cyclic amines were normalized to the internal standard and the relative amounts in [%] in comparison to the normalized area of one 10 mM external standard of each compound was calculated. As the imines of such unsubstituted heterocycles tend to form dimers and trimers^{237,238} with high boiling points they could not completely be detected and were therefore not included in this analysis. The further optimization and investigation of this reaction cascade is also ongoing work of another PhD project at the Institute of Technical Biochemistry. The preliminary results with the comparisons of the three IREDs in combination with PuO-*Re* wt and the polyamine substrates **28**, **29** and **31** are summarized in Table 34.

After oxidation by PuO-*Re* all three polyamines could successfully be converted with all three IREDs to the cyclic amines pyrrolidine **40**, piperidine **42** and 3-methylpiperidine **44**. The control reactions showed that both enzymes had to be active for the complete transformation to the heterocyclic amine. The formations of the heterocyclic amines varied, but were always lower in case of 1,4-diaminobutane **28** (leading to pyrrolidine **40**) as substrate, compared to polyamines **29** and **31**, which both lead to a six-

membered piperidine product. In contrast, in the reactions with inactivated PuO-*Re* the polyamine substrate was not converted at all and after inactivation of the IREDs, only parts of the imine intermediates (**39** corresponding to pyrrolidine **40**, **41** to piperidine **42** and **43** to 3-methylpiperidine **44**, respectively) could be detected, but no heterocyclic amines. In addition in the samples with polyamine **31** after inactivation of the IREDs, no full substrate consumption was observed. About 10% of the residual polyamine could be detected, whereas it was fully consumed in the reaction with both enzymes being active. This could be an indicator for potential product inhibition of this cyclic imine on PuO-*Re* activity. Exemplarily this transformation is shown in Figure 34 for PuO-*Re* and *R*-IRED-*Sr* with 1,5-diamino-2-methylpentane **31** as substrate and the cyclic amine **44** as product in which the 3 h reaction time was sufficient for full substrate consumption (Table 34 and Figure 34).

Table 34: Analysis of the reaction cascade with purified proteins (PuO-*Re* and IREDs) for the conversion of 10 mM of the polyamines **28**, **29** and **31** into the heterocyclic amines **40**, **42** and **44**. Single reactions were performed of each biotransformation and the reactions stopped after 3 h. Control reactions were done in which always one of each enzymes was inactivated (indicated by the red background in Table 34). For analysis the peak areas were normalized to the internal standard and the ratio in [%] compared to one external 10 mM standard of the polyamines and heterocyclic amines was calculated. The imine intermediates were not examined in this work as they can form dimers and trimers with too high boiling points for the GC based analysis. In most reactions with both enzymes being active high conversions to the heterocyclic amines could be found and no residual polyamines were detected. In contrast, in the samples with inactivated PuO-*Re* no conversions of the polyamines were observed. After inactivation of the IRED full conversion of polyamines **28** and **29** was observed, but no cyclic amine detected. Also for **31** no cyclic amine could be detected, but in addition about 10% of the residual polyamine was found, an indicator for potential product inhibition of this imine on the activity of PuO-*Re*. -: not detected or analyzed as only parts of the imine (monomer/dimer) were detected.

polyamine substrate						
	28 [%]	40 [%]	29 [%]	42 [%]	31 [%]	44 [%]
PuO- <i>Re</i> (active) <i>R</i> -IRED- <i>Sr</i> (active)	-	51	-	> 99	-	95
PuO- <i>Re</i> (inactive) <i>R</i> -IRED- <i>Sr</i> (active)	> 99	-	> 99	-	> 99	-
PuO- <i>Re</i> (active) <i>R</i> -IRED- <i>Sr</i> (inactive)	-	-	-	-	13	-
PuO- <i>Re</i> (active) <i>R</i> -IRED- <i>St</i> (active)	-	4	-	> 99	-	> 99
PuO- <i>Re</i> (inactive) <i>R</i> -IRED- <i>St</i> (active)	> 99	-	> 99	-	> 99	-
PuO- <i>Re</i> (active) <i>R</i> -IRED- <i>St</i> (inactive)	-	-	-	-	9	-
PuO- <i>Re</i> (active) <i>S</i> -IRED- <i>Pe</i> (active)	-	62	-	84	-	94
PuO- <i>Re</i> (inactive) <i>S</i> -IRED- <i>Pe</i> (active)	> 99	-	> 99	-	> 99	-
PuO- <i>Re</i> (active) <i>S</i> -IRED- <i>Pe</i> (inactive)	-	-	-	-	9	-

The GC traces for the conversion of diaminobutane **28** to pyrrolidine **40** and diaminopentane **29** to piperidine **42** with PuO-*Re* and *R*-IRED-*Sr* can be found in Figure S82 and Figure S83, respectively. The transformations with PuO-*Re* and *R*-IRED-*St* with **28**, **29** and **31** to **40**, **42** and **44**, respectively are

3 RESULTS

shown in Figure S84, Figure S85 and Figure S86. The transformations of the three polyamines with PuO-*Re* and S-IRED-*Pe* are shown in Figure S87, Figure S88 and Figure S89.

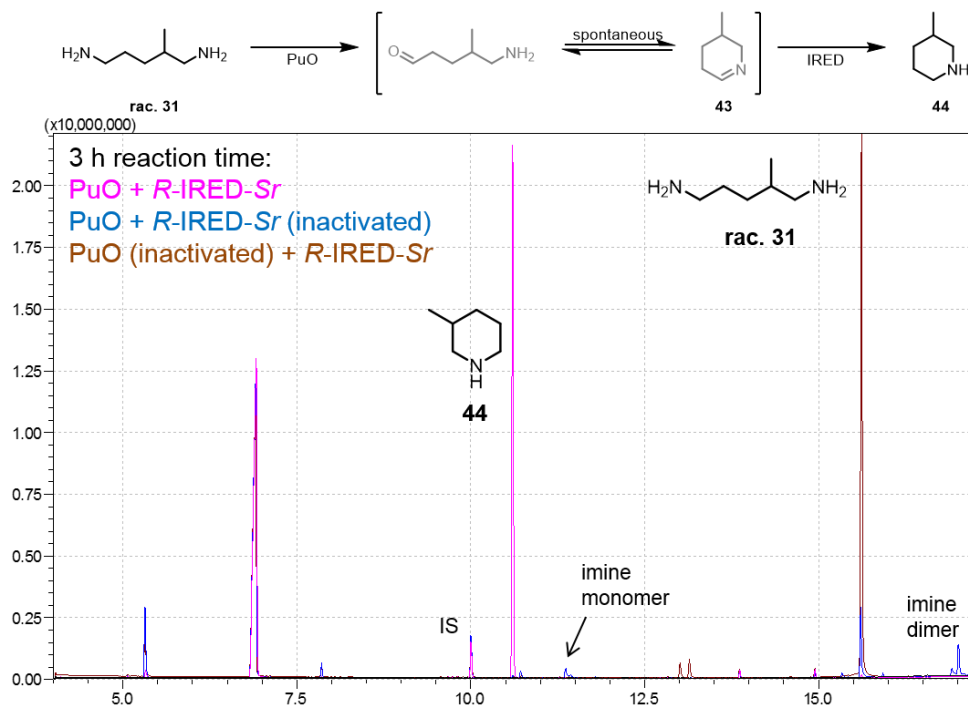


Figure 34: Conversion of polyamine **31** to the cyclic amine product **44** by the combination of purified PuO-*Re* and R-IRED-*Sr*. In the reaction with both enzymes being active (pink) the substrate is fully consumed in the 3 h reaction time and transformed to the product **44**. After inactivation of one of the enzymes (R-IRED-*Sr* inactivated in blue or PuO-*Re* inactivated in brown) either the polyamine is not converted (brown) or small amounts of the imine intermediates (blue) could be detected. In addition for this substrate after inactivation of the IRED no complete substrate consumption was detected, indicating some kind of product inhibition on PuO-*Re*. The reaction scheme on top assumes that the sterically less demanding amine group of **31** is oxidized, however the regioselectivity of PuO-*Re* has to be determined. Depending on this regioselectivity also different imine intermediates are formed, however this information is lost after reduction of the cyclic imine by an IRED. IS = internal standard.

3.9.2 Cascade reaction with whole cells expressing PuO-*Re* and the IREDs

To avoid the laborious purification of several enzymes, it was finally shown that the reaction cascade can be transformed to a host cell expressing both enzymes at the same time. After overnight expression, the cells were washed and used as whole cell biocatalyst as described for the IREDs above (see 3.3). As model substrate polyamine **31** was selected due to the high conversion by using purified enzymes and as it represents an unnatural polyamine in contrast to 1,4-diaminobutane **28** and 1,5-diaminopentane **29** (see 3.9.1). All three strains were able to transform the polyamine to the cyclic amine product **44**. As shown in Figure 35 for the *E. coli* strain JW5510 expressing PuO-*Re* and S-IRED-*Pe* simultaneously for a reaction time of up to 20 h, the amount of product **44** increased. The analysis of the GC peak areas^{VI} underlined this increase in product formation over time (Table 35). Nevertheless the overall performance was poor compared to the use of purified enzymes as it is obvious by the large peak corresponding to the residual substrate (see Figure 35 and Table 35). The use of the

^{VI}: The ratios of the polyamine substrate **31** and the heterocyclic amine product **44** in [%] were calculated from the GC areas. The comparison to the standard, as performed above, was not possible, as the volume of the sample taken was different due to the cells.

other two IREDs (*R*-IRED-Sr and *R*-IRED-St) yielded comparable results (Table 35) and the chromatograms for these transformations are shown in Figure S90 and Figure S91.

Table 35: Analysis of the GC areas for the transformation of polyamine **31** into the heterocyclic amine **44** by whole cells expressing PuO-*Re* and an IRED simultaneously. Single reactions were performed and regularly samples taken. After derivatization and GC analysis the fractions corresponding to the polyamine substrate and the amine product were calculated in [%]. For the given reaction time of 20 h the formed product increased in all cases, however compared to the performance of isolated enzymes the overall substrate consumption and product formation was poor. -: not detected.

time [h]	<i>E. coli</i> JW5510 with PuO- <i>Re</i> and <i>R</i> -IRED-Sr		<i>E. coli</i> JW5510 with PuO- <i>Re</i> and <i>R</i> -IRED-St		<i>E. coli</i> JW5510 with PuO- <i>Re</i> and <i>S</i> -IRED- <i>Pe</i>	
	31 [%]	44 [%]	31 [%]	44 [%]	31 [%]	44 [%]
0	> 99	-	> 99	-	> 99	-
3	94.6	5.4	90.9	9.1	94.1	5.9
6	93.2	6.8	87.2	12.8	92.4	7.6
20	92.2	7.8	86.8	13.2	90.5	9.5

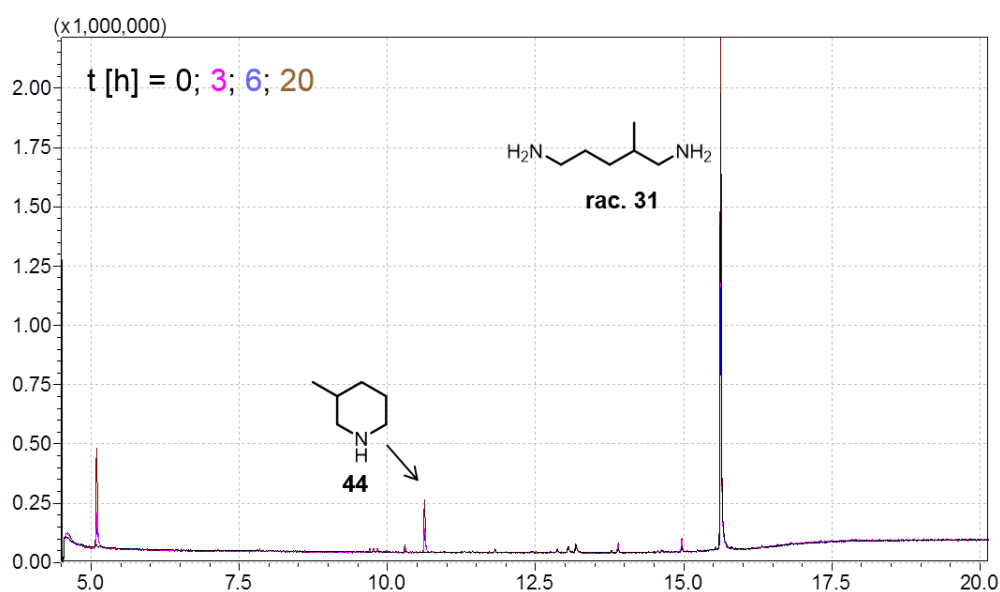


Figure 35: Whole cell biotransformation of polyamine **31** to the cyclic amine **44** with *E. coli* JW5510 expressing PuO-*Re* and *S*-IRED-*Pe* simultaneously. For the reaction time of 20 h the amount of product slightly increased. Compared to the performance of isolated enzymes the consumption of the substrate and transformation to the amine was poor.

4 DISCUSSION

4.1 Identification, selection and definition of enzymes of the IRED family

4.1.1 The importance of IREDs as novel biocatalysts for the generation of chiral amines

Biocatalytic methods for the generation of chiral amines have emerged as promising alternative to chemical means. Unfortunately, until recently the amines accessible were limited by the available enzymes. Traditionally lipases are employed, also on an industrial scale, for kinetic resolution of racemic amines.^{239,240} Mechanistically however they only provide access to primary amines.⁶⁰ The same is true for ω -TAs, ammonia lyases and amino acid or amine dehydrogenases.^{50,62,65,92,241} For ω -TAs an exception has been described,^{154,155} and for ammonia lyases by protein engineering the amine nucleophile scope was expanded, enabling access to substituted secondary amines, derived from aspartic acid.⁹⁸ As both methods are not broadly applicable, for quite some time deracemizations relying on amine oxidases were the biocatalytic method of choice to access secondary and tertiary amines.^{2,43} In most cases the (S)-selective MAO-N was applied, which has throughout the last about 15 years undergone extensive evolution to broaden its substrate scope.^{110–113,115} To access the other enantiomer, (R)-selective amine oxidases for deracemizations were generated by protein engineering.^{119,120} Another just recently patented enzymatic method for preparation of chiral secondary and tertiary amines involves the reductive amination of ketones with opine dehydrogenase variants.^{106,107}

Alternatively, the novel enzyme class of the IREDs received considerable interest since their first description by Mitsukura *et al.* about 5 years ago.¹³⁷ In contrast to MAO-N and opine dehydrogenases, it was shown for IRED wt enzymes that they are active on imines that lead to chiral primary, secondary and tertiary amines.^{139,142–152} This versatility and the high selectivities that were described for the IREDs promoted their use as biocatalysts, what is reflected in a rapid growing number of known and characterized enzymes published especially in the last two years.^{139,142–152} Impressively, in one work 50 novel enzymes were cloned and tested for the reduction of 3*H*-indoles¹⁵⁰ and in another work the pharma company Roche has published their investigations on 20 novel IREDs.¹⁴⁹ Within the Chem21 project, which started in October 2012²⁴² several research groups and GlaxoSmithKline expressed considerable interest in these enzymes and a larger number of IRED genes was ordered and will now be characterized in ongoing works. The characterization of them will probably shed more details on the mechanism and origin of these enzymes as well as their relation to other enzymes. Overall, keeping the enormous potential of the IREDs in mind and the attention they instantly gained, it is expected that the number of IREDs and the application of them in biocatalysis will grow even faster.

4.1.2 Defining and expanding the known sequence space of IREDs

The above mentioned rapid increase in known and confirmed IREDs required an in detail analysis how to exactly define these enzymes with respect to related enzymes. The early classification in (R)- type and (S)- type enzymes from two different superfamilies was based on the transformation of imine substrate **1** performed by literature known IREDs^{138,139,142,143} and the three novel IREDs characterized

during this work.¹⁴⁵ The selection of these novel IREDs from *Streptosporangium roseum* DSM 43021 (*R*-IRED-*Sr*), *Streptomyces turgidiscabies* (*R*-IRED-*St*) and *Paenibacillus elgii* (*S*-IRED-*Pe*) was based on the combination of biochemical information about the three at this time published IREDs from *Streptomyces* sp.^{138–142} with bioinformatics sequence analyses. As therefore only few criteria could be applied to reduce the sequence space, very stringent sequence thresholds were applied to select the members for the first version of the “Imine Reductase Engineering Database” resulting in only about 350 protein entries.¹⁴⁵ The establishment of (*R*)- type IRED and (*S*)- type IRED superfamilies resulted also in the first classification system of these enzymes. Yet, as the number of characterized IREDs has steadily increased a few exceptions from this selectivity pattern were described,^{148,149} but the overall majority of IREDs from these two families follows the classification. As such a designation greatly facilitates the communication it will be kept in the current discussion of this work.

With the proof that even more distantly related enzymes, not part of the two superfamilies of (*R*)- type and (*S*)- type IREDs are functional,^{146,149,150} the threshold how to define an IRED had to be reconsidered. This resulted in an updated version of the “Imine Reductase Engineering Database”,¹⁵² but also alternative classification systems were conceived, based on the C-terminal clustering of IRED sequences.¹⁴⁹ The currently proposed definition of an IRED on a sequence level relies on global sequence similarity to known IREDs and the match to two IRED specific motifs.¹⁵² The first motif describes the IRED specific cofactor binding region (GLGxMGx₅[ATS]x₄Gx₄[VIL]WNR[TS]x₂[KR]) and the second one characterizes the proposed active site (Gx[DE]x[GDA]x[APS]x₃[K]x[ASL]x[LMVIAG]).¹⁵² The combination of these information allows discriminating IREDs from the closest related family, the β-HADs (sequence identity up to 35%).¹⁵² These two motifs are sufficient to cover all currently described IREDs and by the application of them in total more than 1400 sequences encoding for over 1100 putative IREDs could be predicted by Fademrecht *et al.*¹⁵²

4.1.3 Cofactor binding of IREDs and mechanistic aspects for the enzymatic imine reduction

The comparison of the IRED specific cofactor binding motif with the cofactor binding motifs of the IRED related family of the β-HADs allowed to predict the preference of all IREDs for NADPH.¹⁵² β-HADs were described to be either NADH- or NADPH-dependent and the motif of the NADPH-dependent enzyme family shares a conserved arginine with IREDs (underlined in the motif described above).^{152,216,217} This preference for NADPH was experimentally confirmed during the characterization of several IREDs with IREDs preferring NADPH over NADH for the reduction reaction by a factor of 5 to over 80.^{138,139,145,146,213} The yellow color of the purified IREDs shown in Figure 11 for the (*R*)- selective enzymes might also be related to the NADPH binding. A spectral analysis of these proteins indicated a peak at 336 nm, close to the generally agreed NADPH maximum of 340 nm. The reason for the (*S*)- selective IRED to remain colorless might be due to some structural differences of the bound NADPH. A highly conserved proline in superfamily 2 ((*S*)- type IREDs) might be the responsible amino acid of the IREDs therefore.¹⁵² In the crystal structure of the (*S*)- selective IRED from *Streptomyces* sp. GF3546 (pdb code: 4OQY)¹⁴⁴ the NAPDH adopts a bend like structure compared to the NAPDH in the structure of the (*R*)- selective enzyme from *Streptomyces kanamyceticus* (pdb code: 3ZHB)¹⁴² (Figure 36). The color could therefore

4 DISCUSSION

be just due to the different conformation of the NADPH, but these difference could also be reflected in different affinities for NADPH. In this concept the yellow colored IREDs should have bound NADPH and the colorless ones not. Preliminary tests to determine the affinity for NADPH of the IREDs were performed during this work, however due to the low sensitivity of the assay, based on NADPH absorbance no conclusions could be drawn from these experiments.

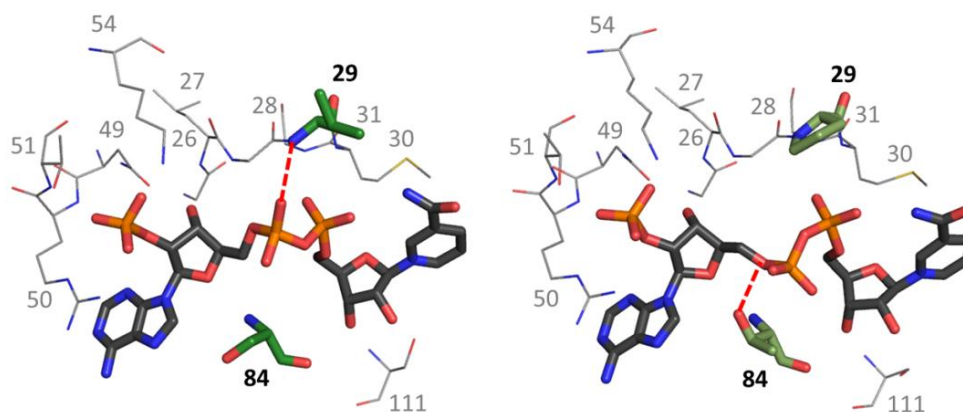


Figure 36: Cofactor binding sites of an (*R*)- type (left) and (*S*)- type (right) IRED. For the comparison the crystal structures of *R*-IRED-*Sk* (pdb code: 3ZHB)¹⁴² and *S*-IRED-*Ss* (pdb code: 4OQY),¹⁴⁴ both containing the NADPH ligand, were used. The conserved proline at standard position 29 in the (*S*)- type IREDs causes the NADPH to adopt a bend at the phosphodiester linkage, stabilized by different hydrogen bonds (red dashes). This figure was provided by Silvia Fademrecht.¹⁵²

The active site motif of IREDs can be used to discriminate them further from the closest related enzyme family, the β -HADs. While these enzymes are characterized by a conserved lysine in their motif representing an essential amino acid for catalysis, this position is only superfamily specific conserved in IREDs.^{152,216} (*R*)- type IREDs possess mainly an Asp at this position and (*S*)- type IREDs a Tyr.^{145,152} In analogy to the role of the conserved Lys in β -HADs, a mechanism for IREDs was proposed involving protonation of the imine to an iminium and hydride transfer from NADPH for the reduction to the amine.¹⁴² Derived from the mechanistic information about other imine reducing enzymes like dihydrofolate reductase (DHFR),^{128,243,244} pyrroline-2-carboxylate reductase¹²⁷ and thiazoline reductase Irp3,¹²⁵ there is some debate about the chronology of these steps, but most likely protonation precedes the hydride transfer.¹⁰⁷

The differentially conserved active sites of (*R*)- and (*S*)- type IREDs however render it questionable whether the protonation actually relies on such a “catalytic” amino acid, as suggested for *R*-IRED-*Sk*,¹⁴² or not. This is further supported by catalytically active (*R*)- type IRED mutants (Table 10 and Table 11)^{145,147} and active wild type IREDs with Ala,¹⁴⁶ Phe¹⁴⁹ and Asn^{149,VII} at this position. In contrast however, the (*S*)- type IREDs all display the conserved Tyr at this position and all of the generated mutants were largely inactive (Table 10).^{145,148} Therefore, different roles of Asp and Tyr, as well as variations in the mechanistic aspects between both (*R*)- and (*S*)- type IREDs can at the moment also not be excluded. This is supported by the fact, that the catalytic constants for the mutants of the (*R*)- selective IREDs decreased only by a factor of about 100 to 400 (Table 11, *R*-IRED-*Sr* and

VII: The characterization of an active IRED with Asn in the active site represents currently unpublished work from the group of Prof. Dr. Nicholas Turner, University of Manchester. The work was presented during Chem21 project meetings and on a poster at the Dechema Summer School “Biotransformations 2014” in Bad Herrenalb, Germany.

R-IRED-*St*, respectively), whereas the knockout of a “true” catalytic residue, the serine in the catalytic triade of proteases for example leads to a decrease of k_{cat}/K_M by a factor of at least 10^5 .²⁴⁵ Due to the very low activity of *S*-IRED-*Pe* Y208A the catalytic constants were not determined, but as already described in biotransformations the mutant protein was in contrast to the *R*-IREDs nearly completely inactive (Table 10).

Further observations on the different roles Asp and Tyr might play for catalysis of an IRED were reported by Man *et al.*¹⁴⁸ During the characterization of the Tyr containing (*S*)- selective IRED from *Streptomyces* sp. GF3546 a more narrow pH profile was found than for the (*R*)- selective Asp containing IREDs *R*-IRED-*Ss* and *R*-IRED-*Sk*.¹⁴⁸ According to the authors, the broader pH profile of the Asp containing IREDs might be related to the role this residue plays for catalysis.¹⁴⁸ Analogously to an Asp in DHFR of *E. coli*, the Asp of the IREDs might function in building up an H-bonding network with H₂O for the protonation of the substrate, whereas the Tyr might serve as direct proton donor.¹⁴⁸

Taken together, at the moment it seems more likely that at least for the (*R*)- type IREDs the previously designated catalytic residue functions more as an important residue for the correct positioning and stabilization of the substrate or in the stabilization of water by building up an H-bonding network, than in a direct catalytic way. As described for DHFR,^{128,244} the source of the proton in the *R*-IRED mediated catalysis might be H₂O. Whether this water molecule has to be coordinated by Asp or other amino acids remains to be discussed. Considering the weakly basic nature of an imine, having a pK_a value of about 8 to 9, at neutral pH it should however be *per se* protonated, alleviating the need for a further proton donating step. The function of the IRED would then mainly be in providing a protein environment for the correct placement and stabilization of the substrate in close proximity to the NADPH bound to the enzyme.

4.2 Biochemical characterization of novel IREDs

After selection of the three novel IREDs (*R*-IRED-*Sr*, *R*-IRED-*St* and *S*-IRED-*Pe*) a basic biochemical characterization of these enzymes was performed to be able to define conditions for their application as biocatalysts. During this work the pH profile, the thermostability and the effect of organic solvents on these enzymes were investigated. Although not that much information about IREDs is available, the three enzymes follow some general trends that seem to be similar for all IREDs.

The reported pH optima for the reduction reaction of the characterized IREDs are all in the neutral range around pH 7.0.^{138,139,146,148,150,151} The same behavior was found for *R*-IRED-*Sr*, *R*-IRED-*St* and *S*-IRED-*Pe* (Figure 13, Figure 14 and Figure 15). In addition all IREDs display a relatively broad pH profile, especially regarding alkaline conditions. *S*-IRED-*Pe* for examples maintained about 50% residual activity at pH 9.0 and showed a comparable broad pH profile than the Asp containing (*R*)-selective IREDs. This is in slight contrast to the above mentioned report by Man *et al.*,¹⁴⁸ but the increase in pH resistance of *S*-IRED-*Pe* might be explained by its generally increased resistance towards non physiological conditions and therefore masking the effect described by Man *et al.*¹⁴⁸

The thermal stability of IREDs is far less investigated than their pH profile. For the first IREDs that were characterized by Mitsukura *et al.*^{138,139} only rudimentary information about their low thermal stability was reported.^{138,139} For *R*-IRED-*Ss* for example it was described that after a 30 min incubation period at

35 °C the reduction activity remained stable and for S-IRED-Ss the optimal temperature was 40 °C.^{138,139} A more detailed characterization of these properties were done by Li *et al.* for the (S)- selective IRED from *Paenibacillus lactis* and the half-life times of this enzyme were determined at 30 °C, 40 °C and 50 °C.¹⁵⁰ With a $T_{1/2}$ of close to 50 h at 50 °C this IRED is assumed to be much more stable than the ones from *Streptomyces* sp., reported by Mitsukura *et al.*^{139,150} S-IRED-Pe originates also from a *Paenibacillus* strain and displays an even higher thermal stability. With a half-life time exceeding 400 h at 50 °C, it is the IRED with the highest thermal stability known to date. In contrast, the (R)- selective IREDs behave most probably comparable to the IREDs characterized by Mitsukura *et al.* and showed significantly lower half-life times and T_{50}^{15} values than S-IRED-Pe (Table 12 and Table 13). Although the genus *Paenibacillus* was not reported to be thermophilic,^{246,247} it is interesting that exactly the two IREDs from these strains show increased thermal stability compared to the other IREDs.

The effect of organic solvents on IRED activity was so far only published for S-IRED-Ss by Mitsukura *et al.*¹³⁹ and again only rudimentary information is available. The enzyme exhibited tolerance against MeOH, but not against EtOH, iProp, acetone and DMSO.¹³⁹ A general relatively high tolerance against MeOH could be confirmed for all three IREDs. In addition to MeOH, seven additional organic solvents were tested. The resulting residual activities correlate well with the thermostability, which in literature is often described to be associated with general stability *versus* denaturing conditions.^{49,248} Whereas for R-IRED-Sr with many solvents at elevated concentrations the residual activities declined to less than 1%, again S-IRED-Pe proved to be the IRED resisting more solvents and tolerating also higher concentrations of them (see 3.2.4). Displaying hardly any loss of activity in the presence of 20% MeOH is an interesting feature of this enzyme as polar organic solvents are usually not very well tolerated by enzymes because they show a high ability to strip of the essential water, contributing to the hydration shell of the enzyme.^{249–251}

For the application of these enzymes as biocatalysts, their substrate spectrum was investigated and kinetic constants recorded to evaluate the substrate acceptance. These points are discussed separately in the following chapter (see 4.3).

4.3 Exploration of the substrate spectrum of the IREDs

4.3.1 Reduction of cyclic and exocyclic imines

Although neither the physiological role, nor a natural substrate of an IRED are known, these enzymes are regarded as promising biocatalysts for the generation of chiral amines. The research that was performed during this project and that was also published in the literature by other groups^{143,146–150} resulted in the elucidation of many cyclic and exocyclic imines as substrates for IREDs. In these biotransformations primary-, secondary- and tertiary amines could be generated, underlining the versatility of IREDs for the preparation of chiral amines. In this project the substrate spectrum of the three novel IREDs was investigated in biotransformations performed with whole cells expressing these enzymes and with purified proteins.

In the initial reports by Mitsukura *et al.* the substrate spectrum of the IREDs was described to be very narrow.^{138,139} On the discovery of R-IRED-Ss a small set of imines, ketones and heterocyclic substrates was investigated, but activity could only be detected for 2-methylpyrroline (imine **1**).¹³⁸ In contrast, for

S-IRED-Ss also activity with the imines **5b**, **5c** and Δ^1 -pyrroline-2-carboxylic acid was described.¹³⁹ Encouraged by these reports, the group of Turner has synthesized a broad range of substituted pyrrolidines, piperideines, isoquinolines and β -carboline and investigated the reduction of them with the two IREDs described by Mitsukura *et al.*^{143,147} In their works, published 2013 and 2015, it was shown that these IREDs possess a much broader substrate spectrum towards cyclic imines than initially thought.^{143,147} Meanwhile also our^{145,213} and other groups^{144,146,149} have investigated pyrrolidines, piperideines, isoquinolines and β -carboline as substrates for IREDs.

Although the structures of (*R*)- and (*S*)- selective IREDs overall share a very similar fold^{142,144,148} and IREDs are also closely related on a sequence level^{145,152} (the sequence identity of *R*-IRED-*Sr* and *R*-IRED-*St* is > 54% and for both enzymes to *S*-IRED-*Pe* ~ 34%^{III}) there are some interesting differences in the substrates accepted. These differences were reported independently by various groups working with different IREDs, allowing to make some general statements about the IRED substrate scope. Cyclic six-membered rings are usually well accepted by both (*R*)- and (*S*)- selective IREDs and many substituents next to the C=N double bond are tolerated.^{143,146–149} Piperideines also tend to show higher conversion rates than pyrrolidines and azepane-derived imines.^{143,147,149} Electron-donating and electron-withdrawing substituents on phenyl rings next to the C=N double bond are usually readily accepted, with the substituents in the *para* position showing beneficial effects on selectivity so far.¹⁴⁷ Isoquinolines are also well accepted by both, (*R*)- and (*S*)- selective IREDs, however giving first indications for a broader substrate spectrum for bulky heterocyclic substrates with (*S*)- selective IREDs.^{143,144,147,149,150} Imine **5c** for example is accepted by these enzymes, but no activity was found with (*R*)- selective IREDs and also other groups did not report activity with *R*-IREDs on this compound.¹⁴⁷ For the even bulkier class of β -carboline also only activity with *S*-IREDs has been reported.^{143–149,213} The extension of the substrate spectrum to indole-derived imines has just recently been described in some of the latest IRED publications by Li *et al.* and Wetzl *et al.*^{149,150} In the work performed by Li *et al.* 50 novel IREDs were tested for this reduction, including *R*-IRED-*St* and *S*-IRED-*Pe*.¹⁵⁰ Interestingly, in this report *R*-IRED-*St* was active, but *S*-IRED-*Pe* not.¹⁵⁰ The most active IRED, however was again an (*S*)- selective IRED from *Paenibacillus lactis*, which did surprisingly not show activity on imine **5b**.¹⁵⁰ As *S*-IRED-*Pe* and the *S*-IRED from *Paenibacillus lactis* are very closely related with a sequence identity of 72.8% and a sequence similarity of 84.9% it seems likely that they possess similar properties and the increased thermostability of these two enzymes compared to all other described IREDs was already discussed above (see 4.2). It might therefore be worth to repeat the experiments reported by Li *et al.* to confirm that *S*-IRED-*Pe* does not show activity with 3*H*-indoles. By such a comparison useful information about amino acids of the active site that contribute to substrate binding and recognition might be acquired, but otherwise this also indicates that the prediction of substrates for a certain class of IREDs is not easily possible. Although altogether *S*-IREDs seem to have a slightly broader substrate spectrum, higher conversion rates in whole cell biotransformations are usually obtained with (*R*)- selective IREDs.^{107,137,143,145–148,201} An overview about the conversions and selectivities obtained in whole cell biotransformations that were performed in this work with *R*-IRED-*Sr*, *R*-IRED-*St* and *S*-IRED-*Pe* and the set of cyclic imine substrates is again given in Figure 37.

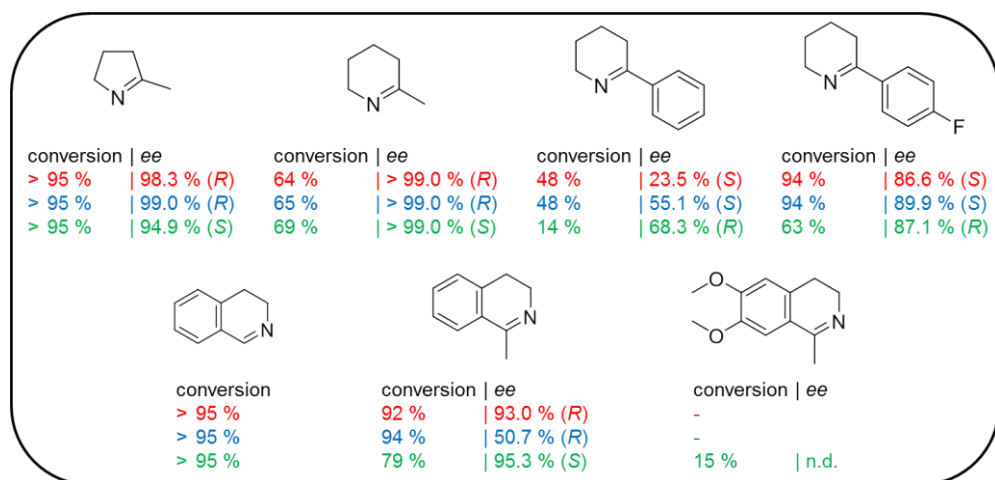


Figure 37: Summary of the product formations in [%] and the enantiomeric excess values in [%] for whole cell biotransformations after 24 h performed in this work employing *E. coli* cells expressing *R*-IRED-*Sr* (red), *R*-IRED-*St* (blue) and *S*-IRED-*Pe* (green). The change in the selectivity from the (*R*)- to the (*S*)- product for *R*-IRED-*Sr* and *R*-IRED-*St* and vice versa in the case of *S*-IRED-*Pe* is caused by a change in the priority of the substituents for the Cahn-Ingold-Prelog assignment.

Work on exocyclic imine substrates is far less reported,^{138,139,146,151} with the investigation of the oxidation reaction on amine substrates by Gand *et al.* being the most thoroughly published study.¹⁴⁶ The investigation of amines for the oxidation reaction is an experimentally much more amenable way for the exploration of the substrate scope as the amines are not prone to hydrolysis like the imines are. However the direct use of exocyclic imine substrates is the synthetically desired reaction and the chemical preparation of imines in organic solvents is a straightforward and established method.²²⁴ In the studies by Mitsukura *et al.* the imines **18** and **23** (precursor of the dialkylation product dibenzylamine **24** which was obtained in small amounts by the repeated reductive amination of benzaldehyde **11** in this work) were tested, but no activity reported.^{138,139} It has therefore to be highlighted that with the IREDs tested in this work activity for these compounds was found. Furthermore, for other exocyclic imines like **7**, **9** and **15** the amine products could be obtained. It seems therefore likely that IREDs are also able to accept a broad range of exocyclic imines as substrates. Based on this data it is however difficult to make some general statements for IRED activity on exocyclic imines as for example imine **7** was accepted by all three IREDs in this work, but **9** and **18** could be reduced only by the *R*-IREDs, with *R*-IRED-*St* showing much higher activities. In contrast **15** was mainly accepted by *R*-IRED-*Sr*, slightly by *S*-IRED-*Pe* and hardly by *R*-IRED-*St*. The broader substrate profile of the *R*-IREDs could in addition be misleading due to a combination of the higher activity these enzymes display and the hydrolytic instability of the exocyclic imine substrates. The further investigation and optimization of the reaction conditions for example by the inclusion of organic solvents to stabilize the imine substrates is therefore advisable to fully exploit IREDs for the reduction of this interesting new class of substrates.

4.3.2 Enantioselectivities for the reduction of imines

The selectivities that were obtained in the IRED-mediated biotransformations with whole cells and purified enzymes are often very high and exceed 99% ee.^{143–147,149,150} The highest selectivities obtained with *R*-IRED-*Sr*, *R*-IRED-*St* and *S*-IRED-*Pe* were all observed for the reduction of imine **3a**, with no traces of the opposite enantiomer detectable. The high selectivities that can be achieved with IREDs

again promote their use as biocatalysts for the stereoselective synthesis of chiral amines. Interestingly for some substrates large differences in the obtained activity and selectivity were observed, again despite the close relationship of the used IREDs. For example the products of the *R*-IRED catalyzed biotransformations performed with isoquinoline **5b** differed quite a lot in selectivity (*R*-IRED-*Sr* 93.0% *ee* and *R*-IRED-*St* 50.7% *ee*). In other cases already a small modifications of the substrate led to a strong change in selectivity as seen for example for piperidine **3b** and **3c**. As long as no structures with bound ligands are available the reasons for these strong differences in selectivity and the possibilities how to engineer IREDs for better selectivity are not clear. Preliminary results from crystallizations with ligands performed in the group of Prof. Dr. Gideon Grogan at the University of York however suggest multiple binding sites for substrates in the active site cleft of the IRED^{VIII}. Having an IRED structure with ligand and different binding modes of it available would help to understand some of the currently reported unexplained behaviors of these enzymes. Man *et al.* and Wetzl *et al.* reported a substrate dependent switch in the enantioselectivity of the used IRED^{148,149} and Hussain *et al.* reported different selectivities of the formed product depending if biotransformations were performed with whole cells or with purified protein.¹⁴⁷

4.3.3 Reduction of carbonyls

The reduction of carbonyls was observed as byproduct during the investigation of the reduction of exocyclic imines with purified IREDs and suspected to originate from contaminants of co-purified KREDs. The hydrolytic instability of such imines produces carbonyl byproducts that can be reduced by these enzymes. For example imine substrates **7** and **9** hydrolyze to benzaldehyde **11** and methylamine **22** or aniline **12**, respectively. Aldehyde dehydrogenase activity is numerously found in *E. coli*, with 44 potential enzyme candidates identified and 13 confirmed ones.^{252,253} Thereof for at least six enzymes activity for the reduction of **11** was confirmed.²⁵² As the investigated substrates most probably do not represent natural ones for IREDs and hence the activity was in general rather poor, enough of the IREDs had to be used to capture the available (unstable) imine. The enzyme loading in these biotransformations was therefore increased over 15-fold compared to the enzyme amount used for the reduction of cyclic imine substrates. The strong increase of the biocatalyst loading has to be considered as thereby also the amounts of the suspected contaminating KREDs, responsible for the carbonyl reduction, are increased. Already slight contaminations like 2% of the total protein will have an enormous impact if the enzyme loading is that much increased. To deal with this, the IREDs had to be sufficiently pure and indeed, the increase in purity led to higher amounts of the amine product formed (see 3.5.2). Together with the biotransformations performed with purified *R*-IRED-*Sr* D191A, that did not produce any amine product but in which alcohol byproduct formation was observed, it seems likely that the aldehyde reduction after the hydrolysis of **7** or **9** was indeed performed by contaminating KREDs. However a weak promiscuous activity of IREDs on carbonyls can also not be excluded at the moment, although all literature reports on carbonyl reduction were unsuccessful.^{138,146,147} Producing IREDs with

^{VIII}: The elucidation of IRED structures with bound ligands represents currently unpublished work from the group of Prof. Dr. Gideon Grogan, University of York. The presentations of these results were done during an IRED project meeting and on the conference Transam 2.0; 2015 in Greifswald, Germany.

an *in vitro* translation system will probably be the most straightforward way to exclude (or confirm) the observed KRED activity as thereby also precise control reactions can be included.

4.3.4 Reduction of activated C=C bonds and others

In an attempt to shed more light into the substrate spectrum of IREDs in the diploma thesis of Sebastian Hofelzer IRED activity with imines, oximes, oxime ethers, benzoquinolines, amidines, activated C=C double bonds and carbonyls was investigated.²¹³ The only substrate of this list that was accepted by the IREDs was cinnamaldehyde **45** and in these biotransformations the activated C=C double bond was reduced. Carbonyl reduction was also found with this substrate, but was considerably lower than the reduction of the C=C double bond. As discussed above this slight reduction might most likely be caused by contaminating KREDs in the enzyme preparation (see 4.3.3). To confirm this promiscuous activity the reactions were repeated during this work.

Again, all three IREDs displayed activity towards the C=C double bond in the Michael system. *R*-IRED-*Sr* and *S*-IRED-*Pe* showed only very low activity and the formation of 3-phenylpropanal **46** was less than 3-5% in 24 h. *R*-IRED-*St* showed the highest activity and about 15% of the product was formed (Table S8). In addition to the C=C reduction also small amounts of a byproduct from the aldehyde reduction were found. Overall the alcohol byproduct was found to be less than 4% and the fully reduced product was not found at all (Table S8). As it was already discussed above, the alcohol formation is assumed to be most likely caused by contaminating ketoreductases in the IRED preparation. The only ene reductase activity in *E. coli* is attributed to the *N*-ethylmaleimide reductase (*E. coli* gene: *nemA*).^{44,254–258} In a thorough investigation of biotransformations performed with several ene reductases expressed recombinantly in *E. coli* however the background activity of NemA was negligible, except for nitroalkenes.²⁵⁸ As it is also the case for the carbonyl reduction (4.3.3), the further purification of the IREDs or the use of a *nemA* knockout strain¹⁷⁵ for production of the enzyme should be performed as additional control to ensure that the reduction of the C=C double bond in **45** represents the first “promiscuous” activity for IREDs.

4.3.5 Investigation of the substrate preference of IREDs and considerations for the search of natural substrates

To get insights in the substrate preference of the IREDs, kinetic constants were recorded with purified proteins and the set of cyclic imine model substrates. Comparable results to the ones that were obtained during this work were meanwhile also published by other research groups^{107,143,147,148,201} and are also in agreement with the results of the biotransformations. A comparison based solely on biotransformations could however be misleading due to differences in the experimental setups that are reported for biotransformations and varying expression levels of the IREDs. Piperideines are well accepted as substrates and preferred over pyrrolidine rings. The k_{cat}/K_M for them is at least 4-fold and up to 160-fold higher, meaning that if both substrates would be present at the same time, the IRED preferable would transform the piperideine scaffold. Comparing cyclic imines **1** and **3a**, **3b** and **3c** it might also be possible that *R*-IRED-*St* has a slightly better performance with larger substrates compared to *R*-IRED-*Sr*. This

could also help to explain the differences in conversion observed during the biotransformation of the exocyclic imine substrates **9** and **18**. The generally lower turnover numbers determined for *S*-IRED-*Pe* might then also help to understand the very low conversion of these substrates with this enzyme as they probably hydrolyze too fast to be transformed efficiently.

Isoquinolines are again well accepted by all IREDs and actually **5** is the substrate with the highest k_{cat}/K_M observed for *S*-IRED-*Pe*. This tendency was not that pronounced with the *R*-IREDs and might again reflect the already suspected broader substrate scope of *S*-IREDs towards more bulky cyclic imine substrates (see also 4.3.1). With some of these substrates inhibitions of the used IREDs were observed at higher concentrations, however therefore also no clear trend could be obtained. Again as all of the three enzymes are closely related (4.3.1) and there are no structures with ligands of them available it is not possible to attribute these differences to the architectures of the active sites of these enzymes.

Further, setting the obtained catalytic efficiencies in relation to the catalytic efficiencies that are assumed for enzymes with their natural substrate (they are supposed to be between $10^5 - 10^8 \text{ M}^{-1} \text{ s}^{-1}$ and thereby at least 10^3 times higher than the typical ones observed for the IREDs)^{259–261} it is tempting to assume that none of the tested substrates so far represents a natural substrate of an IRED. Due to their homology IREDs were in most cases wrongly annotated as glycerol-3-phosphate dehydrogenases and 6-phosphogluconate dehydrogenases, however in none of the literature reports (including *R*-IRED-*Sr*, *R*-IRED-*St* and *S*-IRED-*Pe*) where activity with such substrates was tested it could be found.^{145–147} Keeping in mind that substrate promiscuity is assumed to be much more widespread than catalytic promiscuity²⁶² it seems likely that the C=N reduction represents the natural activity and does not represent a promiscuous reaction, but without knowing more about the mechanism of these enzymes the confirmation therefore is still outstanding.

4.4 Application of IREDs as whole cell biocatalysts

The use of IREDs in whole cell bioreductions has the advantage of a simple preparation of the biocatalyst and the possibility to use the host metabolism for *in situ* cofactor regeneration, although also the use of isolated enzymes might be beneficial to avoid competing side reactions and eliminate transport barriers.^{38,45,46,62}

Most of the biotransformations with the cyclic imine substrates in this work were performed with whole cells expressing the IREDs. As cyclic imine substrates are hydrolytically relatively stable, competing side reactions like the reductions of the corresponding carbonyl hydrolysis products of exocyclic imines were not observed. However other problems that might arise and were also observed, are related to the cellular metabolism. The loss of cell fitness is a considerable problem and for whole cell biotransformations always fresh cells had to be used as after freezing the activity considerably decreased. As IREDs survive several freeze/thaw cycles without any impact on activity, it is most probably the case that the host metabolism suffers by this procedure. This then might lead to an insufficient cofactor regeneration capacity. The cofactor regeneration capacity is already suspected to be limited and the use of glucose as additional energy source is crucial. In the diploma thesis of Sebastian Hofelzer it was shown, that otherwise hardly any conversions were obtained.²¹³ Furthermore, Nagasawa *et al.* reported in a patent covering *R*-IRED-*Ss* that the co-expression of a glucose

dehydrogenase from *Bacillus* sp. resulted in about twofold higher imine reducing activity.¹⁴¹ This limitation is also obvious, when working with *R*-IRED-*Sr* and *R*-IRED-*St*. During the reduction of substrates **1** and **3a** in whole cell biotransformations full substrate consumption in less than 3 h and less than 0.5 h was observed. Knowing the maximal turnover numbers of the enzymes for these substrates (Table 17 and Table 18) however, it is likely that substrate **3a** should have been transformed even faster. Further information for the inability of the host metabolism to satisfactorily regenerate the NADPH can be derived from the biotransformations with the *R*-IRED mutants (*R*-IRED-*Sr* D191A and *R*-IRED-*St* D193A). In whole cell biotransformations with them, conversion rates decrease to about 15% and 5%, respectively. In contrast, the purified enzymes showed 10- to 100-fold decreased turnover numbers. This indicates that the whole cell biotransformations employing the wild type enzymes should be faster if one considers solely the IRED activity (the expression level of the wt enzymes and the mutants was equal, based on SDS gel analysis). Next to limitations of the cofactor regeneration capacity however also transport limitations could account for this.

Another constraint for using whole cells arises from limitations in the recovery of the product, as it was observed with amines **4a** and **4b**. In both cases 10 mM of the imine substrate was used and fully consumed during the biotransformation, but the maximal detected product yield was about 70%. Next to limitations in the recovery of products from complex biological samples, also the possibility that the host strain might metabolize the substrate or product should be considered. Metabolization of the imine substrate was detected in case of isoquinoline **5c**, where the cells harboring an empty pBAD33 plasmid consumed about 20% of the substrate (Figure S12).

4.5 Applications with purified IREDs

4.5.1 Reduction of exocyclic imine substrates and analytical challenges for their detection

The main investigations performed with purified IREDs aimed for the reduction of exocyclic imine substrates and their use in reductive amination reactions. For both of these parts it is important to keep the hydrolytic sensitive nature of the imine substrate in mind and the therewith associated challenge for their detection.

The hydrolysis of such exocyclic imines is very rapid and for example with imine **7** directly after the setup by GC analysis the imine **7** and the aldehyde **11** could be detected in a ratio of about 60/40. As observed in the negative control with heat inactivated IRED, this ratio did not change (see also Table 24), indicating a potential equilibrium. However the work-up of these samples dramatically influenced the conditions and hence the analytical result. First, the extraction into the organic solvent eliminates the water and might promote imine formation or at least increase the stability. Second, for extraction of the amines the pH of the samples was raised to > 14. The change in pH also changes the protonation status of the amine hydrolysis products, with the deprotonated amine being a nucleophile capable of imine formation. The combination of these factors led to an overestimation of the imine fraction detected. In control experiments it was tested that small amines like methylamine **22** are either not or only poorly extracted. Imine formation in the organic phase after extraction is then either not supported by the conditions (solvent MTBE) or might be neglected. The GC results for these combinations will therefore

most likely give the equilibrium of carbonyl/imine during the workup. In contrast, when working with imines **9** and **18** also the amine nucleophile **12** was extracted. In the negative controls for all of these electron rich substrates (**9**, **15** and **18**) their hydrolysis could be followed for a period of several hours, what could indicate a slightly higher hydrolytic stability. It is however also possible that the amount of imine detected by HPLC in these cases is falsified due to re-formation of the imine substrate after the sample workup (solvents ammoniumbicarbonate buffer and acetonitrile).

To get further insights into the imine formation, Maïke Lenz^{IX} performed NMR experiments.¹⁵¹ By NMR spectroscopy directly the imine fraction in the aqueous buffer could be detected without changing the conditions for workup as required for GC or HPLC analysis. Being aware of the different acidities of hydrogen and deuterium, ($pD = pH + 0.4$),^{263,264} it was possible to estimate the true imine fraction. For the condensation of aldehyde **11** and amine **22** at the respective pH of 8.2 the imine fraction is about 32% and not > 80% as detected by GC, thereby confirming the overestimation (Figure 38 and Table S11; the reference value with 500 mM of the nucleophile has to be used for the comparison).¹⁵¹

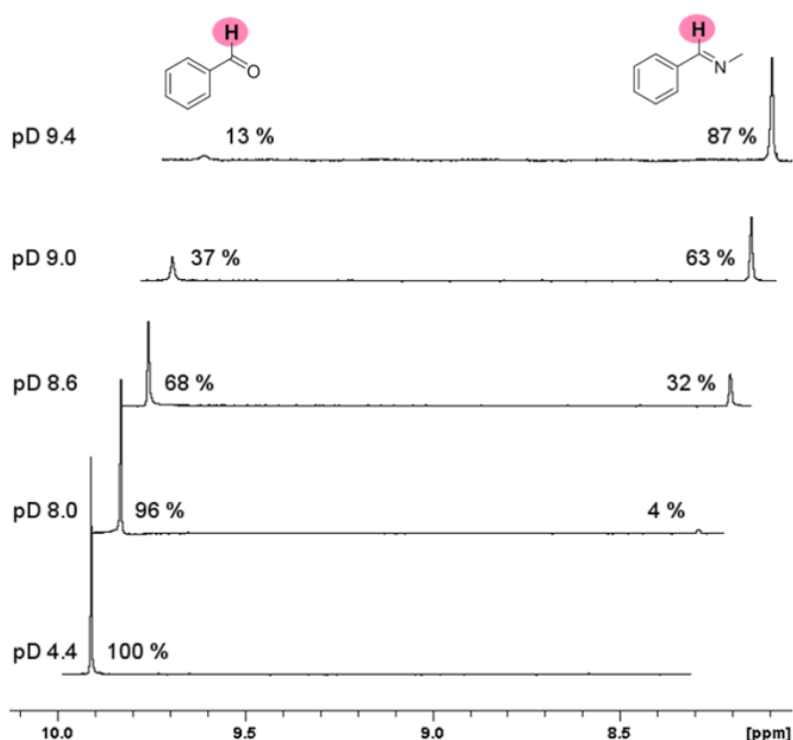


Figure 38: ¹H-NMR spectra to follow the condensation of aldehyde **11** and amine **22** for the formation of imine **7** at different pH conditions, increasing from pH 4.0 to 9.0. As solvent for the NMR experiments D₂O was used. The pD was calculated by the following correction $pD = pH + 0.4$.^{263,264} Above the respective pH of 8.2, substantial amounts of imine **7** could be detected. This figure was provided by Maïke Lenz.¹⁵¹

Disadvantages of the NMR experiments are the low sensitivity of this technique. For example, for the reaction of acetophenone with methylamine no imine formation could be detected, but IREDs are capable of product formation (see 3.6.2).¹⁵¹ The detection limit of the ¹H-NMR is permissively estimated to be above 500 μM, thereby highlighting the potential of IREDs to reduce also low amounts of imines.¹⁵¹

^{IX}: Biocatalysis group, Institute of Technical Biochemistry, University of Stuttgart.

Summarized it could be said that when working with exocyclic imine substrates, the IRED activity or amount of enzyme has to be high enough to capture the available imine substrate before it completely hydrolyzes. As already mentioned in 4.3.1, the optimization of the reaction conditions to reduce the hydrolysis by performing biotransformations in low water containing media will be advisable, as is the engineering of IREDs to show higher activity and stability for these conditions.

4.5.2 Reductive amination reactions – the potential of IREDs

A significant advancement for the use of an IRED is to exploit their reductive potential directly for stereoselective intermolecular reactions to generate novel C-N bonds from carbonyls and amines. Enzymes to perform such reductive amination reactions (“reductive aminases”) have long been sought after and this reaction has been described as one of the most aspirational ones.²⁶⁵ As it is difficult to achieve highly selective reductive aminations by chemical catalysts,^{16,20} enzymes with their exquisite selectivity appear to be promising catalysts for such challenging reactions. Indeed, the reductive amination of α - and β - keto acids to produce amino acids and derivatives thereof is performed with natural and engineered enzymes also on an industrial scale.^{44,77,83,84,266,267} The enzymatic reductive amination of unfunctionalized ketones however was only described in one work with an enzyme from *Streptomyces virginiae* IFO 12827,²⁶⁸ without any follow-up results published. The lack of such enzymes represented a significant disadvantage and by protein engineering the group of Bommarius has for the first time, and later also other groups, promoted to generate amine dehydrogenases from amino acid dehydrogenase scaffolds.^{85–89} Most amino acid dehydrogenase are L-selective and these were used as scaffolds for the evolved amine dehydrogenase. In all of these cases the selectivity of the enzymes was kept.^{85–89} To be able to obtain the opposite enantiomers, a D-selective amino acid dehydrogenase with broad substrate scope was developed,⁸¹ but no such amine dehydrogenase for reductive aminations has been described, yet. Still, these enzymes are restricted to ammonia as nitrogen source, as ω -TAs are. They are formally also able to perform reductive amination reactions, however require the amine to be supplied as a co-substrate and hence are not able to assimilate free ammonia.^{50,64,65} To overcome these limitations researchers from Codexis Inc. have engineered opine dehydrogenase variants with up to 29 mutations, acquired over eleven rounds of directed evolution, to perform a wide variety of reductive aminations, producing chiral secondary and tertiary amines.^{106,107}

While Codexis Inc. had to evolve several different enzymes, each for specific reductive amination reactions,^{106,107} results that were obtained during this work with *R*-IRED-*Sr* indicated a broad applicability of this enzyme with respect to the carbonyl compounds but also the amine nucleophile range.¹⁵¹ Independently from this work, the reductive amination with IREDs has also been reported in an earlier published work by the group of Prof. Dr. Michael Müller, however only with methylamine **22** as nucleophile and a maximum of 8.8% conversion and 76% ee was obtained.¹⁴⁴ Interestingly for the synthetic application of IREDs is that the enantiocomplementary nature of the (*R*)- and (*S*)- type IREDs was maintained in the reductive amination reactions. Huber *et al.* used the *S*-IREDs from *Streptomyces* sp. GF3546 and *S. aurantiacus*, resulting in the (*S*)- products,¹⁴⁴ whereas the use of *R*-IRED-*Sr* in this work produced the (*R*)- enantiomers, with higher enantiomeric excess values and higher conversions (see 3.6).¹⁵¹ The progress in using IREDs as catalysts for enzymatic reductive

aminations that was obtained during this work and recently published¹⁵¹ underlines the enormous potential of these enzymes to fill the gap originating from missing such synthetically desirable enzymes, beside the developments of amine dehydrogenases and opine dehydrogenases.

4.5.3 Optimizations for enzymatic reductive amination reactions

Optimization of the reductive amination reaction in this work was mainly done by shifting the equilibrium of the carbonyl and amine compound to the imine intermediate. The use of stronger nucleophiles resulted in a higher fraction of the imine intermediate. Next, by increasing the amine concentration up to a 50-fold molar excess over the carbonyl and by shifting the pH of the reaction media into alkaline conditions, the amount of the reactive amine species was increased, again enhancing the imine formation.

The final amine concentration of 500 mM however, does not have to be the optimum for the imine forming reaction. Codexis Inc. for example used up to 1.6 M of the amine^{106,107} and amine dehydrogenases were used with up to 5 M NH₄Cl.⁸⁷ As both enzymes, amine dehydrogenases and opine dehydrogenases, are described to perform a “true” bimolecular reaction and possess a carbonyl and an amine binding site, the high excess of the amine is required to suppress the oxidative deamination and to drive the reaction to completion.^{44,107,241} In contrast, the recent works with IREDs indicate that they reduce imines that are formed spontaneously in the aqueous buffer system and hence an higher excess of the amine than tested yet, or increase in the pH might further enhance the imine fraction¹⁵¹ (see also NMR experiments, discussed in 4.5.1). The optimum however has to be determined for each single amine nucleophile and will probably also depend on the used enzyme. With amines **21** and **22** for example at concentrations up to 500 mM no negative effects on the conversions were observed, but with aniline **12** at concentrations of 100 mM conversions decreased, indicating some kind of inhibition (3.6.1). The same is true for the pH of the reaction. By increasing it, the fraction of the deprotonated amine is enhanced, resulting in an equilibrium shift towards the imine. Work on reductive aminations performed in the Müller group was done at pH values ranging from 9.2 to 9.8, without systematically investigating their effect.¹⁴⁴ A further increase in the pH might likely be beneficial for the position of this equilibrium, however will also go in line with decreased enzyme activity (see 3.2.1) and one has to consider that at higher pH values IREDs are also able to catalyze the oxidation reaction with amines as substrates.^{138,139,146} To further shift the position of the equilibrium, water eliminating or reducing conditions by inclusion of organic solvents in the enzymatic reductive amination reaction hold great promise for optimization.

Next to the position of the carbonyl/amine – imine equilibrium also the kinetics of imine formation have to be taken into account. In general, the chemistry of imine formation is well understood, but usually these reactions are performed in aqueous free media.^{218,269} Under these conditions slightly acidic pH values are reported to be beneficial for the reaction due to the activation of the carbonyl.¹⁴ Imine formation and hydrolysis in aqueous environment is far less reported in literature^{218,219,270,271} but from investigations in this work it seems possible that the kinetics of imine formation also could become rate limiting. During the reductive amination of acetophenone **20** the enzyme loading was increased 4-fold but the conversion rates did not increase to the same extent. Determining the kinetic constants for the

reductive amination reaction also gave some indications for this. While the maximal determined turnover numbers of **11** with **22** at conditions with 1- and 10 equivalents of the nucleophile reach about the same level, at 50-fold excess they are increased (Table 29). If the imine formation would become the rate limiting step, such an effect could be explained. In this case the determined k_{cat} values should also be designated as $k_{\text{cat app}}$ (as the rate determining step for this reaction would be k_0 for the imine formation in the reaction scheme at the top of Figure 26).

The optimization of the reaction conditions for the reductive amination resulted at the same time in a beneficial side effect. Shifting the conditions towards imine formation suppressed the carbonyl reduction. This was highest (~ 6%) for nucleophiles **12** and **21** with aldehyde **11** at equimolar concentrations and decreased considerably to < 1% for nucleophile **22** (Table S10, Table S11, Table S12). This decrease could again be related to different issues. By increasing the fraction of the imine intermediate it might be the case that there is less of the carbonyl available for the supposed competing KREDs, or the conditions beneficial for imine formation also reduce the suspected KRED activity.

4.5.4 Kinetic characterization of the reductive amination reaction

Although without further knowledge about the reaction mechanism and the true substrate of the IREDs the recorded kinetics represent a simplification and the first steps of the reaction (k_0 for the formation of the imine substrate and k_1 for formation of the *ES* complex, reaction scheme provided in top of Figure 26) are treated as a “black box” this data gives valuable information about the reductive amination reaction in total. The data was recorded under the premise of a steady state equilibrium and that the imine has completely formed before the reaction started. This was ensured by preparation of the substrate solution (the mix of aldehyde **11** and amine **22** in buffer with the respective pH) ahead of the reaction start. In addition it is expected that the imine is the single substrate for the IRED and that the enzyme does not have different binding sites for two substrates.

The determined apparent K_M values correlate with the expected conditions for imine formation indicating that they directly reflect the relative amount of substrate the enzyme is exposed to. In this way these values represent a very powerful tool to assess the effect of optimizing the reaction conditions. By NMR also the actual imine fraction was estimated (data shown in 4.5.1) and thereof the equilibrium constant ($K_{\text{eq}} = \frac{[\text{imine}]}{[\text{aldehyde}][\text{amine}]}$) for the imine forming reaction can be calculated. With this K_{eq} it should be possible to calculate a “true” imine concentration in the substrate solutions and use this information for data fitting, thereby estimating the real affinity (K_M) of the enzyme for the substrate. This was done, but problems emerged by the insensitivity of the NMR to determine accurately the imine concentration. At unfavorable conditions (pH 8.0 and less than 50-fold excess of the amine and pH 9.0 with equimolar amine concentrations) no imine formation could be observed and in the other cases the calculated K_{eq} differed quite a lot. The correction of the imine fraction with the different calculated K_{eq} resulted in affinities in the range of 0.08-0.45 mM of *R*-IRED-*Sr* for imine **7** (for details see 7.7).

As already discussed above the determined turnover numbers might be masked by limitations in the kinetics of the imine forming reaction. Further experiments and optimizations should therefore be done to clarify this fact. Besides to the spectrophotometric analysis, the turnover numbers can also be calculated from the conversion rates of the biotransformations (Table 27, Table S11, Figure S52 and

Figure S53). The values calculated for these experiments ($2.23 \times 10^{-3} \text{ s}^{-1}$ for pH 8.0 with an equimolar concentration of **22** and $7.77 \times 10^{-3} \text{ s}^{-1}$ in the case of 10-fold excess) resemble quite well the ones determined in the photometric assay (Table 29). In the work by Huber *et al.* also the turnover number for the reductive amination of the ketone substrate was calculated and given with $2.8 \times 10^{-6} \text{ s}^{-1}$.^{144,X} Calculation of the turnover numbers for the reductive amination of ketone **20** with the amines **21** and **22** results for the best conditions in about $175 \times 10^{-6} \text{ s}^{-1}$ for the reaction with **21** (see Figure S56) and $292 \times 10^{-6} \text{ s}^{-1}$ for the reductive amination employing **22** (see Figure S58). These values are about two orders of magnitude higher than the one reported by Huber *et al.*¹⁴⁴ Considering that in the work of Huber with ketone **22**, no product formation was obtained,²⁷² the results achieved in this work might at least partially be owed to the selectivity and activity differences of (*R*)- type and (*S*)- type IREDs, but could also reflect the further optimized reaction conditions, as ketone **22** is a challenging substrate for direct reductive aminations.²²⁴ As discussed, the turnover numbers of the IRED catalyzed reductive aminations are rather low and most of the optimization steps aimed to enhance the imine formation either by higher pH conditions or by increased concentrations of the reactants. Further, the inclusion of organic solvents is an option, but all of these steps represent unphysiological conditions and are likely to decrease the activity of an IRED. For more efficient applications of IREDs in enzymatic reductive amination procedures it is therefore required not only to optimize the reaction conditions, but also the activity and stability of the biocatalyst as it was done with many of the nowadays industrially applied enzymes.^{38,39,42,48,156,273}

4.6 Establishing cascade reactions with IREDs

4.6.1 The selection of an amine oxidase and the investigation of its substrate scope

Enzymatic cascade reactions hold great promise for future synthetic challenges as enzymes often operate under relatively similar conditions and due to their high selectivity can be combined, avoiding unwanted side reactions and laborious isolation steps.^{257,274–276} Saturated nitrogen containing heterocyclic compounds are frequent motifs in pharmaceuticals¹² and IREDs show high activity for the reduction of cyclic imines, making such a cascade a promising proof of principle showcase. Chemical-biocatalytical cascades for these targets were already described by the groups of Kroutil and Turner.^{122,154} In these works ω -TAs were employed for the amination of diketones to trigger their self-cyclization to cyclic imines.^{122,154} For the subsequent reduction however in both cases chemical reagents were used.^{122,154} As an alternative starting point, based on renewable resources for such a reaction cascade polyamines were identified in a “retrobiosynthetic” analysis.²⁷⁷ Polyamines already contain the required number of carbon atoms and nitrogen. In addition polyamines or modified version of them are well known metabolic intermediates with a wealth of biological functions^{278–281} and the natural ones are easily accessible from amino acids by decarboxylation with overproducing strains described.^{157,158} The difficulty however lies in the cyclization of such an amine, a reaction not directly accessible by chemical catalysts or enzymes. The selective transformation of one of the amine groups into a carbonyl to promote the formation of a cyclic imine, followed by the reduction with an IRED therefore practically represents

^X: The turnover number for this substrate was calculated from the conversion rate, experimental details are given in the PhD thesis of T. Huber, online available at the University of Freiburg.²⁷²

an intramolecular reductive amination. The enzymatic conversion of the amine into the carbonyl is most straightforward accomplished by polyamine oxidases (see also Scheme 11) with PuO-*Re* being the best characterized member of this family of enzymes.^{161,165–173}

To address different polyamines that would directly lead to modified *N*-heterocycles the substrate scope of PuO-*Re* was investigated with a variety of non-natural polyamine substrates. The substrate panel was composed of symmetric and asymmetric polyamines with oxygen and nitrogen heteroatoms, as well as methyl-substituted branched polyamines. Next to the activity measurements also the affinities for some of these polyamines were determined. In general the trend published in literature could be confirmed.¹⁶¹ The enzyme displayed high activity on its natural substrate 1,4-diaminobutane **28** but already small modifications of the substrate led to a sharp decrease in activity. After determining the kinetic constants it became obvious, that the affinity of the enzyme to these substrates was still high enough to facilitate saturate it. Without the exception of *N*-aminopropyl-1,4-diaminobutane **34** which shows slightly lower affinities, all K_M values were in the low μM range. This exception of amine **34** might reflect the challenge arising from longer polyamines to accommodate the active site or the difficulty for the enzyme to discriminate between the two highly similar terminal amino groups. In contrast the turnover numbers for most non-natural polyamines strongly dropped, indicating that although the affinity is high the binding of these substrates does not proceed in a way that supports the path to the transition state of the reaction.^{229,230} The narrow activity profile of the enzyme has already been described with natural polyamines and has its origin in the highly evolved active site for polyamine **28**. The perfect positioning of this substrate in proximity to the flavin cofactor was already 1976 hypothesized by Swain and DeSa to be mediated by an anionic point (Glu or Asp residue).¹⁶⁶ Later after resolving the crystal structure of PuO-*Re* this hypothesis was confirmed and the anionic point identified as a glutamate at position 324.¹⁷¹

4.6.2 Mutagenesis of PuO-*Re* to enhance the activity for non-natural polyamines

To shift the substrate spectrum of PuO-*Re* towards longer and non-natural polyamines mutagenesis was performed. This has been proven to be a powerful tool for the expansion of the substrate spectrum of several enzymes.^{38,39,42,48,156,273} For example MAO-N initially displayed highest activity with a few aliphatic monoamines^{108,109} but over several rounds of directed evolution it was evolved for the oxidation of a broad range of primary-, secondary- and tertiary amines.^{110–117,282,283}

In a first attempt it was investigated to shift the anionic point by a single point mutation that exchanges Glu with Asp. The side chain of this amino acid is one carbon atom shorter and ideally the space that is created can then be filled by longer polyamines. The mutant was generated and the activities tested. It indeed displayed activity changes for the tested polyamines but the mutation resulted mainly in a dramatic loss of activity (**28** decreased to 0.3% and **29** to about 2.7%). In 2013 the book of the conference “Flavins and Flavoproteins 2011” appeared online and in one chapter a more detailed investigation of this mutant was published.¹⁷² The affinities and catalytic efficiencies determined by Kopacz *et al.* more clearly demonstrate the shift in the substrate spectrum.¹⁷²

For further mutagenesis no rational approach could be outlined. The amino acids in the active site seem to be highly specialized and in total 7^v channels were identified leading into the active site of the enzyme.

Therefore a random mutagenesis strategy starting with an epPCR was pursued, resulting in the successful identification of several mutants. Of these mutants, the characterization of two (PuO-*Re* E203G and PuO-*Re* I154V E203V) is included in this study. The substitution of Glu to Gly resulted in strongly increased activities for the tested substrates as did the substitution with Val. It is assumed that by the modification with these smaller amino acids the channel leading into the active site is enlarged, allowing the easier access of substrates to the active site. In addition this position is located at the outer chamber of the active site¹⁷¹ and hence also directly more space for longer polyamines like **34** could be created. This additional space might also explain the higher affinity PuO-*Re* E203G displays for **34**. The change in activity and affinity compared to the wild type is impressively shown in Figure 29 illustrating the over 10-fold increased catalytic efficiency of the mutant. The use of this parameter in such a way can however be misleading as two enzymes can possess the same k_{cat}/K_M but display completely different activities.^{227,228} In contrast it is best used to evaluate the reaction of one enzyme for different substrates, thereby allowing to judge how well an enzyme is able to discriminate between them (as done in Figure 30).^{227,228} By comparing the relative k_{cat}/K_M values the achieved shift in the substrate spectrum becomes even more obvious. 1,4-diaminobutane **28** is still the best substrate for all mutants, but polyamine **34** is converted by the wild type with about 1% of this efficiency and with PuO-*Re* E203G it reaches already 25% (Table 31, Table 32 and Figure 30).

The successful identification of two mutants at the same position (E203G and E203V) makes it likely that this position represents an interesting hotspot that should be targeted for further mutagenesis. The fact that this position also aligns one of the channels allowed the generation of more focused libraries, surrounding position E203. The second mutagenesis round consisted of site-saturation libraries of two residues in the active site and several positions that align this channel. Due to an U-formed shape of the tertiary structure at this position however the amino acids surrounding E203 have many potential interaction partners (Figure 31) and not all library combinations proposed by Reetz for a CASTing process²³⁴ could be made during this work. The screening of the saturation mutagenesis libraries resulted in much higher “hit” rates of positive candidates than did the screening of the epPCR library. Nevertheless, the successful identification of the hotspot and the associated channel relied on the random approach and the generation of a glycine substitution would usually be carefully considered as due to the high flexibility of this very small amino acid often structural changes are introduced.

The characterization of the promising mutants identified in the site-saturation approach, underlined the versatility of position E203 for increasing the activity of the enzyme. Next to Gly and Val many other small amino acids like Ala, Ser, and Cys were found at this position. In addition at the simultaneously targeted position V201 also Ser and Ala were found in the sequencing results of the active mutants. The characterized mutants summarized in Figure 33 represent the most promising ones and showed for many substrates higher activities at saturating conditions. The most impressive increase in activity was found for the methyl substituted polyamine **33**. Whereas the wt enzyme did hardly show any activity on this substrate most mutants displayed activity, with an up to 25-fold increase for PuO-*Re* E203G. In Figure 33 also some mutants with lower activity are shown and they were investigated to confirm the importance of these positions. This included mutations in the channel (double mutant L168 F169) or at its entrance (D104). Further, the active site position L207 proved to be an interesting target for mutagenesis and resulted for most of the substrates in higher activities. In contrast, the other library

targeting an active site amino acid (M174) resulted in only poorly active variants. A simultaneous saturation mutagenesis approach targeting position E203 and L207 should obviously be made in future as these amino acids are in close proximity and interestingly due to the U-formed tertiary structure, the side chains of these amino acids point in totally different directions in the crystal structure (Figure 31).

4.6.3 Application of IREDs in cascade reactions

The application of IREDs and PuO-*Re* in cascade reactions to generate *N*-heterocycles was investigated with purified proteins and with whole cells, expressing both enzymes simultaneously. In this work initial experiments for this reaction cascade were performed and are now continued in another PhD project at the Institute of Technical Biochemistry.

For the reactions with purified proteins in most cases fast conversions were obtained, resulting in full substrate consumption (Table 34). This confirms that the enzymes in principle work well together. While some of these reactions proceeded efficiently (Figure 34: *R*-IRED-*Sr* employed in the transformation of polyamine **31** to the cyclic amine product **44**, full conversion) others worked less well (Figure S84: polyamine **28** to the cyclic amine product **40** with *R*-IRED-*St*, resulting in only about 4% of the cyclic amine). Indeed, it was generally observed, that when starting with polyamines **29** or **31** higher product formations were obtained, compared to polyamine **28** as a starting point. Further, with polyamine **31** no full substrate consumption was observed with PuO-*Re* in case the IREDs were inactivated. This could indicate some kind of product inhibition of the imine on PuO-*Re* activity. Also the differences in product formation might be explained by the different activities and properties of the enzymes with the substrates. PuO-*Re* prefers polyamine **28**, which leads to a pyrroline scaffold, but all IREDs prefer piperidine substrates. In addition IREDs tend to be inhibited by too high substrate concentrations and this is severe for pyrroline substrates compared to piperidines. A better balancing of the enzymes in the reaction might help to avoid bottlenecks and inhibition of the IREDs (substrate) or PuO-*Re* (product), however during this work only equimolar ratios were tested.

The low amounts of the detected imine intermediate in the reaction with the inactivated IREDs might again reflect the analytical difficulties in detection of imines. For unsubstituted pyrrolines and piperidines it was described that they tend to form dimers and trimers in solution, with the trimer being the most stable structure.^{237,238} Such high molecular weight complexes however possess most probably too high boiling points and were therefore not detected by GC.

The simultaneous coexpression of these enzymes and the conversion of polyamine **31** to the heterocyclic amine **44** could also be shown with whole cell biocatalysts, albeit in contrast to the reactions with purified proteins lower conversions were obtained. As most of the substrate was not consumed (Table 35, Figure 35, Figure S90 and Figure S91), it seems likely that the cells did not take up the strongly charged polyamines. To overcome this polyamine transporters might be targeted as they are reported to be highly specific^{284,285} and most probably are very inefficient for the uptake of non-natural polyamines. Otherwise also permeabilization of the cells by chemical or physical methods can be taken into account, but for the redox reaction of the IREDs the cofactor regeneration capacity has to be considered. The insufficient ability of the host cells to regenerate the NADPH was already discussed above (see 4.4). In addition, in the reactions with purified proteins catalase was included to prevent H₂O₂

damage to the enzyme. A coexpression of such an enzyme might also be beneficial to prevent the host strain from oxidative stress.²⁸⁶ Further, the information about the enzyme ratios that can be derived from the reaction cascade with purified proteins will help to define and optimize the genetic context. This could lead to an optimized expression and better balancing of the enzymes. Finally the combination with additional enzymes to decorate the heterocyclic products is an attractive goal. Several steps have to be done to reach a full application of such a “designer” bug,^{287,288} but the proof that this orthogonal pathway can be implemented was achieved.

5 CONCLUSION AND OUTLOOK

After the discovery of the IRED family in 2010¹³⁷ the number of enzymes described and the knowledge about them has steadily increased, especially in the latest two years. The importance of this novel enzyme family is explained by the fact that they represent the first extension of enzymatic reduction catalysts for C=N double bonds that can also be used for a broad range of synthetic applications (including chiral secondary- and tertiary amines). Together with ketoreductases (KRED, C=O reduction) and ene reductases (ERED, reduction of activated C=C bonds) IREDs now comprise the biocatalytic reduction toolbox and these enzymes might together simply be summarized as “X”REDs (Figure 39).

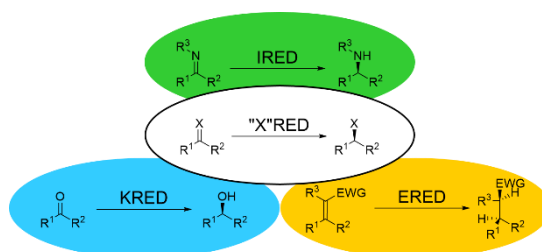


Figure 39: The “X”RED family composed of KREDs (C=O reduction) and EREDs (reduction of activated C=C bonds; EWG: electron withdrawing group) is now extended by the IREDs (C=N reduction).

During this work valuable contributions to this rapidly emerging field were made. For the first time it was shown that there are many more functional IREDs stored in the sequence space than initially assumed.¹⁴⁵ These discoveries were used to assign the IREDs into families and derive information about their mechanism.¹⁴⁵ Later also the increasing diversity was included and clear criteria defined how to discriminate IREDs from their closest related enzymes.¹⁵² The characterization of the three selected enzymes that was performed in this work and the exploration of their substrate spectrum provided useful information, not only for these IREDs but for the whole family as this data extended the molecular knowledge about the published IREDs.

An application of IREDs in cascade reactions for the formation of heterocyclic amines from linear precursors was shown and by extending the reaction scope of the IREDs away from the “classical” reduction of cyclic imines to reductive aminations the chemical potential of these enzymes was investigated.¹⁵¹ Future directions of IRED research will probably include the discovery and characterization of many more of these important enzymes. The resolution of new crystal structures with bound ligands and the combination of these information with data from their characterization and mechanistic studies will help to shed light on how these enzymes work and their physiological role. By enzyme engineering the activity, stability, the substrate scope and the selectivity for the products of these enzymes could be enhanced but the establishment of a suitable HTS assay is an initially required step. The suitability of the IREDs to be integrated in cascade reactions will also increase the number of their applications. Finally, further research on the reaction scope of these enzymes could be inspired by the reactivity of the imine substrates. The majority of described applications with imines is related to reductive aminations,²⁸⁹ but also their enantioselective alkylation and allylation was described.²⁹⁰ Combining this reactivity with the recent advantages biocatalysis has harvested by engineering non-natural reactions into protein scaffolds^{51–56} outlines an exciting future for IREDs.

6 REFERENCES

1. Nugent, T. C. *Chiral Amine Synthesis*. (Wiley-VCH Verlag GmbH & Co. KGaA, 2010).
2. Ghislieri, D. & Turner, N. J. Biocatalytic Approaches to the Synthesis of Enantiomerically Pure Chiral Amines. *Top. Catal.* **57**, 284–300 (2014).
3. Breuer, M., Ditrich, K., Habicher, T., Hauer, B., Keßeler, M., Stürmer, R. & Zelinski, T. Industrial Methods for the Production of Optically Active Intermediates. *Angew. Chem. Int. Ed.* **43**, 788–824 (2004).
4. Roose, P., Eller, K., Henkes, E., Rossbacher, R. & Höke, H. in *Ullmann's Encyclopedia of Industrial Chemistry* 1–55 (Wiley-VCH Verlag GmbH & Co. KGaA, 2015).
5. Wu, G. Amino acids: metabolism, functions, and nutrition. *Amino Acids* **37**, 1–17 (2009).
6. Mascavage, L. M., Jasmin, S., Sonnet, P. E., Wilson, M. & Dalton, D. R. in *Ullmann's Encyclopedia of Industrial Chemistry* 326–416 (Wiley-VCH Verlag GmbH & Co. KGaA, 2010).
7. Ziegler, J. & Facchini, P. J. Alkaloid Biosynthesis: Metabolism and Trafficking. *Annu. Rev. Plant Biol.* **59**, 735–769 (2008).
8. Hagel, J. M., Krizevski, R., Marsolais, F., Lewinsohn, E. & Facchini, P. J. Biosynthesis of amphetamine analogs in plants. *Trends Plant Sci.* **17**, 404–412 (2012).
9. Nugent, T. C. & El-Shazly, M. Chiral Amine Synthesis - Recent Developments and Trends for Enamide Reduction, Reductive Amination, and Imine Reduction. *Adv. Synth. Catal.* **352**, 753–819 (2010).
10. Sheldon, R. A. *Chirotechnology: Industrial Synthesis of Optically Active Compounds*. (New York: Marcel Dekker, Inc., 1993).
11. Agranat, I., Caner, H. & Caldwell, J. Putting chirality to work: the strategy of chiral switches. *Nat. Rev. Drug Discov.* **1**, 753–768 (2002).
12. Carey, J. S., Laffan, D., Thomson, C. & Williams, M. T. Analysis of the reactions used for the preparation of drug candidate molecules. *Org. Biomol. Chem.* **4**, 2337–2347 (2006).
13. Gnas, Y. & Glorius, F. Chiral Auxiliaries - Principles and Recent Applications. *Synthesis* **2006**, 1899–1930 (2006).
14. Wang, C. & Xiao, J. Asymmetric reductive amination. *Top. Curr. Chem.* **343**, 261–282 (2014).
15. Rouf, A. & Taneja, S. C. Synthesis of Single-enantiomer Bioactive Molecules: A Brief Overview. *Chirality* **26**, 63–78 (2014).
16. Li, W. & Zhang, X. *Stereoselective Formation of Amines*. (Springer Berlin Heidelberg, 2014).
17. Samant, R. N. & Chandalia, S. B. Separation of racemic mixtures: optical resolution of DL-2-amino-1-butanol. *Ind. Eng. Chem. Process Des. Dev.* **24**, 426–429 (1985).
18. Yamada, K. & Tomioka, K. Copper-Catalyzed Asymmetric Alkylation of Imines with Dialkylzinc and Related Reactions. *Chem. Rev.* **108**, 2874–2886 (2008).
19. Alinezhad, H., Yavari, H. & Salehian, F. Recent Advances in Reductive Amination Catalysis and Its Applications. *Curr. Org. Chem.* **19**, 1021–1049 (2015).
20. Tararov, V. I. & Börner, A. Approaching Highly Enantioselective Reductive Amination. *Synlett* 203–211 (2005).
21. Blaser, H.-U., Malan, C., Pugin, B., Spindler, F., Steiner, H. & Studer, M. Selective Hydrogenation

- for Fine Chemicals: Recent Trends and New Developments. *Adv. Synth. Catal.* **345**, 103–151 (2003).
22. Blaser, H.-U. The Chiral Switch of (S)-Metolachlor: A Personal Account of an Industrial Odyssey in Asymmetric Catalysis. *Adv. Synth. Catal.* **344**, 17–31 (2002).
 23. Blaser, H.-U., Pugin, B., Spindler, F. & Thommen, M. From a Chiral Switch to a Ligand Portfolio for Asymmetric Catalysis. *Acc. Chem. Res.* **40**, 1240–1250 (2007).
 24. Hoffmann, S., Seayad, A. M. & List, B. A Powerful Brønsted Acid Catalyst for the Organocatalytic Asymmetric Transfer Hydrogenation of Imines. *Angew. Chem. Int. Ed.* **44**, 7424–7427 (2005).
 25. Storer, R. I., Carrera, D. E., Ni, Y. & MacMillan, D. W. C. Enantioselective Organocatalytic Reductive Amination. *J. Am. Chem. Soc.* **128**, 84–86 (2006).
 26. Ouellet, S. G., Walji, A. M. & MacMillan, D. W. C. Enantioselective Organocatalytic Transfer Hydrogenation Reactions using Hantzsch Esters. *Acc. Chem. Res.* **40**, 1327–1339 (2007).
 27. Wakchaure, V. N., Zhou, J., Hoffmann, S. & List, B. Catalytic Asymmetric Reductive Amination of α -Branched Ketones. *Angew. Chem. Int. Ed.* **49**, 4612–4614 (2010).
 28. Vogt, P. F. & Gerulis, J. J. in *Ullmann's Encyclopedia of Industrial Chemistry* 1–20 (Wiley-VCH Verlag GmbH & Co. KGaA, 2000).
 29. Zhao, D., Kuethe, J. T., Journet, M., Peng, Z. & Humphrey, G. R. Efficient and Practical Synthesis of (R)-2-Methylpyrrolidine. *J. Org. Chem.* **71**, 4336–4338 (2006).
 30. Shimizu, S., Watanabe, N., Kataoka, T., Shoji, T., Abe, N., Morishita, S. & Ichimura, H. in *Ullmann's Encyclopedia of Industrial Chemistry* 183–228 (Wiley-VCH Verlag GmbH & Co. KGaA, 2000).
 31. Glorius, F., Spielkamp, N., Holle, S., Goddard, R. & Lehmann, C. W. Efficient Asymmetric Hydrogenation of Pyridines. *Angew. Chem. Int. Ed.* **43**, 2850–2852 (2004).
 32. Binanzer, M., Hsieh, S. & Bode, J. W. Catalytic Kinetic Resolution of Cyclic Secondary Amines. *J. Am. Chem. Soc.* **133**, 19698–19701 (2011).
 33. Doller, D., Davies, R. & Chackalamannil, S. A practical preparation of (R)- and (S)-N-Boc-2-methylpiperidines. *Tetrahedron: Asymmetry* **8**, 1275–1278 (1997).
 34. Williams, G. D., Pike, R. A., Wade, C. E. & Wills, M. A One-Pot Process for the Enantioselective Synthesis of Amines via Reductive Amination under Transfer Hydrogenation Conditions. *Org. Lett.* **5**, 4227–4230 (2003).
 35. Cowart, M., Pratt, J. K., Stewart, A. O., Bennani, Y. L., Esbenshade, T. A. & Hancock, A. A. A new class of potent non-imidazole H₃ antagonists: 2-aminoethylbenzofurans. *Bioorg. Med. Chem. Lett.* **14**, 689–693 (2004).
 36. Sun, M., Zhao, C., Gfesser, G. A., Thiffault, C., Miller, T. R., Marsh, K., Wetter, J., Curtis, M., Faghieh, R., Esbenshade, T. A., Hancock, A. A. & Cowart, M. Synthesis and SAR of 5-Amino- and 5-(Aminomethyl)benzofuran Histamine H₃ Receptor Antagonists with Improved Potency. *J. Med. Chem.* **48**, 6482–6490 (2005).
 37. Krajewski, K., Zhang, Y., Parrish, D., Deschamps, J., Roller, P. P. & Pathak, V. K. New HIV-1 reverse transcriptase inhibitors based on a tricyclic benzothiophene scaffold: Synthesis, resolution, and inhibitory activity. *Bioorg. Med. Chem. Lett.* **16**, 3034–3038 (2006).
 38. Bornscheuer, U. T., Huisman, G. W., Kazlauskas, R. J., Lutz, S., Moore, J. C. & Robins, K.

- Engineering the third wave of biocatalysis. *Nature* **485**, 185–194 (2012).
39. Reetz, M. T. Biocatalysis in Organic Chemistry and Biotechnology: Past, Present, and Future. *J. Am. Chem. Soc.* **135**, 12480–12496 (2013).
 40. Bommarius, A. S. Biocatalysis: A Status Report. *Annu. Rev. Chem. Biomol. Eng.* **6**, 319–345 (2015).
 41. Davids, T., Schmidt, M., Böttcher, D. & Bornscheuer, U. T. Strategies for the discovery and engineering of enzymes for biocatalysis. *Curr. Opin. Chem. Biol.* **17**, 215–220 (2013).
 42. Turner, N. J. Directed evolution drives the next generation of biocatalysts. *Nat. Chem. Biol.* **5**, 567–573 (2009).
 43. Kohls, H., Steffen-Munsberg, F. & Höhne, M. Recent achievements in developing the biocatalytic toolbox for chiral amine synthesis. *Curr. Opin. Chem. Biol.* **19**, 180–192 (2014).
 44. Wildeman, S. M. A. De, Sonke, T., Schoemaker, H. E. & May, O. Biocatalytic Reductions: From Lab Curiosity to ‘First Choice’. *Acc. Chem. Res.* **40**, 1260–1266 (2007).
 45. Moore, J. C., Pollard, D. J., Kosjek, B. & Devine, P. N. Advances in the Enzymatic Reduction of Ketones. *Acc. Chem. Res.* **40**, 1412–1419 (2007).
 46. Torrelo, G., Hanefeld, U. & Hollmann, F. Biocatalysis. *Catal. Letters* **145**, 309–345 (2015).
 47. Ni, Y., Holtmann, D. & Hollmann, F. How Green is Biocatalysis? To Calculate is To Know. *ChemCatChem* **6**, 930–943 (2014).
 48. Bommarius, A. S., Blum, J. K. & Abrahamson, M. J. Status of protein engineering for biocatalysts: how to design an industrially useful biocatalyst. *Curr. Opin. Chem. Biol.* **15**, 194–200 (2011).
 49. Bommarius, A. S. & Paye, M. F. Stabilizing biocatalysts. *Chem. Soc. Rev.* **42**, 6534–6565 (2013).
 50. Nestl, B. M., Hammer, S. C., Nebel, B. A. & Hauer, B. New Generation of Biocatalysts for Organic Synthesis. *Angew. Chem. Int. Ed.* **53**, 3070–3095 (2014).
 51. Röthlisberger, D., Khersonsky, O., Wollacott, A. M., Jiang, L., DeChancie, J., Betker, J., Gallaher, J. L., Althoff, E. A., Zanghellini, A., Dym, O., Albeck, S., Houk, K. N., Tawfik, D. S. & Baker, D. Kemp elimination catalysts by computational enzyme design. *Nature* **453**, 190–195 (2008).
 52. Jiang, L., Althoff, E. A., Clemente, F. R., Doyle, L., Röthlisberger, D., Zanghellini, A., Gallaher, J. L., Betker, J. L., Tanaka, F., Barbas, C. F., Hilvert, D., Houk, K. N., Stoddard, B. L. & Baker, D. De novo computational design of retro-aldol enzymes. *Science* **319**, 1387–1391 (2008).
 53. Siegel, J. B., Zanghellini, A., Lovick, H. M., Kiss, G., Lambert, A. R., St Clair, J. L., Gallaher, J. L., Hilvert, D., Gelb, M. H., Stoddard, B. L., Houk, K. N., Michael, F. E. & Baker, D. Computational design of an enzyme catalyst for a stereoselective bimolecular Diels-Alder reaction. *Science* **329**, 309–313 (2010).
 54. Coelho, P. S., Brustad, E. M., Kannan, A. & Arnold, F. H. Olefin cyclopropanation via carbene transfer catalyzed by engineered cytochrome P450 enzymes. *Science* **339**, 307–310 (2013).
 55. McIntosh, J. A., Coelho, P. S., Farwell, C. C., Wang, Z. J., Lewis, J. C., Brown, T. R. & Arnold, F. H. Enantioselective Intramolecular C-H Amination Catalyzed by Engineered Cytochrome P450 Enzymes In Vitro and In Vivo. *Angew. Chem. Int. Ed.* **52**, 9309–9312 (2013).
 56. Hammer, S. C., Marjanovic, A., Dominicus, J. M., Nestl, B. M. & Hauer, B. Squalene hopene cyclases are protonases for stereoselective Brønsted acid catalysis. *Nat. Chem. Biol.* **11**, 121–126 (2014).

57. Savile, C. K., Janey, J. M., Mundorff, E. C., Moore, J. C., Tam, S., Jarvis, W. R., Colbeck, J. C., Krebber, A., Fleitz, F. J., Brands, J., Devine, P. N., Huisman, G. W. & Hughes, G. J. Biocatalytic asymmetric synthesis of chiral amines from ketones applied to sitagliptin manufacture. *Science* **329**, 305–309 (2010).
58. Balkenhohl, F., Ditrich, K., Hauer, B. & Ladner, W. Optisch aktive Amine durch Lipase-katalysierte Methoxyacetylierung. *J. für Prakt. Chemie/Chemiker-Zeitung* **339**, 381–384 (1997).
59. Höhne, M. & Bornscheuer, U. T. Biocatalytic Routes to Optically Active Amines. *ChemCatChem* **1**, 42–51 (2009).
60. Jaeger, K.-E., Dijkstra, B. W. & Reetz, M. T. Bacterial Biocatalysts: Molecular Biology, Three-Dimensional Structures, and Biotechnological Applications of Lipases. *Annu. Rev. Microbiol.* **53**, 315–351 (1999).
61. Karl, U. & Andrea, S. BASF's ChiPros® chiral building blocks: The cornerstones of your API syntheses! *Chim. Oggi* **27**, 66–69 (2009).
62. Hollmann, F., Arends, I. W. C. E. & Holtmann, D. Enzymatic reductions for the chemist. *Green Chem.* **13**, 2285–2313 (2011).
63. Fuchs, M., Farnberger, J. E. & Kroutil, W. The Industrial Age of Biocatalytic Transamination. *Eur. J. Org. Chem.* **2015**, 6965–6982 (2015).
64. Koszelewski, D., Lavandera, I., Clay, D., Guebitz, G. M., Rozzell, D. & Kroutil, W. Formal Asymmetric Biocatalytic Reductive Amination. *Angew. Chem. Int. Ed.* **47**, 9337–9340 (2008).
65. Koszelewski, D., Tauber, K., Faber, K. & Kroutil, W. ω -Transaminases for the synthesis of non-racemic α -chiral primary amines. *Trends Biotechnol.* **28**, 324–332 (2010).
66. Green, A. P., Turner, N. J. & O'Reilly, E. Chiral Amine Synthesis Using ω -Transaminases: An Amine Donor that Displaces Equilibria and Enables High-Throughput Screening. *Angew. Chem. Int. Ed.* **53**, 10714–10717 (2014).
67. Holzer, A. K., Hiebler, K., Mutti, F. G., Simon, R. C., Lauterbach, L., Lenz, O. & Kroutil, W. Asymmetric Biocatalytic Amination of Ketones at the Expense of NH_3 and Molecular Hydrogen. *Org. Lett.* **17**, 2431–2433 (2015).
68. Malik, M. S., Park, E.-S. & Shin, J.-S. Features and technical applications of ω -transaminases. *Appl. Microbiol. Biotechnol.* **94**, 1163–1171 (2012).
69. Truppo, M. D., Rozzell, J. D. & Turner, N. J. Efficient Production of Enantiomerically Pure Chiral Amines at Concentrations of 50 g/L Using Transaminases. *Org. Process Res. Dev.* **14**, 234–237 (2010).
70. Simon, R. C., Richter, N., Busto, E. & Kroutil, W. Recent Developments of Cascade Reactions Involving ω -Transaminases. *ACS Catal.* **4**, 129–143 (2014).
71. Höhne, M., Schätzle, S., Jochens, H., Robins, K. & Bornscheuer, U. T. Rational assignment of key motifs for function guides in silico enzyme identification. *Nat. Chem. Biol.* **6**, 807–813 (2010).
72. Scheidt, T., Land, H., Anderson, M., Chen, Y., Berglund, P., Yi, D. & Fessner, W.-D. Fluorescence-Based Kinetic Assay for High-Throughput Discovery and Engineering of Stereoselective ω -Transaminases. *Adv. Synth. Catal.* **357**, 1721–1731 (2015).
73. Schrewe, M., Ladkau, N., Bühler, B. & Schmid, A. Direct Terminal Alkylamino-Functionalization via Multistep Biocatalysis in One Recombinant Whole-Cell Catalyst. *Adv. Synth. Catal.* **355**,

- 1693–1697 (2013).
74. Sattler, J. H., Fuchs, M., Tauber, K., Mutti, F. G., Faber, K., Pfeffer, J., Haas, T. & Kroutil, W. Redox Self-Sufficient Biocatalyst Network for the Amination of Primary Alcohols. *Angew. Chem. Int. Ed.* **51**, 9156–9159 (2012).
 75. Sehl, T., Hailes, H. C., Ward, J. M., Wardenga, R., von Lieres, E., Offermann, H., Westphal, R., Pohl, M. & Rother, D. Two Steps in One Pot: Enzyme Cascade for the Synthesis of Nor(pseudo)ephedrine from Inexpensive Starting Materials. *Angew. Chem. Int. Ed.* **52**, 6772–6775 (2013).
 76. Sehl, T., Hailes, H. C., Ward, J. M., Menyes, U., Pohl, M. & Rother, D. Efficient 2-step biocatalytic strategies for the synthesis of all nor(pseudo)ephedrine isomers. *Green Chem.* **16**, 3341–3348 (2014).
 77. Ohshima, T. & Soda, K. in *Bioprocesses and Applied Enzymology* **42**, 187–209 (Springer-Verlag, 1990).
 78. Sekimoto, T., Matsuyama, T., Fukui, T. & Tanizawa, K. Evidence for lysine 80 as general base catalyst of leucine dehydrogenase. *J. Biol. Chem.* **268**, 27039–27045 (1993).
 79. Vanhooke, J. L., Thoden, J. B., Brunhuber, N. M., Blanchard, J. S. & Holden, H. M. Phenylalanine dehydrogenase from *Rhodococcus* sp. M4: high-resolution X-ray analyses of inhibitory ternary complexes reveal key features in the oxidative deamination mechanism. *Biochemistry* **38**, 2326–2339 (1999).
 80. Brunhuber, N. M., Thoden, J. B., Blanchard, J. S. & Vanhooke, J. L. *Rhodococcus* L-phenylalanine dehydrogenase: kinetics, mechanism, and structural basis for catalytic specificity. *Biochemistry* **39**, 9174–9187 (2000).
 81. Vedha-Peters, K., Gunawardana, M., Rozzell, J. D. & Novick, S. J. Creation of a broad-range and highly stereoselective D-amino acid dehydrogenase for the one-step synthesis of D-amino acids. *J. Am. Chem. Soc.* **128**, 10923–10929 (2006).
 82. Zhang, K., Li, H., Cho, K. M. & Liao, J. C. Expanding metabolism for total biosynthesis of the nonnatural amino acid L-homoalanine. *Proc. Natl. Acad. Sci.* **107**, 6234–6239 (2010).
 83. Li, H. & Liao, J. C. Development of an NADPH-Dependent Homophenylalanine Dehydrogenase by Protein Engineering. *ACS Synth. Biol.* **3**, 13–20 (2014).
 84. Zhang, D., Chen, X., Zhang, R., Yao, P., Wu, Q. & Zhu, D. Development of β -Amino Acid Dehydrogenase for the Synthesis of β -Amino Acids via Reductive Amination of β -Keto Acids. *ACS Catal.* **5**, 2220–2224 (2015).
 85. Abrahamson, M. J., Vázquez-Figueroa, E., Woodall, N. B., Moore, J. C. & Bommarius, A. S. Development of an Amine Dehydrogenase for Synthesis of Chiral Amines. *Angew. Chem. Int. Ed.* **51**, 3969–3972 (2012).
 86. Abrahamson, M. J., Wong, J. W. & Bommarius, A. S. The Evolution of an Amine Dehydrogenase Biocatalyst for the Asymmetric Production of Chiral Amines. *Adv. Synth. Catal.* **355**, 1780–1786 (2013).
 87. Bommarius, B. R., Schürmann, M. & Bommarius, A. S. A novel chimeric amine dehydrogenase shows altered substrate specificity compared to its parent enzymes. *Chem. Commun.* **50**, 14953–14955 (2014).

88. Ye, L. J., Toh, H. H., Yang, Y., Adams, J. P., Snajdrova, R. & Li, Z. Engineering of Amine Dehydrogenase for Asymmetric Reductive Amination of Ketone by Evolving *Rhodococcus* Phenylalanine Dehydrogenase. *ACS Catal.* **5**, 1119–1122 (2015).
89. Chen, F.-F., Liu, Y.-Y., Zheng, G.-W. & Xu, J.-H. Asymmetric Amination of Secondary Alcohols by using a Redox-Neutral Two-Enzyme Cascade. *ChemCatChem* **7**, 3838–3841 (2015).
90. Mutti, F. G., Knaus, T., Scrutton, N. S., Breuer, M. & Turner, N. J. Conversion of alcohols to enantiopure amines through dual-enzyme hydrogen-borrowing cascades. *Science* **349**, 1525–1529 (2015).
91. Asano, Y., Kato, Y., Levy, C., Baker, P. & Rice, D. Structure and Function of Amino Acid Ammonia-lyases. *Biocatal. Biotransform.* **22**, 133–140 (2004).
92. MacDonald, M. J. & D’Cunha, G. B. Erratum: A modern view of phenylalanine ammonia lyase. *Biochem. Cell Biol.* **85**, 759–759 (2007).
93. Lovelock, S. L. & Turner, N. J. Bacterial *Anabaena variabilis* phenylalanine ammonia lyase: A biocatalyst with broad substrate specificity. *Bioorg. Med. Chem.* **22**, 5555–5557 (2014).
94. Lovelock, S. L., Lloyd, R. C. & Turner, N. J. Phenylalanine Ammonia Lyase Catalyzed Synthesis of Amino Acids by an MIO-Cofactor Independent Pathway. *Angew. Chem. Int. Ed.* **53**, 4652–4656 (2014).
95. Parmeggiani, F., Lovelock, S. L., Weise, N. J., Ahmed, S. T. & Turner, N. J. Synthesis of D- and L-phenylalanine derivatives by phenylalanine ammonia lyases: a multienzymatic cascade process. *Angew. Chem. Int. Ed.* **54**, 4608–4611 (2015).
96. Ahmed, S. T., Parmeggiani, F., Weise, N. J., Flitsch, S. L. & Turner, N. J. Chemoenzymatic Synthesis of Optically Pure L- and D-Biarylalanines through Biocatalytic Asymmetric Amination and Palladium-Catalyzed Arylation. *ACS Catal.* **5**, 5410–5413 (2015).
97. Heberling, M. M., Wu, B., Bartsch, S. & Janssen, D. B. Priming ammonia lyases and aminomutases for industrial and therapeutic applications. *Curr. Opin. Chem. Biol.* **17**, 250–260 (2013).
98. Raj, H., Szymański, W., de Villiers, J., Rozeboom, H. J., Veetil, V. P., Reis, C. R., de Villiers, M., Dekker, F. J., de Wildeman, S., Quax, W. J., Thunnissen, A.-M. W. H., Feringa, B. L., Janssen, D. B. & Poelarends, G. J. Engineering methylaspartate ammonia lyase for the asymmetric synthesis of unnatural amino acids. *Nat. Chem.* **4**, 478–484 (2012).
99. Resch, V., Schrittwieser, J. H., Siirola, E. & Kroutil, W. Novel carbon–carbon bond formations for biocatalysis. *Curr. Opin. Biotechnol.* **22**, 793–799 (2011).
100. Schrittwieser, J. H., Groenendaal, B., Resch, V., Ghislieri, D., Wallner, S., Fischereeder, E.-M., Fuchs, E., Grischek, B., Sattler, J. H., Macheroux, P., Turner, N. J. & Kroutil, W. Deracemization By Simultaneous Bio-oxidative Kinetic Resolution and Stereo-inversion. *Angew. Chem. Int. Ed.* **53**, 3731–3734 (2014).
101. Winkler, A., Hartner, F., Kutchan, T. M., Glieder, A. & Macheroux, P. Biochemical Evidence That Berberine Bridge Enzyme Belongs to a Novel Family of Flavoproteins Containing a Bi-covalently Attached FAD Cofactor. *J. Biol. Chem.* **281**, 21276–21285 (2006).
102. Stöckigt, J., Antonchick, A. P., Wu, F. & Waldmann, H. The Pictet-Spengler Reaction in Nature and in Organic Chemistry. *Angew. Chem. Int. Ed.* **50**, 8538–8564 (2011).

103. Maresh, J. J., Giddings, L., Friedrich, A., Loris, E. A., Panjikar, S., Trout, B. L., Stöckigt, J., Peters, B. & O'Connor, S. E. Strictosidine synthase: mechanism of a Pictet-Spengler catalyzing enzyme. *J. Am. Chem. Soc.* **130**, 710–723 (2008).
104. Wu, F., Zhu, H., Sun, L., Rajendran, C., Wang, M., Ren, X., Panjikar, S., Cherkasov, A., Zou, H. & Stöckigt, J. Scaffold Tailoring by a Newly Detected Pictet–Spenglerase Activity of Strictosidine Synthase: From the Common Tryptoline Skeleton to the Rare Piperazino-indole Framework. *J. Am. Chem. Soc.* **134**, 1498–1500 (2012).
105. Lichman, B. R., Lamming, E. D., Pesnot, T., Smith, J. M., Hailes, H. C. & Ward, J. M. One-pot triangular chemoenzymatic cascades for the syntheses of chiral alkaloids from dopamine. *Green Chem.* **17**, 852–855 (2015).
106. Chen, H., Moore, J., Collier, S. J., Smith, D., Nazor, J., Hughes, G., Janey, J., Huisman, G., Novick, S., Agard, N., Alvizo, O., Cope, G., Yeo, W. L., Sukumaran, J. & Ng, S. (Codexis Inc.), Engineered imine reductases and methods for the reductive amination of ketone and amine compounds., WO2013170050A1. (2013).
107. Schrittwieser, J. H., Velikogne, S. & Kroutil, W. Biocatalytic Imine Reduction and Reductive Amination of Ketones. *Adv. Synth. Catal.* **357**, 1655–1685 (2015).
108. Schilling, B. & Lerch, K. Amine oxidases from *Aspergillus niger*: identification of a novel flavin-dependent enzyme. *Biochim. Biophys. Acta, Gen. Subj.* **1243**, 529–537 (1995).
109. Sablin, S. O., Yankovskaya, V., Bernard, S., Cronin, C. N. & Singer, T. P. Isolation and characterization of an evolutionary precursor of human monoamine oxidases A and B. *Eur. J. Biochem.* **253**, 270–279 (1998).
110. Alexeeva, M., Enright, A., Dawson, M. J., Mahmoudian, M. & Turner, N. J. Deracemization of α -Methylbenzylamine Using an Enzyme Obtained by In Vitro Evolution. *Angew. Chem. Int. Ed.* **41**, 3177–3180 (2002).
111. Carr, R., Alexeeva, M., Enright, A., Eve, T. S. C., Dawson, M. J. & Turner, N. J. Directed Evolution of an Amine Oxidase Possessing both Broad Substrate Specificity and High Enantioselectivity. *Angew. Chem. Int. Ed.* **42**, 4807–4810 (2003).
112. Carr, R., Alexeeva, M., Dawson, M. J., Gotor-Fernández, V., Humphrey, C. E. & Turner, N. J. Directed Evolution of an Amine Oxidase for the Preparative Deracemisation of Cyclic Secondary Amines. *ChemBioChem* **6**, 637–639 (2005).
113. Dunsmore, C. J., Carr, R., Fleming, T. & Turner, N. J. A Chemo-Enzymatic Route to Enantiomerically Pure Cyclic Tertiary Amines. *J. Am. Chem. Soc.* **128**, 2224–2225 (2006).
114. Rowles, I., Malone, K. J., Etchells, L. L., Willies, S. C. & Turner, N. J. Directed Evolution of the Enzyme Monoamine Oxidase (MAO-N): Highly Efficient Chemo-enzymatic Deracemisation of the Alkaloid (\pm)-Crispine A. *ChemCatChem* **4**, 1259–1261 (2012).
115. Ghislieri, D., Green, A. P., Pontini, M., Willies, S. C., Rowles, I., Frank, A., Grogan, G. & Turner, N. J. Engineering an Enantioselective Amine Oxidase for the Synthesis of Pharmaceutical Building Blocks and Alkaloid Natural Products. *J. Am. Chem. Soc.* **135**, 10863–10869 (2013).
116. Köhler, V., Bailey, K. R., Znabet, A., Raftery, J., Helliwell, M. & Turner, N. J. Enantioselective Biocatalytic Oxidative Desymmetrization of Substituted Pyrrolidines. *Angew. Chem. Int. Ed.* **49**, 2182–2184 (2010).

117. Atkin, K. E., Reiss, R., Koehler, V., Bailey, K. R., Hart, S., Turkenburg, J. P., Turner, N. J., Brzozowski, A. M. & Grogan, G. The Structure of Monoamine Oxidase from *Aspergillus niger* Provides a Molecular Context for Improvements in Activity Obtained by Directed Evolution. *J. Mol. Biol.* **384**, 1218–1231 (2008).
118. Turner, N. J. Deracemisation methods. *Curr. Opin. Chem. Biol.* **14**, 115–121 (2010).
119. Yasukawa, K., Nakano, S. & Asano, Y. Tailoring D-Amino Acid Oxidase from the Pig Kidney to R-Stereoselective Amine Oxidase and its Use in the Deracemization of α -Methylbenzylamine. *Angew. Chem. Int. Ed.* **53**, 4428–4431 (2014).
120. Heath, R. S., Pontini, M., Bechi, B. & Turner, N. J. Development of an R-Selective Amine Oxidase with Broad Substrate Specificity and High Enantioselectivity. *ChemCatChem* **6**, 996–1002 (2014).
121. Li, T., Liang, J., Ambrogelly, A., Brennan, T., Gloor, G., Huisman, G., Lalonde, J., Lekhal, A., Mijts, B., Muley, S., Newman, L., Tobin, M., Wong, G., Zaks, A. & Zhang, X. Efficient, Chemoenzymatic Process for Manufacture of the Boceprevir Bicyclic [3.1.0]Proline Intermediate Based on Amine Oxidase-Catalyzed Desymmetrization. *J. Am. Chem. Soc.* **134**, 6467–6472 (2012).
122. O'Reilly, E., Iglesias, C., Ghislieri, D., Hopwood, J., Galman, J. L., Lloyd, R. C. & Turner, N. J. A Regio- and Stereoselective ω -Transaminase/Monoamine Oxidase Cascade for the Synthesis of Chiral 2,5-Disubstituted Pyrrolidines. *Angew. Chem. Int. Ed.* **53**, 2447–2450 (2014).
123. O'Reilly, E., Iglesias, C. & Turner, N. J. Monoamine Oxidase- ω -Transaminase Cascade for the Deracemisation and Dealkylation of Amines. *ChemCatChem* **6**, 992–995 (2014).
124. Köhler, V., Wilson, Y. M., Dürrenberger, M., Ghislieri, D., Churakova, E., Quinto, T., Knörr, L., Häussinger, D., Hollmann, F., Turner, N. J. & Ward, T. R. Synthetic cascades are enabled by combining biocatalysts with artificial metalloenzymes. *Nat. Chem.* **5**, 93–99 (2012).
125. Meneely, K. M. & Lamb, A. L. Two Structures of a Thiazolinyl Imine Reductase from *Yersinia enterocolitica* Provide Insight into Catalysis and Binding to the Nonribosomal Peptide Synthetase Module of HMWP1. *Biochemistry* **51**, 9002–9013 (2012).
126. Fichman, Y., Gerdes, S. Y., Kovács, H., Szabados, L., Zilberstein, A. & Csonka, L. N. Evolution of proline biosynthesis: enzymology, bioinformatics, genetics, and transcriptional regulation. *Biol. Rev.* **90**, 1065–1099 (2015).
127. Goto, M., Muramatsu, H., Mihara, H., Kurihara, T., Esaki, N., Omi, R., Miyahara, I. & Hirotsu, K. Crystal Structures of Δ^1 -Piperideine-2-carboxylate/ Δ^1 -Pyrroline-2-carboxylate Reductase Belonging to a New Family of NAD(P)H-dependent Oxidoreductases. *J. Biol. Chem.* **280**, 40875–40884 (2005).
128. Schnell, J. R., Dyson, H. J. & Wright, P. E. Structure, Dynamics, and Catalytic Function of Dihydrofolate Reductase. *Annu. Rev. Biophys. Biomol. Struct.* **33**, 119–140 (2004).
129. Li, H., Williams, P., Micklefield, J., Gardiner, J. M. & Stephens, G. A dynamic combinatorial screen for novel imine reductase activity. *Tetrahedron* **60**, 753–758 (2004).
130. Chimni, S. S. & Singh, R. J. Bioreduction of a carbon–nitrogen double bond using immobilized baker's yeast - a first report. *World J. Microbiol. Biotechnol.* **14**, 247–250 (1998).
131. Vaijayanthi, T. & Chadha, A. Asymmetric reduction of aryl imines using *Candida parapsilosis*

- ATCC 7330. *Tetrahedron: Asymmetry* **19**, 93–96 (2008).
132. Espinoza-Moraga, M., Petta, T., Vasquez-Vasquez, M., Laurie, V. F., Moraes, L. A. B. & Santos, L. S. Bioreduction of β -carboline imines to amines employing *Saccharomyces bayanus*. *Tetrahedron: Asymmetry* **21**, 1988–1992 (2010).
133. Mirabal-Gallardo, Y., Soriano, M. D. P. C. & Santos, L. S. Stereoselective bioreduction of β -carboline imines through cell-free extracts from earthworms (*Eisenia foetida*). *Tetrahedron: Asymmetry* **24**, 440–443 (2013).
134. Dürrenberger, M., Heinisch, T., Wilson, Y. M., Rossel, T., Nogueira, E., Knörr, L., Mutschler, A., Kersten, K., Zimbron, M. J., Pierron, J., Schirmer, T. & Ward, T. R. Artificial Transfer Hydrogenases for the Enantioselective Reduction of Cyclic Imines. *Angew. Chem. Int. Ed.* **50**, 3026–3029 (2011).
135. Wilson, Y. M., Dürrenberger, M., Nogueira, E. S. & Ward, T. R. Neutralizing the Detrimental Effect of Glutathione on Precious Metal Catalysts. *J. Am. Chem. Soc.* **136**, 8928–8932 (2014).
136. Robles, V. M., Dürrenberger, M., Heinisch, T., Lledós, A., Schirmer, T., Ward, T. R. & Maréchal, J.-D. Structural, Kinetic, and Docking Studies of Artificial Imine Reductases Based on Biotin–Streptavidin Technology: An Induced Lock-and-Key Hypothesis. *J. Am. Chem. Soc.* **136**, 15676–15683 (2014).
137. Mitsukura, K., Suzuki, M., Tada, K., Yoshida, T. & Nagasawa, T. Asymmetric synthesis of chiral cyclic amine from cyclic imine by bacterial whole-cell catalyst of enantioselective imine reductase. *Org. Biomol. Chem.* **8**, 4533–4535 (2010).
138. Mitsukura, K., Suzuki, M., Shinoda, S., Kuramoto, T., Yoshida, T. & Nagasawa, T. Purification and Characterization of a Novel (*R*)-Imine Reductase from *Streptomyces* sp. GF3587. *Biosci. Biotechnol. Biochem.* **75**, 1778–1782 (2011).
139. Mitsukura, K., Kuramoto, T., Yoshida, T., Kimoto, N., Yamamoto, H. & Nagasawa, T. A NADPH-dependent (*S*)-imine reductase (SIR) from *Streptomyces* sp. GF3546 for asymmetric synthesis of optically active amines: purification, characterization, gene cloning, and expression. *Appl. Microbiol. Biotechnol.* **97**, 8079–8086 (2013).
140. Nagasawa, T., Yoshida, T., Ishida, K., Yamamoto, H. & Kimoto, N. (Daicel Chemical Industries, Ltd.) Process for production of optically active amine derivative, WO2010024445A1. (2010).
141. Nagasawa, T., Yoshida, T., Ishida, K., Yamamoto, H. & Kimoto, N. (Daicel Chemical Industries Ltd.) Process for production of optically active amine derivative, WO2010024444A1. (2010).
142. Rodríguez-Mata, M., Frank, A., Wells, E., Leipold, F., Turner, N. J., Hart, S., Turkenburg, J. P. & Grogan, G. Structure and Activity of NADPH-Dependent Reductase Q1EQE0 from *Streptomyces kanamyceticus*, which Catalyses the *R*-Selective Reduction of an Imine Substrate. *ChemBioChem* **14**, 1372–1379 (2013).
143. Leipold, F., Hussain, S., Ghislieri, D. & Turner, N. J. Asymmetric Reduction of Cyclic Imines Catalyzed by a Whole-Cell Biocatalyst Containing an (*S*)-Imine Reductase. *ChemCatChem* **5**, 3505–3508 (2013).
144. Huber, T., Schneider, L., Präg, A., Gerhardt, S., Einsle, O. & Müller, M. Direct Reductive Amination of Ketones: Structure and Activity of *S*-Selective Imine Reductases from *Streptomyces*. *ChemCatChem* **6**, 2248–2252 (2014).

145. Scheller, P. N., Fademrecht, S., Hofelzer, S., Pleiss, J., Leipold, F., Turner, N. J., Nestl, B. M. & Hauer, B. Enzyme Toolbox: Novel Enantiocomplementary Imine Reductases. *ChemBioChem* **15**, 2201–2204 (2014).
146. Gand, M., Müller, H., Wardenga, R. & Höhne, M. Characterization of three novel enzymes with imine reductase activity. *J. Mol. Catal. B: Enzym.* **110**, 126–132 (2014).
147. Hussain, S., Leipold, F., Man, H., Wells, E., France, S. P., Mulholland, K. R., Grogan, G. & Turner, N. J. An (*R*)-Imine Reductase Biocatalyst for the Asymmetric Reduction of Cyclic Imines. *ChemCatChem* **7**, 579–583 (2015).
148. Man, H., Wells, E., Hussain, S., Leipold, F., Hart, S., Turkenburg, J. P., Turner, N. J. & Grogan, G. Structure, Activity and Stereoselectivity of NADPH-Dependent Oxidoreductases Catalysing the *S*-Selective Reduction of the Imine Substrate 2-Methylpyrroline. *ChemBioChem* **16**, 1052–1059 (2015).
149. Wetzl, D., Berrera, M., Sandon, N., Fishlock, D., Ebeling, M., Müller, M., Hanlon, S., Wirz, B. & Iding, H. Expanding the Imine Reductase Toolbox by Exploring the Bacterial Protein-Sequence Space. *ChemBioChem* **16**, 1749–1756 (2015).
150. Li, H., Luan, Z.-J., Zheng, G.-W. & Xu, J.-H. Efficient Synthesis of Chiral Indolines using an Imine Reductase from *Paenibacillus lactis*. *Adv. Synth. Catal.* **357**, 1692–1696 (2015).
151. Scheller, P. N., Lenz, M., Hammer, S. C., Hauer, B. & Nestl, B. M. Imine Reductase-Catalyzed Intermolecular Reductive Amination of Aldehydes and Ketones. *ChemCatChem* **7**, 3239–3242 (2015).
152. Fademrecht, S., Scheller, P. N., Nestl, B. M., Hauer, B. & Pleiss, J. Identification of imine reductase-specific sequence motifs. *Proteins* **84**, 600–610 (2016).
153. Heath, R. S., Pontini, M., Hussain, S. & Turner, N. J. Combined Imine Reductase and Amine Oxidase Catalyzed Deracemization of Nitrogen Heterocycles. *ChemCatChem* **8**, 117–120 (2016).
154. Simon, R. C., Grischek, B., Zepeck, F., Steinreiber, A., Belaj, F. & Kroutil, W. Regio- and Stereoselective Monoamination of Diketones without Protecting Groups. *Angew. Chem. Int. Ed.* **51**, 6713–6716 (2012).
155. Simon, R. C., Zepeck, F. & Kroutil, W. Chemoenzymatic Synthesis of All Four Diastereomers of 2,6-Disubstituted Piperidines through Stereoselective Monoamination of 1,5-Diketones. *Chem. Eur. J.* **19**, 2859–2865 (2013).
156. Otte, K. B. & Hauer, B. Enzyme engineering in the context of novel pathways and products. *Curr. Opin. Biotechnol.* **35**, 16–22 (2015).
157. Qian, Z. G., Xia, X. X. & Lee, S. Y. Metabolic engineering of *Escherichia coli* for the production of putrescine: A four carbon diamine. *Biotechnol. Bioeng.* **104**, 651–662 (2009).
158. Qian, Z. G., Xia, X. X. & Lee, S. Y. Metabolic engineering of *Escherichia coli* for the production of cadaverine: A five carbon diamine. *Biotechnol. Bioeng.* **108**, 93–103 (2011).
159. Kurihara, S., Oda, S., Tsuboi, Y., Kim, H. G., Oshida, M., Kumagai, H. & Suzuki, H. γ -Glutamylputrescine Synthetase in the Putrescine Utilization Pathway of *Escherichia coli* K-12. *J. Biol. Chem.* **283**, 19981–19990 (2008).
160. Foster, A., Barnes, N., Speight, R., Morris, P. C. & Keane, M. A. Role of amine oxidase

- expression to maintain putrescine homeostasis in *Rhodococcus opacus*. *Enzyme Microb. Technol.* **52**, 286–295 (2013).
161. van Hellemond, E. W., van Dijk, M., Heuts, D. P. H. M., Janssen, D. B. & Fraaije, M. W. Discovery and characterization of a putrescine oxidase from *Rhodococcus erythropolis* NCIMB 11540. *Appl. Microbiol. Biotechnol.* **78**, 455–463 (2008).
162. Di Fusco, M., Federico, R., Boffi, A., Maccone, A., Favero, G. & Mazzei, F. Characterization and application of a diamine oxidase from *Lathyrus sativus* as component of an electrochemical biosensor for the determination of biogenic amines in wine and beer. *Anal. Bioanal. Chem.* **401**, 707–716 (2011).
163. Bóka, B., Adányi, N., Szamos, J., Virág, D. & Kiss, A. Putrescine biosensor based on putrescine oxidase from *Kocuria rosea*. *Enzyme Microb. Technol.* **51**, 258–262 (2012).
164. Lee, J.-I. & Kim, Y.-W. Characterization of amine oxidases from *Arthrobacter aurescens* and application for determination of biogenic amines. *World J. Microbiol. Biotechnol.* **29**, 673–682 (2013).
165. DeSa, R. J. Putrescine oxidase from *Micrococcus rubens*. Purification and properties of the enzyme. *J. Biol. Chem.* **247**, 5527–5534 (1972).
166. Swain, W. F. & DeSa, R. J. Mechanism of action of putrescine oxidase. *Biochim. Biophys. Acta, Enzymol.* **429**, 331–341 (1976).
167. Okada, M., Kawashima, S. & Imahori, K. Substrate specificity and reaction mechanism of putrescine oxidase. *J. Biochem.* **86**, 97–104 (1979).
168. Okada, M., Kawashima, S. & Imahori, K. Mode of inactivation of putrescine oxidase by 1-ethyl-3-(3-dimethylaminopropyl)carbodiimide or metal ions. *J. Biochem.* **88**, 481–488 (1980).
169. Ishizuka, H., Horinouchi, S. & Beppu, T. Putrescine oxidase of *Micrococcus rubens*: primary structure and *Escherichia coli*. *J. Gen. Microbiol.* **139**, 425–432 (1993).
170. van Hellemond, E. W., Mazon, H., Heck, A. J., van den Heuvel, R. H. H., Heuts, D. P. H. M., Janssen, D. B. & Fraaije, M. W. ADP Competes with FAD Binding in Putrescine Oxidase. *J. Biol. Chem.* **283**, 28259–28264 (2008).
171. Kopacz, M. M., Rovidá, S., van Duijn, E., Fraaije, M. W. & Mattevi, A. Structure-Based Redesign of Cofactor Binding in Putrescine Oxidase. *Biochemistry* **50**, 4209–4217 (2011).
172. Kopacz, M. M., Kholodova, I., Rovidá, S., Mattevi, A. & Fraaije, M. W. in *Flavins and Flavoproteins 2011* (eds. Miller, S. M., Hille, R. & Palfey, B. A.) 163–168 (Lulu.com, 2013).
173. Kopacz, M. M., Heuts, D. P. H. M. & Fraaije, M. W. Kinetic mechanism of putrescine oxidase from *Rhodococcus erythropolis*. *FEBS J.* **281**, 4384–4393 (2014).
174. Guzman, L. M., Belin, D., Carson, M. J. & Beckwith, J. Tight regulation, modulation, and high-level expression by vectors containing the arabinose PBAD promoter. *J. Bacteriol.* **177**, 4121–4130 (1995).
175. Baba, T., Ara, T., Hasegawa, M., Takai, Y., Okumura, Y., Baba, M., Datsenko, K. A., Tomita, M., Wanner, B. L. & Mori, H. Construction of *Escherichia coli* K-12 in-frame, single-gene knockout mutants: the Keio collection. *Mol. Syst. Biol.* **2**, 2006.0008 (2006).
176. Hanahan, D. Studies on transformation of *Escherichia coli* with plasmids. *J. Mol. Biol.* **166**, 557–580 (1983).

177. Green, M. R. & Sambrook, J. *Molecular cloning - A Laboratory Manual*. (Cold Spring Harbor Laboratory Press, Cold Spring Harbor, New York, 2012).
178. Korbie, D. J. & Mattick, J. S. Touchdown PCR for increased specificity and sensitivity in PCR amplification. *Nat. Protoc.* **3**, 1452–1456 (2008).
179. Mitchell, L. A., Cai, Y., Taylor, M., Noronha, A. M., Chuang, J., Dai, L. & Boeke, J. D. Multichange Isothermal Mutagenesis: A New Strategy for Multiple Site-Directed Mutations in Plasmid DNA. *ACS Synth. Biol.* **2**, 473–477 (2013).
180. Gibson, D. G., Young, L., Chuang, R., Venter, J. C., Hutchison, C. A. & Smith, H. O. Enzymatic assembly of DNA molecules up to several hundred kilobases. *Nat. Methods* **6**, 343–345 (2009).
181. Gibson, D. G. Enzymatic assembly of overlapping DNA fragments. *Methods Enzymol.* **498**, 349–361 (2011).
182. Papworth, C., Greener, A. & Braman, J. C. Highly Efficient Double-Stranded, Site-Directed Mutagenesis with the Chameleon Kit. *Strateg. Mol. Biol.* **7**, 38–40 (1996).
183. Cirino, P. C., Mayer, K. M. & Umeno, D. Generating mutant libraries using error-prone PCR. *Methods Mol. Biol.* **231**, 3–9 (2003).
184. Kille, S., Acevedo-Rocha, C. G., Parra, L. P., Zhang, Z.-G., Opperman, D. J., Reetz, M. T. & Acevedo, J. P. Reducing Codon Redundancy and Screening Effort of Combinatorial Protein Libraries Created by Saturation Mutagenesis. *ACS Synth. Biol.* **2**, 83–92 (2013).
185. Firth, A. E. & Patrick, W. M. GLUE-IT and PEDEL-AA: new programmes for analyzing protein diversity in randomized libraries. *Nucleic Acids Res.* **36**, W281–W285 (2008).
186. Bio-Rad Deutschland|Protein Blotting Detection and Imaging|Date Accessed: 2015/11/26.
187. Holt, A. & Palcic, M. M. A peroxidase-coupled continuous absorbance plate-reader assay for flavin monoamine oxidases, copper-containing amine oxidases and related enzymes. *Nat. Protoc.* **1**, 2498–2505 (2006).
188. T.C.McIlvaine. A buffer solution for colorimetric comparison. *J. Biol. Chem.* **49**, 183–186 (1921).
189. Reetz, M. T. & Carballeira, J. D. Iterative saturation mutagenesis (ISM) for rapid directed evolution of functional enzymes. *Nat. Protoc.* **2**, 891–903 (2007).
190. Motulsky, H. & Christopoulos, A. *Fitting Models to Biological Data using Linear and Nonlinear Regression. A practical guide to curve fitting*. (GraphPad Software Inc., San Diego CA, 2003).
191. Wu, B., Ako, R. & Hu, M. A Useful Microsoft Excel Add-in Program for Modeling Steady-state Enzyme Kinetics. *Pharm. Anal. Acta* S11:003 (2012).
192. Kemmer, G. & Keller, S. Nonlinear least-squares data fitting in Excel spreadsheets. *Nat. Protoc.* **5**, 267–281 (2010).
193. Dobos, A., Hidvegi, E. & Somogyi, G. P. Comparison of Five Derivatizing Agents for the Determination of Amphetamine-Type Stimulants in Human Urine by Extractive Acylation and Gas Chromatography-Mass Spectrometry. *J. Anal. Toxicol.* **36**, 340–344 (2012).
194. Cunha, S. C., Faria, M. A. & Fernandes, J. O. Gas Chromatography–Mass Spectrometry Assessment of Amines in Port Wine and Grape Juice after Fast Chloroformate Extraction/Derivatization. *J. Agric. Food Chem.* **59**, 8742–8753 (2011).
195. Kanemitsu, T., Umehara, A., Haneji, R., Nagata, K. & Itoh, T. A simple proline-based organocatalyst for the enantioselective reduction of imines using trichlorosilane as a reductant.

- Tetrahedron* **68**, 3893–3898 (2012).
196. Tang, W., Johnston, S., Li, C., Iggo, J. a, Bacsa, J. & Xiao, J. Cooperative Catalysis: Combining an Achiral Metal Catalyst with a Chiral Brønsted Acid Enables Highly Enantioselective Hydrogenation of Imines. *Chem. Eur. J.* **19**, 14187–14193 (2013).
 197. Pei, Y.-N., Deng, Y., Li, J.-L., Liu, L. & Zhu, H.-J. New chiral biscarboline *N,N'*-dioxide derivatives as catalyst in enantioselective reduction of ketoimines with trichlorosilane. *Tetrahedron Lett.* **55**, 2948–2952 (2014).
 198. Davis, B. G., Maughan, M. A. T., Chapman, T. M., Villard, R. & Courtney, S. Novel Cyclic Sugar Imines: Carbohydrate Mimics and Easily Elaborated Scaffolds for Aza-Sugars. *Org. Lett.* **4**, 103–106 (2002).
 199. Movassaghi, M. & Chen, B. Stereoselective intermolecular formal [3+3] cycloaddition reaction of cyclic enamines and enones. *Angew. Chem. Int. Ed.* **46**, 565–568 (2007).
 200. Kandula, M. Compositions and Methods for the Treatment of Cancer, WO2013017977 A1. 1–76 (2013).
 201. Grogan, G. & Turner, N. J. InspiRED by Nature: NADPH-Dependent Imine Reductases (IREDs) as Catalysts for the Preparation of Chiral Amines. *Chem. Eur. J.* **22**, 1900–1907 (2016).
 202. Momoko, H., Kunihiro, K. & Hiroaki, Y. (Daicel Chemical Industries, Ltd.) Enzymic preparation method for optically active amine derivatives from imines by using imine reductase, JP2011177029A. (2011).
 203. Altschul, S. F., Madden, T. L., Schäffer, A. A., Zhang, J., Zhang, Z., Miller, W. & Lipman, D. J. Gapped BLAST and PSI-BLAST: a new generation of protein database search programs. *Nucleic Acids Res.* **25**, 3389–3402 (1997).
 204. Benson, D. A., Cavanaugh, M., Clark, K., Karsch-Mizrachi, I., Lipman, D. J., Ostell, J. & Sayers, E. W. GenBank. *Nucleic Acids Res.* **41**, D36–D42 (2013).
 205. Vogel, C. Systematic analysis of the sequence-structure-function relationships of thiamine diphosphate-dependent enzymes. (Universität Stuttgart, 2015).
 206. Salis, H. M., Mirsky, E. A. & Voigt, C. A. Automated design of synthetic ribosome binding sites to control protein expression. *Nat. Biotechnol.* **27**, 946–950 (2009).
 207. Chen, H., Bjercknes, M., Kumar, R. & Jay, E. Determination of the optimal aligned spacing between the Shine – Dalgarno sequence and the translation initiation codon of *Escherichia coli* mRNAs. *Nucleic Acids Res.* **22**, 4953–4957 (1994).
 208. Ringquist, S., Shinedling, S., Barrick, D., Green, L., Binkley, J., Stormo, G. D. & Gold, L. Translation initiation in *Escherichia coli*: sequences within the ribosome-binding site. *Mol. Microbiol.* **6**, 1219–1229 (1992).
 209. Shultzaberger, R. K., Bucheimer, R. E., Rudd, K. E. & Schneider, T. D. Anatomy of *Escherichia coli* ribosome binding sites. *J. Mol. Biol.* **313**, 215–228 (2001).
 210. Kimple, M. E. & Sondek, J. in *Current Protocols in Protein Science* **Chapter 9**, 9.9.1–9.9.19 (John Wiley & Sons, Inc., 2004).
 211. Lichty, J. J., Malecki, J. L., Agnew, H. D., Michelson-Horowitz, D. J. & Tan, S. Comparison of affinity tags for protein purification. *Protein Expr. Purif.* **41**, 98–105 (2005).
 212. Waugh, D. S. An overview of enzymatic reagents for the removal of affinity tags. *Protein Expr.*

- Purif.* **80**, 283–293 (2011).
213. Hofelzer, S. Charakterisierung neuer Mitglieder der Familie der Iminreduktases. (Universität Stuttgart, 2014).
214. Gräslund, S., Nordlund, P., Weigelt, J., Bray, J., Gileadi, O., Knapp, S., Oppermann, U., Arrowsmith, C., Hui, R., Ming, J., Dhe-Paganon, S., Park, H., Savchenko, A., Yee, A., Edwards, A., Vincentelli, R., Cambillau, C., Kim, R., Kim, S.-H., *et al.* Protein production and purification. *Nat. Methods* **5**, 135–146 (2008).
215. Alzari, P. M., Berglund, H., Berrow, N. S., Blagova, E., Busso, D., Cambillau, C., Campanacci, V., Christodoulou, E., Eiler, S., Fogg, M. J., Folkers, G., Geerlof, A., Hart, D., Haouz, A., Herman, M. D., Macieira, S., Nordlund, P., Perrakis, A., Quevillon-Cheruel, S., *et al.* Implementation of semi-automated cloning and prokaryotic expression screening: the impact of SPINE. *Acta Crystallogr. Sect. D: Biol. Crystallogr.* **62**, 1103–1113 (2006).
216. Lokanath, N. K., Ohshima, N., Takio, K., Shiromizu, I., Kuroishi, C., Okazaki, N., Kuramitsu, S., Yokoyama, S., Miyano, M. & Kunishima, N. Crystal Structure of Novel NADP-dependent 3-Hydroxyisobutyrate Dehydrogenase from *Thermus thermophilus* HB8. *J. Mol. Biol.* **352**, 905–917 (2005).
217. Reitz, S., Alhapel, A., Essen, L.-O. & Pierik, A. J. Structural and Kinetic Properties of a β -Hydroxyacid Dehydrogenase Involved in Nicotinate Fermentation. *J. Mol. Biol.* **382**, 802–811 (2008).
218. Godoy-Alcántar, C., Yatsimirsky, A. K. & Lehn, J.-M. Structure-stability correlations for imine formation in aqueous solution. *J. Phys. Org. Chem.* **18**, 979–985 (2005).
219. Crisalli, P. & Kool, E. T. Water-Soluble Organocatalysts for Hydrazone and Oxime Formation. *J. Org. Chem.* **78**, 1184–1189 (2013).
220. Kluger, R. & Tittmann, K. Thiamin Diphosphate Catalysis: Enzymic and Nonenzymic Covalent Intermediates. *Chem. Rev.* **108**, 1797–1833 (2008).
221. Humphrey, A. J. & O'Hagan, D. Tropane alkaloid biosynthesis. A century old problem unresolved. *Nat. Prod. Rep.* **18**, 494–502 (2001).
222. Gaston, M. A., Zhang, L., Green-Church, K. B. & Krzycki, J. A. The complete biosynthesis of the genetically encoded amino acid pyrrolysine from lysine. *Nature* **471**, 647–650 (2011).
223. Brotzel, F., Chu, Y. C. & Mayr, H. Nucleophilicities of Primary and Secondary Amines in Water. *J. Org. Chem.* **72**, 3679–3688 (2007).
224. Abdel-Magid, A. F., Carson, K. G., Harris, B. D., Maryanoff, C. A. & Shah, R. D. Reductive Amination of Aldehydes and Ketones with Sodium Triacetoxyborohydride. Studies on Direct and Indirect Reductive Amination Procedures. *J. Org. Chem.* **61**, 3849–3862 (1996).
225. Huisman, G. W. & Collier, S. J. On the development of new biocatalytic processes for practical pharmaceutical synthesis. *Curr. Opin. Chem. Biol.* **17**, 284–292 (2013).
226. O'Reilly, E. & Turner, N. J. Enzymatic cascades for the regio- and stereoselective synthesis of chiral amines. *Perspect. Sci.* **4**, 55–61 (2015).
227. Eisenthal, R., Danson, M. J. & Hough, D. W. Catalytic efficiency and k_{cat}/K_M : a useful comparator? *Trends Biotechnol.* **25**, 247–249 (2007).
228. Koshland, D. E. The Application and Usefulness of the Ratio k_{cat}/K_M . *Bioorg. Chem.* **30**, 211–213

- (2002).
229. Schramm, V. L. Enzymatic transition states and transition state analog design. *Annu. Rev. Biochem.* **67**, 693–720 (1998).
230. Schramm, V. L. Enzymatic Transition States, Transition-State Analogs, Dynamics, Thermodynamics, and Lifetimes. *Annu. Rev. Biochem.* **80**, 703–732 (2011).
231. Alexeeva, M., Carr, R. & Turner, N. J. Directed evolution of enzymes: new biocatalysts for asymmetric synthesis. *Org. Biomol. Chem.* **1**, 4133–4137 (2003).
232. Weiß, M. S., Pavlidis, I. V., Vickers, C., Höhne, M. & Bornscheuer, U. T. Glycine Oxidase Based High-Throughput Solid-Phase Assay for Substrate Profiling and Directed Evolution of (*R*)- and (*S*)-Selective Amine Transaminases. *Anal. Chem.* **86**, 11847–11853 (2014).
233. Pavelka, A., Chovancova, E. & Damborsky, J. HotSpot Wizard: a web server for identification of hot spots in protein engineering. *Nucleic Acids Res.* **37**, W376–W383 (2009).
234. Reetz, M. T., Bocola, M., Carballeira, J. D., Zha, D. & Vogel, A. Expanding the Range of Substrate Acceptance of Enzymes: Combinatorial Active-Site Saturation Test. *Angew. Chem. Int. Ed.* **44**, 4192–4196 (2005).
235. Reetz, M. T., Wang, L.-W. & Bocola, M. Directed Evolution of Enantioselective Enzymes: Iterative Cycles of CASTing for Probing Protein-Sequence Space. *Angew. Chem. Int. Ed.* **45**, 1236–1241 (2006).
236. Li, M., Binda, C., Mattevi, A. & Edmondson, D. E. Functional role of the ‘aromatic cage’ in human monoamine oxidase B: structures and catalytic properties of Tyr435 mutant proteins. *Biochemistry* **45**, 4775–4784 (2006).
237. Claxton, G. P., Allen, L. & Grisar, J. M. 2,3,4,5-Tetrahydropyridine Trimer. *Org. Synth.* 118 (2003).
238. Baxter, G., Melville, J. C. & Robins, D. J. Stabilisation of 3,4-Dihydro-2*H*-pyrrole (1-Pyrroline) by Complexation with Zinc Iodide. *Synlett* **1991**, 359–360 (1991).
239. Schmid, A., Hollmann, F., Park, J. B. & Bühler, B. The use of enzymes in the chemical industry in Europe. *Curr. Opin. Biotechnol.* **13**, 359–366 (2002).
240. Jaeger, K. E. & Reetz, M. T. Microbial lipases form versatile tools for biotechnology. *Trends Biotechnol.* **16**, 396–403 (1998).
241. Brunhuber, N. M. W. & Blanchard, J. S. The Biochemistry and Enzymology of Amino Acid Dehydrogenases. *Crit. Rev. Biochem. Mol. Biol.* **29**, 415–467 (1994).
242. Aldridge, S. Industry backs biocatalysis for greener manufacturing. *Nat. Biotechnol.* **31**, 95–96 (2013).
243. Czekster, C. M., Vandemeulebroucke, A. & Blanchard, J. S. Kinetic and Chemical Mechanism of the Dihydrofolate Reductase from *Mycobacterium tuberculosis*. *Biochemistry* **50**, 367–375 (2011).
244. Morrison, J. F. & Stone, S. R. Mechanism of the reaction catalyzed by dihydrofolate reductase from *Escherichia coli*: pH and deuterium isotope effects with NADPH as the variable substrate. *Biochemistry* **27**, 5499–5506 (1988).
245. Polgár, L. The catalytic triad of serine peptidases. *Cell. Mol. Life Sci.* **62**, 2161–2172 (2005).
246. Kim, D.-S., Bae, C.-Y., Jeon, J.-J., Chun, S.-J., Oh, H. W., Hong, S. G., Baek, K.-S., Moon, E. Y.

- & Bae, K. S. *Paenibacillus elgii* sp. nov., with broad antimicrobial activity. *Int. J. Syst. Evol. Microbiol.* **54**, 2031–2035 (2004).
247. Ding, R., Li, Y., Qian, C. & Wu, X. Draft Genome Sequence of *Paenibacillus elgii* B69, a Strain with Broad Antimicrobial Activity. *J. Bacteriol.* **193**, 4537–4537 (2011).
248. Arnold, F. H., Wintrode, P. L., Miyazaki, K. & Gershenson, A. How enzymes adapt: lessons from directed evolution. *Trends Biochem. Sci.* **26**, 100–106 (2001).
249. Klivanov, A. M. Why are enzymes less active in organic solvents than in water? *Trends Biotechnol.* **15**, 97–101 (1997).
250. Klivanov, A. M. Improving enzymes by using them in organic solvents. *Nature* **409**, 241–246 (2001).
251. Doukyu, N. & Ogino, H. Organic solvent-tolerant enzymes. *Biochem. Eng. J.* **48**, 270–282 (2010).
252. Kunjapur, A. M. & Prather, K. L. J. Microbial Engineering for Aldehyde Synthesis. *Appl. Environ. Microbiol.* **81**, 1892–1901 (2015).
253. Rodriguez, G. M. & Atsumi, S. Toward aldehyde and alkane production by removing aldehyde reductase activity in *Escherichia coli*. *Metab. Eng.* **25**, 227–237 (2014).
254. Miura, K., Tomioka, Y., Suzuki, H., Yonezawa, M., Hishinuma, T. & Mizugaki, M. Molecular Cloning of the *nema* Gene Encoding *N*-Ethylmaleimide Reductase from *Escherichia coli*. *Biol. Pharm. Bull.* **20**, 110–112 (1997).
255. Stueckler, C., Reiter, T. C., Baudendistel, N. & Faber, K. Nicotinamide-independent asymmetric bioreduction of C=C-bonds via disproportionation of enones catalyzed by enoate reductases. *Tetrahedron* **66**, 663–667 (2010).
256. Durchschein, K., Hall, M. & Faber, K. Unusual reactions mediated by FMN-dependent ene- and nitro-reductases. *Green Chem.* **15**, 616–619 (2013).
257. Muschiol, J., Peters, C., Oberleitner, N., Mihovilovic, M. D., Bornscheuer, U. T. & Rudroff, F. Cascade catalysis – strategies and challenges en route to preparative synthetic biology. *Chem. Commun.* **51**, 5798–5811 (2015).
258. Reiß, T., Hummel, W., Hanlon, S. P., Iding, H. & Gröger, H. The Organic-Synthetic Potential of Recombinant Ene Reductases: Substrate-Scope Evaluation and Process Optimization. *ChemCatChem* **7**, 1302–1311 (2015).
259. Khersonsky, O. & Tawfik, D. S. Enzyme Promiscuity: A Mechanistic and Evolutionary Perspective. *Annu. Rev. Biochem.* **79**, 471–505 (2010).
260. Aharoni, A., Gaidukov, L., Khersonsky, O., Gould, S. M., Roodveldt, C. & Tawfik, D. S. The ‘evolvability’ of promiscuous protein functions. *Nat. Genet.* **37**, 73–76 (2005).
261. Bornscheuer, U. T. & Kazlauskas, R. J. Catalytic Promiscuity in Biocatalysis: Using Old Enzymes to Form New Bonds and Follow New Pathways. *Angew. Chem. Int. Ed.* **43**, 6032–6040 (2004).
262. Khersonsky, O., Malitsky, S., Rogachev, I. & Tawfik, D. S. Role of Chemistry versus Substrate Binding in Recruiting Promiscuous Enzyme Functions. *Biochemistry* **50**, 2683–2690 (2011).
263. Mikkelsen, K. & Nielsen, S. O. ACIDITY MEASUREMENTS WITH THE GLASS ELECTRODE IN H₂O-D₂O MIXTURES. *J. Phys. Chem.* **64**, 632–637 (1960).
264. Krężel, A. & Bal, W. A formula for correlating p*K*_a values determined in D₂O and H₂O. *J. Inorg. Biochem.* **98**, 161–166 (2004).

265. Constable, D. J. C., Dunn, P. J., Hayler, J. D., Humphrey, G. R., Leazer, Jr., J. L., Linderman, R. J., Lorenz, K., Manley, J., Pearlman, B. A., Wells, A., Zaks, A. & Zhang, T. Y. Key green chemistry research areas - a perspective from pharmaceutical manufacturers. *Green Chem.* **9**, 411–420 (2007).
266. Ohshima, T. & Soda, K. in *Stereoselective Biocatalysis* (ed. Patel, R. N.) 877–903 (Marcel Dekker, Inc., 1990).
267. Zhu, D. & Hua, L. Biocatalytic asymmetric amination of carbonyl functional groups - a synthetic biology approach to organic chemistry. *Biotechnol. J.* **4**, 1420–1431 (2009).
268. Itoh, N., Yachi, C. & Kudome, T. Determining a novel NAD⁺-dependent amine dehydrogenase with a broad substrate range from *Streptomyces virginiae* IFO 12827: purification and characterization. *J. Mol. Catal. B: Enzym.* **10**, 281–290 (2000).
269. Lei, Q., Wei, Y., Talwar, D., Wang, C., Xue, D. & Xiao, J. Fast Reductive Amination by Transfer Hydrogenation 'on Water'. *Chem. Eur. J.* **19**, 4021–4029 (2013).
270. Fuentes-Martínez, Y., Godoy-Alcántar, C., Medrano, F. & Dikiy, A. Kanamycin A: imine formation in aqueous solution. *J. Phys. Org. Chem.* **25**, 1395–1403 (2012).
271. Saggiomo, V. & Lüning, U. On the formation of imines in water—a comparison. *Tetrahedron Lett.* **50**, 4663–4665 (2009).
272. Huber, T. Biokatalytische Reduktive Aminierung. (Albert-Ludwigs-Universität Freiburg, 2014).
273. Li, Y. & Cirino, P. C. Recent advances in engineering proteins for biocatalysis. *Biotechnol. Bioeng.* **111**, 1273–1287 (2014).
274. Ricca, E., Brucher, B. & Schrittwieser, J. H. Multi-Enzymatic Cascade Reactions: Overview and Perspectives. *Adv. Synth. Catal.* **353**, 2239–2262 (2011).
275. Oroz-Guinea, I. & García-Junceda, E. Enzyme catalysed tandem reactions. *Curr. Opin. Chem. Biol.* **17**, 236–249 (2013).
276. Sigrist, R., Costa, B. Z. da, Marsaioli, A. J. & de Oliveira, L. G. Nature-inspired enzymatic cascades to build valuable compounds. *Biotechnol. Adv.* **33**, 394–411 (2015).
277. Turner, N. J. & O'Reilly, E. Biocatalytic retrosynthesis. *Nat. Chem. Biol.* **9**, 285–288 (2013).
278. Igarashi, K. & Kashiwagi, K. Polyamines: Mysterious Modulators of Cellular Functions. *Biochem. Biophys. Res. Commun.* **271**, 559–564 (2000).
279. Tobar, J. & Tchen, T. T. Identification of (+)-hydroxyputrescine (1,4-diaminobutan-2-ol) from a *Pseudomonas* species. *J. Biol. Chem.* **246**, 1262–1265 (1971).
280. Biastoff, S., Brandt, W. & Dräger, B. Putrescine N-methyltransferase – The start for alkaloids. *Phytochemistry* **70**, 1708–1718 (2009).
281. Ober, D., Tholl, D., Martin, W. & Hartmann, T. Homospermidine synthase of *Rhodospseudomonas viridis*: Substrate specificity and effects of the heterologously expressed enzyme on polyamine metabolism of *Escherichia coli*. *J. Gen. Appl. Microbiol.* **42**, 411–419 (1996).
282. Atkin, K. E., Reiss, R., Turner, N. J., Brzozowski, A. M. & Grogan, G. Cloning, expression, purification, crystallization and preliminary X-ray diffraction analysis of variants of monoamine oxidase from *Aspergillus niger*. *Acta Crystallogr. Sect. F: Struct. Biol. Cryst. Commun.* **64**, 182–185 (2008).
283. Ghislieri, D., Houghton, D., Green, A. P., Willies, S. C. & Turner, N. J. Monoamine Oxidase

- (MAO-N) Catalyzed Deracemization of Tetrahydro- β -carbolines: Substrate Dependent Switch in Enantioselectivity. *ACS Catal.* **3**, 2869–2872 (2013).
284. Igarashi, K. & Kashiwagi, K. Polyamine transport in bacteria and yeast. *Biochem. J.* **344**, 633–642 (1999).
285. Igarashi, K., Ito, K. & Kashiwagi, K. Polyamine uptake systems in *Escherichia coli*. *Res. Microbiol.* **152**, 271–278 (2001).
286. Imlay, J. A. The molecular mechanisms and physiological consequences of oxidative stress: lessons from a model bacterium. *Nat. Rev. Microbiol.* **11**, 443–454 (2013).
287. Lee, J. W., Na, D., Park, J. M., Lee, J., Choi, S. & Lee, S. Y. Systems metabolic engineering of microorganisms for natural and non-natural chemicals. *Nat. Chem. Biol.* **8**, 536–546 (2012).
288. Felnagle, E. A., Chaubey, A., Noey, E. L., Houk, K. N. & Liao, J. C. Engineering synthetic recursive pathways to generate non-natural small molecules. *Nat. Chem. Biol.* **8**, 518–526 (2012).
289. Kobayashi, S. & Ishitani, H. Catalytic Enantioselective Addition to Imines. *Chem. Rev.* **99**, 1069–1094 (1999).
290. Denmark, S. E., Nakajima, N. & Nicaise, O. J.-C. Asymmetric Addition of Organolithium Reagents to Imines. *J. Am. Chem. Soc.* **116**, 8797–8798 (1994).
291. Cahn, R. S., Ingold, C. & Prelog, V. Specification of Molecular Chirality. *Angew. Chem. Int. Ed.* **5**, 385–415 (1966).
292. Needleman, S. B. & Wunsch, C. D. A general method applicable to the search for similarities in the amino acid sequence of two proteins. *J. Mol. Biol.* **48**, 443–453 (1970).
293. Rice, P., Longden, I. & Bleasby, A. EMBOSS: The European Molecular Biology Open Software Suite. *Trends Genet.* **16**, 276–277 (2000).
294. McWilliam, H., Li, W., Uludag, M., Squizzato, S., Park, Y. M., Buso, N., Cowley, A. P. & Lopez, R. Analysis Tool Web Services from the EMBL-EBI. *Nucleic Acids Res.* **41**, W597–W600 (2013).
295. Quinto, T., Schwizer, F., Zimbron, J. M., Morina, A., Köhler, V. & Ward, T. R. Expanding the Chemical Diversity in Artificial Imine Reductases Based on the Biotin-Streptavidin Technology. *ChemCatChem* **6**, 1010–1014 (2014).
296. He, B. & Lloyd, D. K. in *Specification of Drug Substances and Products - Development of Analytical Methods* (eds. Riley, C. M., Rosanske, T. W. & Rabel-Riley, S. R.) 193–222 (Elsevier, 2013).

7 SUPPORTING INFORMATION

7.1 Michaelis-Menten plots of IREDs and mutants with substrate 2-methylpyrroline 1

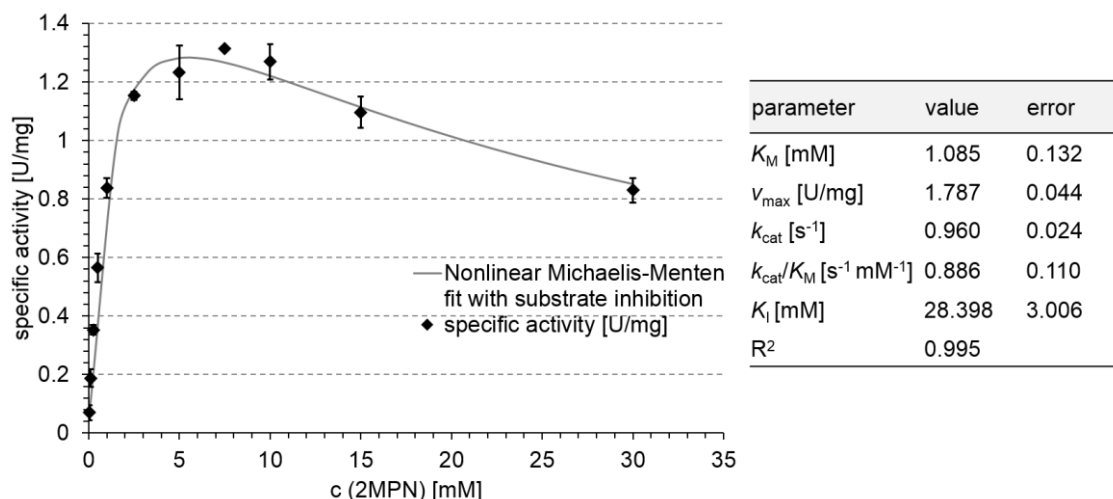


Figure S1: Determination of kinetic constants for *R*-IRED-*Sr* with substrate 1. Due to lower activities at higher substrate concentrations, the Michaelis-Menten equation was adapted to substrate inhibition: $v = (v_{max} \times [S]) / (K_M + [S] \times (1 + ([S]/K_I)))$. All activities were determined in triplicates and the error bars show the standard deviation.

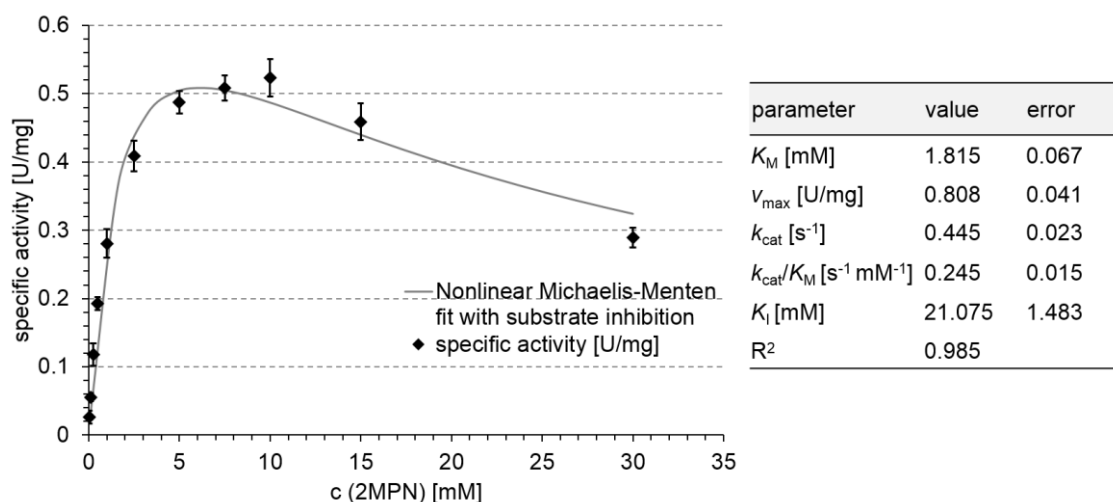


Figure S2: Determination of kinetic constants for *R*-IRED-*St* with substrate 1. Due to lower activities at higher substrate concentrations, the Michaelis-Menten equation was adapted to substrate inhibition: $v = (v_{max} \times [S]) / (K_M + [S] \times (1 + ([S]/K_I)))$. All activities were determined in triplicates and the error bars show the standard deviation.

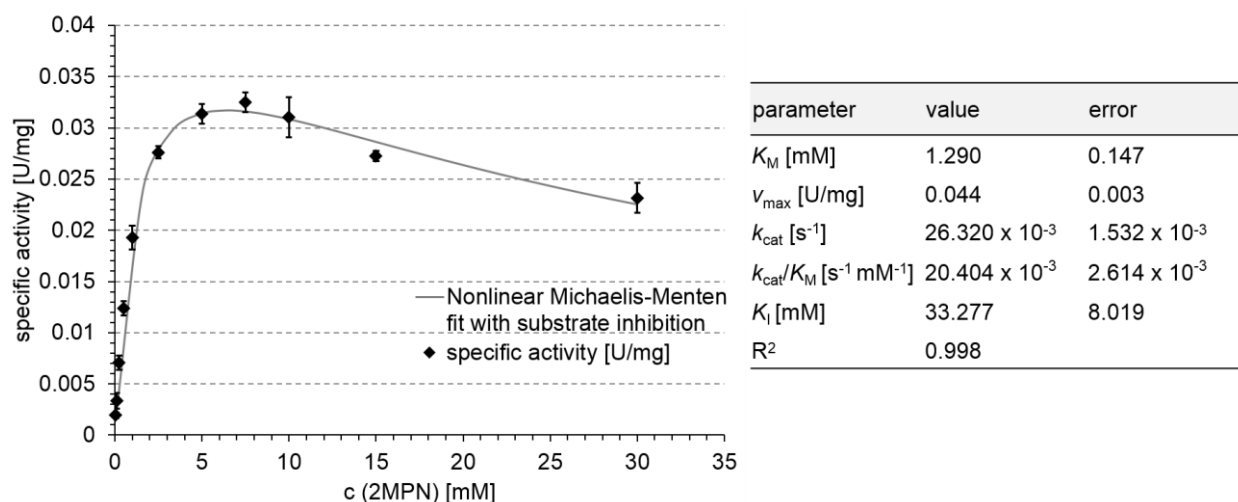


Figure S3: Determination of kinetic constants for S-IRED-Pe with substrate 1. Due to lower activities at higher substrate concentrations, the Michaelis-Menten equation was adapted to substrate inhibition: $v = (v_{max} \times [S]) / (K_M + [S] \times (1 + ([S]/K_I)))$. All activities were determined in triplicates and the error bars show the standard deviation.

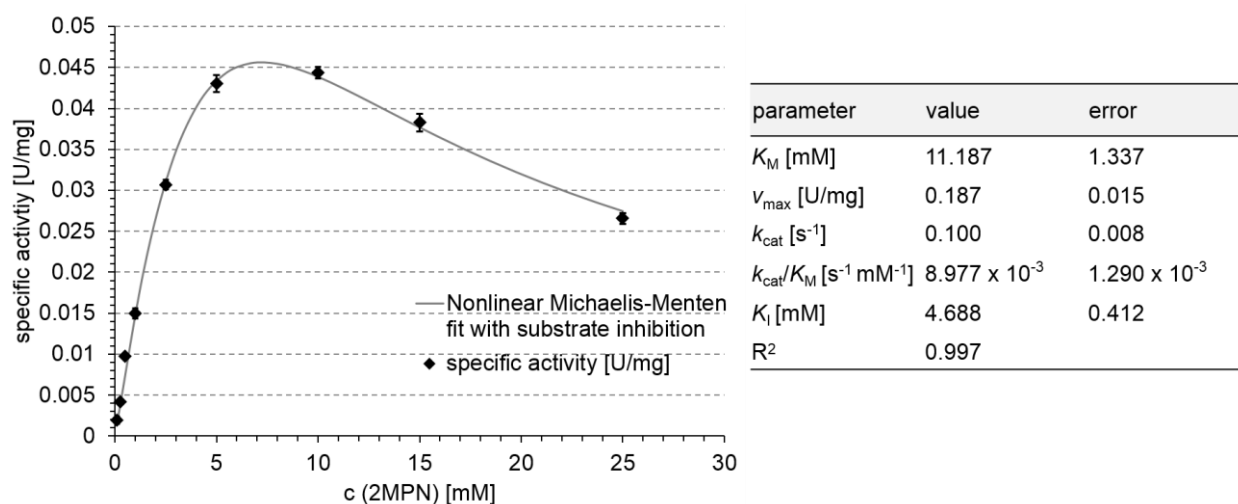


Figure S4: Determination of kinetic constants for R-IRED-Sr D191A with substrate 1. Due to lower activities at higher substrate concentrations, the Michaelis-Menten equation was adapted to substrate inhibition: $v = (v_{max} \times [S]) / (K_M + [S] \times (1 + ([S]/K_I)))$. All activities were determined in triplicates and the error bars show the standard deviation.

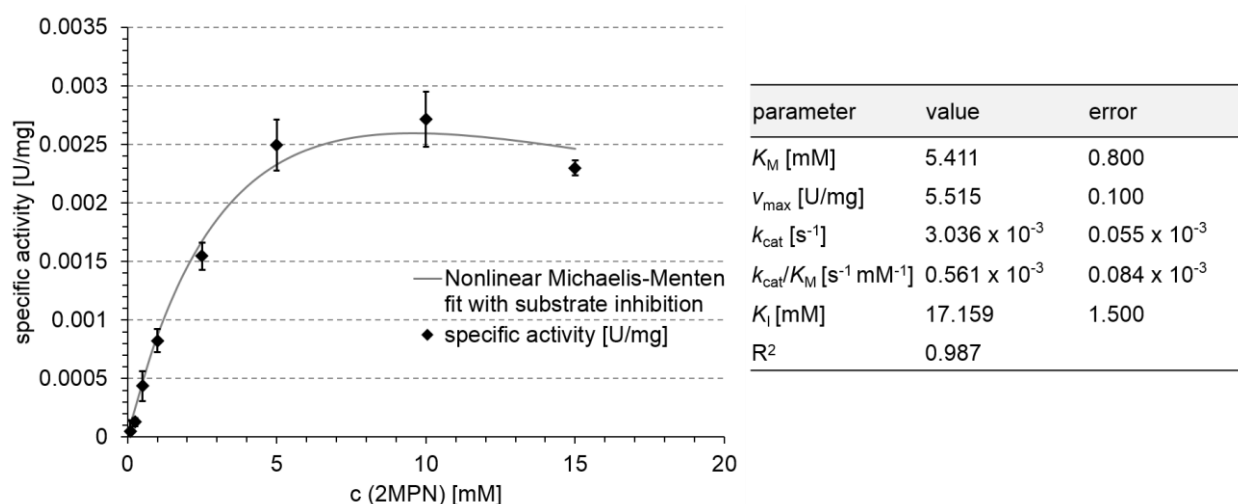
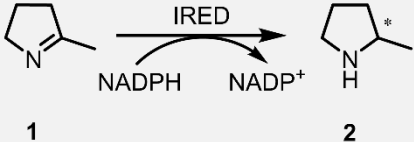


Figure S5: Determination of kinetic constants for R-IRED-St D193A with substrate 1. Due to lower activities at higher substrate concentrations, the Michaelis-Menten equation was adapted to substrate inhibition: $v = (v_{max} \times [S]) / (K_M + [S] \times (1 + ([S]/K_I)))$. All activities were determined in triplicates and the error bars show the standard deviation.

7.2 Biotransformations with IREDs

7.2.1 IRED catalyzed whole cell biotransformations and chiral GC/HPLC-traces for determination of product formations and determination of the enantiomeric excess in these biotransformations

Table S1: Product formations and enantiomeric excess values in [%] for the reduction of **1** with whole cells expressing IREDs and mutants of them. All biotransformations were performed in triplicates. The values in this table give the average of such a triplicate and the errors represent the standard deviation. As the values determined for *S*-IRED-*Pe* Y208A after 3 h and 5 h were very low and not in the optimal range for detection with the applied method they are given in parentheses. -: not detected.

IRED									<i>ee</i> [%] after 24 h
	0 h	0.5 h	1 h	product formation [%]		8 h	24 h		
<i>R</i> -IRED- <i>Sr</i>	0.77 ± 0.22	46.29 ± 0.42	89.79 ± 2.89	> 99	> 99	> 99	> 99	98.26 ± 0.01 (<i>R</i>)	
<i>R</i> -IRED- <i>St</i>	0.88 ± 0.24	29.58 ± 1.49	64.59 ± 4.19	> 99	> 99	> 99	> 99	99.02 ± 0.02 (<i>R</i>)	
<i>S</i> -IRED- <i>Pe</i>	0.58 ± 0.21	18.66 ± 0.12	38.07 ± 0.38	77.25 ± 1.52	88.97 ± 3.92	94.54 ± 1.33	96.84 ± 1.01	94.92 ± 0.00 (<i>S</i>)	
<i>R</i> -IRED- <i>Sr</i> D191A	< 1	7.22 ± 0.14	14.89 ± 0.32	33.25 ± 1.55	43.44 ± 2.79	58.32 ± 4.21	63.73 ± 3.81	91.43 ± 0.09 (<i>R</i>)	
<i>R</i> -IRED- <i>St</i> D193A	-	1.11 ± 0.23	2.17 ± 0.06	5.77 ± 0.21	9.07 ± 0.17	13.40 ± 0.35	17.42 ± 2.40	94.13 ± 0.03 (<i>R</i>)	
<i>S</i> -IRED- <i>Pe</i> Y208A	-	-	-	(0.08)	(0.22)	0.37 ± 0.18	0.88 ± 0.21	65.66 ± 0.25 (<i>S</i>)	

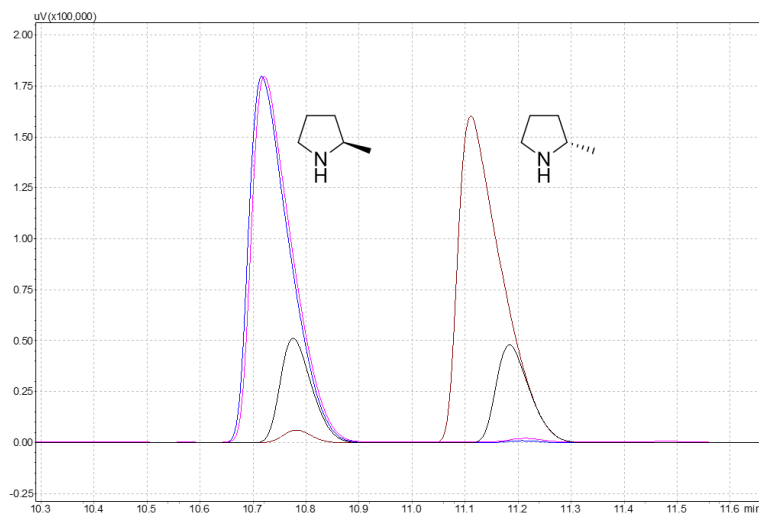


Figure S6: Chiral GC-traces for the separation of the enantiomers of product **2** and determination of the enantiomeric excess in IRED catalyzed whole cell biotransformations. Black: racemic **2**, pink *R*-IRED-*Sr* 98.3% *ee*; blue: *R*-IRED-*St* 99.0% *ee* and brown: *S*-IRED-*Pe* 94.9% *ee*. Assignment of the enantiomers was done by comparison with commercial available samples of (*R*)-**2** and (*S*)-**2**.

7 SUPPORTING INFORMATION

Table S2: Product formations and enantiomeric excess values in [%] for IRED catalyzed whole cell biotransformations with piperidine substrates **3a**, **3b** and **3c**. All biotransformations were performed in triplicates. The values in this table give the average of such a triplicate and the errors represent the standard deviation. Product formation with substrate **3a** at 0 h is most probably caused by too slow sample preparation after starting the biotransformation. Biotransformations were set up in the order *R*-IRED-*Sr*, *R*-IRED-*St* and *S*-IRED-*Pe* last. -: not detected; n.d.: not determined.

3a: R = methyl
3b: R = phenyl
3c: R = *p*-fluorophenyl
4a: R = methyl
4b: R = phenyl
4c: R = *p*-fluorophenyl

imine	time [h]	<i>R</i> -IRED- <i>Sr</i>		<i>R</i> -IRED- <i>St</i>		<i>S</i> -IRED- <i>Pe</i>	
		product formation [%]	ee [%]	product formation [%]	ee [%]	product formation [%]	ee [%]
3a	0	0.37 ± 0.04	n.d.	2.08 ± 0.15	n.d.	5.93 ± 0.00	n.d.
	0.5	63.62 ± 3.94	n.d.	63.67 ± 3.30	n.d.	43.32 ± 4.18	n.d.
	1	64.38 ± 1.48	n.d.	66.99 ± 2.72	n.d.	58.95 ± 4.00	n.d.
	3	67.18 ± 4.47	n.d.	66.17 ± 2.72	n.d.	74.89 ± 8.17	n.d.
	5	66.00 ± 4.15	> 99 (<i>R</i>)	71.52 ± 4.49	> 99 (<i>R</i>)	78.14 ± 4.95	> 99 (<i>S</i>)
	8	64.22 ± 2.21	> 99 (<i>R</i>)	69.86 ± 7.11	> 99 (<i>R</i>)	74.18 ± 6.89	> 99 (<i>S</i>)
	24	64.35 ± 8.15	> 99 (<i>R</i>)	64.81 ± 2.02	> 99 (<i>R</i>)	69.00 ± 1.04	> 99 (<i>S</i>)
3b	0	-	n.d.	0.05 ± 0.00	n.d.	-	n.d.
	0.5	10.89 ± 0.21	n.d.	17.77 ± 0.85	58.24 ± 10.43 (<i>S</i>)	0.11 ± 0.00	n.d.
	1	20.88 ± 0.31	32.24 ± 20.66 (<i>S</i>)	29.69 ± 0.84	51.97 ± 8.92 (<i>S</i>)	1.06 ± 0.11	n.d.
	3	36.75 ± 1.96	23.74 ± 0.41 (<i>S</i>)	46.91 ± 1.99	n.d.	4.85 ± 0.08	n.d.
	5	39.95 ± 1.56	22.60 ± 1.94 (<i>S</i>)	48.67 ± 0.99	53.67 ± 3.32 (<i>S</i>)	7.33 ± 0.12	72.31 ± 6.10 (<i>R</i>)
	8	43.62 ± 1.26	20.98 ± 4.24 (<i>S</i>)	50.05 ± 2.09	54.58 ± 1.83 (<i>S</i>)	9.54 ± 0.30	69.32 ± 1.63 (<i>R</i>)
	24	48.02 ± 1.83	23.22 ± 0.41 (<i>S</i>)	47.79 ± 1.20	55.96 ± 0.30 (<i>S</i>)	14.22 ± 0.19	67.89 ± 0.53 (<i>R</i>)
3c	0	-	n.d.	-	n.d.	-	n.d.
	0.5	23.93 ± 1.26	n.d.	52.43 ± 1.61	89.61 ± 0.03 (<i>S</i>)	3.13 ± 0.06	n.d.
	1	46.47 ± 2.34	87.07 ± 0.09 (<i>S</i>)	82.26 ± 4.96	89.92 ± 0.05 (<i>S</i>)	8.17 ± 1.05	n.d.
	3	86.32 ± 4.46	86.52 ± 0.04 (<i>S</i>)	93.83 ± 8.39	89.96 ± 0.01 (<i>S</i>)	24.88 ± 1.98	n.d.
	5	91.68 ± 4.93	86.45 ± 0.02 (<i>S</i>)	> 99	n.d.	36.03 ± 3.89	87.20 ± 0.05 (<i>R</i>)
	8	89.79 ± 8.17	n.d.	96.11 ± 3.42	n.d.	49.95 ± 1.39	87.11 ± 0.01 (<i>R</i>)
	24	94.06 ± 4.37	n.d.	94.39 ± 5.22	n.d.	63.00 ± 0.41	87.00 ± 0.02 (<i>R</i>)

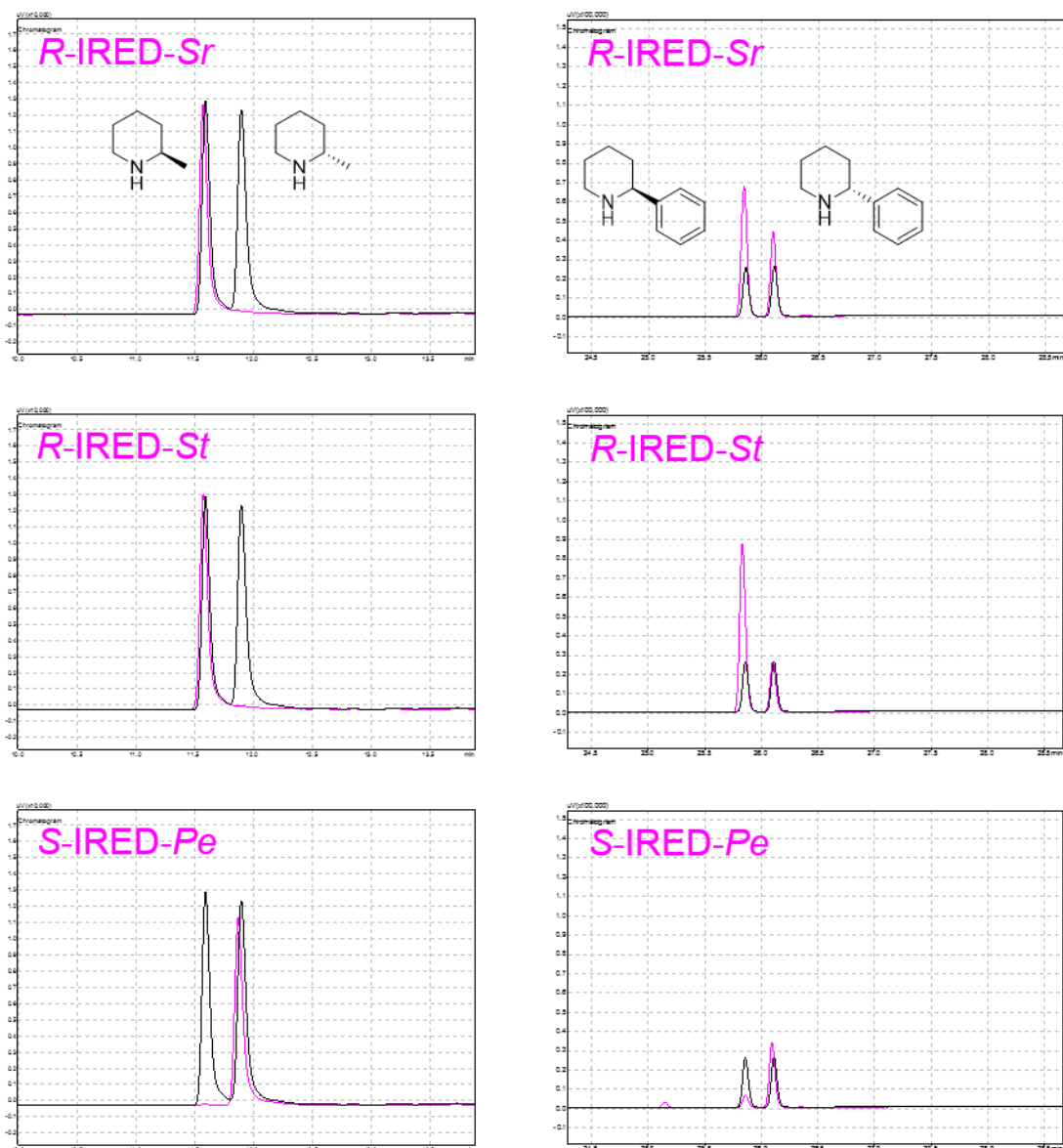


Figure S7: Chiral GC-traces for the separation of the enantiomers of product **4a** (left side) and **4b** (right side) to determine the enantiomeric excess in IRED catalyzed whole cell biotransformations. Black: racemic **4a** or **4b**. Examples of biotransformation samples are always shown in pink with *R*-IRED-*Sr* in the top row, *R*-IRED-*St* in the middle and *S*-IRED-*Pe* in the bottom row. Enantiomeric excess values are given in Table S2. Assignment of the enantiomers was done by comparison with commercial available (*S*)-**4a** and by analogy to amine product **2a**. Assignment for product (*R*)-**4b** and (*S*)-**4b** is based on literature reference.¹⁴⁷

7 SUPPORTING INFORMATION

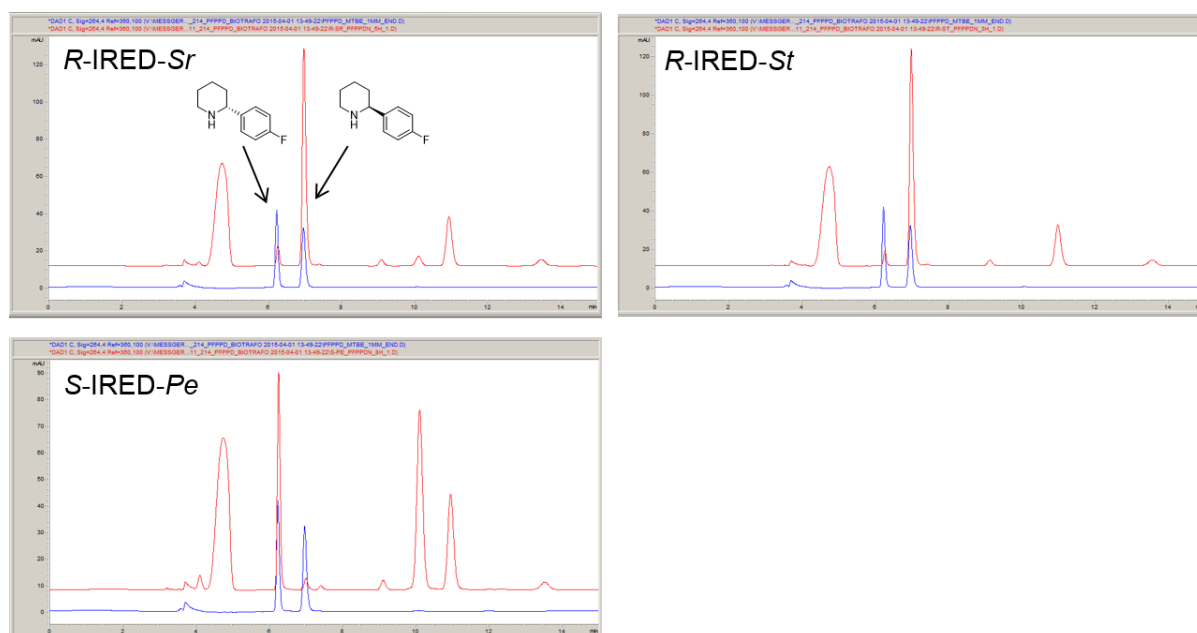


Figure S8: Chiral HPLC traces for the separation of the enantiomers of product **4c** to determine the enantiomeric excess in IRED catalyzed whole cell biotransformations. Blue: racemic **4c**, examples of biotransformation samples are always shown in red with *R*-IRED-*Sr* on top left, *R*-IRED-*St* on top right and *S*-IRED-*Pe* in the bottom row. Enantiomeric excess values are given in Table S2. Assignment of product (*R*)-**4c** and (*S*)-**4c** is based on literature references.¹⁴⁷

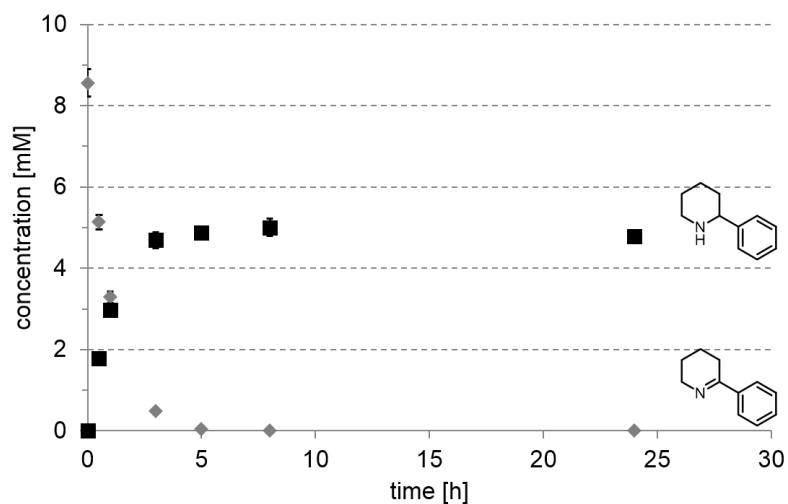


Figure S9: Exemplarily the whole cell biotransformation for the conversion of substrate **3b** into amine product **4b** is shown for the triplicate of *R*-IRED-*St*; *R*-IRED-*Sr* yielded comparable results. As explained in the main text, the substrate is fully consumed, but the amount of product detected is limited to about 50%. It might be possible that the cells consume the substrate/product or that the recovery from the complex biological sample is limited as it is also the case for isoquinoline **5c** (Figure S12).

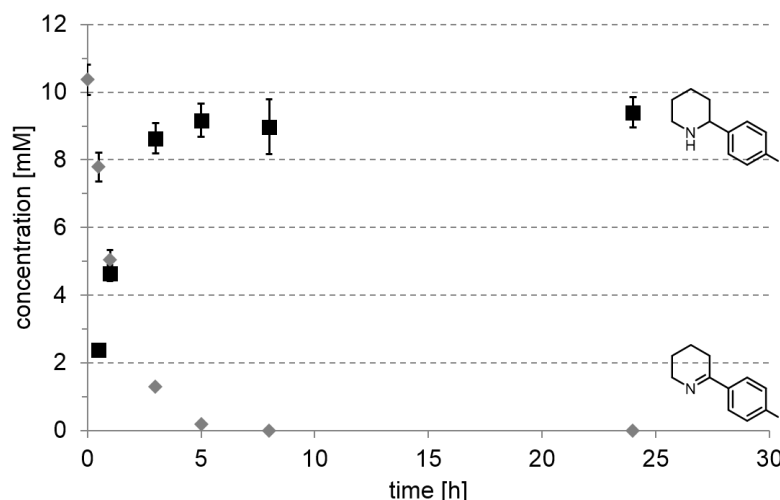


Figure S10: Exemplarily the whole cell biotransformation for the conversion of substrate **3c** into amine product **4c** is shown for the triplicate of *R*-IRED-*Sr*; *R*-IRED-*St* yielded comparable results. In contrast to substrate **3b**, which was also fully consumed, this product could nearly fully be recovered.

Table S3: Product formations and enantiomeric excess values in [%] for IRED catalyzed whole cell biotransformations with isoquinoline substrates **5a**, **5b** and **5c**. All biotransformations were performed in triplicates. The values in this table give the average of such a triplicate and the errors represent the standard deviation. Product formation with substrate **5a** and **5b** at 0 h is caused most probably due to the too slow sample preparation after starting the biotransformation. Biotransformations were set up in the order *R*-IRED-*Sr*, *R*-IRED-*St* and *S*-IRED-*Pe* last. For the assumed (*S*)-selectivity of *S*-IRED-*Pe* with substrate **5c**, please see footnote^{IV}. -: not detected; n.d.: not determined; n.a.: not available.

		5a: R ¹ = H, R ² = H 5b: R ¹ = methyl, R ² = H 5c: R ¹ = methyl, R ² = methoxy		6a: R ¹ = H, R ² = H 6b: R ¹ = methyl, R ² = H 6c: R ¹ = methyl, R ² = methoxy			
imine	time [h]	<i>R</i> -IRED- <i>Sr</i> product formation [%] ee [%]	<i>R</i> -IRED- <i>St</i> product formation [%] ee [%]	<i>S</i> -IRED- <i>Pe</i> product formation [%] ee [%]			
5a	0	0.92 ± 0.74	n.a.	1.52 ± 0.54	n.a.	1.42 ± 0.58	n.a.
	0.5	37.65 ± 0.18	n.a.	41.27 ± 0.31	n.a.	37.57 ± 0.57	n.a.
	1	75.52 ± 4.18	n.a.	83.75 ± 2.91	n.a.	67.14 ± 0.91	n.a.
	3	>99	n.a.	97.27 ± 4.05	n.a.	95.00 ± 2.32	n.a.
	5	>99	n.a.	>99	n.a.	>99	n.a.
	8	>99	n.a.	>99	n.a.	>99	n.a.
	24	>99	n.a.	>99	n.a.	>99	n.a.
5b	0	1.87 ± 0.30	n.d.	1.99 ± 0.21	n.d.	1.67 ± 0.21	n.d.
	0.5	28.97 ± 0.87	n.d.	18.32 ± 0.40	n.d.	3.69 ± 0.33	n.d.
	1	51.59 ± 3.32	n.d.	37.14 ± 0.93	n.d.	9.25 ± 0.31	n.d.
	3	80.00 ± 9.23	n.d.	86.51 ± 4.62	n.d.	24.14 ± 2.33	n.d.
	5	95.71 ± 4.72	91.26 ± 1.80 (<i>R</i>)	96.29 ± 1.78	51.12 ± 0.18 (<i>R</i>)	40.61 ± 1.30	93.15 ± 0.66 (<i>S</i>)
	8	99.32 ± 6.35	93.02 ± 0.07 (<i>R</i>)	98.06 ± 3.63	50.79 ± 0.16 (<i>R</i>)	54.75 ± 2.45	95.32 ± 0.17 (<i>S</i>)
	24	91.51 ± 6.71	93.02 ± 0.15 (<i>R</i>)	94.18 ± 4.14	50.71 ± 0.09 (<i>R</i>)	79.42 ± 4.75	94.89 ± 0.06 (<i>S</i>)
5c	0	-	n.d.	-	n.d.	-	n.d. (<i>S</i>)
	0.5	-	n.d.	-	n.d.	-	n.d. (<i>S</i>)
	1	-	n.d.	-	n.d.	-	n.d. (<i>S</i>)
	3	-	n.d.	-	n.d.	3.22 ± 0.14	n.d. (<i>S</i>)
	5	-	n.d.	-	n.d.	5.69 ± 0.83	n.d. (<i>S</i>)
	8	-	n.d.	-	n.d.	9.62 ± 0.85	n.d. (<i>S</i>)
	24	-	n.d.	-	n.d.	14.82 ± 0.75	n.d. (<i>S</i>)
	30	-	n.d.	-	n.d.	17.44 ± 0.33	n.d. (<i>S</i>)
	48	-	n.d.	-	n.d.	28.09 ± 4.94	n.d. (<i>S</i>)

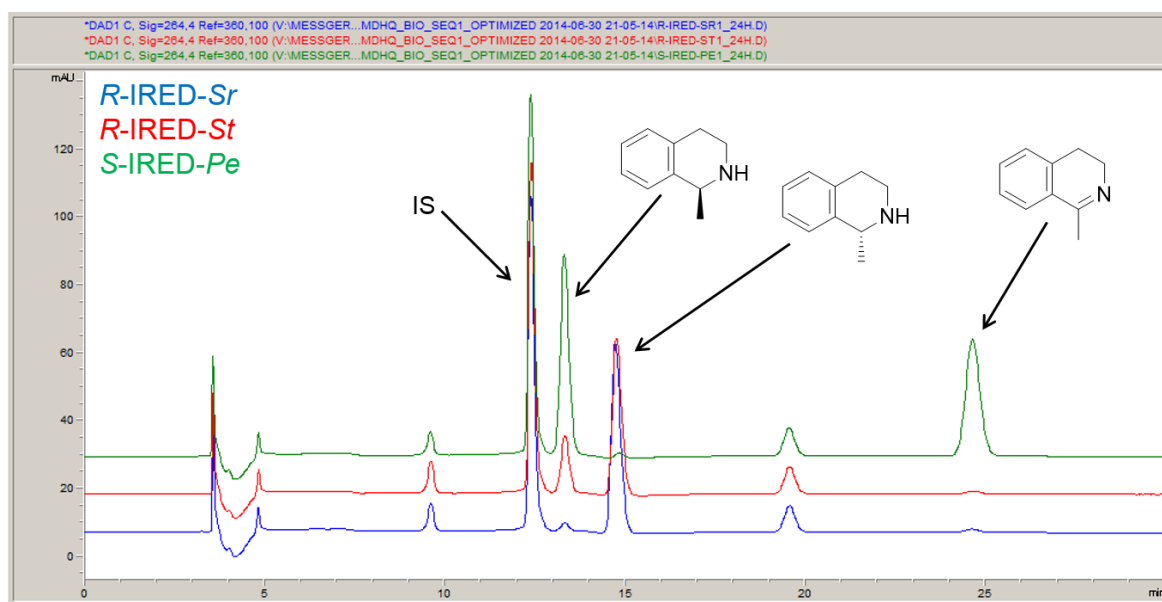


Figure S11: Chiral HPLC traces for the separation of the enantiomers of product **6b** to determine the enantiomeric excess in IRED catalyzed whole cell biotransformations. Blue: Biotransformation with *R*-IRED-*Sr*, red: Biotransformation with *R*-IRED-*St* and green: Biotransformation with *S*-IRED-*Pe*. Enantiomeric excess values are given in Table S3. Assignment of the enantiomers was done as described by Leipold *et al.*¹⁴³ IS = internal standard.

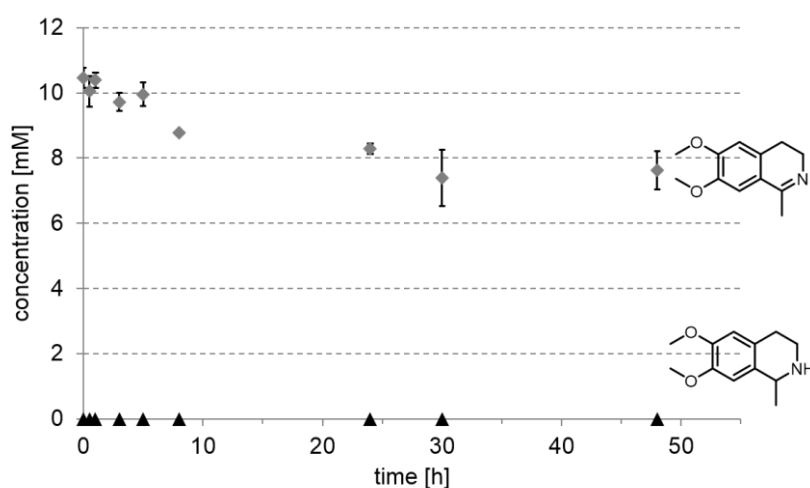
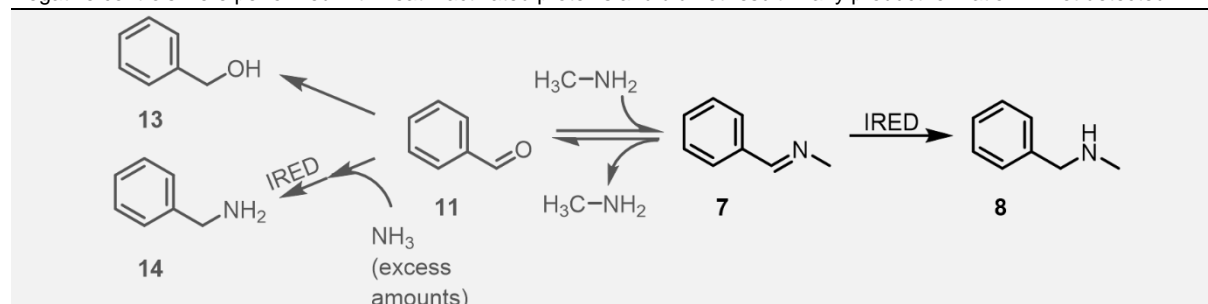


Figure S12: Consumption of substrate **5c** by *E. coli* JW5510 cells harboring an empty pBAD33 plasmid. These cells were used as control for IRED catalyzed whole cell biotransformations and the mock biotransformation performed in triplicates. The error bars in Figure S12 represent the standard deviation of the triplicate. About 20% of the substrate is consumed (or could not be recovered from the complex biological sample), but no formation of product **6c** was observed. Negative controls for the other imine substrates did not show any substrate consumption.

7.2.2 Biotransformations with purified IREDs and GC/HPLC-traces for determination of product formations and determination of the enantiomeric excess in these biotransformations

Table S4: Reduction of imine **7** to amine **8** by purified IREDs. Hydrolysis of **7** generates aldehyde **11** which further reacted to **13** and **14**. For details see main text. The biotransformations were performed in triplicates with purified proteins from the same purification batch. The values in this table give the average of such a triplicate and the error represents the standard deviation. Negative controls were performed with heat inactivated proteins and did not result in any product formation. -: not detected.



IRED	time [h]	substrate consumption [%] and product formation [%]				
		7	8	11	13	14
R-IRED-Sr	0	54.15 ± 1.19	-	45.85 ± 1.11	-	-
	0.5	48.50 ± 1.28	6.45 ± 0.19	42.29 ± 2.67	2.76 ± 0.23	-
	1	45.73 ± 1.36	9.81 ± 0.26	40.03 ± 1.54	4.44 ± 0.16	-
	3	34.96 ± 0.59	22.77 ± 0.84	29.54 ± 0.49	12.73 ± 0.86	-
	5	23.40 ± 0.24	30.69 ± 0.92	19.43 ± 0.23	21.64 ± 1.14	4.84 ± 0.47
	8	12.13 ± 0.49	37.61 ± 0.85	8.95 ± 0.51	33.26 ± 1.95	8.04 ± 0.52
	24	-	42.01 ± 0.92	-	46.22 ± 1.95	11.77 ± 0.15
R-IRED-St	0	52.87 ± 0.09	-	47.13 ± 2.43	-	-
	0.5	48.70 ± 0.30	6.02 ± 0.25	45.28 ± 1.49	-	-
	1	47.33 ± 0.28	8.26 ± 0.29	44.41 ± 2.39	-	-
	3	42.31 ± 0.82	15.26 ± 0.09	40.00 ± 1.53	2.43 ± 0.39	-
	5	38.21 ± 1.05	21.30 ± 0.42	37.66 ± 0.65	2.83 ± 0.09	-
	8	33.59 ± 0.18	29.31 ± 0.86	33.79 ± 0.96	3.30 ± 0.10	-
	24	18.87 ± 0.37	56.67 ± 0.36	20.11 ± 0.69	4.35 ± 0.23	-
S-IRED-Pe	0	51.80 ± 1.65	-	48.20 ± 3.14	-	-
	0.5	52.27 ± 1.29	-	47.73 ± 0.92	-	-
	1	52.54 ± 1.02	-	47.46 ± 1.39	-	-
	3	51.23 ± 0.86	4.22 ± 0.37	44.56 ± 0.67	-	-
	5	50.48 ± 1.52	5.50 ± 0.34	44.01 ± 2.60	-	-
	8	50.02 ± 1.68	7.19 ± 0.28	42.79 ± 2.46	-	-
	24	44.08 ± 1.39	13.92 ± 0.51	38.18 ± 1.77	3.83 ± 0.55	-

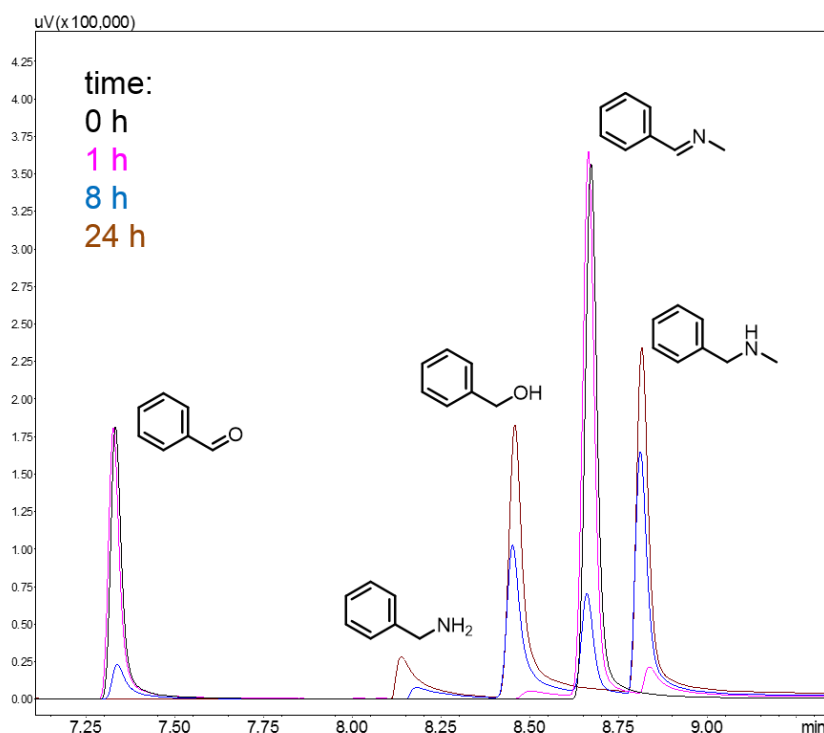


Figure S13: Exemplary GC-traces overlay for the reduction of imine **7** to amine **8**. The samples after 0 h (black), 1 h (pink), 8 h (blue) and 24 h (brown) for the reaction catalyzed by purified *R*-IRED-*Sr* are shown. The hydrolysis product **11** further reacted to **13** (benzylalcohol) and **14** (benzylamine). For details see the main text.

Table S5: Reduction of imine **9** to amine **10** by purified IREDS. Hydrolysis of **9** generates aldehyde **11** and amine **12**. Aldehyde **11** further reacted to **13** and **14**. For details see main text. The biotransformations were performed in triplicates with purified proteins from the same purification batch. The values in this table give the average of such a triplicate and the error represents the standard deviation. Negative controls were performed with heat inactivated proteins and did not result in any product formation. -: not detected.

IRED	time [h]	substrate consumption [%] and product formation [%]					
		9	10	11	12	13	14
<i>R</i> -IRED- <i>Sr</i>	0	87.35 ± 5.29	-	12.65 ± 0.51	10.18 ± 0.33	-	-
	0.5	36.84 ± 5.76	0.68 ± 0.03	56.96 ± 3.41	51.49 ± 2.50	3.73 ± 0.38	1.80 ± 0.18
	1	9.43 ± 1.79	0.91 ± 0.11	77.97 ± 3.83	76.69 ± 1.50	9.07 ± 0.60	2.61 ± 0.20
	3	15.40 ± 1.91	3.58 ± 0.64	57.87 ± 2.79	72.33 ± 3.30	19.93 ± 1.08	3.21 ± 0.19
	5	4.05 ± 0.96	3.17 ± 0.71	53.65 ± 2.62	88.80 ± 3.01	34.56 ± 2.44	4.56 ± 0.32
	8	4.08 ± 0.66	4.81 ± 0.79	39.87 ± 3.05	87.07 ± 3.36	45.77 ± 1.42	5.47 ± 0.12
	24	1.94 ± 0.43	6.49 ± 2.65	19.84 ± 4.55	87.14 ± 6.33	64.14 ± 2.77	7.59 ± 0.46
<i>R</i> -IRED- <i>Sr</i>	0	86.27 ± 1.62	0.79 ± 0.05	12.94 ± 0.25	11.36 ± 0.03	-	-
	0.5	35.43 ± 4.71	9.75 ± 0.18	53.07 ± 0.78	47.77 ± 0.95	0.34 ± 0.03	1.41 ± 0.17
	1	7.94 ± 1.09	11.89 ± 0.42	76.54 ± 4.17	71.06 ± 3.66	1.68 ± 0.04	1.96 ± 0.07
	3	16.86 ± 0.31	33.90 ± 1.63	44.68 ± 1.61	43.08 ± 1.42	2.73 ± 0.10	1.83 ± 0.05
	5	4.58 ± 1.34	34.03 ± 4.86	51.75 ± 2.03	57.42 ± 1.94	6.50 ± 0.27	3.15 ± 0.13
	8	5.90 ± 2.59	56.39 ± 11.54	29.17 ± 4.10	33.13 ± 6.38	5.85 ± 1.26	2.69 ± 0.64
	24	1.65 ± 0.28	67.00 ± 13.99	16.56 ± 2.33	25.60 ± 2.74	10.49 ± 0.82	4.30 ± 0.39

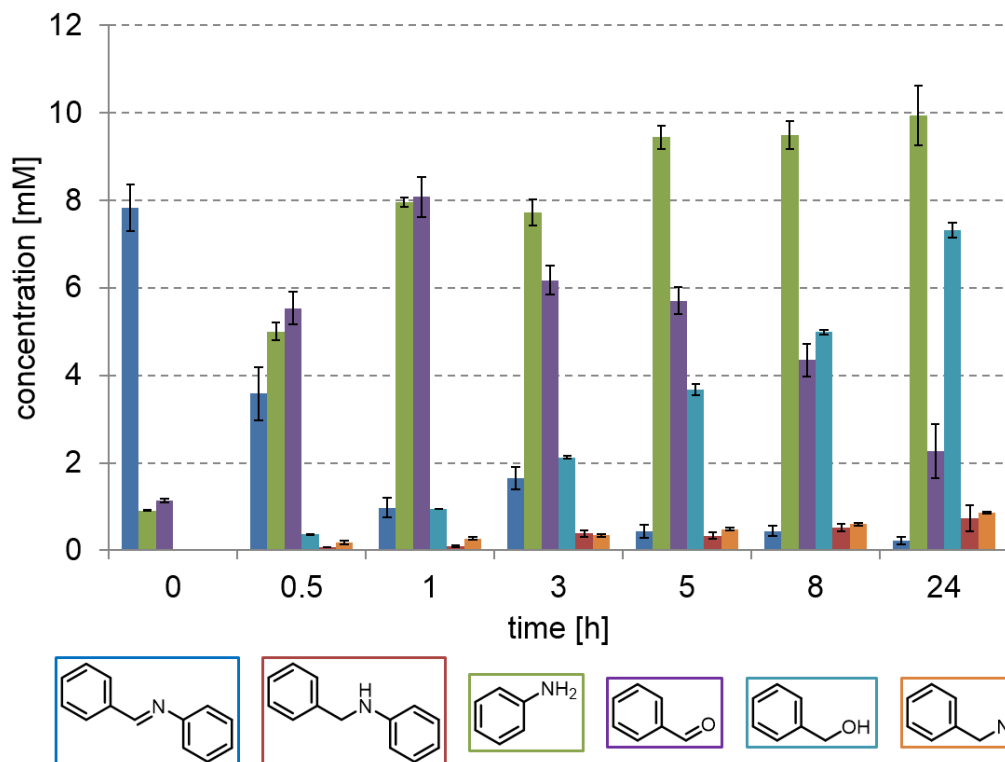


Figure S14: Graphical representation of the *R*-IRED-*Sr* catalyzed biotransformation of imine **9** (dark blue) to amine **10** (red). *R*-IRED-*Sr* was selected for presentation as in this biotransformation the formation of the byproducts is better visualized than with *R*-IRED-*St*. The hydrolysis product aniline **12** (green) can react back to form the substrate **9**, but the aldehyde **11** (purple) can also be further reduced to alcohol **13** (light blue) and reductively aminated to amine **14** (orange).

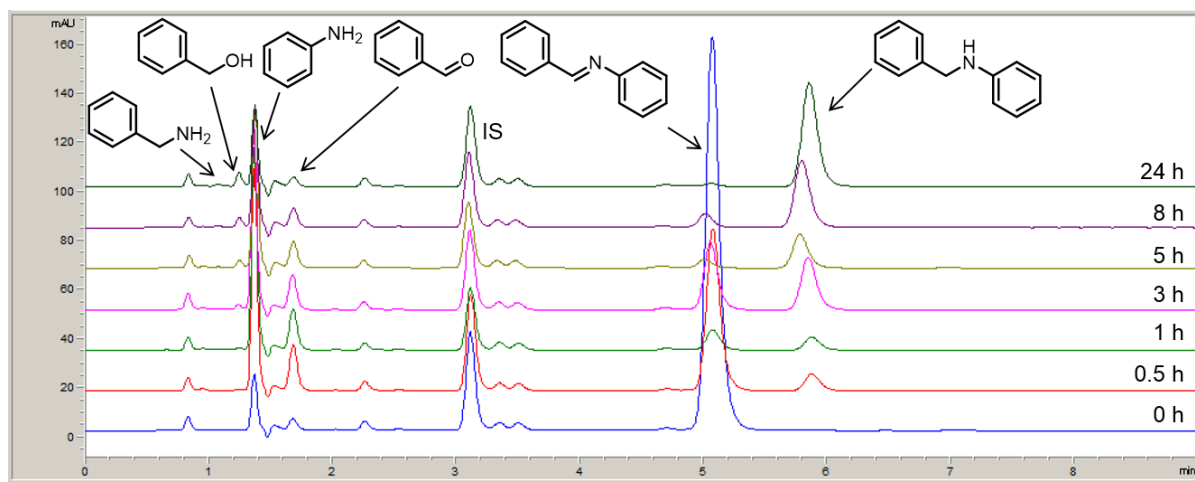


Figure S15: Exemplary HPLC traces for the reduction of imine **9** to amine **10**. The reduction catalyzed by purified *R*-IRED-*St* over 24 h is shown as with this enzyme the formation of product **10** is more pronounced than with *R*-IRED-*Sr*. Next to the substrate and product also the hydrolysis products (aldehyde **11** and amine **12**) and the byproducts (alcohol **13** and amine **14**) were detected. For a more detailed explanation see main text. The UV signal at 220 nm was used for generation of this Figure as it provides in general the highest sensitivity, however note that not all substances have their absorbance maxima at this wavelength. Quantification was done at the maximum specific absorbance wavelength. IS = internal standard.

7 SUPPORTING INFORMATION

Table S6: Full dataset for the formation of benzhydrylamine **16** and the hydrolytic byproduct benzophenone **17** in [%] in a biotransformation with purified *R*-IRED-*Sr*. For the negative control, the IRED was heat inactivated by treatment at 95 °C for 10 min. All reactions were performed in triplicates with purified proteins from the same purification batch. The values in this table give the average of such a triplicate and the errors represent the standard deviation. Further reduction of **17** to the alcohol was not observed. -: not detected.

product formation [%]				
time [h]	<i>R</i> -IRED- <i>Sr</i>		negative control	
	16	17	16	17
0	-	3.98 ± 0.10	-	3.22 ± 0.34
0.5	21.60 ± 0.72	21.11 ± 0.32	-	29.20 ± 0.70
1	34.22 ± 0.98	30.91 ± 0.42	-	45.32 ± 0.19
3	47.56 ± 0.37	40.75 ± 1.78	-	76.90 ± 2.35
5	48.71 ± 0.15	41.92 ± 1.41	-	84.78 ± 4.02
8	49.46 ± 0.24	42.49 ± 1.66	-	81.43 ± 1.27
24	52.55 ± 2.94	45.84 ± 1.55	-	88.48 ± 2.64

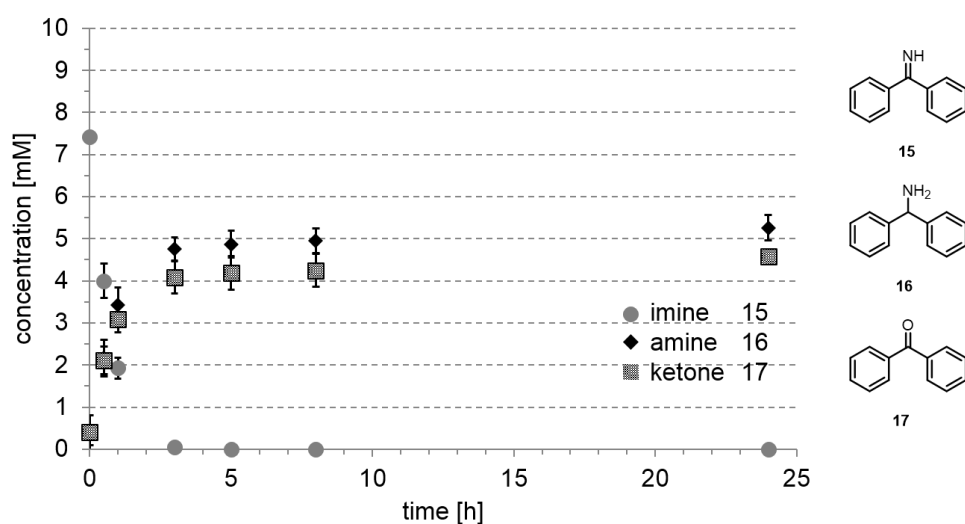


Figure S16: Time course for the reduction and the hydrolysis of 10 mM benzophenoneimine **15** to the amine product **16** and the ketone **17** in a biotransformation with purified *R*-IRED-*Sr*. The biotransformation was performed in triplicates with purified protein of the same purification batch. Values in Figure S16 give the average of the triplicate and the error bars represent the standard deviation. The pure hydrolysis to ketone **17**, visible in the negative control with heat inactivated *R*-IRED-*Sr* is shown in Figure S17.

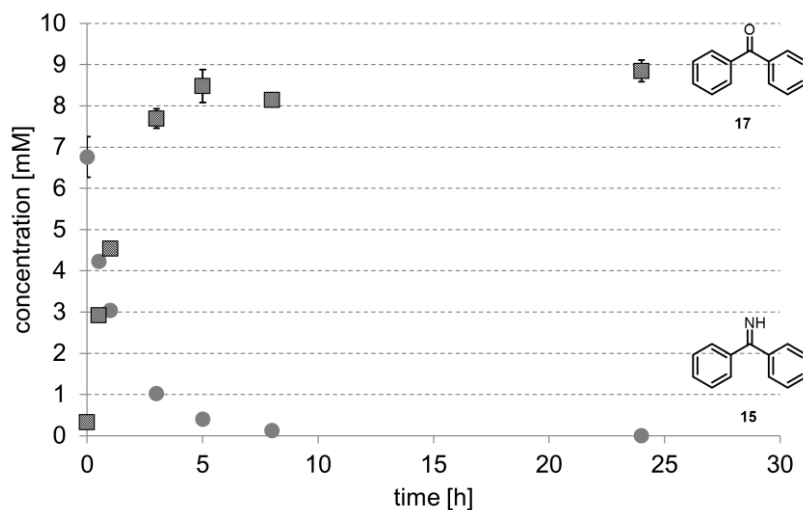


Figure S17: Time course for the hydrolysis of 10 mM benzophenoneimine **15** to the ketone **17** in a mock biotransformation with heat inactivated *R*-IRED-*Sr*. The control reaction was done in triplicates and the error bars represent the standard deviation.

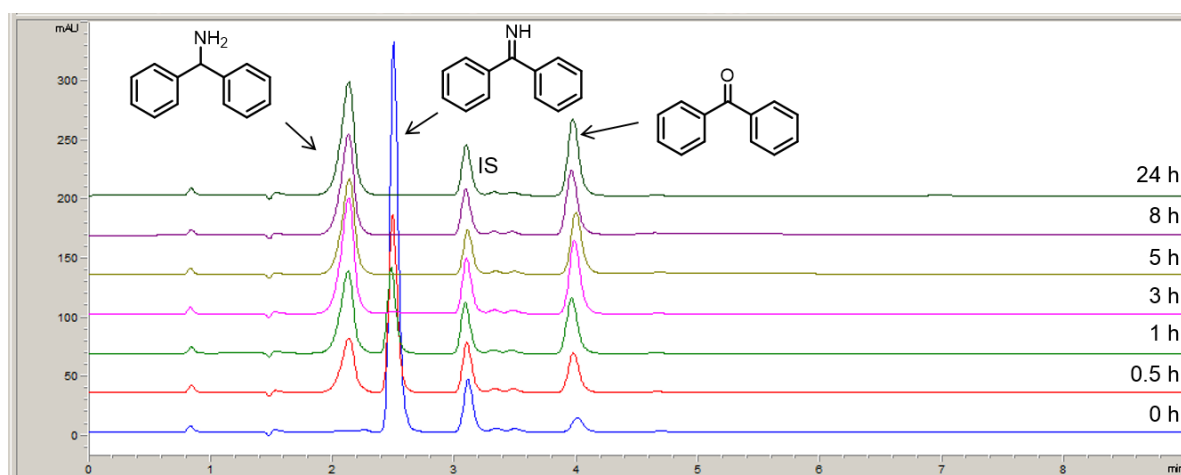


Figure S18: Exemplary HPLC traces for the reduction of imine **15** to amine **16** catalyzed by purified *R*-IRED-*Sr* over 24 h. Next to the substrate and product also the hydrolysis product, ketone **17** was detected. The UV signal at 220 nm was used for generation of this Figure as it provides in general the highest sensitivity, however note that not all substances have their absorbance maxima at this wavelength. Quantification was done at the maximum specific absorbance wavelength. IS = internal standard.

7 SUPPORTING INFORMATION

Table S7: Product formations and stereoselectivities in [%] for the reduction of **18** to amine product **19** by (*R*)-selective IREDs. Imine substrate **18** hydrolyzes to the byproducts **12** and **20**. Further reduction of **20** to 1-phenylethanol was not observed or is below the detection limit. The biotransformations were performed in triplicates with purified proteins from the same purification batch. The values in this table give the average of such a triplicate and the errors represent the standard deviation. Negative controls were performed with heat inactivated proteins and did not result in any product formation. -: not detected; n.d.: not determined.

IRED	time [h]	substrate consumption [%] and product formation [%]				ee [%] of 19
		18	19	20	12	
<i>R</i> -IRED- <i>Sr</i>	0	82.30 ± 6.05	-	1.05 ± 0.06	1.01 ± 0.06	n.d.
	0.5	54.61 ± 6.61	-	1.92 ± 0.13	2.00 ± 0.15	n.d.
	1	65.77 ± 11.04	-	3.36 ± 0.15	3.55 ± 0.14	n.d.
	3	43.51 ± 11.30	1.48 ± 0.23	8.60 ± 0.27	9.59 ± 0.28	n.d.
	5	23.20 ± 7.20	2.56 ± 0.96	13.42 ± 0.73	14.97 ± 0.29	91.81 ± 1.57 (<i>R</i>)
	8	19.85 ± 6.65	2.82 ± 0.35	20.81 ± 0.78	24.62 ± 0.44	90.39 ± 2.85 (<i>R</i>)
	24	50.35 ± 17.44	10.18 ± 5.65	38.17 ± 2.47	38.28 ± 0.86	94.24 ± 0.50 (<i>R</i>)
<i>R</i> -IRED- <i>St</i>	0	59.07 ± 7.78	-	0.63 ± 0.06	0.57 ± 0.06	n.d.
	0.5	54.61 ± 6.61	-	1.92 ± 0.13	2.00 ± 0.15	n.d.
	1	37.19 ± 4.35	21.32 ± 1.08	2.67 ± 0.09	2.78 ± 0.13	n.d.
	3	19.30 ± 3.87	47.71 ± 2.57	5.46 ± 0.33	5.65 ± 0.34	n.d.
	5	5.89 ± 1.57	49.51 ± 4.27	6.39 ± 0.32	6.83 ± 0.41	88.62 ± 0.06 (<i>R</i>)
	8	1.65 ± 0.87	30.22 ± 4.02	7.92 ± 0.42	8.74 ± 0.64	88.23 ± 0.25 (<i>R</i>)
	24	13.44 ± 5.68	83.85 ± 20.47	9.76 ± 2.06	7.96 ± 1.52	87.75 ± 0.33 (<i>R</i>)

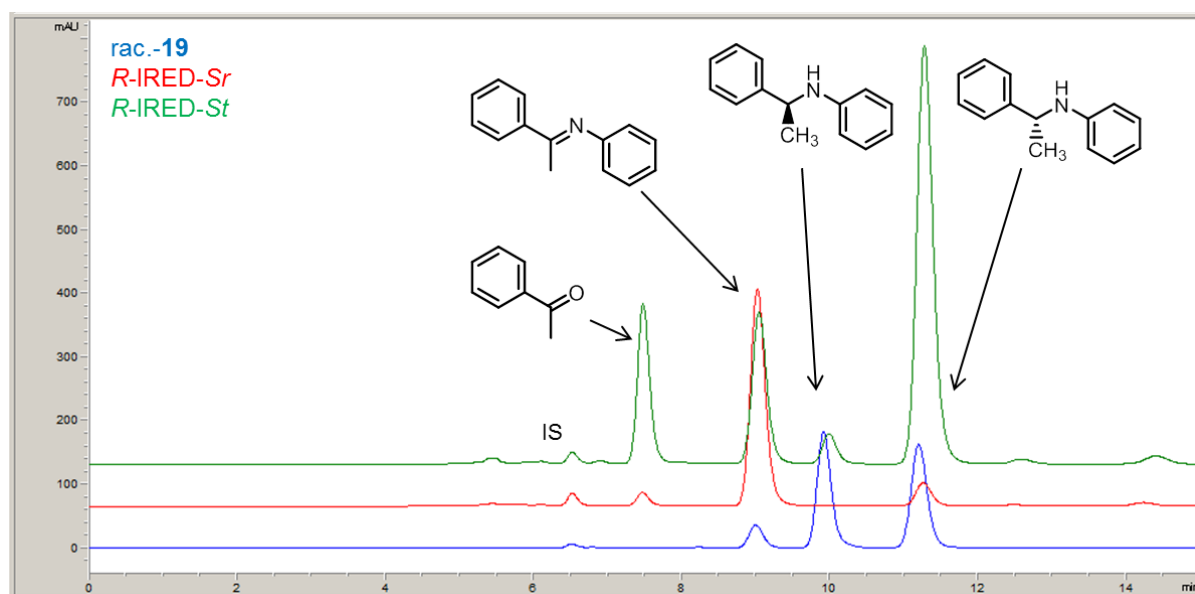
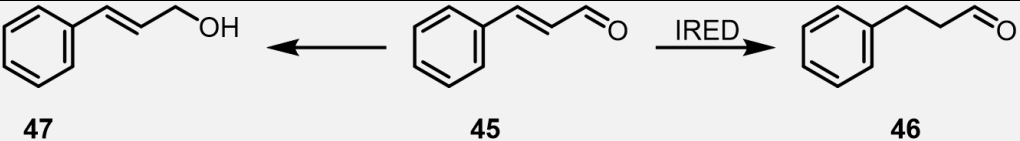


Figure S19: Chiral HPLC traces for the separation of the enantiomers of product **19** to determine the enantiomeric excess in biotransformations with purified *R*-IREDs. Blue: racemic-**19**. Red: Biotransformation with *R*-IRED-*Sr*, green: Biotransformation with *R*-IRED-*St*. Enantiomeric excess values are given in Table S7. Assignment of the enantiomers was done as described in literature.^{195–197} As the substrate (imine **18**) at high concentrations overlaps with the (*S*)-enantiomer of the product it was hydrolyzed by the addition of acidic Et₂O (2 M HCl in Et₂O), followed by a washing procedure to remove parts of aniline **12**, which shows higher water solubility than ketone **20**. For the analysis of the sample on HPLC the compounds had to be extracted again into an organic solvent, requiring a pH shift to > 14, leading to the potential partial reformation of the imine. By this procedure the fraction of imine **18** was reduced and the ratio of **12**:**20** increased towards the ketone. IS = internal standard.

Table S8: Reduction of cinnamaldehyde **45** to 3-phenylpropanal **46** by purified *R*-IRED-*St* and formation of the alcohol byproduct **47** in [%]. Product formation with the other two IREDs was found to be in the range of 3-5% in 24 h. All biotransformations were performed in triplicates with purified proteins from the same purification batch. The values in this table give the average of such a triplicate and the errors represent the standard deviation. Negative controls were performed with heat inactivated proteins and did not result in any product formation. -: not detected.

			
product formation [%]			
<i>R</i> -IRED- <i>St</i>			
time [h]	46	47	
0	-	-	
0.5	0.74 ± 0.06	1.21 ± 0.11	
1	1.55 ± 0.15	1.24 ± 0.11	
3	4.95 ± 0.30	1.94 ± 0.69	
5	7.89 ± 0.54	2.30 ± 1.48	
8	11.18 ± 0.58	3.49 ± 0.79	
24	15.83 ± 0.95	3.56 ± 1.00	

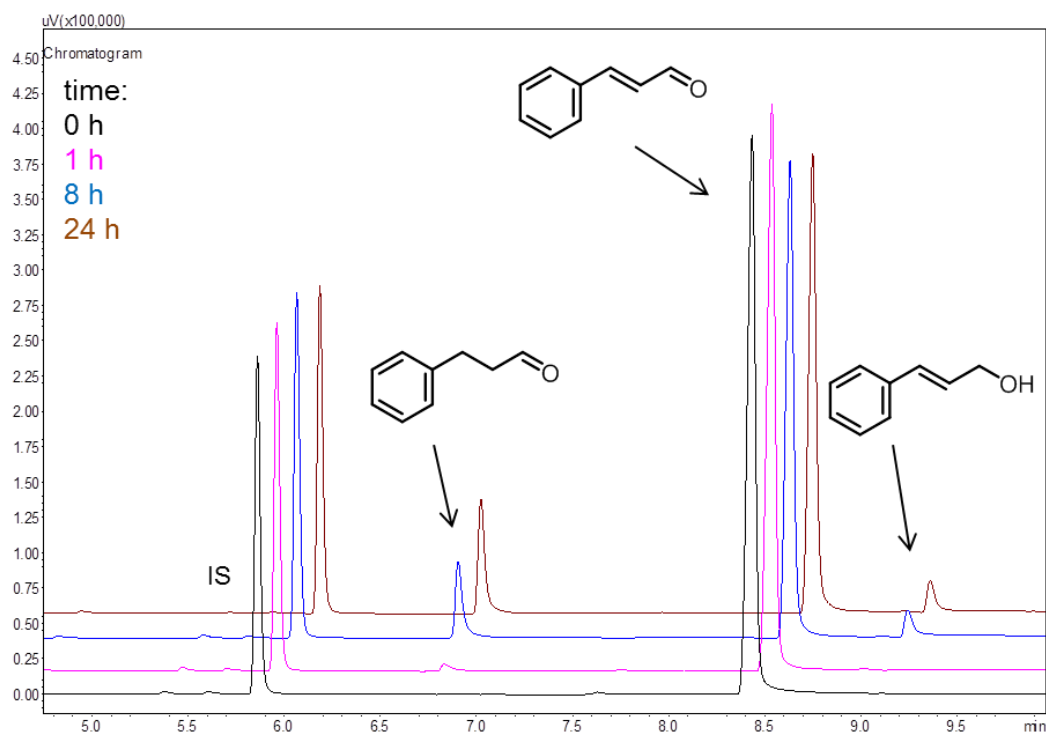


Figure S20: Exemplary GC-traces for the reduction of the activated C=C double bond in **45** to aldehyde **46** and formation of the alcohol byproduct. The samples after 0 h (black), 1 h (pink), 8 h (blue) and 24 h (brown) for the reaction catalyzed by purified *R*-IRED-*St* are shown. IS = internal standard.

7.3 Characterization of the IREDs

7.3.1 Thermostability

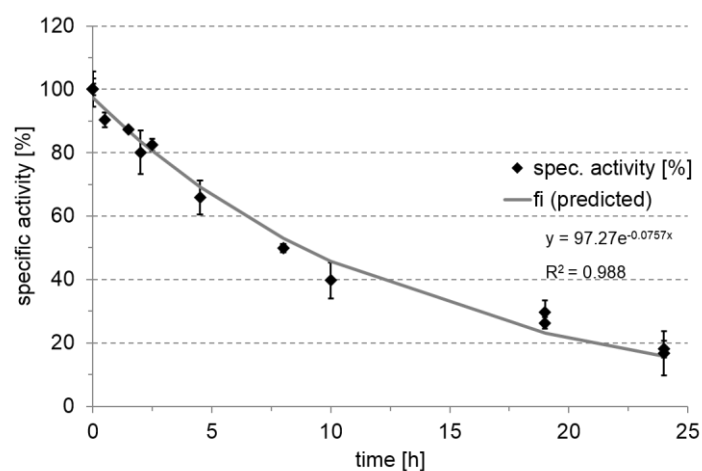


Figure S21: Specific activities for the reduction of **1** in [%] to determine the half-life time of *R*-IRED-*Sr* for incubation at 30 °C. Activities were determined in triplicates and the errors give the standard deviation. The decreasing activities were fitted to an exponential decay function of the formula $A=A_0 \cdot e^{-\lambda t}$ with A_0 representing the specific activity at $t = 0$ h.

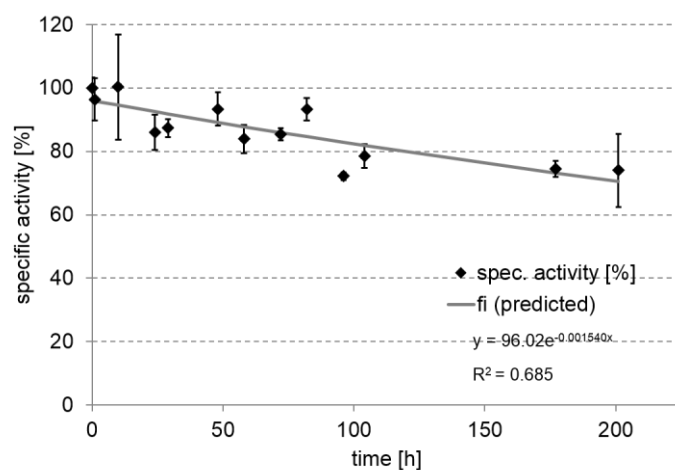


Figure S22: Specific activities for the reduction of **1** in [%] to determine the half-life time of *S*-IRED-*Pe* for incubation at 50 °C. Activities were determined in triplicates and the errors give the standard deviation. The decreasing activities were fitted to an exponential decay function of the formula $A=A_0 \cdot e^{-\lambda t}$ with A_0 representing the specific activity at $t = 0$ h.

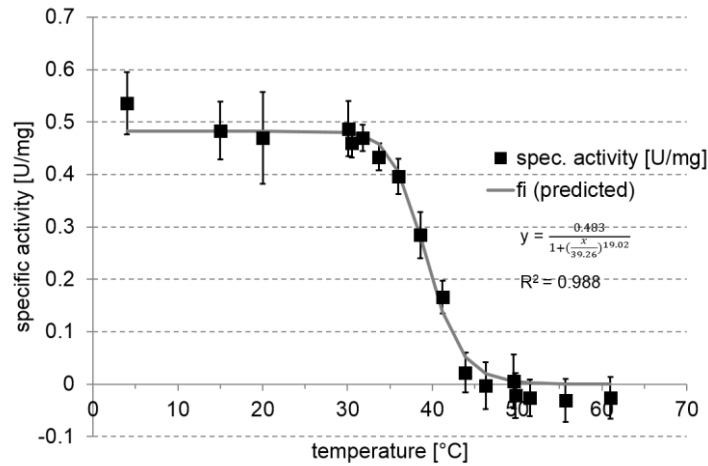


Figure S23: Specific activities for the reduction of **1** in [U/mg] with *R-IRED-Sr* after incubation at different temperatures for 15 min. Activities were determined in triplicates and the errors give the standard deviation. Activities were fitted to a sigmoidal dose-response curve to determine the T_{50}^{15} . Using the above shown data *R-IRED-Sr* displayed 50% residual activity when incubated at 38.81 °C for a period of 15 min.

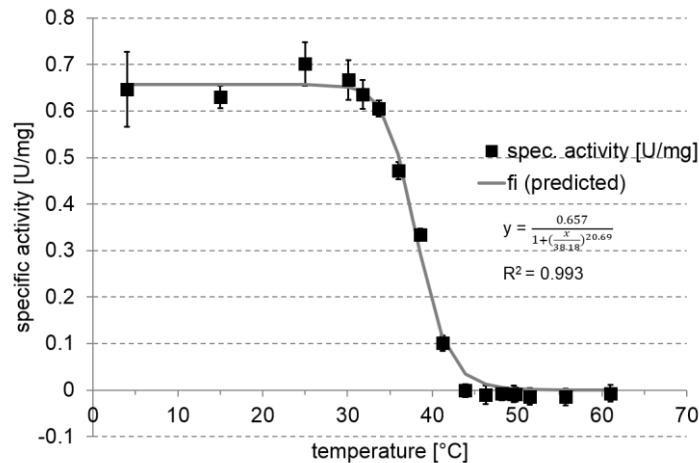


Figure S24: Specific activities for the reduction of **1** in [U/mg] with *R-IRED-St* after incubation at different temperatures for 15 min. Activities were determined in triplicates and the errors give the standard deviation. Activities were fitted to a sigmoidal dose-response curve to determine the T_{50}^{15} . Using the above shown data *R-IRED-St* displayed 50% residual activity when incubated at 38.24 °C for a period of 15 min.

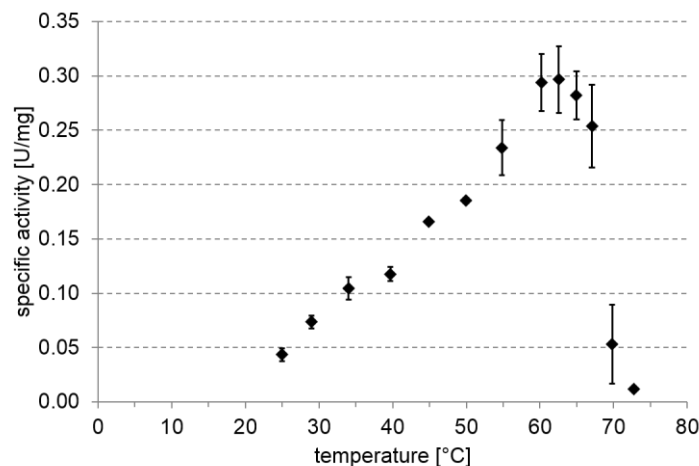


Figure S25: Specific activities for the reduction of **1** in [U/mg] with *S-IRED-Pe* recorded at different temperatures. Activities were determined in triplicates and the errors give the standard deviation. The maximum activity was found at around 65 °C, followed by a rapid loss due to the denaturation of the enzyme. An increase of about 10 °C resulted in an approximate doubling of the reaction rate.

7.3.2 Specific activities of the IREDs in the presence of different water miscible organic solvents

Table S9: Specific activities in [U/mg] of the three IREDs in the presence of varying (5%-25%) concentrations of water miscible organic solvents. All activities were determined in triplicates by photometrically monitoring the decrease of the NADPH absorbance for the reduction of 5 mM substrate 1. The solvents tested were: methanol (MeOH), ethanol (EtOH), isopropyl alcohol (iProp), acetonitrile (ACN), dimethyl sulfoxide (DMSO), glycerol, acetone and *tert*-butyl alcohol (*t*-BuOH). The specific activities of these IRED preparations in the solvent free reference system (50 mM NaPi buffer pH 7.0) were for *R*-IRED-*Sr*: 3.43 ± 0.02 U/mg, for *R*-IRED-*St*: 0.97 ± 0.02 U/mg and for *S*-IRED-*Pe*: $39.86 \times 10^{-3} \pm 1.30 \times 10^{-3}$ U/mg. -: not detected.

solvent	solvent [%]	specific activity [U/mg]		
		<i>R</i> -IRED- <i>Sr</i>	<i>R</i> -IRED- <i>St</i>	<i>S</i> -IRED- <i>Pe</i>
MeOH	5 %	2.06 ± 0.05	0.52 ± 0.03	$48.67 \times 10^{-3} \pm 1.68 \times 10^{-3}$
	10 %	1.44 ± 0.03	0.37 ± 0.02	$47.08 \times 10^{-3} \pm 2.57 \times 10^{-3}$
	15 %	0.74 ± 0.11	0.29 ± 0.02	$39.30 \times 10^{-3} \pm 1.08 \times 10^{-3}$
	20 %	0.32 ± 0.03	0.20 ± 0.02	$40.09 \times 10^{-3} \pm 1.11 \times 10^{-3}$
	25 %	0.11 ± 0.02	0.11 ± 0.02	$25.86 \times 10^{-3} \pm 0.52 \times 10^{-3}$
EtOH	5 %	0.79 ± 0.05	0.23 ± 0.01	$21.82 \times 10^{-3} \pm 0.82 \times 10^{-3}$
	10 %	0.40 ± 0.01	0.10 ± 0.00	$14.78 \times 10^{-3} \pm 0.29 \times 10^{-3}$
	15 %	0.09 ± 0.01	0.05 ± 0.00	$10.22 \times 10^{-3} \pm 0.05 \times 10^{-3}$
	20 %	0.08 ± 0.00	0.06 ± 0.00	$11.61 \times 10^{-3} \pm 0.69 \times 10^{-3}$
	25 %	-	0.03 ± 0.02	$4.83 \times 10^{-3} \pm 0.30 \times 10^{-3}$
iProp	5 %	0.38 ± 0.02	0.13 ± 0.01	$9.03 \times 10^{-3} \pm 0.71 \times 10^{-3}$
	10 %	0.11 ± 0.00	0.06 ± 0.01	$4.75 \times 10^{-3} \pm 0.19 \times 10^{-3}$
	15 %	-	0.03 ± 0.00	$1.93 \times 10^{-3} \pm 0.18 \times 10^{-3}$
	20 %	-	0.02 ± 0.00	$1.26 \times 10^{-3} \pm 0.06 \times 10^{-3}$
	25 %	-	-	$0.90 \times 10^{-3} \pm 0.47 \times 10^{-3}$
ACN	5 %	1.06 ± 0.05	0.27 ± 0.01	$15.92 \times 10^{-3} \pm 0.31 \times 10^{-3}$
	10 %	0.26 ± 0.02	0.13 ± 0.01	$9.80 \times 10^{-3} \pm 0.66 \times 10^{-3}$
	15 %	-	0.03 ± 0.01	$4.76 \times 10^{-3} \pm 0.38 \times 10^{-3}$
	20 %	-	0.04 ± 0.03	$3.22 \times 10^{-3} \pm 0.34 \times 10^{-3}$
	25 %	-	-	$1.97 \times 10^{-3} \pm 0.17 \times 10^{-3}$
DMSO	5 %	1.83 ± 0.06	0.38 ± 0.02	$25.06 \times 10^{-3} \pm 1.64 \times 10^{-3}$
	10 %	1.34 ± 0.08	0.26 ± 0.01	$14.60 \times 10^{-3} \pm 2.25 \times 10^{-3}$
	15 %	0.74 ± 0.03	0.18 ± 0.00	$6.92 \times 10^{-3} \pm 0.41 \times 10^{-3}$
	20 %	0.46 ± 0.03	0.12 ± 0.00	$4.02 \times 10^{-3} \pm 0.22 \times 10^{-3}$
	25 %	0.30 ± 0.09	0.06 ± 0.00	$2.08 \times 10^{-3} \pm 0.18 \times 10^{-3}$
glycerol	5 %	2.72 ± 0.12	0.56 ± 0.01	$41.51 \times 10^{-3} \pm 0.79 \times 10^{-3}$
	10 %	2.36 ± 0.26	0.49 ± 0.02	$38.06 \times 10^{-3} \pm 1.57 \times 10^{-3}$
	15 %	1.61 ± 0.10	0.66 ± 0.05	$30.40 \times 10^{-3} \pm 0.64 \times 10^{-3}$
	20 %	1.55 ± 0.15	0.58 ± 0.03	$28.55 \times 10^{-3} \pm 0.62 \times 10^{-3}$
	25 %	0.73 ± 0.03	0.43 ± 0.03	$25.01 \times 10^{-3} \pm 1.08 \times 10^{-3}$
acetone	5 %	0.65 ± 0.05	0.23 ± 0.06	$15.88 \times 10^{-3} \pm 0.87 \times 10^{-3}$
	10 %	0.30 ± 0.03	0.13 ± 0.05	$9.21 \times 10^{-3} \pm 0.94 \times 10^{-3}$
	15 %	0.12 ± 0.02	0.05 ± 0.01	$4.58 \times 10^{-3} \pm 0.54 \times 10^{-3}$
	20 %	0.06 ± 0.02	0.03 ± 0.00	$2.85 \times 10^{-3} \pm 0.18 \times 10^{-3}$
	25 %	-	0.01 ± 0.01	$1.78 \times 10^{-3} \pm 0.42 \times 10^{-3}$
<i>t</i> -BuOH	5 %	0.42 ± 0.19	0.12 ± 0.00	$10.99 \times 10^{-3} \pm 0.29 \times 10^{-3}$
	10 %	0.05 ± 0.04	0.04 ± 0.02	$2.92 \times 10^{-3} \pm 0.35 \times 10^{-3}$
	15 %	-	-	$1.03 \times 10^{-3} \pm 0.04 \times 10^{-3}$
	20 %	-	-	$0.52 \times 10^{-3} \pm 0.18 \times 10^{-3}$
	25 %	-	-	$0.90 \times 10^{-3} \pm 0.00 \times 10^{-3}$

7.3.3 HPLC-SEC runs for determination of the IRED purity

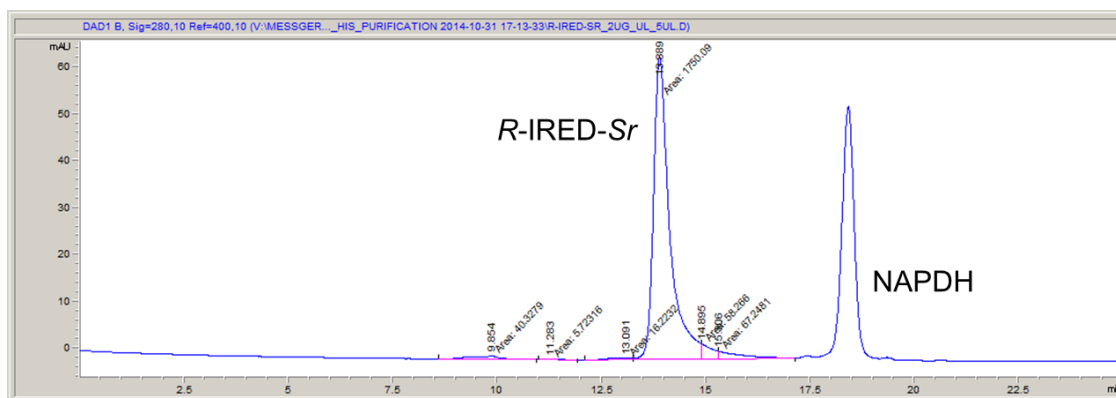


Figure S26: HPLC-SEC analysis of *R-IRED-Sr* wild type. 5 μ l of the protein diluted to a concentration of 2 μ g/ μ l was injected. The purity of the IRED was calculated to be about 90.3%. The peak at 13.89 min indicates that *R-IRED-Sr* forms a dimer in solution, the peak at 18.4 min corresponds to the NADPH added for storage (see also Figure S33).

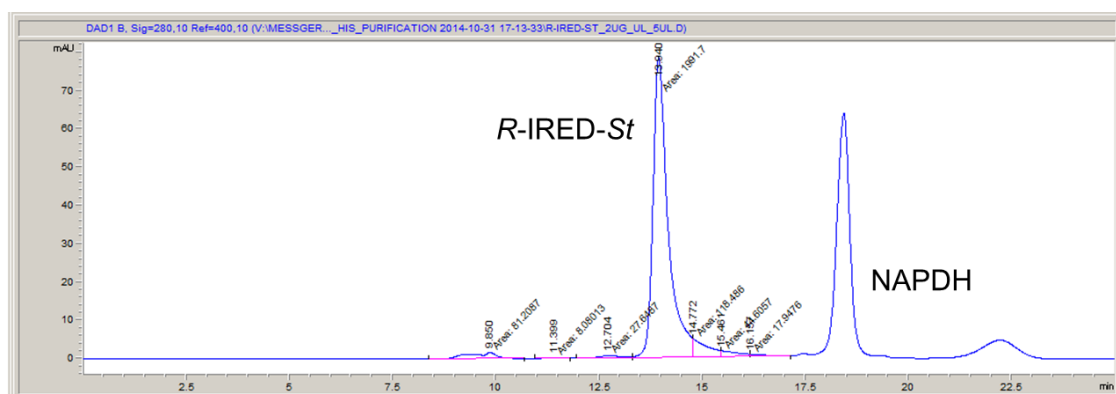


Figure S27: HPLC-SEC analysis of *R-IRED-St* wild type. 5 μ l of the protein diluted to a concentration of 2 μ g/ μ l was injected. The purity of the IRED was calculated to be about 87.0%. The peak at 13.94 min indicates that *R-IRED-St* forms a dimer in solution, the peak at 18.4 min corresponds to the NADPH added for storage (see also Figure S33).

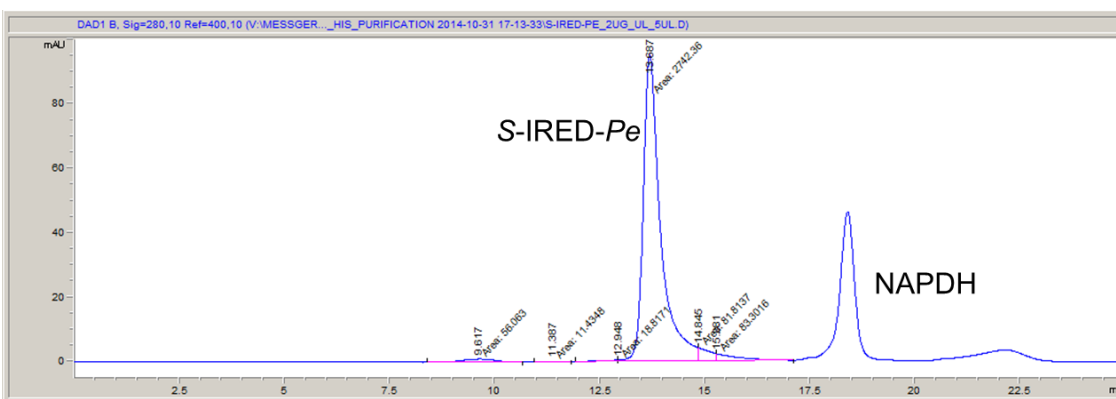


Figure S28: HPLC-SEC analysis of *S-IRED-Pe* wild type. 5 μ l of the protein diluted to a concentration of 2 μ g/ μ l was injected. The purity of the IRED was calculated to be about 91.6%. The peak at 13.69 min indicates that *S-IRED-Pe* forms a dimer in solution, the peak at 18.4 min corresponds to the NADPH added for storage (see also Figure S33).

7 SUPPORTING INFORMATION

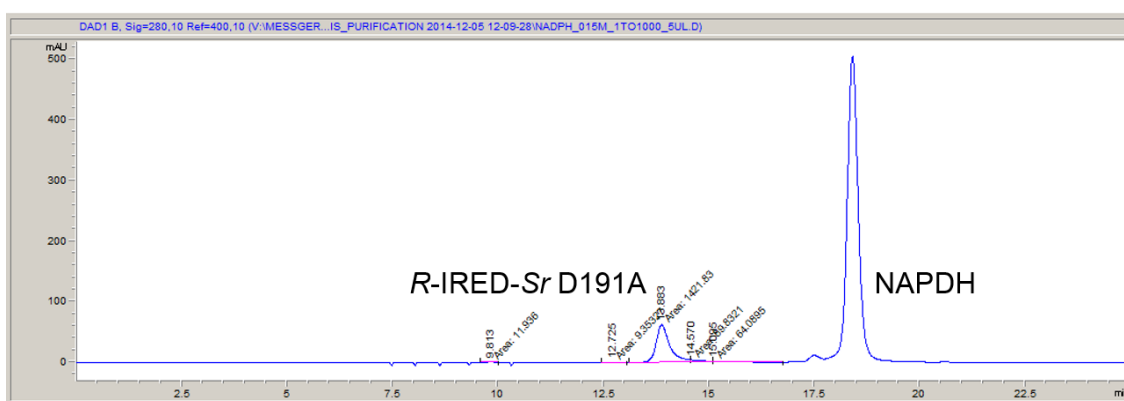


Figure S29: HPLC-SEC analysis of *R-IRED-Sr D191A*. 5 μ l of the protein diluted to a concentration of 2 μ g/ μ l was injected. The purity of the IRED was calculated to be about 89.0%. The peak at 13.88 min indicates that *R-IRED-Sr D191A* forms a dimer in solution, the peak at 18.4 min corresponds to the NADPH added for storage (see also Figure S33).

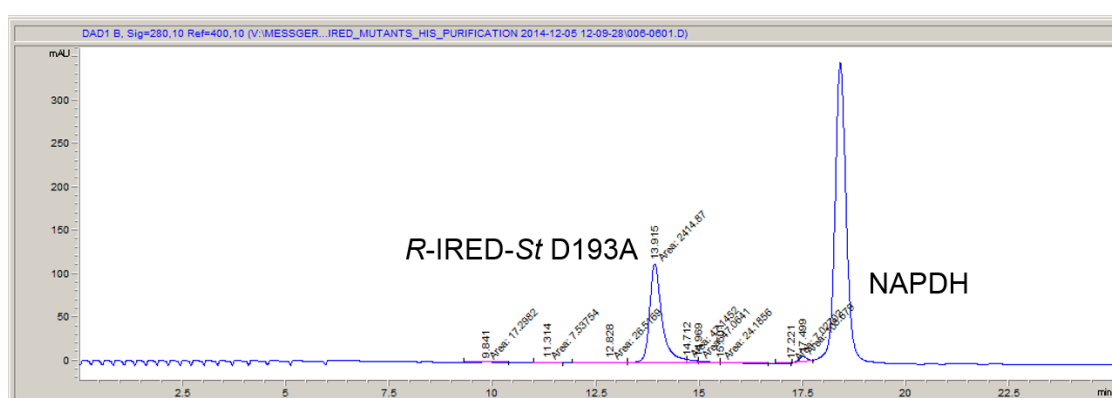


Figure S30 HPLC-SEC analysis of *R-IRED-St D193A* wild type. 5 μ l of the protein diluted to a concentration of 2 μ g/ μ l was injected. The purity of the IRED was calculated to be about 89.4%. The peak at 13.91 min indicates that *R-IRED-St D193A* forms a dimer in solution, the peak at 18.4 min corresponds to the NADPH added for storage (see also Figure S33).

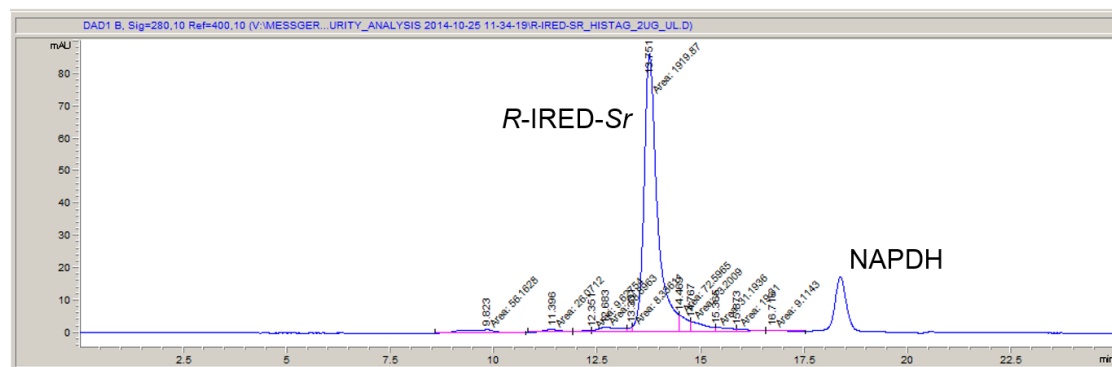


Figure S31: HPLC-SEC analysis of *R-IRED-Sr* wild type. 5 μ l of the protein diluted to a concentration of 2 μ g/ μ l was injected. The purity of the IRED was calculated to be about 84.0%. The peak at 13.75 min indicates that *R-IRED-Sr* forms a dimer in solution, the peak at 18.4 min corresponds to the NADPH added for storage (see also Figure S33). Optimization of the Ni^{2+} -NTA purification procedure yielded *R-IRED-Sr* with a purity of close to 90 % (Figure S26).

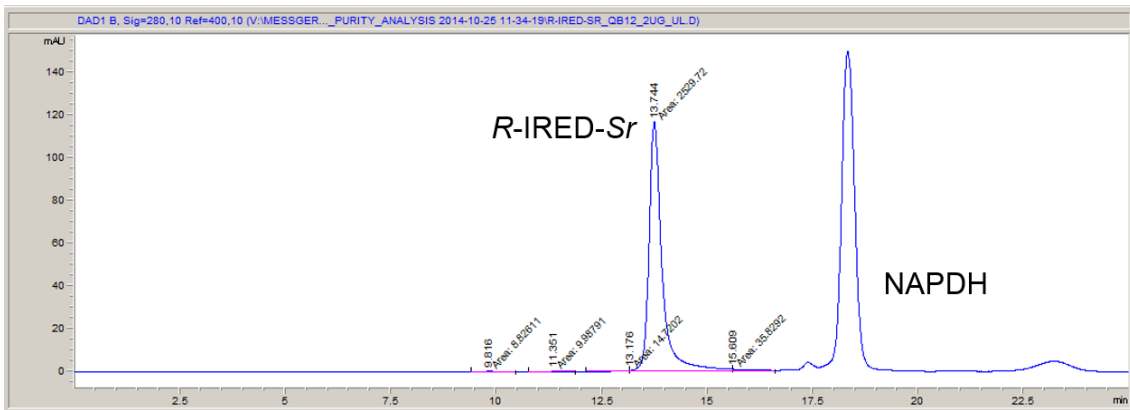


Figure S32: HPLC-SEC analysis of fraction B12 of the MonoQ purified *R*-IRED-Sr wild type. 5 μ l of the protein diluted to a concentration of 2 μ g/ μ l was injected. The purity of the IRED was calculated to be about 97.3%. The peak at 13.74 min indicates that *R*-IRED-Sr forms a dimer in solution, the peak at 18.4 min corresponds to the NADPH added for storage (see also Figure S33). Note the increase in purity from the *R*-IRED-Sr preparation in Figure S31 which was used for the ion-exchange chromatography.

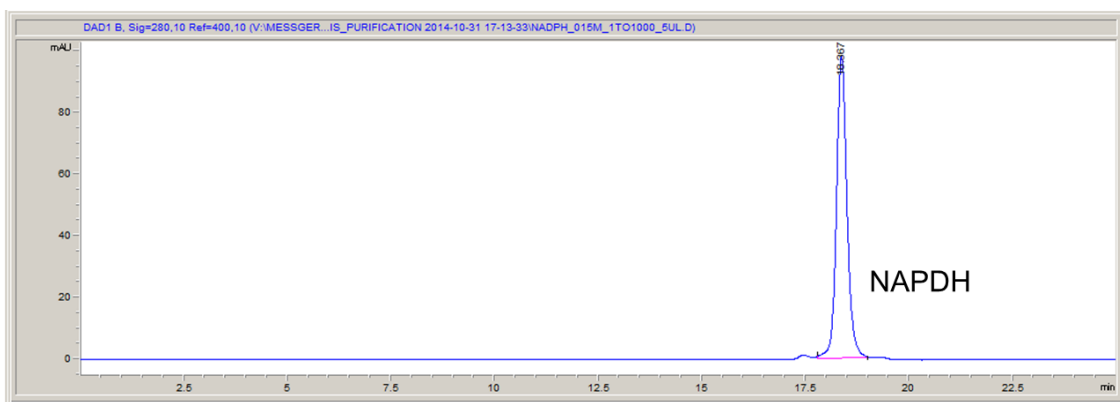


Figure S33: Injection of 5 μ l NADPH solution (150 μ M).

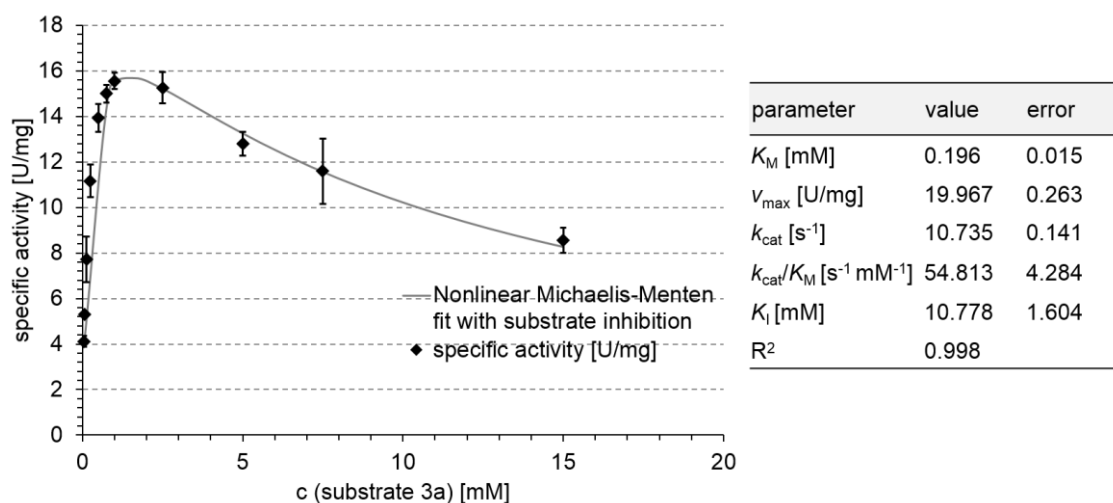
7.4 Michaelis-Menten plots of IREDs with cyclic imine substrates **3a** to **3c** and **5a** to **5b**

Figure S34: Determination of kinetic constants for *R*-IRED-*Sr* with substrate **3a**. Due to lower activities at higher substrate concentrations, the Michaelis-Menten equation was adapted to substrate inhibition: $v = (v_{max} \times [S]) / (K_M + [S] \times (1 + ([S]/K_I)))$. All activities were determined in triplicates and the error bars show the standard deviation.

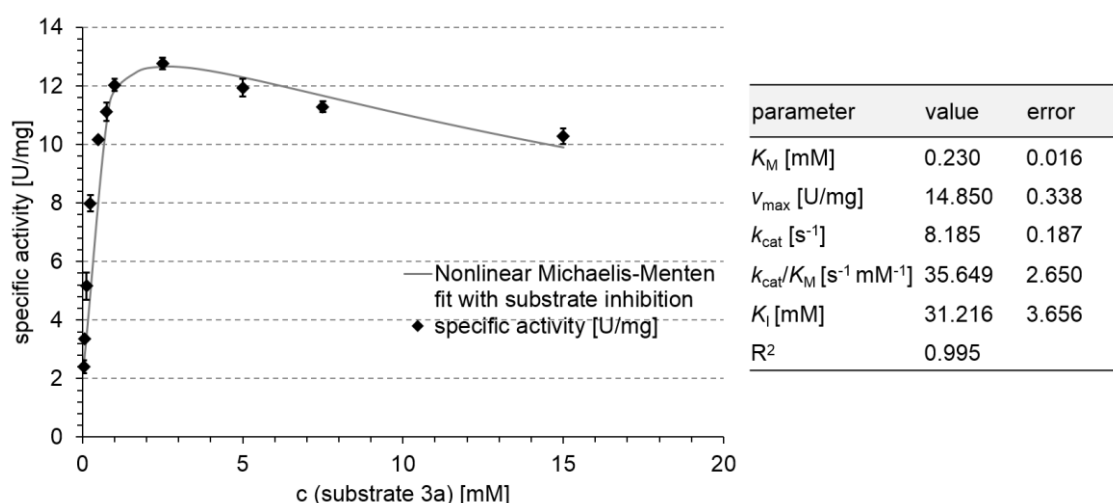


Figure S35: Determination of kinetic constants for *R*-IRED-*St* with substrate **3a**. Due to lower activities at higher substrate concentrations, the Michaelis-Menten equation was adapted to substrate inhibition: $v = (v_{max} \times [S]) / (K_M + [S] \times (1 + ([S]/K_I)))$. All activities were determined in triplicates and the error bars show the standard deviation.

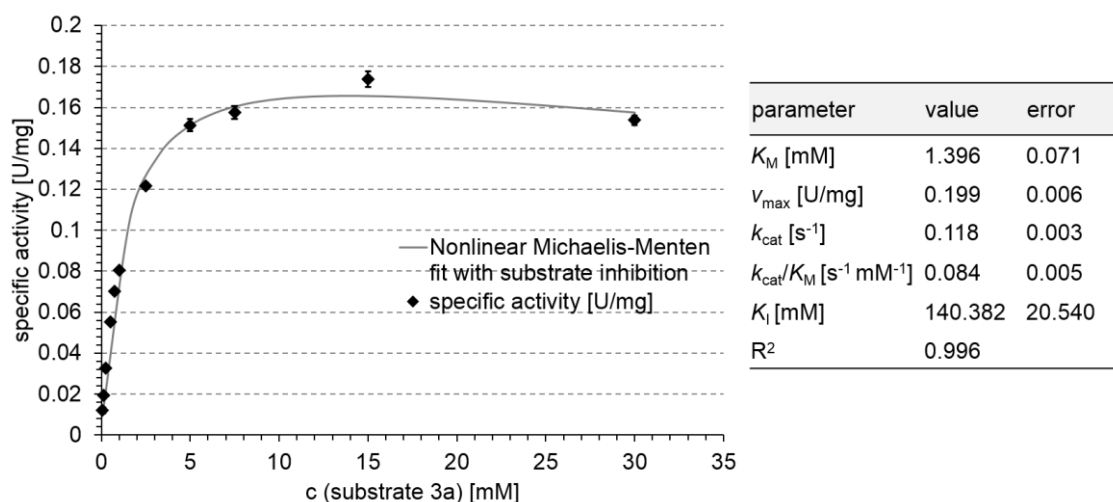


Figure S36: Determination of kinetic constants for *S*-IRED-*Pe* with substrate **3a**. Due to lower activities at higher substrate concentrations, the Michaelis-Menten equation was adapted to substrate inhibition: $v = (v_{max} \times [S]) / (K_M + [S] \times (1 + ([S]/K_I)))$. All activities were determined in triplicates and the error bars show the standard deviation.

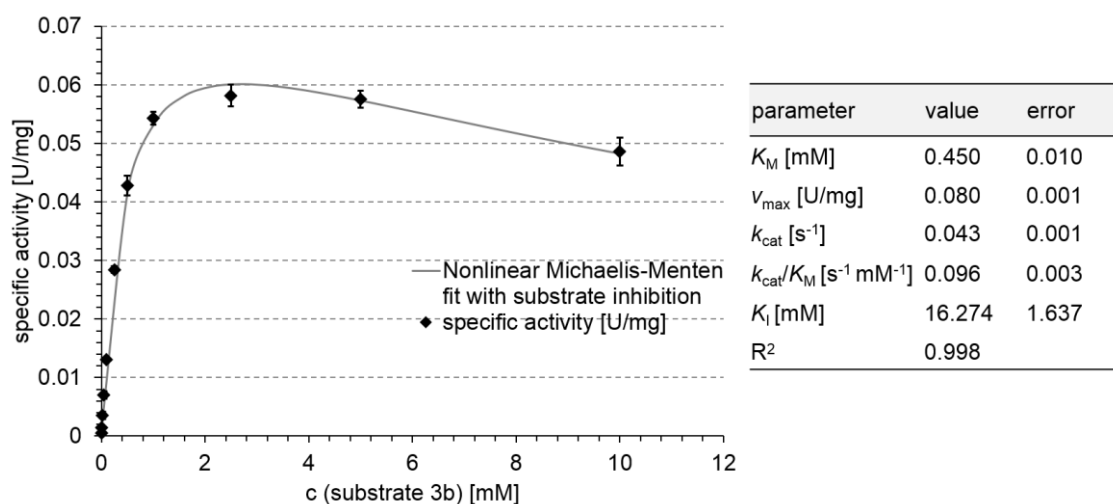


Figure S37: Determination of kinetic constants for *R*-IRED-*Sr* with substrate **3b**. Due to lower activities at higher substrate concentrations, the Michaelis-Menten equation was adapted to substrate inhibition: $v = (v_{max} \times [S]) / (K_M + [S] \times (1 + ([S]/K_I)))$. All activities were determined in triplicates and the error bars show the standard deviation.

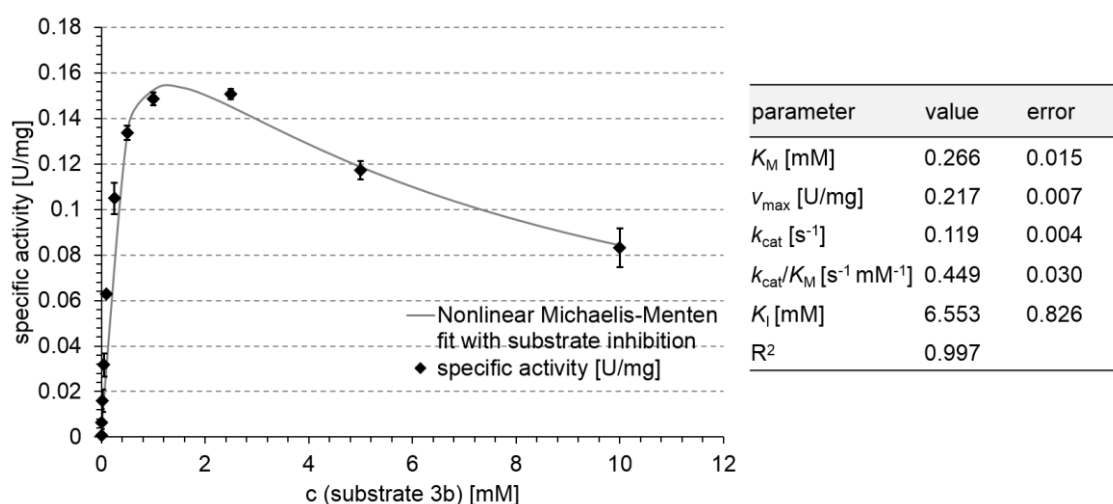


Figure S38: Determination of kinetic constants for *R*-IRED-*St* with substrate **3b**. Due to lower activities at higher substrate concentrations, the Michaelis-Menten equation was adapted to substrate inhibition: $v = (v_{max} \times [S]) / (K_M + [S] \times (1 + ([S]/K_I)))$. All activities were determined in triplicates and the error bars show the standard deviation.

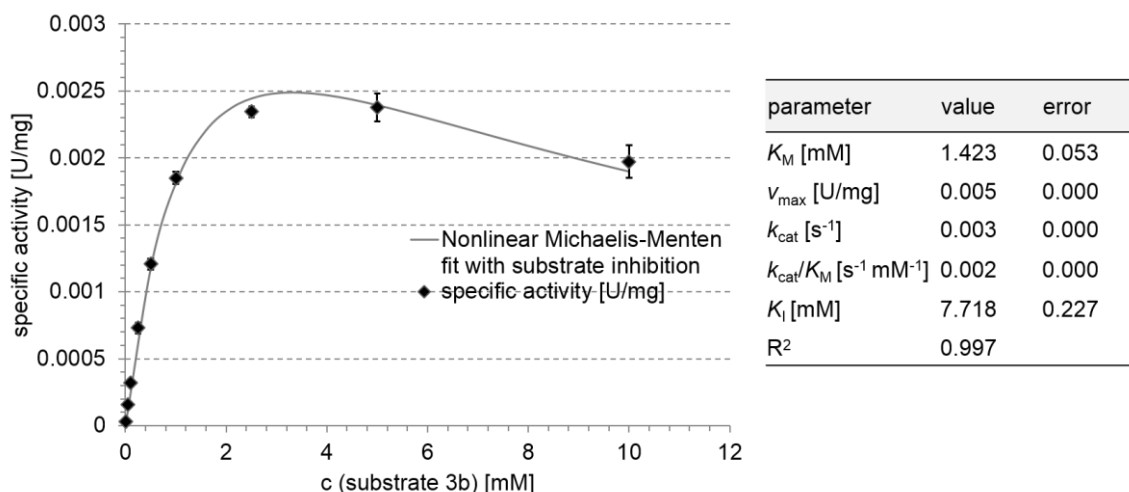


Figure S39: Determination of kinetic constants for *S*-IRED-*Pe* with substrate **3b**. Due to lower activities at higher substrate concentrations, the Michaelis-Menten equation was adapted to substrate inhibition: $v = (v_{max} \times [S]) / (K_M + [S] \times (1 + ([S]/K_I)))$. All activities were determined in triplicates and the error bars show the standard deviation.

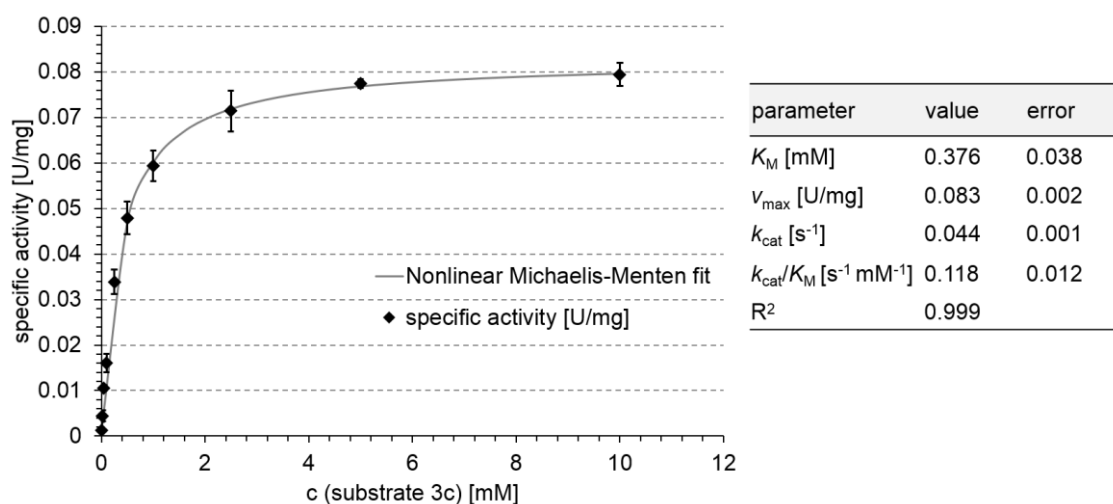


Figure S40: Determination of kinetic constants for *R*-IRED-*Sr* with substrate **3c**. All activities were determined in triplicates and the error bars show the standard deviation.

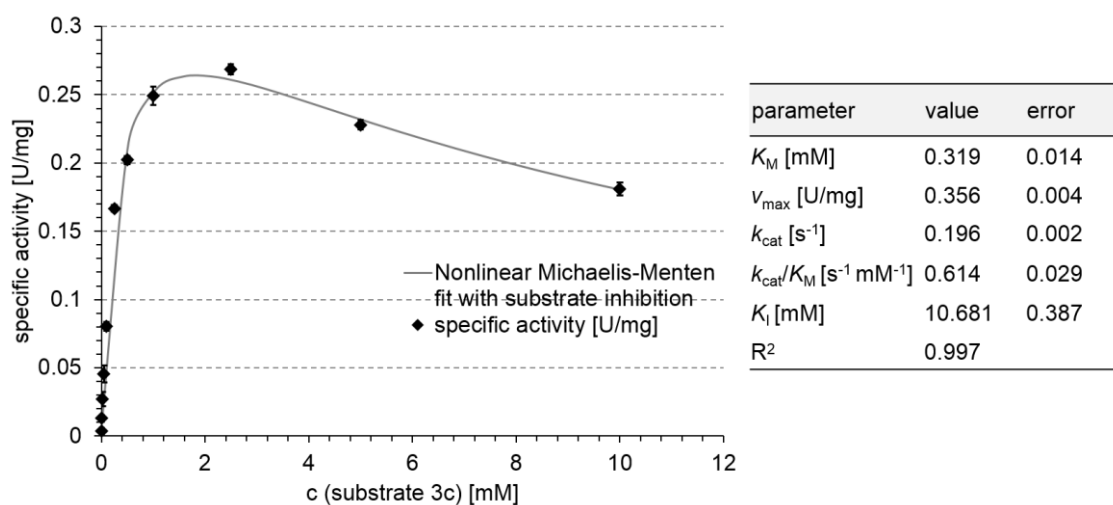


Figure S41: Determination of kinetic constants for *R*-IRED-*St* with substrate **3c**. Due to lower activities at higher substrate concentrations, the Michaelis-Menten equation was adapted to substrate inhibition: $v = (v_{max} \times [S]) / (K_M + [S] \times (1 + ([S]/K_I)))$. All activities were determined in triplicates and the error bars show the standard deviation.

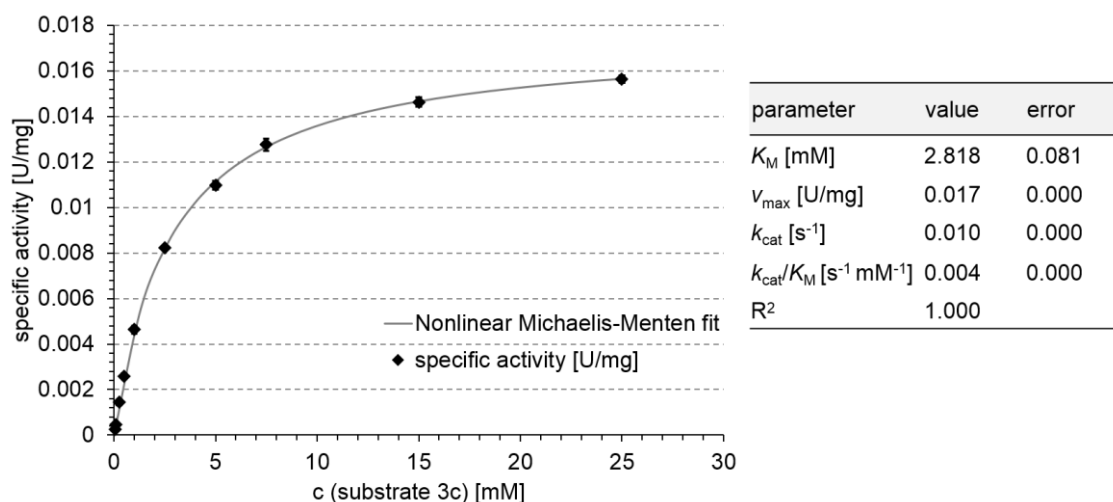


Figure S42: Determination of kinetic constants for S-IRED-Pe with substrate **3c**. All activities were determined in triplicates and the error bars show the standard deviation.

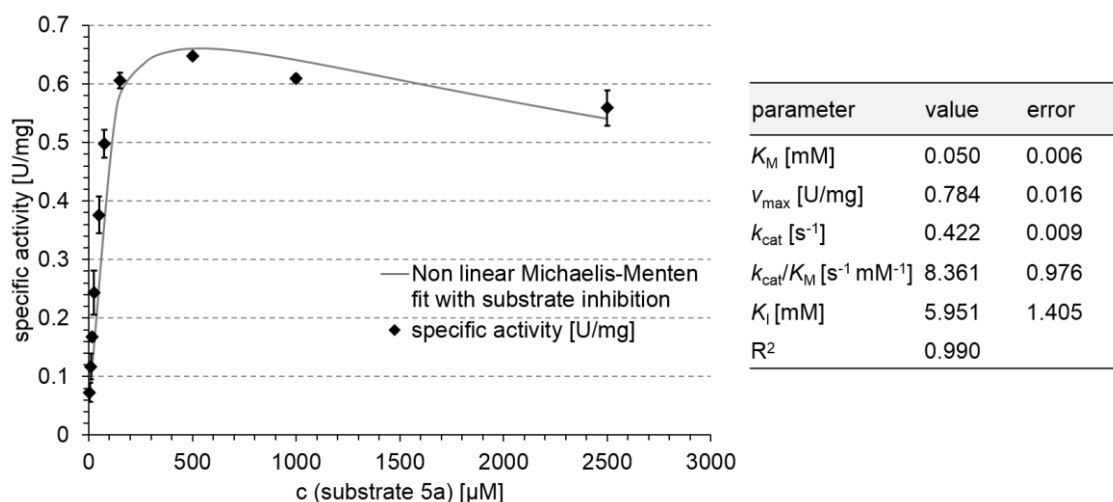


Figure S43: Determination of kinetic constants for R-IRED-Sr with substrate **5a**. Due to lower activities at higher substrate concentrations, the Michaelis-Menten equation was adapted to substrate inhibition: $v = (v_{max} \times [S]) / (K_M + [S] \times (1 + ([S]/K_I)))$. All activities were determined in triplicates and the error bars show the standard deviation.

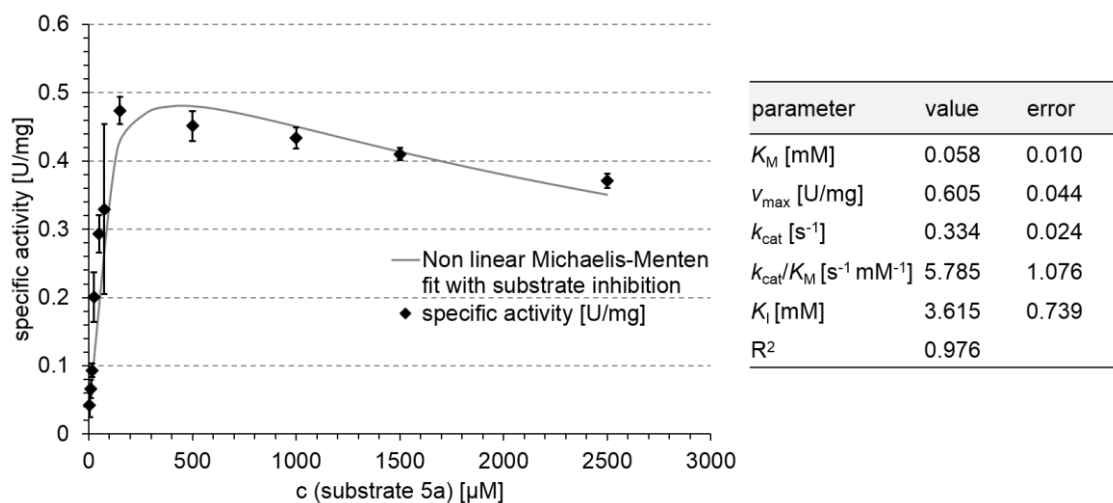


Figure S44: Determination of kinetic constants for R-IRED-St with substrate **5a**. Due to lower activities at higher substrate concentrations, the Michaelis-Menten equation was adapted to substrate inhibition: $v = (v_{max} \times [S]) / (K_M + [S] \times (1 + ([S]/K_I)))$. All activities were determined in triplicates and the error bars show the standard deviation.

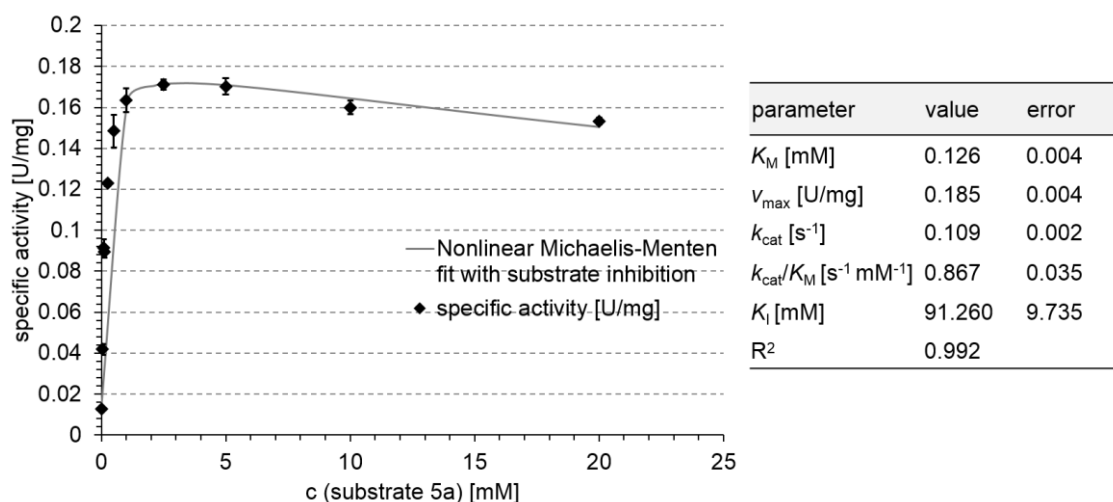


Figure S45: Determination of kinetic constants for *S*-IRED-*Pe* with substrate **5a**. Due to lower activities at higher substrate concentrations, the Michaelis-Menten equation was adapted to substrate inhibition: $v = (v_{max} \times [S]) / (K_M + [S] \times (1 + ([S]/K_I)))$. All activities were determined in triplicates and the error bars show the standard deviation.

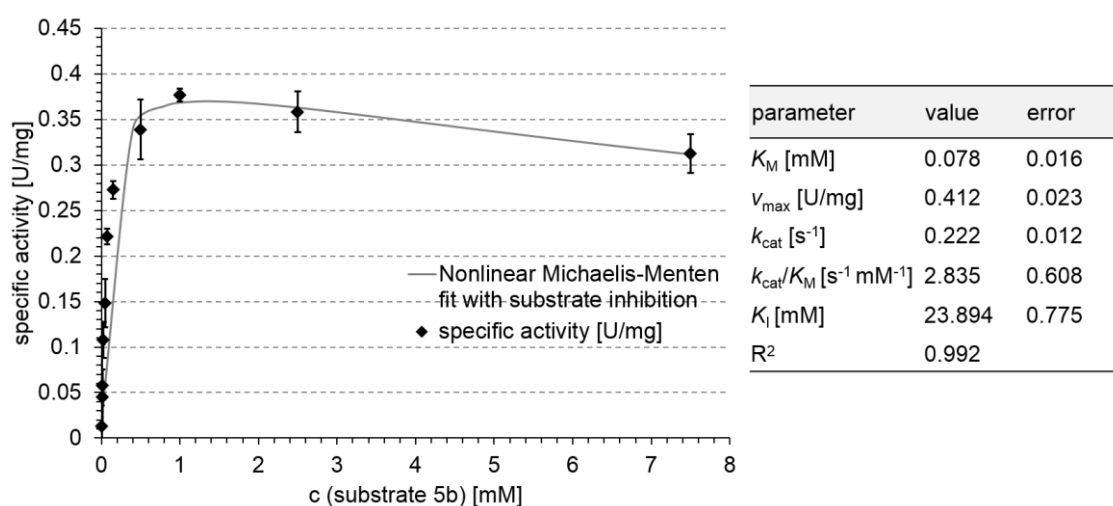


Figure S46: Determination of kinetic constants for *R*-IRED-*Sr* with substrate **5b**. Due to lower activities at higher substrate concentrations, the Michaelis-Menten equation was adapted to substrate inhibition: $v = (v_{max} \times [S]) / (K_M + [S] \times (1 + ([S]/K_I)))$. All activities were determined in triplicates and the error bars show the standard deviation.

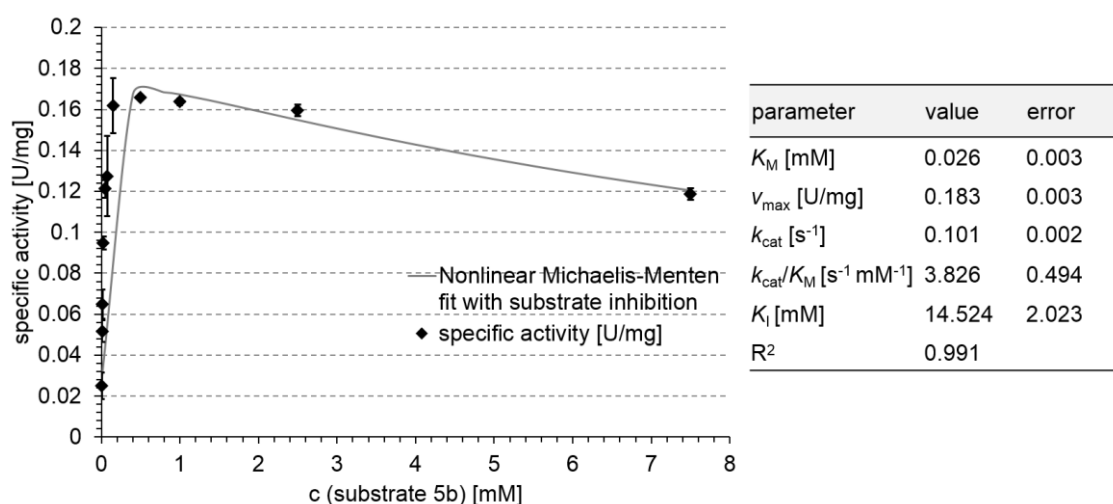


Figure S47: Determination of kinetic constants for *R*-IRED-*St* with substrate **5b**. Due to lower activities at higher substrate concentrations, the Michaelis-Menten equation was adapted to substrate inhibition: $v = (v_{max} \times [S]) / (K_M + [S] \times (1 + ([S]/K_I)))$. All activities were determined in triplicates and the error bars show the standard deviation.

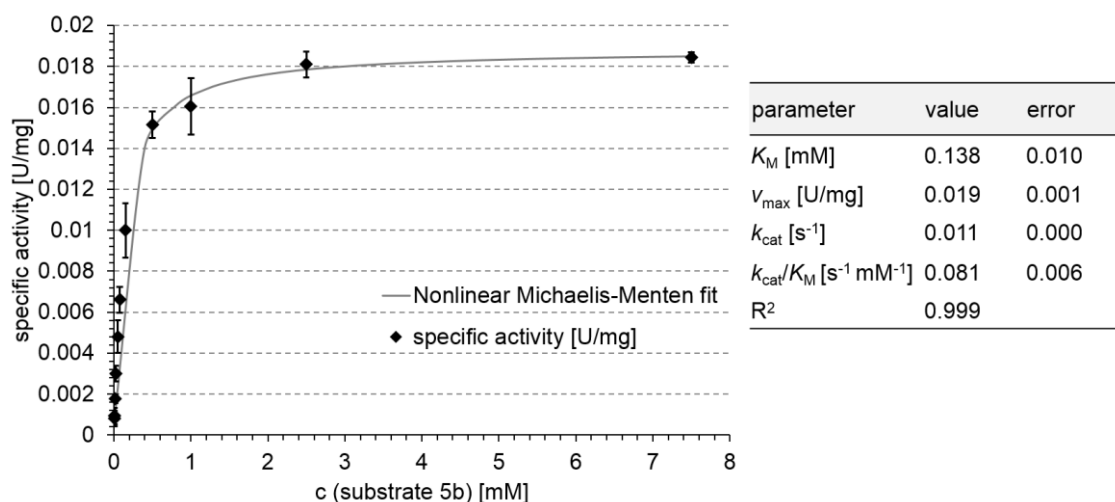
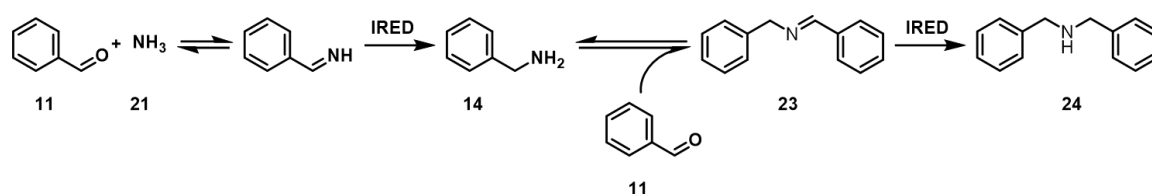


Figure S48: Determination of kinetic constants for S-IRED-Pe with substrate **5b**. All activities were determined in triplicates and the error bars show the standard deviation.

7.5 The reductive amination of aldehydes and ketones



Scheme S1: reaction scheme for the formation of the dialkylation product **24** by the repeated reductive amination of **11**.

Table S10: Product formations in [%] for the reductive amination of benzaldehyde **11** with increasing equivalents of ammonia **21** as nucleophile. All reactions were done with purified proteins of the same purification batch in triplicates at a pH of 8.0. Negative controls were performed with heat inactivated enzyme and did not show any product formation. The errors were calculated from the standard deviation. Formation of the imine intermediate might be overestimated as for the extraction the pH was raised. -: not detected.

eq 21												
	1	10	50	1	10	50	1	10	50	1	10	50
1 h	-	-	< 0.5	0.70 ± 0.03	6.36 ± 0.11	13.09 ± 0.42	-	-	-	-	-	-
3 h	-	5.04 ± 0.40	15.29 ± 0.68	3.81 ± 0.02	16.38 ± 0.25	22.53 ± 0.25	-	-	-	< 0.5	-	-
5 h	0.54 ± 0.13	12.04 ± 0.44	32.79 ± 0.91	5.07 ± 0.18	20.97 ± 0.95	19.58 ± 0.48	-	-	-	1.58 ± 0.04	0.67	< 0.5
8 h	1.25 ± 0.13	21.43 ± 0.28	48.03 ± 0.76	6.11 ± 0.09	16.02 ± 0.30	4.69 ± 0.26	< 0.5	< 0.5	-	2.55 ± 0.04	1.54 ± 0.05	0.77 ± 0.02
24 h	6.60 ± 0.25	51.22 ± 2.13	60.66 ± 1.12	6.30 ± 0.16	2.35 ± 0.11	-	2.18 ± 0.06	3.15 ± 0.03	< 0.5	6.94 ± 0.26	4.78 ± 0.18	1.40 ± 0.02

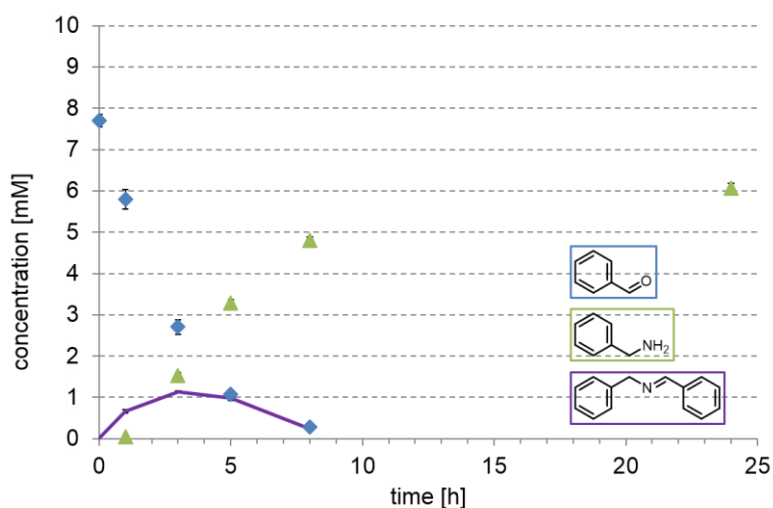


Figure S49: Time course for the reductive amination of **11** (blue) with 50-fold molar excess of amine nucleophile **21** by *R*-IRED-Sr. The biotransformation was performed in triplicates with purified protein. The initial formed product **14** (green) acts as an additional nucleophile leading to the formation of imine intermediate **23** (purple). **23** can be further reduced to the dialkylation product **24**. Figure S49 illustrates the appearance and the disappearance of the intermediate **23**. For a better overview the dialkylation product **24** and the formation of byproduct **13** (benzylalcohol) are not shown here.

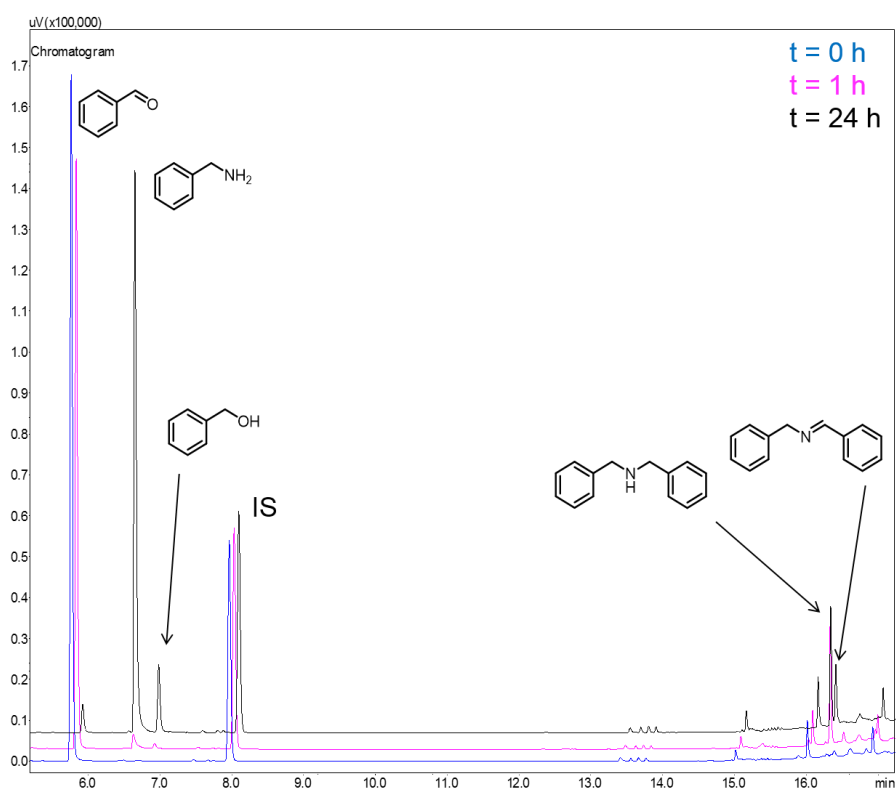
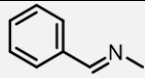
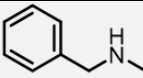
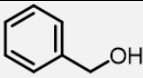


Figure S50: Overlay of chromatograms of the reductive amination of benzaldehyde **11** with ammonia **21** at 10-fold excess after 0 h (blue), 1 h (pink) and 24 h (black). IS = internal standard.

Table S11: Product formations in [%] for the reductive amination of benzaldehyde **11** with different increasing equivalents of methylamine **22** as nucleophile. All reactions were done with purified proteins of the same purification batch in triplicates at a pH of 8.0. Negative controls were performed with heat inactivated enzyme and did not show any product formation. The errors were calculated from the standard deviation. Formation of the imine intermediate might be overestimated as for the extraction the pH was raised. -: not detected.

eq 22									
	1	10	50	1	10	50	1	10	50
0 h	55.49 ± 2.10	82.50 ± 6.60	80.95 ± 1.73	-	-	-	-	-	-
1 h	41.60 ± 0.83	35.41 ± 0.74	10.87 ± 1.24	5.54 ± 0.22	32.82 ± 0.56	57.95 ± 3.28	-	-	-
3 h	29.38 ± 2.16	1.40 ± 0.08	-	19.40 ± 1.15	67.23 ± 2.21	75.51 ± 0.50	< 0.5	-	-
5 h	23.69 ± 2.88	-	-	30.67 ± 4.29	72.01 ± 2.69	70.89 ± 3.18	1.34 ± 0.17	-	-
8 h	16.04 ± 0.89	-	-	34.64 ± 1.29	71.56 ± 3.31	73.33 ± 3.80	2.33 ± 0.08	-	-
24 h	2.05 ± 0.13	-	-	51.18 ± 2.75	66.19 ± 0.48	68.98 ± 4.08	5.55 ± 0.27	-	-

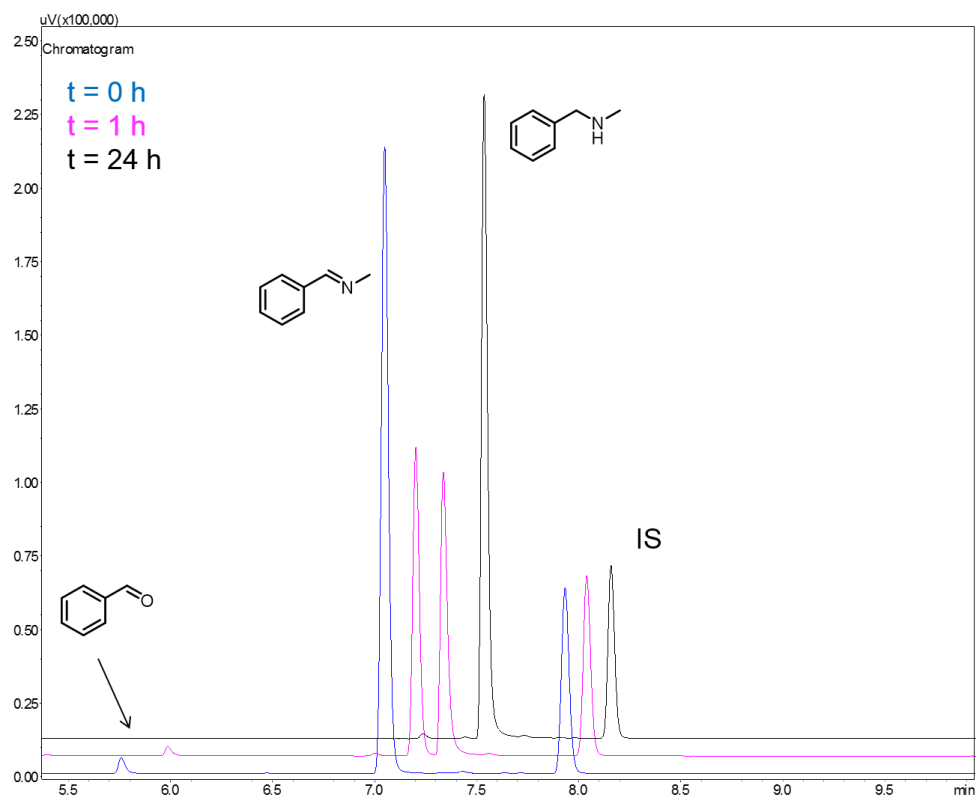


Figure S51: Overlay of chromatograms of the reductive amination of benzaldehyde **11** with methylamine **22** at 10-fold excess after 0 h (blue), 1 h (pink) and 24 h (black). IS = internal standard.

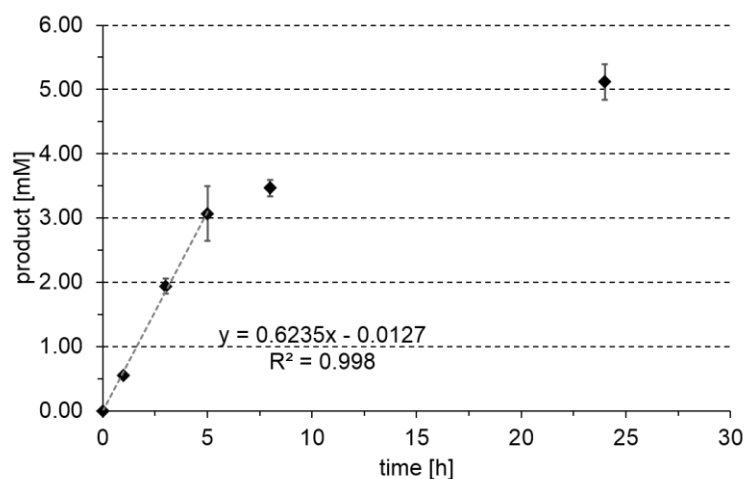


Figure S52: Time course for the formation of the amination product in the reductive amination reaction of 10 mM benzaldehyde **11** with one equivalent of methylamine **22** as nucleophile at pH 8.0, catalyzed by *R*-IREd-Sr. All biotransformations were done with purified proteins of the same purification batch in triplicates. The errors were calculated from the standard deviation. Out of this data the turnover number is calculated to be $2.23 \times 10^{-3} \text{ s}^{-1}$.

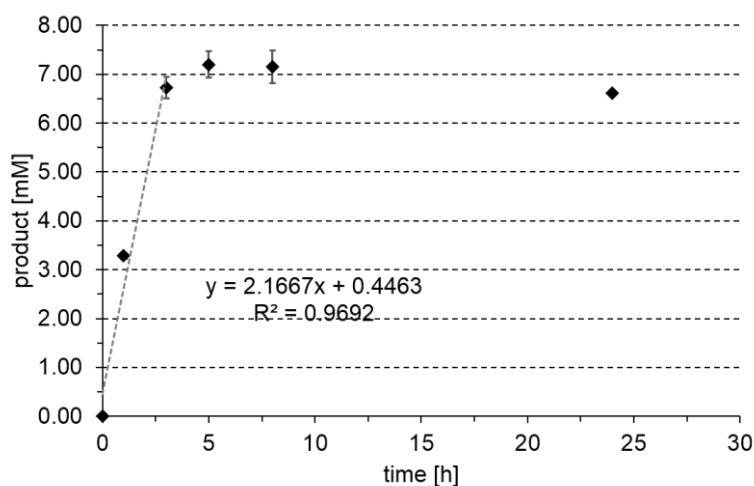
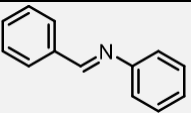
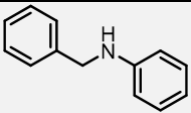
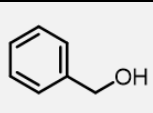


Figure S53: Time course for the formation of the amination product in the reductive amination reaction of 10 mM benzaldehyde **11** with ten equivalents of methylamine **22** as nucleophile at pH 8.0, catalyzed by *R*-IREd-Sr. All biotransformations were done with purified proteins of the same purification batch in triplicates. The errors were calculated from the standard deviation. Out of this data the turnover number is calculated to be $7.77 \times 10^{-3} \text{ s}^{-1}$.

Table S12: Product formations in [%] for the reductive amination of 10 mM benzaldehyde **11** with aniline **12** as nucleophile. All reactions were done with purified proteins of the same purification batch in triplicates at a pH of 8.0. Negative controls were performed with heat inactivated enzyme and did not show any product formation. The errors were calculated from the standard deviation. Formation of the imine intermediate might be overestimated as for the extraction the pH was raised. -: not detected.

			
	product formation [%]		
eq 12	1	1	1
0 h	2.46 ± 0.20	-	-
1 h	3.02 ± 0.21	4.06 ± 0.16	-
3 h	2.91 ± 0.10	9.61 ± 0.33	-
5 h	2.80 ± 0.09	15.08 ± 0.63	1.22 ± 0.03
8 h	1.02 ± 0.09	13.44 ± 1.30	2.42 ± 0.6
24 h	-	24.97 ± 5.28	7.20 ± 0.45

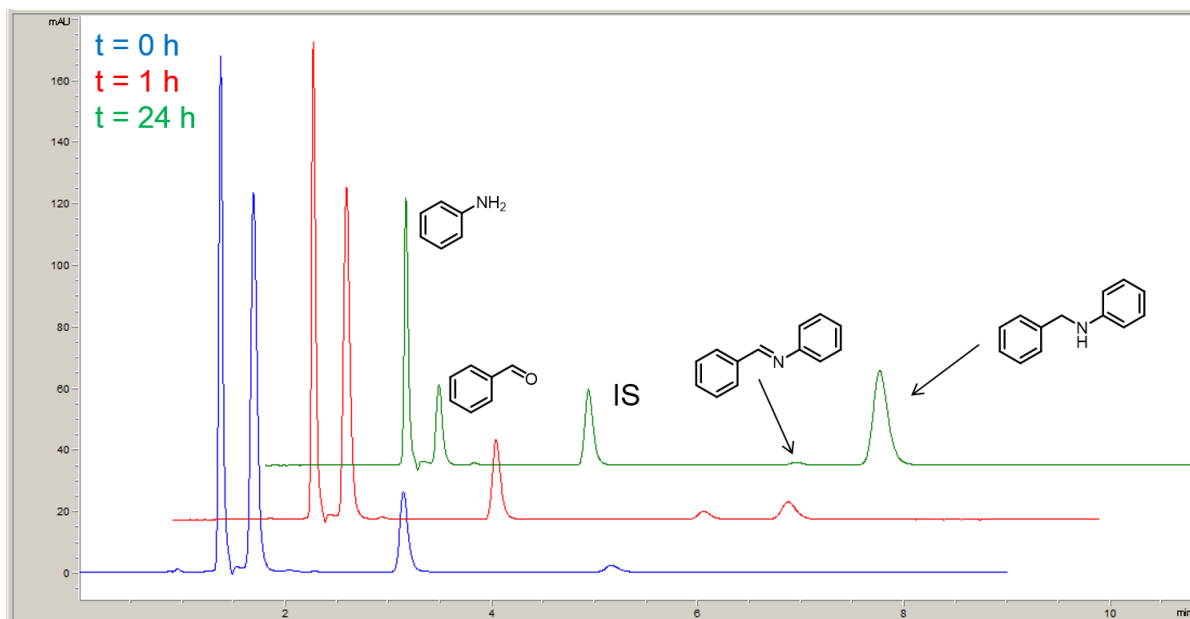
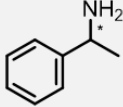


Figure S54: Overlay of chromatograms of the reductive amination of benzaldehyde **11** with aniline **12** at equimolar concentrations monitored at 240 nm after 0 h (blue), 1 h (red) and 24 h (green). Due to its poor absorbance at this wavelength and the low amounts formed, the byproduct benzylalcohol is not visible in Figure S54. IS = internal standard.

Table S13: Product formations and enantiomeric excess values in [%] for the reductive amination of 10 mM acetophenone **20** with ammonia **21** as nucleophile. All reactions were done with purified proteins of the same purification batch in triplicates at a pH of 8.0, 8.5 and 9.0. The amine nucleophile was used at 50-fold excess in all cases. Negative controls were performed with heat inactivated enzyme and did not show any product formation. The errors were calculated from the standard deviation. Byproduct formation (reduction of the carbonyl to the alcohol) was detectable only in traces for all conditions. -: not detected; n.d.: not determined; ^[a]: reactions performed with 10 mg/ml *R*-IRED-Sr.

pH								
	8.0		8.5		9.0		9.0 ^[a]	
	product [%]	ee [%]	product [%]	ee [%]	product [%]	ee [%]	product [%]	ee [%]
1 h	-	n.d.	-	n.d.	-	n.d.	< 0.5	n.d.
3 h	-	n.d.	-	n.d.	< 0.5	n.d.	0.87 ± 0.02	94.11 ± 4.70
5 h	< 0.5	n.d.	< 0.5	n.d.	0.77 ± 0.05	n.d.	2.28 ± 0.06	97.52 ± 0.34
8 h	0.81 ± 0.02	91.22 ± 8.57	1.16 ± 0.02	96.48 ± 0.37	2.42 ± 0.05	96.85 ± 0.21	4.48 ± 0.09	97.67 ± 0.25
24 h	5.45 ± 0.03	96.55 ± 0.22	7.09 ± 0.07	97.56 ± 0.39	10.12 ± 0.06	97.66 ± 0.16	15.82 ± 0.66	97.07 ± 0.07

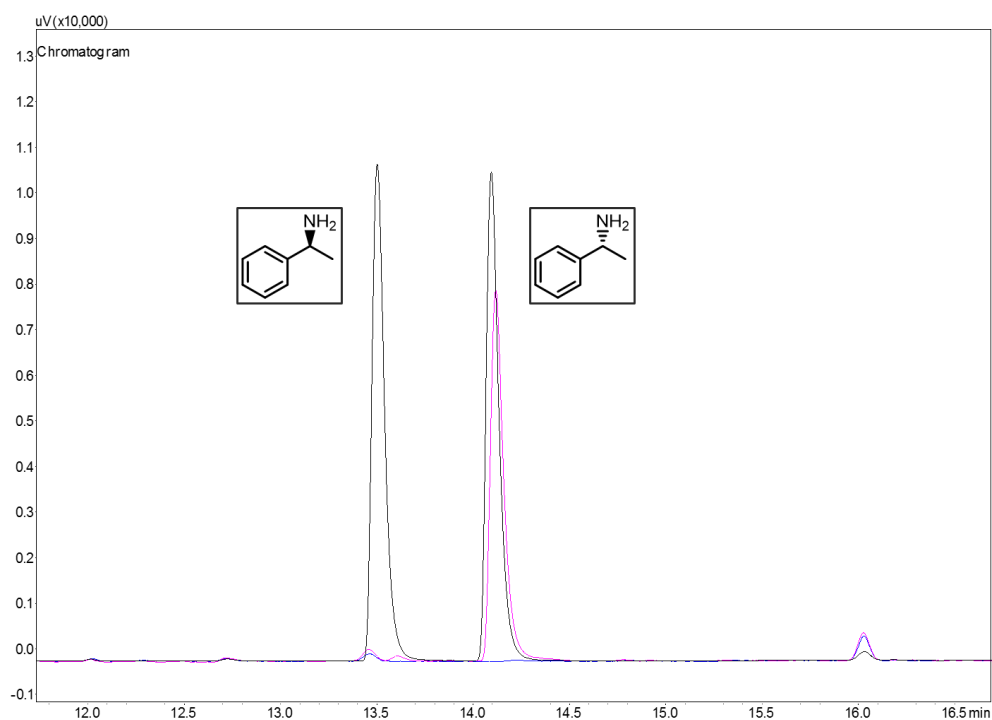


Figure S55: Overlay of chiral GC chromatograms for determination of the enantiomeric excess of 1-phenylethylamine **26** in biotransformations with *R*-IREd-Sr. Black: racemic **26** ((*S*)- enantiomer elutes first, assignment was done with commercially available reference material of (*R*)-**26** and (*S*)-**26**); pink: biotransformation with *R*-IREd-Sr, **20** as substrate and **21** as nucleophile; blue: negative control (biotransformation with heat inactivated enzyme). Biotransformations with *R*-IREd-Sr produced (*R*)-**26** with an enantiomeric excess of > 97%.

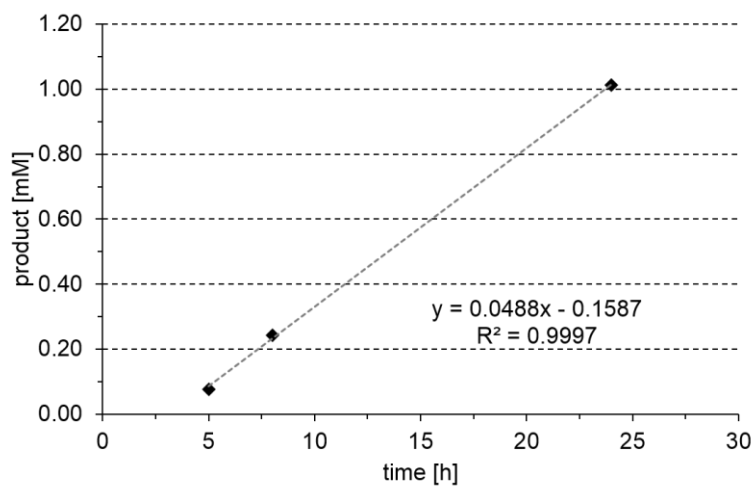


Figure S56: Time course for formation of the amination product in the reductive amination reaction of acetophenone **20** with 50 equivalents of ammonia **21** as nucleophile at pH 9.0 in the reactions catalyzed by 2.5 mg/ml *R*-IREd-Sr. All biotransformations were done with purified proteins of the same purification batch in triplicates. The errors were calculated from the standard deviation. Out of this data the turnover number is calculated to be $175 \times 10^{-6} \text{ s}^{-1}$.

Table S14: Product formations and enantiomeric excess values in [%] for the reductive amination of 10 mM acetophenone **20** with methylamine **22** as nucleophile. All reactions were done with purified proteins of the same purification batch in triplicates at a pH of 8.0, 8.5 and 9.0. The amine nucleophile was used at 50-fold excess in all cases. Negative controls were performed with heat inactivated enzyme and did not show any product formation. The errors were calculated from the standard deviation. Byproduct formation (reduction of the carbonyl to the alcohol), was detectable only in traces for all conditions. -: not detected; n.d.: not determined; ^[a]: reactions performed with 10 mg/ml *R*-IRED-Sr.

pH	8.0		8.5		9.0		9.0 ^[a]	
	product [%]	ee [%]	product [%]	ee [%]	product [%]	ee [%]	product [%]	ee [%]
1 h	-	n.d.	< 0.5	n.d.	< 0.5	n.d.	1.37 ± 0.02	n.d.
3 h	< 0.5	n.d.	1.03 ± 0.03	n.d.	1.70 ± 0.11	n.d.	6.90 ± 0.37	86.33 ± 1.64
5 h	1.13 ± 0.03	n.d.	2.53 ± 0.17	n.d.	3.38 ± 0.09	n.d.	8.86 ± 0.20	86.83 ± 0.23
8 h	2.75 ± 0.02	86.46 ± 2.49	4.68 ± 0.06	86.80 ± 0.62	6.49 ± 0.16	87.49 ± 0.48	13.83 ± 0.32	86.54 ± 0.29
24 h	8.57 ± 0.08	86.70 ± 0.37	15.19 ± 0.22	86.33 ± 0.33	18.95 ± 1.02	86.31 ± 0.12	39.18 ± 1.38	86.64 ± 0.04

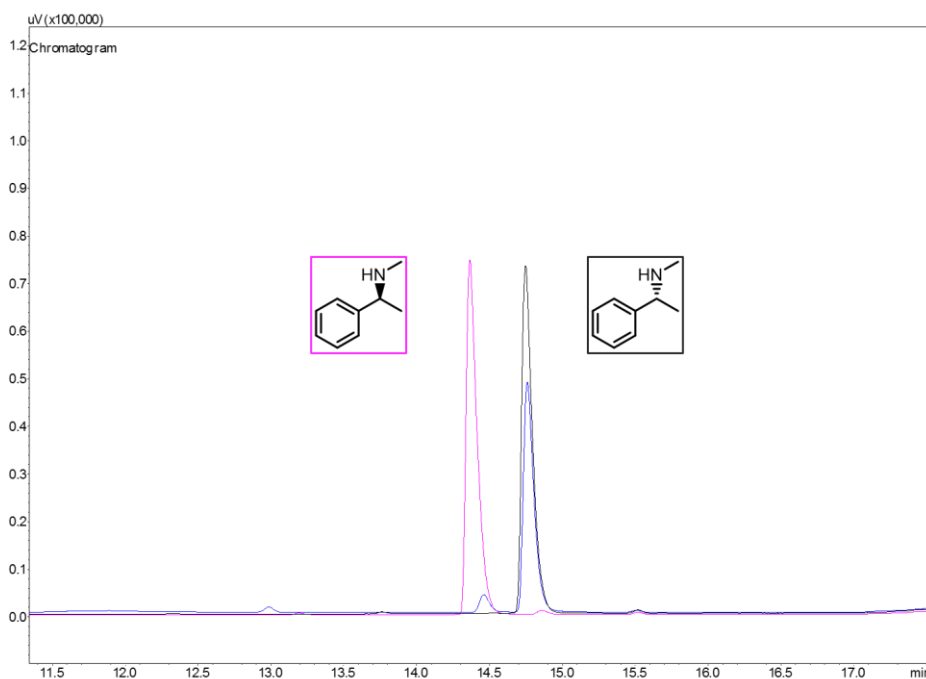


Figure S57: Overlay of chiral GC chromatograms for determination of the enantiomeric excess of *N*- α -dimethylbenzylamine **27** in biotransformations with *R*-IRED-Sr. Black: (*R*)-**27**; pink: (*S*)-**27**, blue biotransformation with *R*-IRED-Sr, **20** as substrate and **22** as nucleophile. Biotransformations with *R*-IRED-Sr produced (*R*)-**27** with an enantiomeric excess of > 86%.

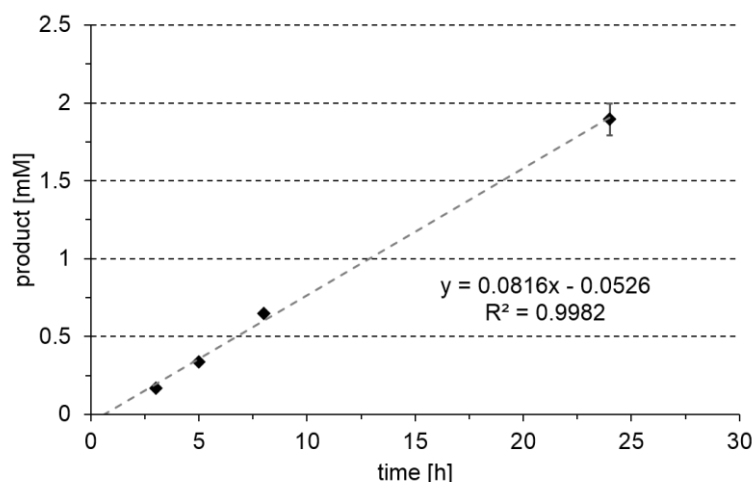


Figure S58: Time course for the formation of the amination product in the reductive amination reaction of acetophenone **20** with 50 equivalents of methylamine **22** as nucleophile at pH 9.0 in the reactions catalyzed by 2.5 mg/ml *R*-IREd-Sr. All biotransformations were done with purified proteins of the same purification batch in triplicates. The errors were calculated from the standard deviation. Out of this data the turnover number is calculated to be $292 \times 10^{-6} \text{ s}^{-1}$.

7.6 Michaelis-Menten plots of *R*-IREd-Sr for the kinetic characterization of the reductive amination of **11** with **22**

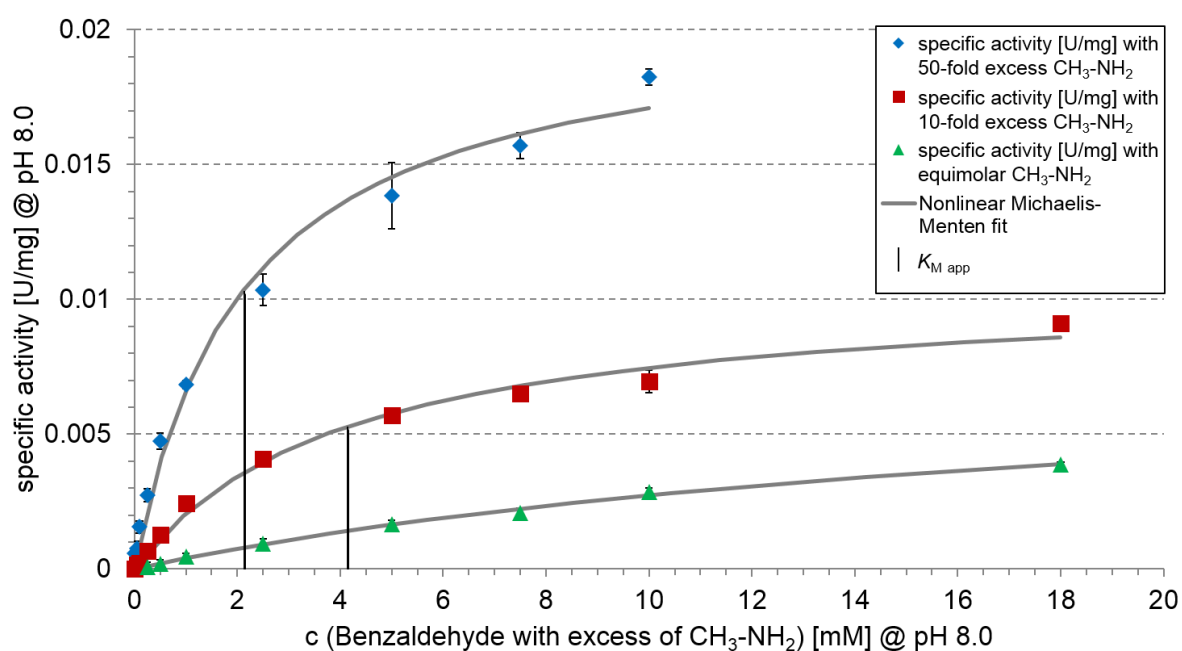


Figure S59: Overlay of the Michaelis-Menten plots for the reductive amination of **11** with different excess amounts of nucleophile **22** at pH 8.0 with *R*-IREd-Sr. Conditions that shift the equilibrium towards imine **7** go along with a decreased $K_{M,app}$ value, directly reflecting the relative amount of substrate the enzyme is exposed to. The apparent affinity at an equimolar concentration of **22** was above the tested conditions and calculated to be $20.47 \pm 5.67 \text{ mM}$ (Table 29).

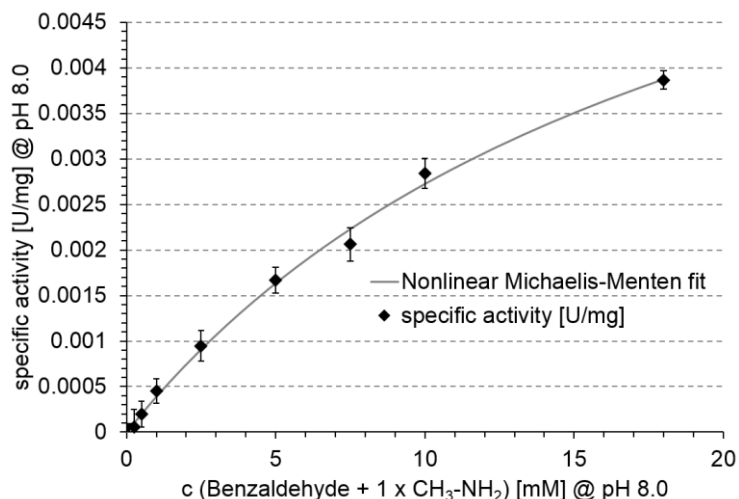


Figure S60: Michaelis-Menten plot for the reductive amination of **11** with equimolar concentration of nucleophile **22** with *R*-IREd-Sr at pH 8.0. All activities were determined in triplicates and the error bars show the standard deviation.

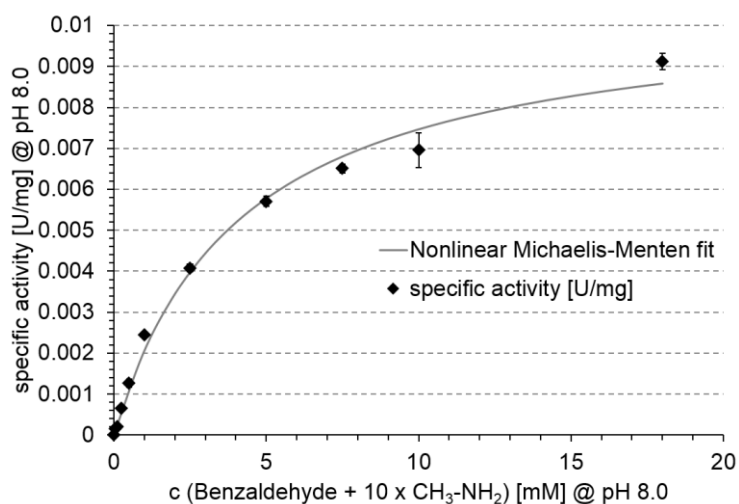


Figure S61: Michaelis-Menten plot for the reductive amination of **11** with 10-fold molar excess of nucleophile **22** with *R*-IREd-Sr at pH 8.0. All activities were determined in triplicates and the error bars show the standard deviation.

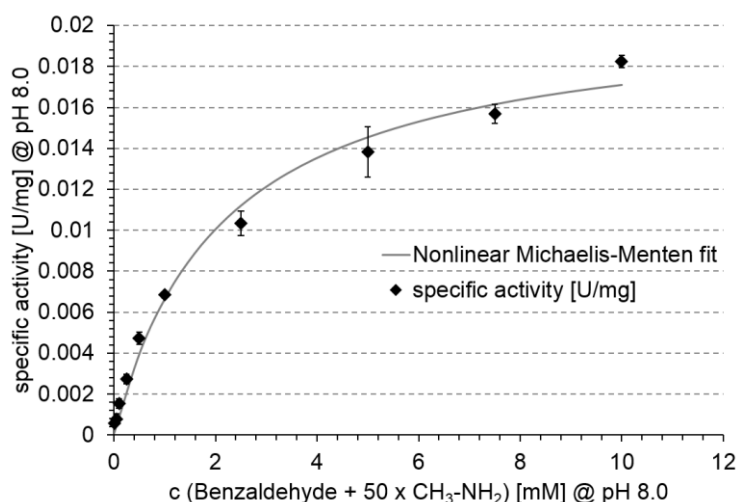


Figure S62: Michaelis-Menten plot for the reductive amination of **11** with 50-fold molar excess of nucleophile **22** with *R*-IREd-Sr at pH 8.0. All activities were determined in triplicates and the error bars show the standard deviation.

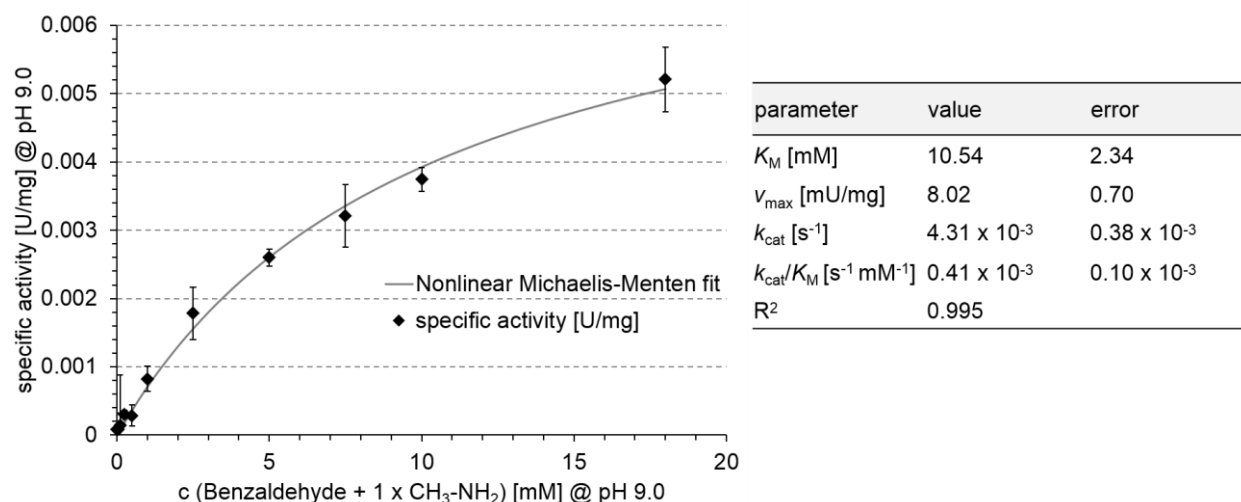


Figure S63: Michaelis-Menten plot for the reductive amination of **11** with equimolar concentration of nucleophile **22** with *R*-IREd-Sr at pH 9.0. All activities were determined in triplicates and the error bars show the standard deviation.

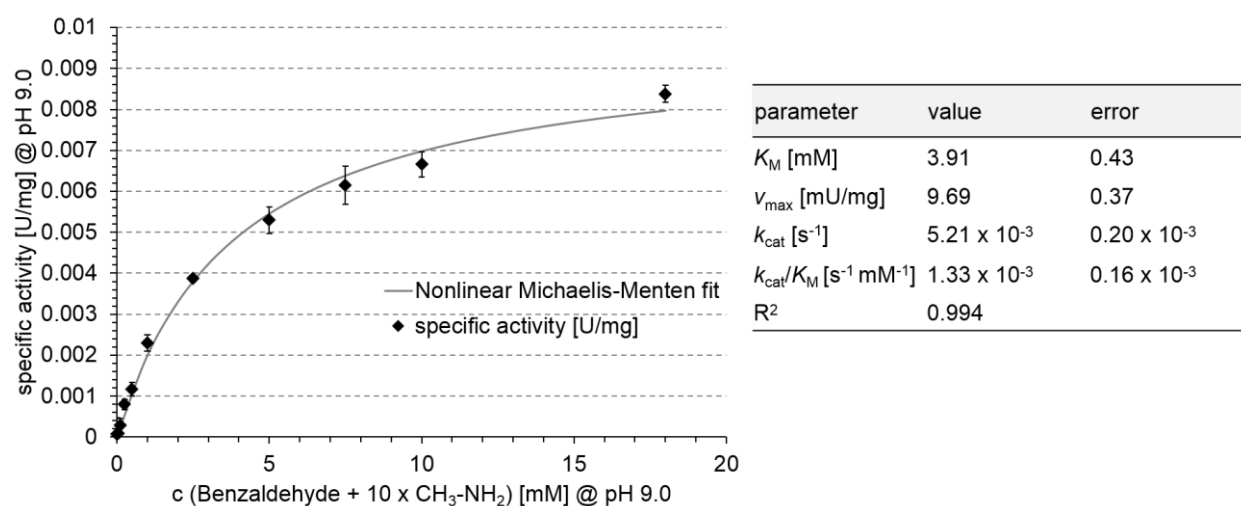


Figure S64: Michaelis-Menten plot for the reductive amination of **11** with 10-fold molar excess of nucleophile **22** with *R*-IREd-Sr at pH 9.0. All activities were determined in triplicates and the error bars show the standard deviation.

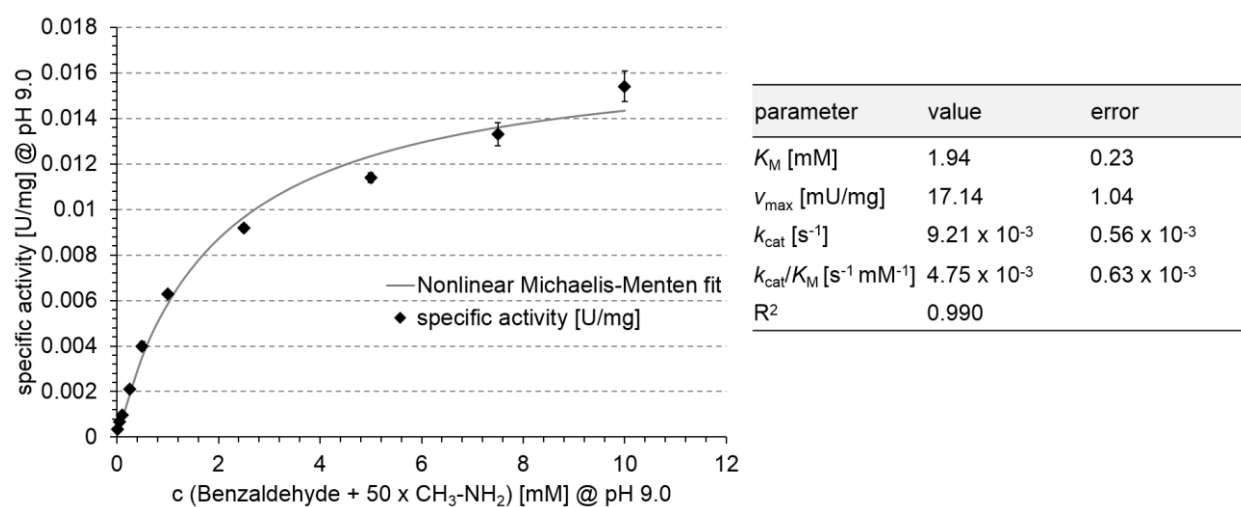


Figure S65: Michaelis-Menten plot for the reductive amination of **11** with 50-fold molar excess of nucleophile **22** with *R*-IREd-Sr at pH 9.0. All activities were determined in triplicates and the error bars show the standard deviation.

7.7 NMR experiments to determine the actual imine fraction and estimation of a “true” K_M value

NMR spectra to determine the actual imine concentration in the reductive amination reaction are shown in Figure 38. For a pH of 9.0 and 8.0 the K_{eq} was calculated by the following formula ($K_{eq} = \frac{[\text{imine}]}{[\text{aldehyde}][\text{amine}]}$) using the known concentrations for the imine, the aldehyde and the amine. The following K_{eq} were calculated from the concentrations derived from the NMR spectra.

pH 9.0: $K_{eq} = 1.36 \times 10^{-2} \text{ mM}^{-1}$

pH 8.0: $K_{eq} = 9.47 \times 10^{-4} \text{ mM}^{-1}$

The calculated K_{eq} were used to correct the imine concentrations in the Michaelis-Menten plots (Figure S65 for pH 9.0 and Figure S62 for pH 8.0). Nonlinear regression with the corrected imine concentrations resulted in “true” K_M values of 0.447 mM for pH 9.0 and 0.081 mM for pH 8.0.

7.8 Oxidation of polyamines by PuO-Re

7.8.1 Analysis of PuO-Re reaction products by GC-MS headspace

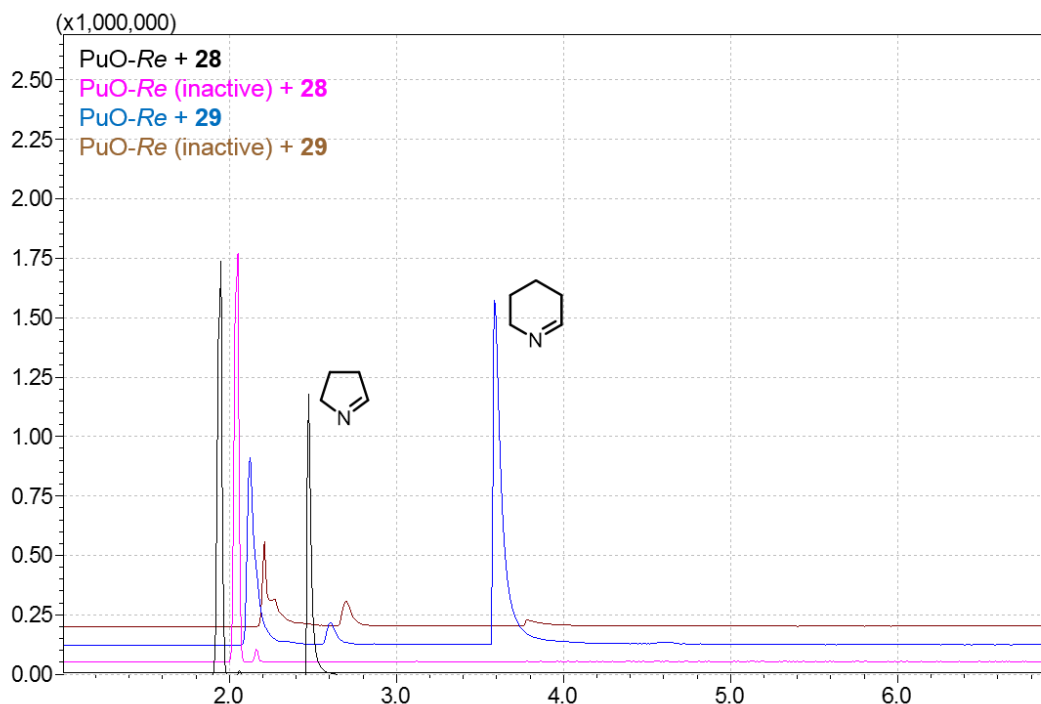


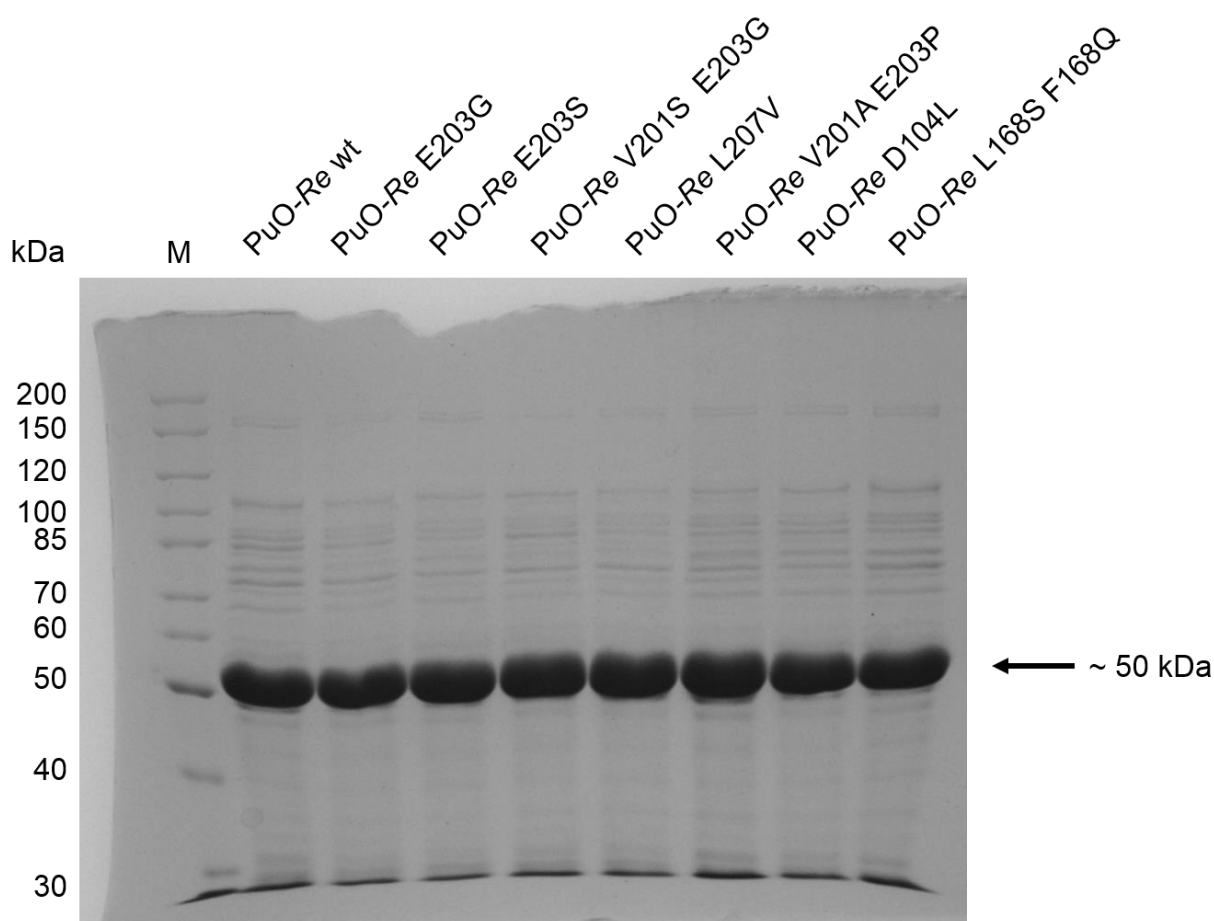
Figure S66: GC-MS headspace analysis of PuO-Re reaction products. To avoid misleading information about imine formation promoted by a change of the sample conditions due to extraction (high pH, organic solvent and derivatization), GC-MS HS was used for analysis. The purified enzyme (10 nM) was incubated with polyamines 1,4-diaminobutane **28** and 1,5-diaminopentane **29** (each 10 mM) for 1 h at 30 °C and 180 rpm. Negative controls were done with previously heat inactivated PuO-Re. A spontaneous cyclization of the formed aminoaldehyde would result in cyclic imines that are much more volatile than the aldehyde or the polyamines and can be detected by GC-HS. GC-MS indicated that the formed peaks correspond to the cyclic imines **39** and **41** resulting from the PuO-Re reaction. Note however that most of the cyclic imines do probably form trimers withstanding detection due to their too high boiling points.^{237,238}

7.8.2 Activity of purified PuO-Re E324D

Table S15: Specific activities in [U/mg] for PuO-Re E324D catalyzed oxidation of polyamine substrates **28**, **29**, **31** and **34** and the relative activity to the wild type enzyme in [%]. The activities of the wild type enzyme are shown in Table 30 and Table S16.

substrate and #		specific activity [U/mg]	activity compared to wild type enzyme [%]
<chem>NCCCCCN</chem>	28	0.041	0.33
<chem>NCCCCCN</chem>	29	0.012	2.65
<chem>CC(C)CCCN</chem>	31	0.003	0.92
<chem>NCCCCNCCCCN</chem>	34	0.008	0.30

7.8.3 Purification of PuO-Re wt and mutants by ion exchange chromatography

Figure S67: 10% SDS-PAGE of a typical Q-Sepharose HP purification of PuO-Re wt (calculated molecular weight 49.4 kDa) and various mutants. 10 μ g total protein were loaded for each sample. The purifications yielded protein in about similar purity. M = molecular weight Marker (Fermentas PageRuler™ unstained protein ladder).

7.8.4 Activity of purified PuO-Re wt and PuO-Re mutants with polyamine substrates **28** to **38**

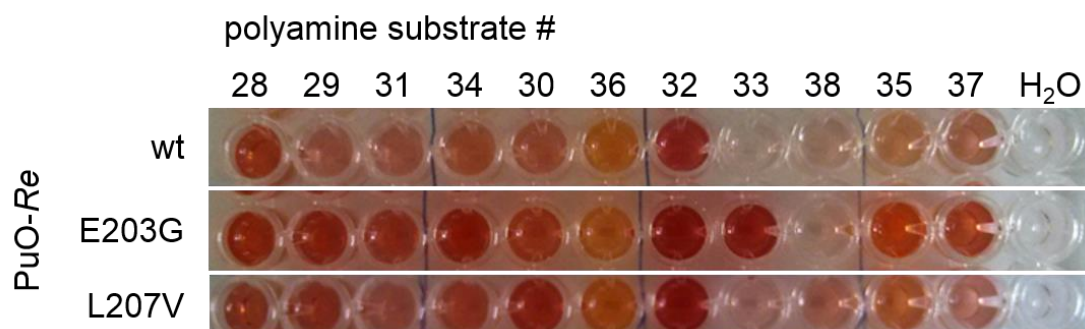


Figure S68: Liquid phase assay with PuO-Re wt, E203G mutant and L207V mutant for the oxidation of polyamines **28** to **38**. The red color originates from aminoantipyrine and vanillic acid that are converted to a quinoneimine dye by H₂O₂ and HRP.¹⁶⁷ After determining the initial activities in the plate reader, the 96 well plate was stored overnight at room temperature. On the next day the picture was taken. As some of the reactions have gone to completion, the color differences are after overnight storage not always directly transferable to differences in the activity. Nevertheless for certain substrates the color formation illustrates very well the activity increase of the mutants, as it is most pronounced visible for polyamine **33**.

Table S16: Specific activities in [U/mg] of purified PuO-Re wt and variants with polyamine substrates **28** to **38**. All activities were determined in triplicates with 10 mM polyamine substrate by monitoring the formation of the enzymatic byproduct H₂O₂ in a coupled spectrophotometric assay with HRP. The enzyme concentrations in the assay were adjusted according to the activity of the polyamine. 1 nM to 4 μM purified PuO-Re wt or mutant were used per reaction. -: not detected.

polyamine substrate #	specific activity [U/mg] PuO-Re variant				
	wt	E203G	E203S	V201S E203G	L207V
28	12.28 ± 0.33	33.80 ± 1.52	18.21 ± 1.06	15.20 ± 1.90	14.30 ± 0.93
29	0.45 ± 0.04	3.32 ± 0.19	2.16 ± 0.18	2.34 ± 0.07	2.07 ± 0.05
30	87.36 × 10 ⁻³ ± 2.64 × 10 ⁻³	0.37 ± 0.02	0.29 ± 0.01	0.25 ± 0.00	0.16 ± 0.00
31	0.33 ± 0.04	1.04 ± 0.09	0.66 ± 0.10	0.98 ± 0.02	0.46 ± 0.02
32	65.62 × 10 ⁻³ ± 3.94 × 10 ⁻³	1.02 ± 0.02	0.98 ± 0.01	0.55 ± 0.02	0.17 ± 0.01
33	3.75 × 10 ⁻³ ± 0.99 × 10 ⁻³	97.75 × 10 ⁻³ ± 3.89 × 10 ⁻³	59.28 × 10 ⁻³ ± 7.78 × 10 ⁻³	51.39 × 10 ⁻³ ± 1.88 × 10 ⁻³	6.76 × 10 ⁻³ ± 0.12 × 10 ⁻³
34	2.63 ± 0.07	9.88 ± 0.34	5.08 ± 0.77	3.38 ± 0.03	1.43 ± 0.02
35	8.13 × 10 ⁻³ ± 0.28 × 10 ⁻³	28.39 × 10 ⁻³ ± 0.57 × 10 ⁻³	11.57 × 10 ⁻³ ± 1.63 × 10 ⁻³	20.25 × 10 ⁻³ ± 1.65 × 10 ⁻³	49.09 × 10 ⁻³ ± 1.42 × 10 ⁻³
36	22.59 × 10 ⁻³ ± 1.18 × 10 ⁻³	13.03 × 10 ⁻³ ± 0.45 × 10 ⁻³	10.93 × 10 ⁻³ ± 1.63 × 10 ⁻³	7.92 × 10 ⁻³ ± 0.54 × 10 ⁻³	37.61 × 10 ⁻³ ± 0.74 × 10 ⁻³
37	9.18 × 10 ⁻³ ± 0.21 × 10 ⁻³	38.77 × 10 ⁻³ ± 2.26 × 10 ⁻³	17.06 × 10 ⁻³ ± 0.27 × 10 ⁻³	31.17 × 10 ⁻³ ± 3.12 × 10 ⁻³	21.22 × 10 ⁻³ ± 1.24 × 10 ⁻³
38	5.36 × 10 ⁻³ ± 5.22 × 10 ⁻³	7.59 × 10 ⁻³ ± 2.55 × 10 ⁻³	4.67 × 10 ⁻³ ± 9.96 × 10 ⁻³	0.49 × 10 ⁻³ ± 4.37 × 10 ⁻³	38.83 × 10 ⁻³ ± 8.14 × 10 ⁻³

7 SUPPORTING INFORMATION

Table S16: continued.

polyamine substrate #	specific activity [U/mg] PuO- <i>Re</i> variant				
	V201A E203P	D104L	L168S F169Q	V201A E203G	A24T V201A E203M
28	13.72 ± 0.11	9.73 ± 1.38	3.71 ± 1.30	22.87 ± 1.31	9.64 ± 0.51
29	1.27 ± 0.03	86.52 × 10 ⁻³ ± 72.15 × 10 ⁻³	0.84 ± 0.29	2.51 ± 0.26	1.36 ± 0.01
30	0.19 ± 0.00	53.11 × 10 ⁻³ ± 1.55 × 10 ⁻³	0.15 ± 0.02	0.32 ± 0.02	0.17 ± 0.01
31	0.48 ± 0.08	82.64 × 10 ⁻³ ± 23.63 × 10 ⁻³	0.43 ± 0.29	0.73 ± 0.11	0.43 ± 0.04
32	0.41 ± 0.02	86.27 × 10 ⁻³ ± 5.30 × 10 ⁻³	21.25 × 10 ⁻³ ± 11.89 × 10 ⁻³	0.76 ± 0.01	0.64 ± 0.01
33	53.21 × 10 ⁻³ ± 1.31 × 10 ⁻³	0.07 × 10 ⁻³ ± 2.88 × 10 ⁻³	-	70.07 × 10 ⁻³ ± 4.59 × 10 ⁻³	51.08 × 10 ⁻³ ± 3.38 × 10 ⁻³
34	0.11 ± 0.01	0.74 ± 0.14	1.80 ± 0.17	4.79 ± 0.49	0.46 ± 0.25
35	8.69 × 10 ⁻³ ± 0.31 × 10 ⁻³	2.76 × 10 ⁻³ ± 0.20 × 10 ⁻³	4.35 × 10 ⁻³ ± 0.33 × 10 ⁻³	20.72 × 10 ⁻³ ± 0.90 × 10 ⁻³	14.99 × 10 ⁻³ ± 0.56 × 10 ⁻³
36	9.29 × 10 ⁻³ ± 0.87 × 10 ⁻³	15.32 × 10 ⁻³ ± 0.82 × 10 ⁻³	7.26 × 10 ⁻³ ± 2.52 × 10 ⁻³	12.31 × 10 ⁻³ ± 2.91 × 10 ⁻³	8.65 × 10 ⁻³ ± 0.38 × 10 ⁻³
37	16.73 × 10 ⁻³ ± 0.53 × 10 ⁻³	4.82 × 10 ⁻³ ± 0.17 × 10 ⁻³	13.16 × 10 ⁻³ ± 0.47 × 10 ⁻³	42.19 × 10 ⁻³ ± 0.76 × 10 ⁻³	14.84 × 10 ⁻³ ± 0.25 × 10 ⁻³
38	4.37 × 10 ⁻³ ± 4.50 × 10 ⁻³	9.28 × 10 ⁻³ ± 6.86 × 10 ⁻³	-	-	-

7.9 Michaelis-Menten plots of putrescine oxidase wild type and mutants

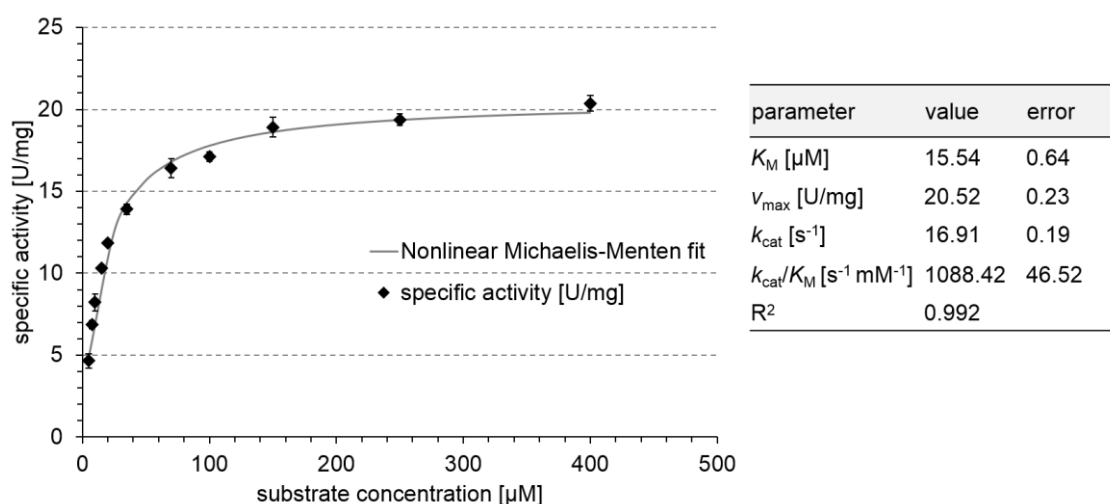


Figure S69: Determination of kinetic constants for PuO-*Re* wild type with substrate **28**. All activities were determined in triplicates and the error bars show the standard deviation.

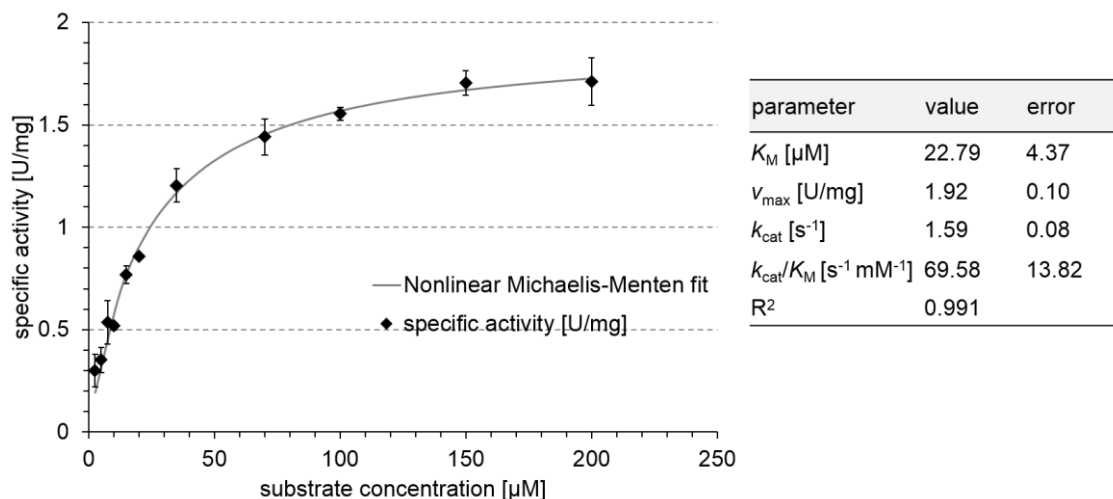


Figure S70: Determination of kinetic constants for PuO-Re wild type with substrate **29**. All activities were determined in triplicates and the error bars show the standard deviation.

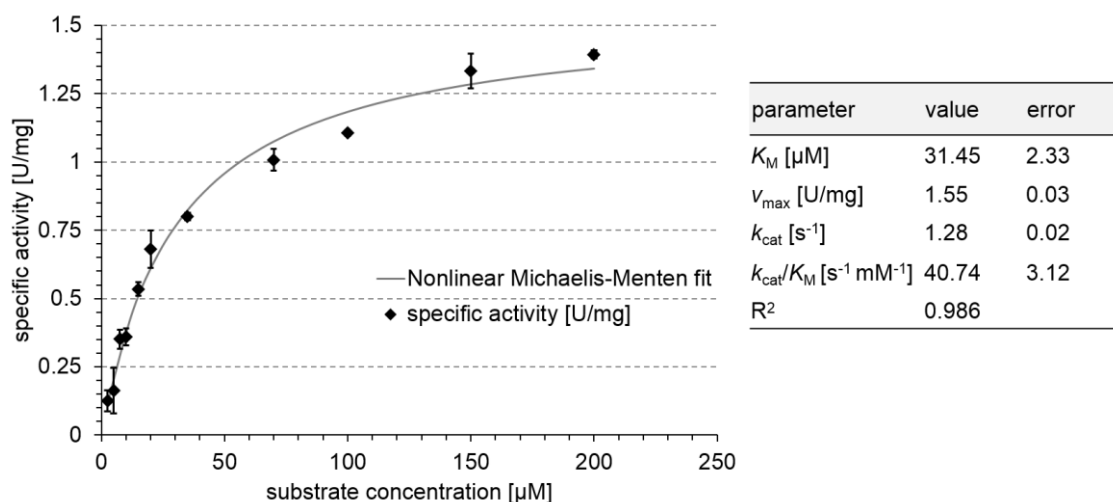


Figure S71: Determination of kinetic constants for PuO-Re wild type with substrate **31**. All activities were determined in triplicates and the error bars show the standard deviation.

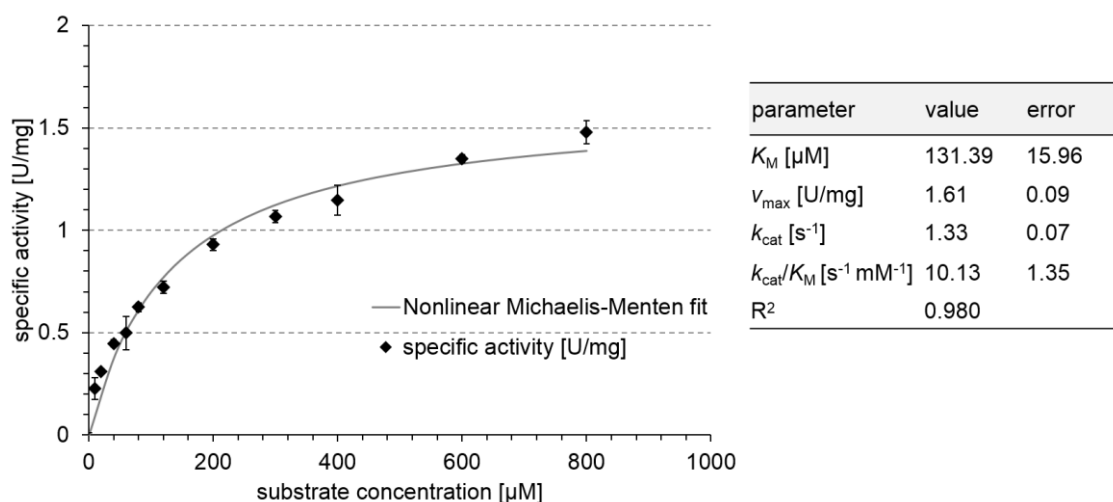


Figure S72: Determination of kinetic constants for PuO-Re wild type with substrate **34**. All activities were determined in triplicates and the error bars show the standard deviation.

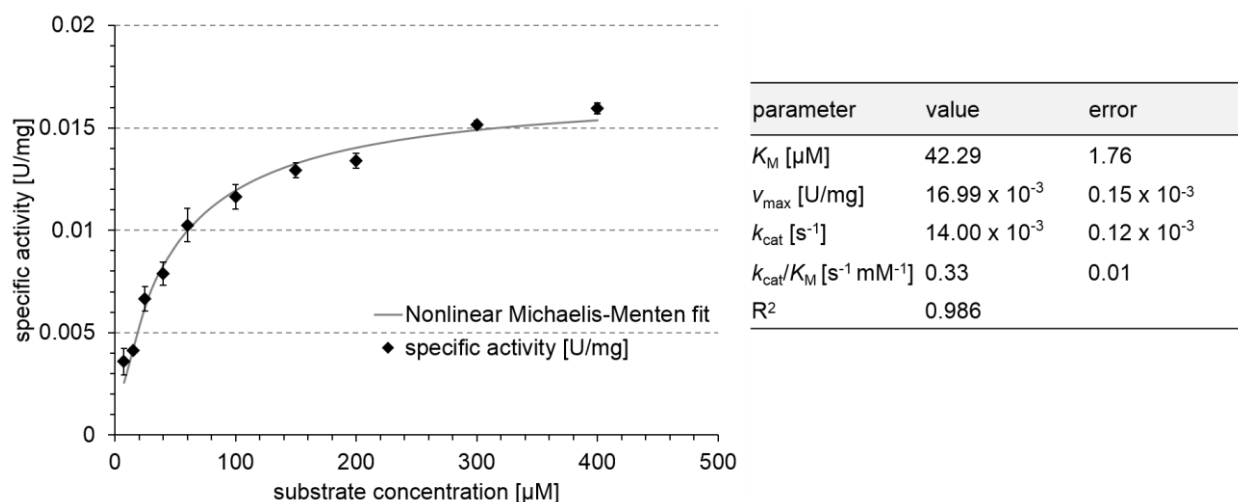


Figure S73: Determination of kinetic constants for PuO-Re wild type with substrate **36**. All activities were determined in triplicates and the error bars show the standard deviation.

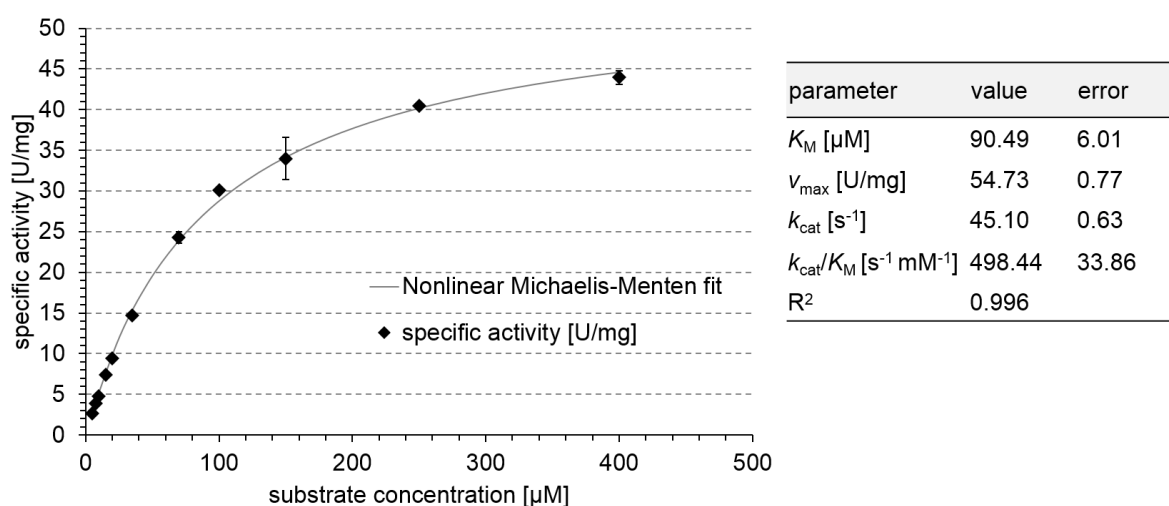


Figure S74: Determination of kinetic constants for PuO-Re E203G with substrate **28**. All activities were determined in triplicates and the error bars show the standard deviation.

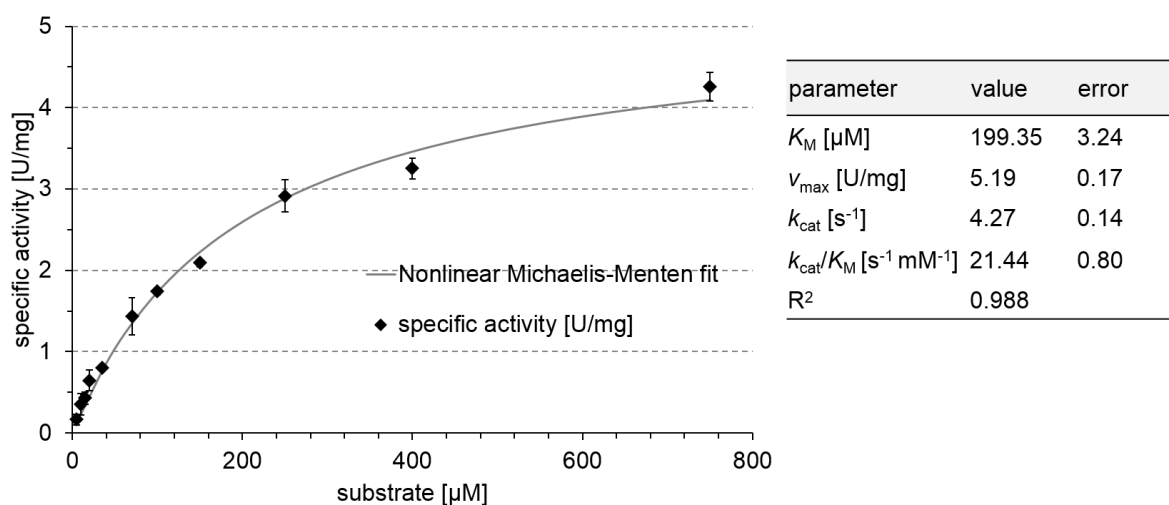


Figure S75: Determination of kinetic constants for PuO-Re E203G with substrate **29**. All activities were determined in triplicates and the error bars show the standard deviation.

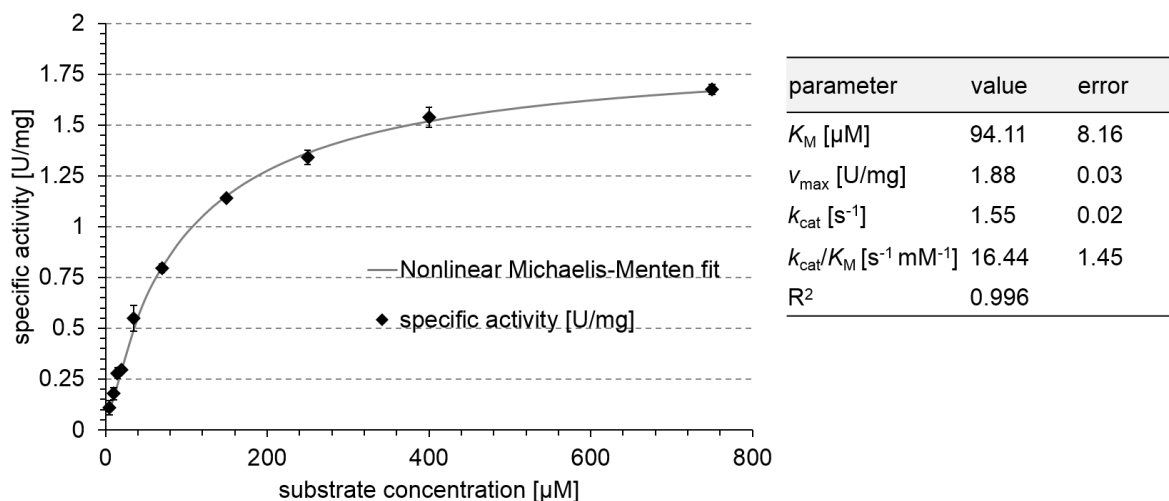


Figure S76: Determination of kinetic constants for PuO-Re E203G with substrate 31. All activities were determined in triplicates and the error bars show the standard deviation.

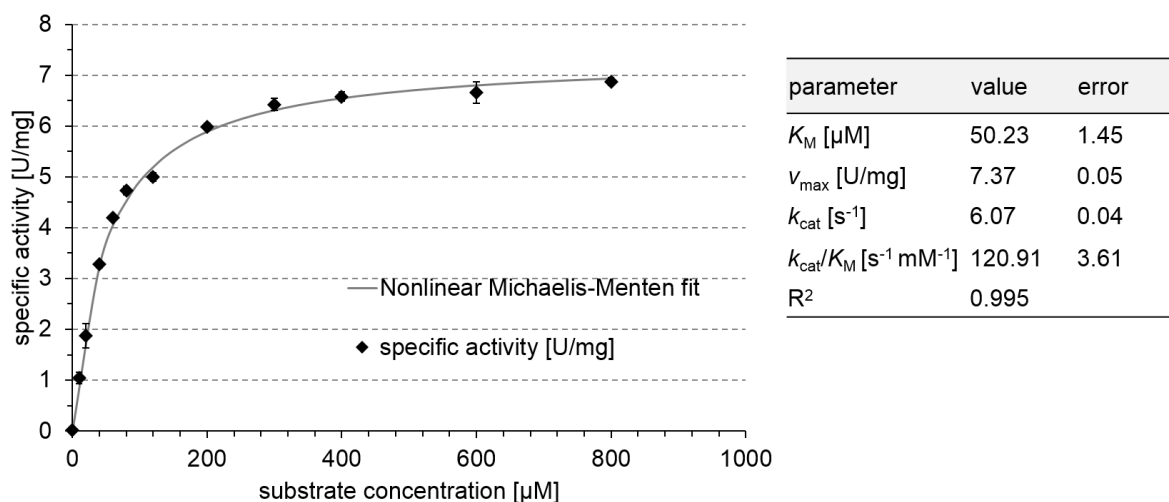


Figure S77: Determination of kinetic constants for PuO-Re E203G with substrate 34. All activities were determined in triplicates and the error bars show the standard deviation.

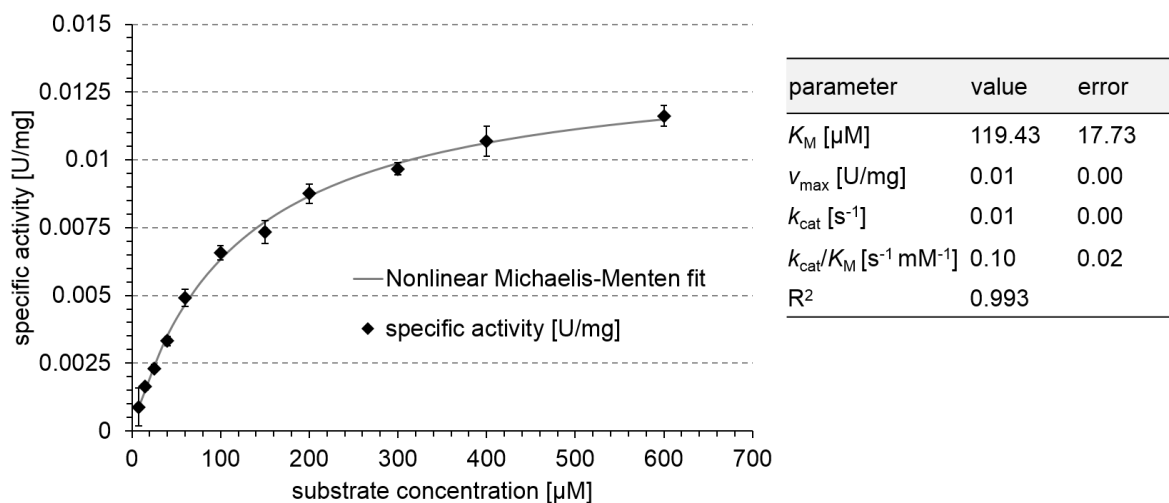


Figure S78: Determination of kinetic constants for PuO-Re E203G with substrate 36. All activities were determined in triplicates and the error bars show the standard deviation.

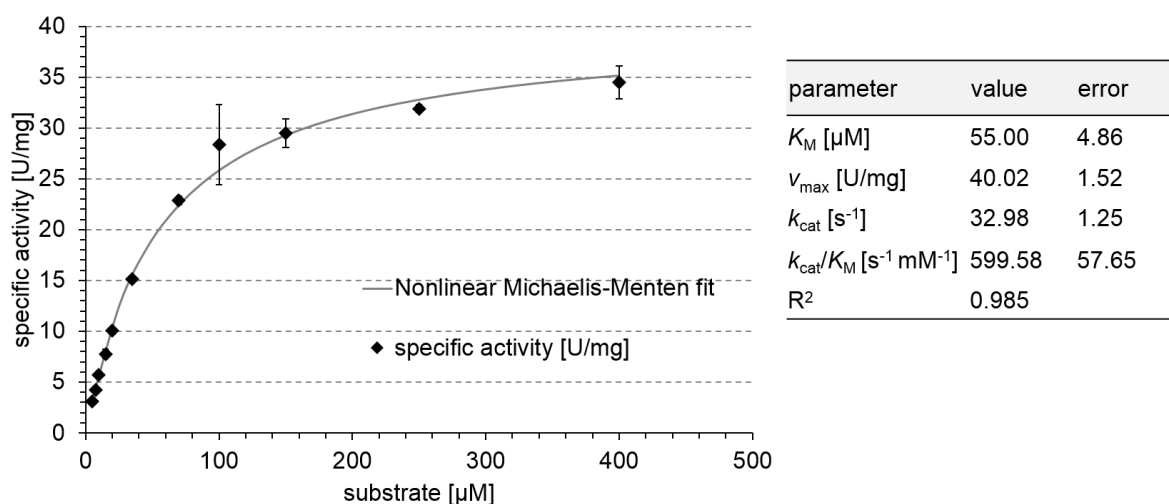


Figure S79: Determination of kinetic constants for PuO-Re I154V E203V with substrate 28. All activities were determined in triplicates and the error bars show the standard deviation.

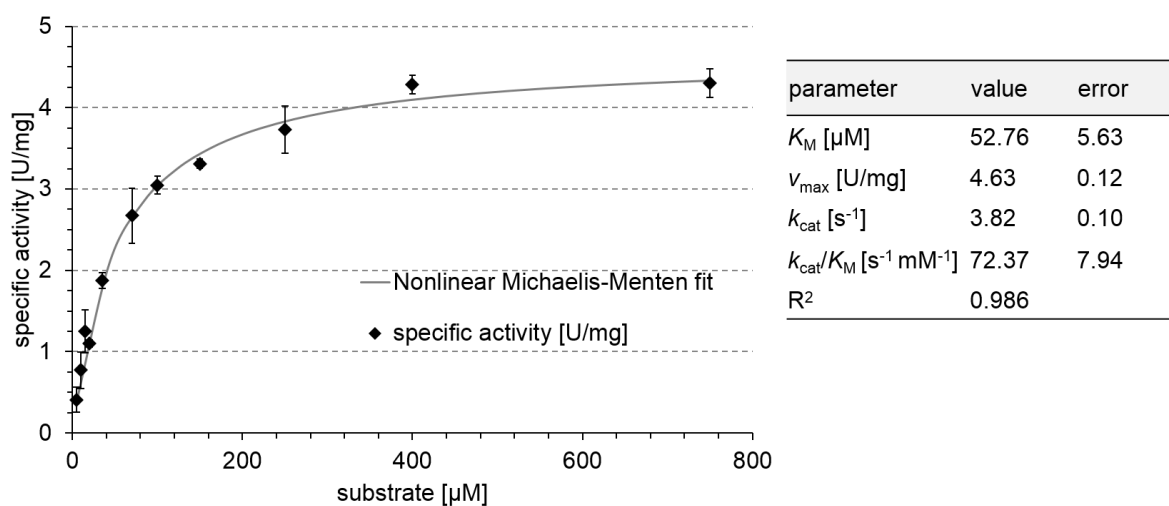


Figure S80: Determination of kinetic constants for PuO-Re I154V E203V with substrate 29. All activities were determined in triplicates and the error bars show the standard deviation.

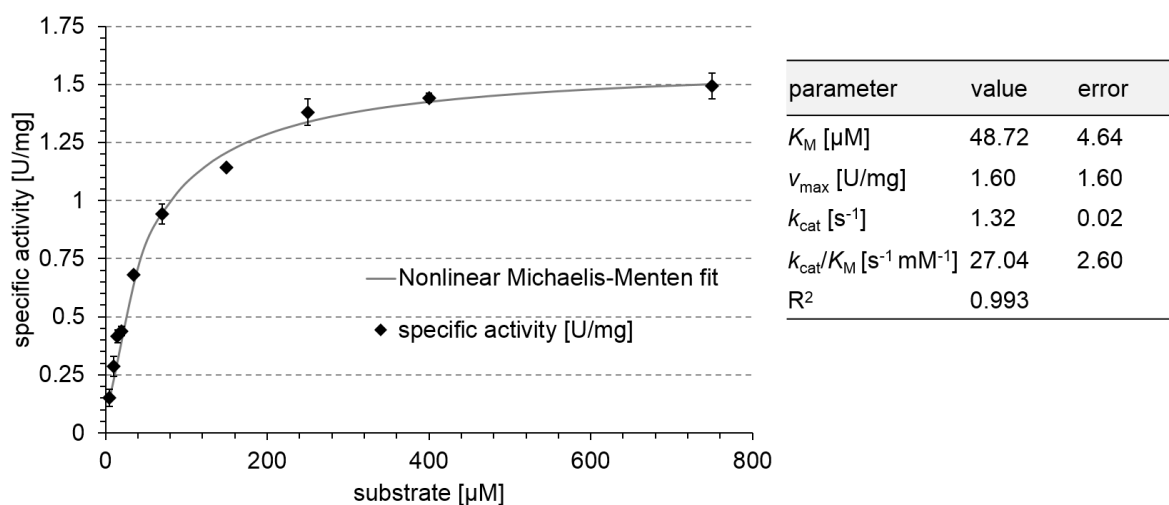


Figure S81: Determination of kinetic constants for PuO-Re I154V E203V with substrate 31. All activities were determined in triplicates and the error bars show the standard deviation.

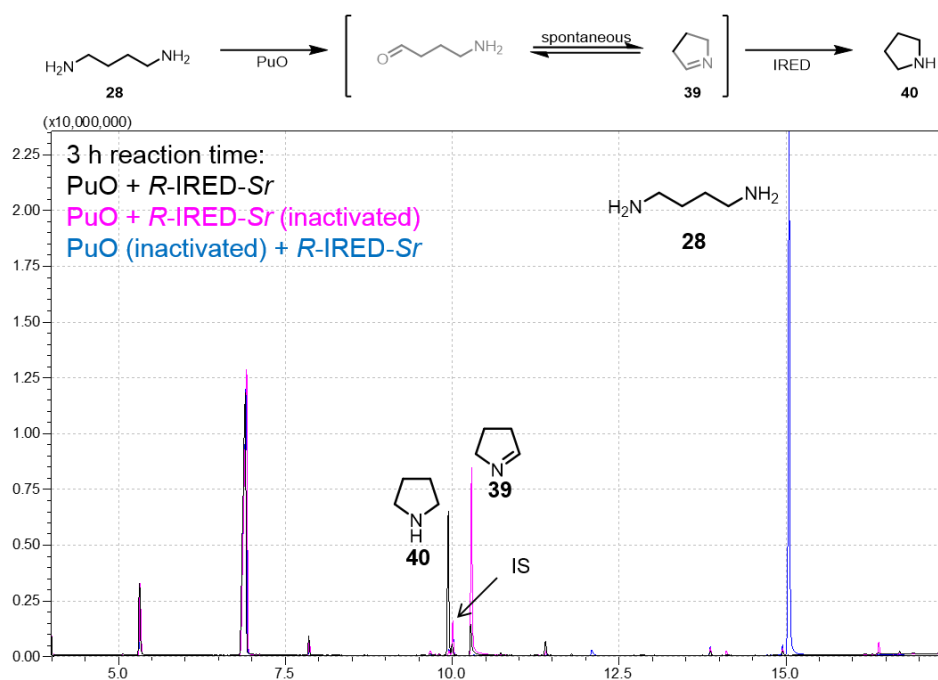
7.10 GC-traces of the cascade reaction with purified proteins to transform polyamines into *N*-heterocycles

Figure S82: Conversion of polyamine **28** to the cyclic amine product **40** by the combination of purified PuO-*Re* and *R*-IRED-*Sr*. In the reaction with both enzymes being active (black) the substrate is fully consumed in the 3 h reaction time and transformed to the product **40**. After inactivation of one of the enzymes (*R*-IRED-*Sr* inactivated in pink or PuO-*Re* inactivated in blue) either the polyamine is not converted (blue) or the imine intermediate **39** (pink) could be detected. It is assumed that most of the imine intermediate forms a trimer. Due to its too high boiling point, the trimer cannot be detected. IS = internal standard.

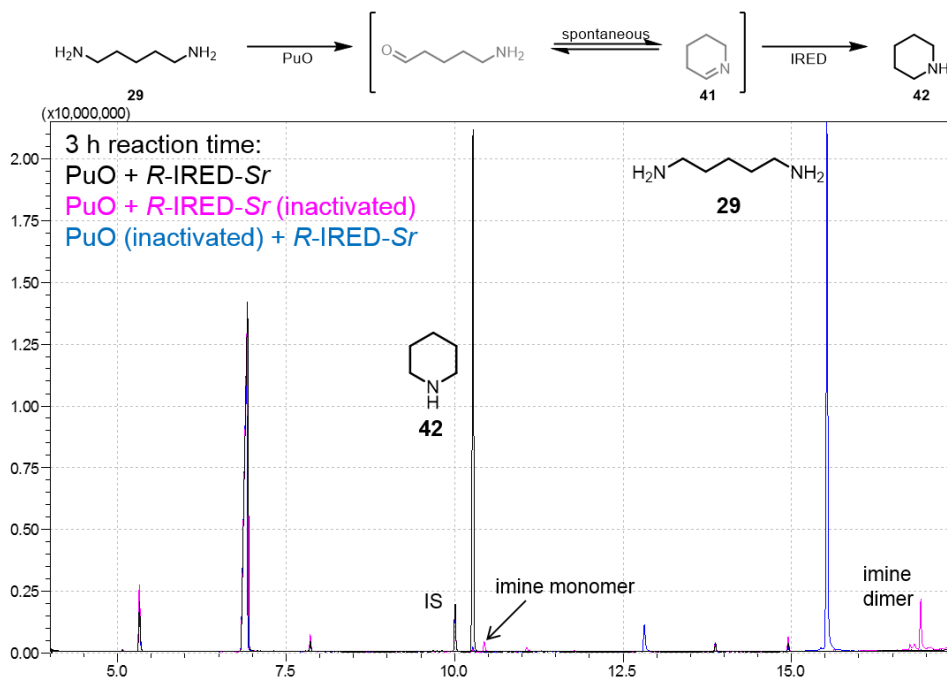


Figure S83: Conversion of polyamine **29** to the cyclic amine product **42** by the combination of purified PuO-*Re* and *R*-IRED-*Sr*. In the reaction with both enzymes being active (black) the substrate is fully consumed in the 3 h reaction time and transformed to the product **42**. After inactivation of one of the enzymes (*R*-IRED-*Sr* inactivated in pink or PuO-*Re* inactivated in blue) either the polyamine is not converted (blue) or small amounts of the imine intermediate (pink) could be detected. It is assumed that most of the imine intermediate forms a trimer. Due to its too high boiling point, the trimer cannot be detected. IS = internal standard.

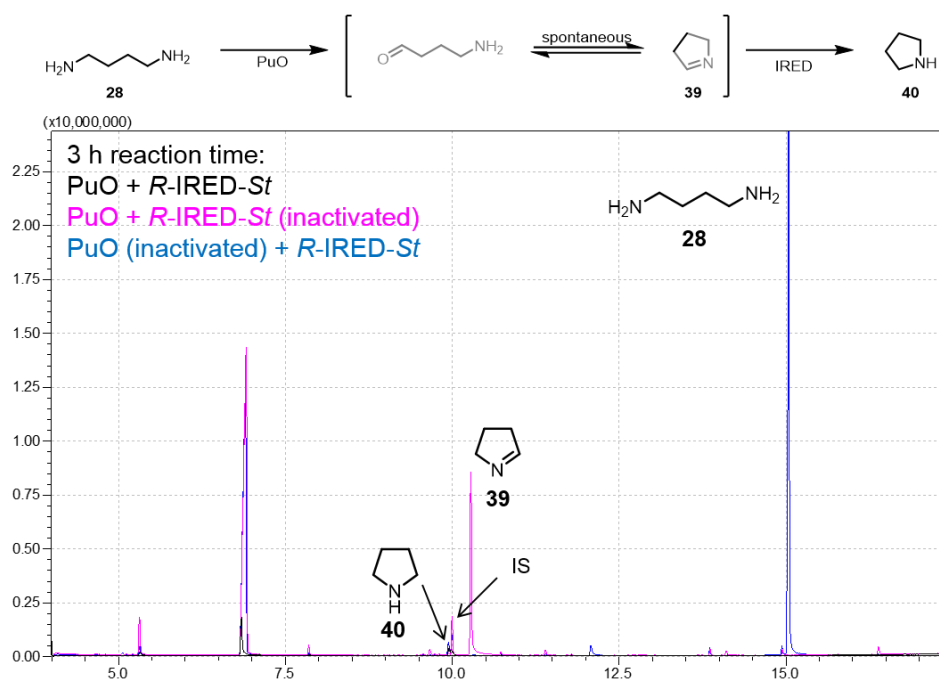


Figure S84: Conversion of polyamine **28** to the cyclic amine product **40** by the combination of purified PuO-*Re* and *R*-IRED-*St*. In the reaction with both enzymes being active (black) the substrate is fully consumed in the 3 h reaction time and transformed to small amounts of product **40**. After inactivation of one of the enzymes (*R*-IRED-*St* inactivated in pink or PuO-*Re* inactivated in blue) either the polyamine is not converted (blue) or the imine intermediate **39** (pink) could be detected. It is assumed that most of the imine intermediate forms a trimer. Due to its too high boiling point, the trimer cannot be detected. IS = internal standard.

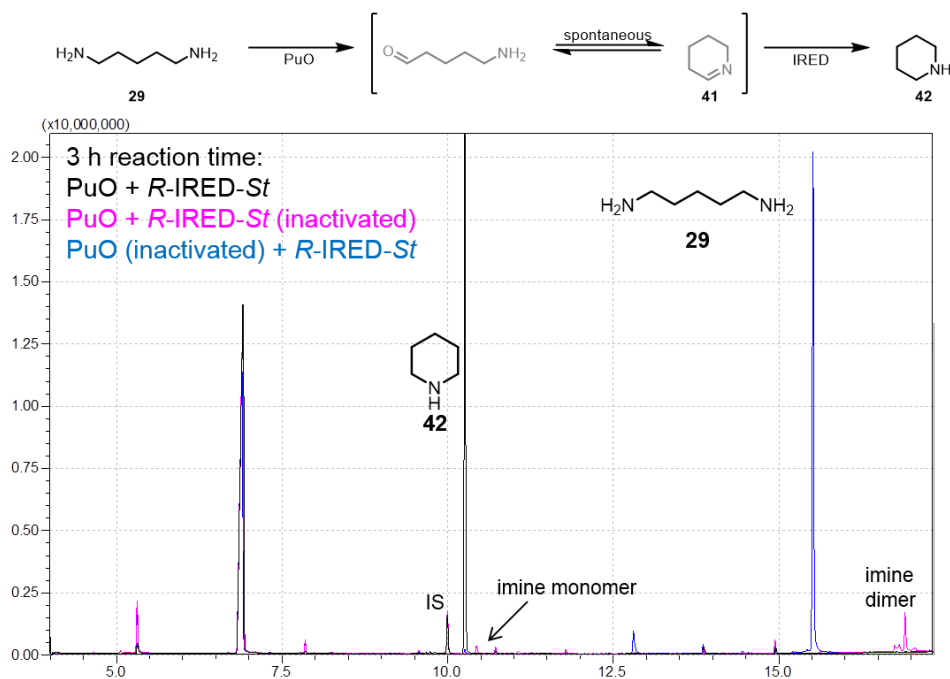


Figure S85: Conversion of polyamine **29** to the cyclic amine product **42** by the combination of purified PuO-*Re* and *R*-IRED-*St*. In the reaction with both enzymes being active (black) the substrate is fully consumed in the 3 h reaction time and transformed to the product **42**. After inactivation of one of the enzymes (*R*-IRED-*St* inactivated in pink or PuO-*Re* inactivated in blue) either the polyamine is not converted (blue) or small amounts of the imine intermediate (pink) could be detected. It is assumed that most of the imine intermediate forms a trimer. Due to its too high boiling point, the trimer cannot be detected. IS = internal standard.

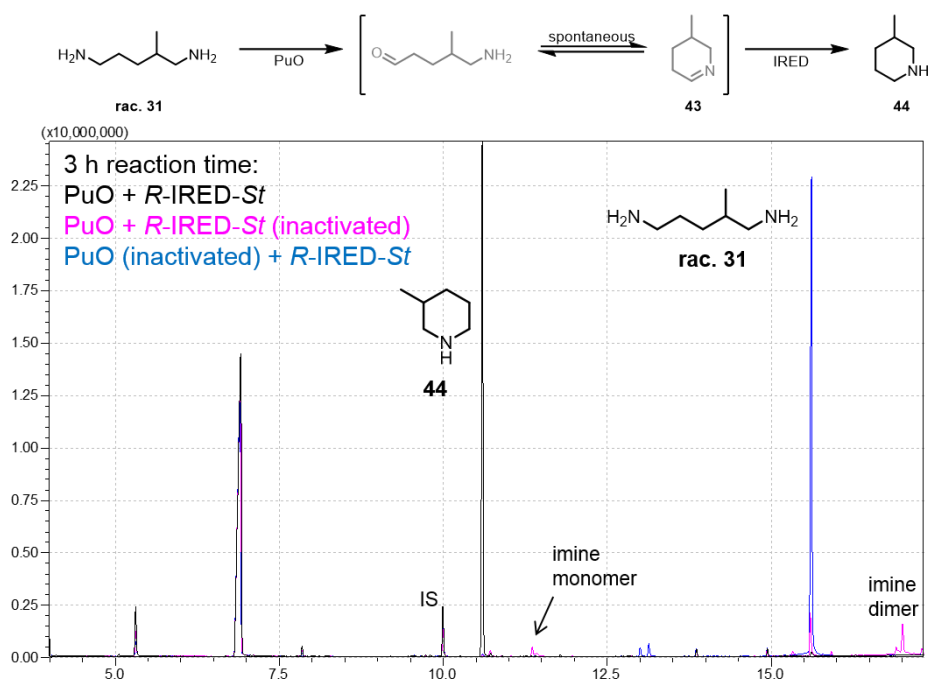


Figure S86: Conversion of polyamine **31** to the cyclic amine product **44** by the combination of purified PuO-*Re* and *R*-IRED-*St*. In the reaction with both enzymes being active (black) the substrate is fully consumed in the 3 h reaction time and transformed to the product **44**. After inactivation of one of the enzymes (*R*-IRED-*St* inactivated in pink or PuO-*Re* inactivated in blue) either the polyamine is not converted (blue) or small amounts of the imine intermediates (pink) could be detected. It is assumed that most of the imine intermediate forms a trimer. Due to its too high boiling point, the trimer cannot be detected. The reaction scheme on top assumes that the sterically less demanding amine group of **31** is oxidized, however the regioselectivity of PuO-*Re* has to be determined. Depending on this regioselectivity also different imine intermediates are formed, however this information is lost after reduction of the cyclic imine by an IRED. IS = internal standard.

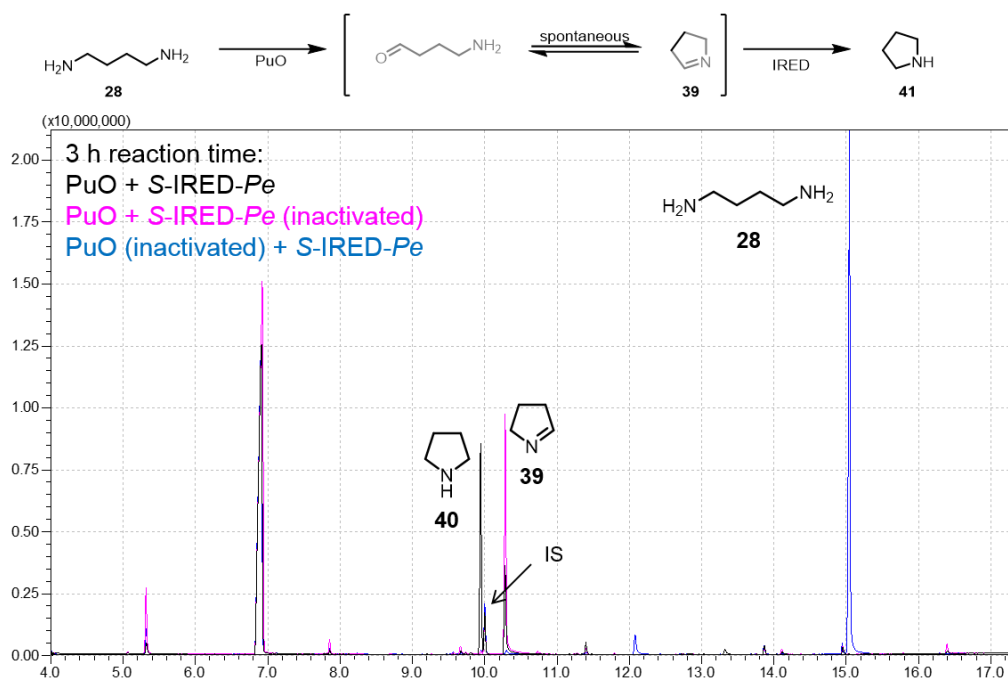


Figure S87: Conversion of polyamine **28** to the cyclic amine product **40** by the combination of purified PuO-*Re* and *S*-IRED-*Pe*. In the reaction with both enzymes being active (black) the substrate is fully consumed in the 3 h reaction time and transformed to the product **40**. After inactivation of one of the enzymes (*S*-IRED-*Pe* inactivated in pink or PuO-*Re* inactivated in blue) either the polyamine is not converted (blue) or the imine intermediate **39** (pink) could be detected. It is assumed that most of the imine intermediate forms a trimer. Due to its too high boiling point, the trimer cannot be detected. IS = internal standard.

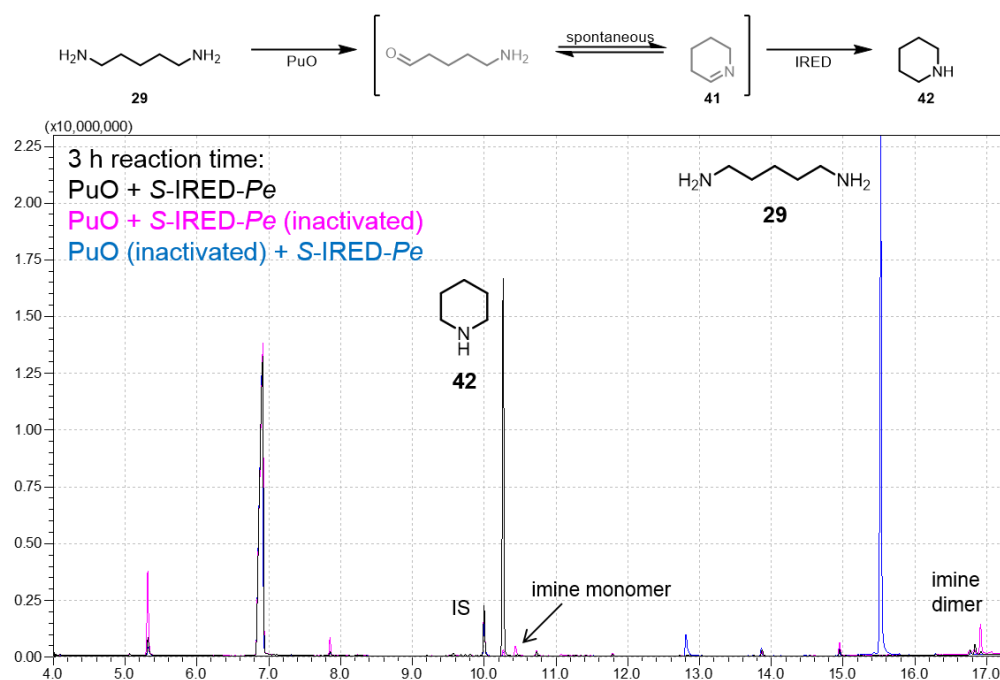


Figure S88: Conversion of polyamine **29** to the cyclic amine product **42** by the combination of purified PuO-*Re* and S-IRED-*Pe*. In the reaction with both enzymes being active (black) the substrate is fully consumed in the 3 h reaction time and transformed to the product **42**. After inactivation of one of the enzymes (*R*-IRED-*Sr* inactivated in pink or PuO-*Re* inactivated in blue) either the polyamine is not converted (blue) or small amounts of the imine intermediate (pink) could be detected. It is assumed that most of the imine intermediate forms a trimer. Due to its too high boiling point, the trimer cannot be detected. IS = internal standard.

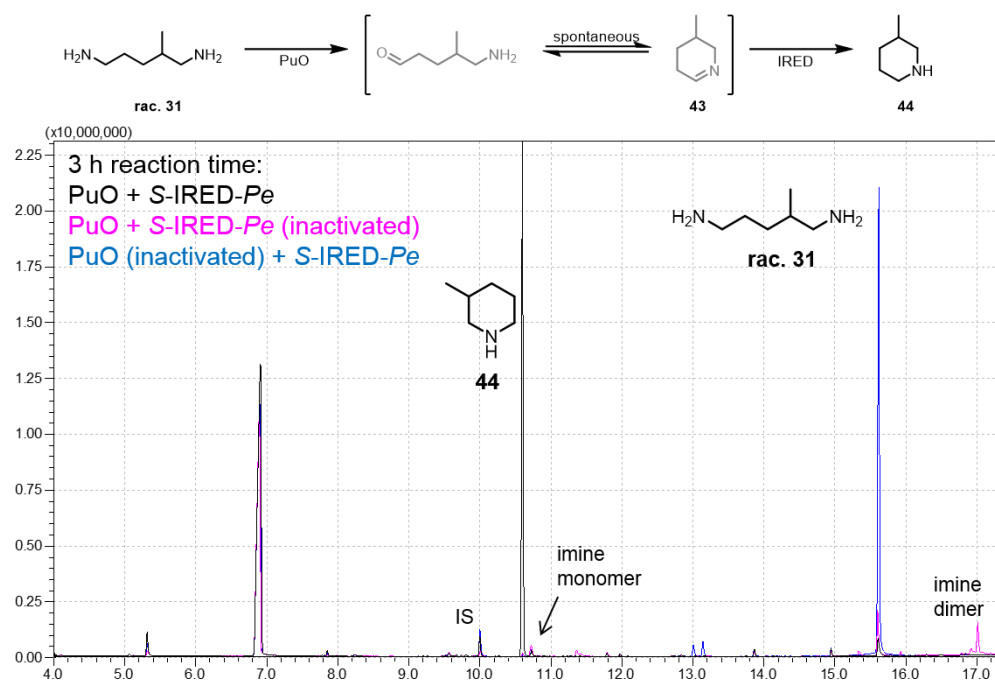


Figure S89: Conversion of polyamine **31** to the cyclic amine product **44** by the combination of purified PuO-*Re* and S-IRED-*Pe*. In the reaction with both enzymes being active (black) the substrate is fully consumed in the 3 h reaction time and transformed to the product **44**. After inactivation of one of the enzymes (S-IRED-*Pe* inactivated in pink or PuO-*Re* inactivated in blue) either the polyamine is not converted (blue) or small amounts of the imine intermediates (pink) could be detected. It is assumed that most of the imine intermediate forms a trimer. Due to its too high boiling point, the trimer cannot be detected. The reaction scheme on top assumes that the sterically less demanding amine group of **31** is oxidized, however the regioselectivity of PuO-*Re* has to be determined. Depending on this regioselectivity also different imine intermediates are formed, however this information is lost after reduction of the cyclic imine by an IRED. IS = internal standard.

7.11 GC-traces of whole cell biotransformations with *E. coli* strains expressing PuO-Re and an IRED simultaneously to transform polyamines into *N*-heterocycles

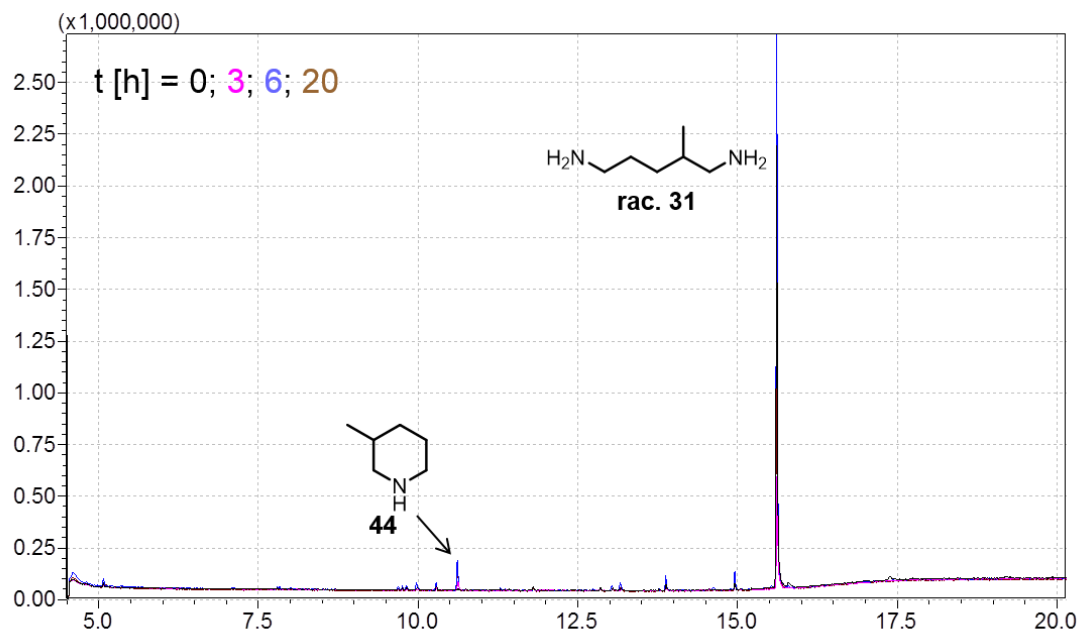


Figure S90: Whole cell biotransformation of polyamine **31** to the cyclic amine **44** with *E. coli* JW5510 expressing PuO-Re and R-IRED-Sr simultaneously. For the reaction time of 20 h the amount of product slightly increases. Compared to the performance of isolated enzymes the consumption of the substrate and transformation to the amine is poor.

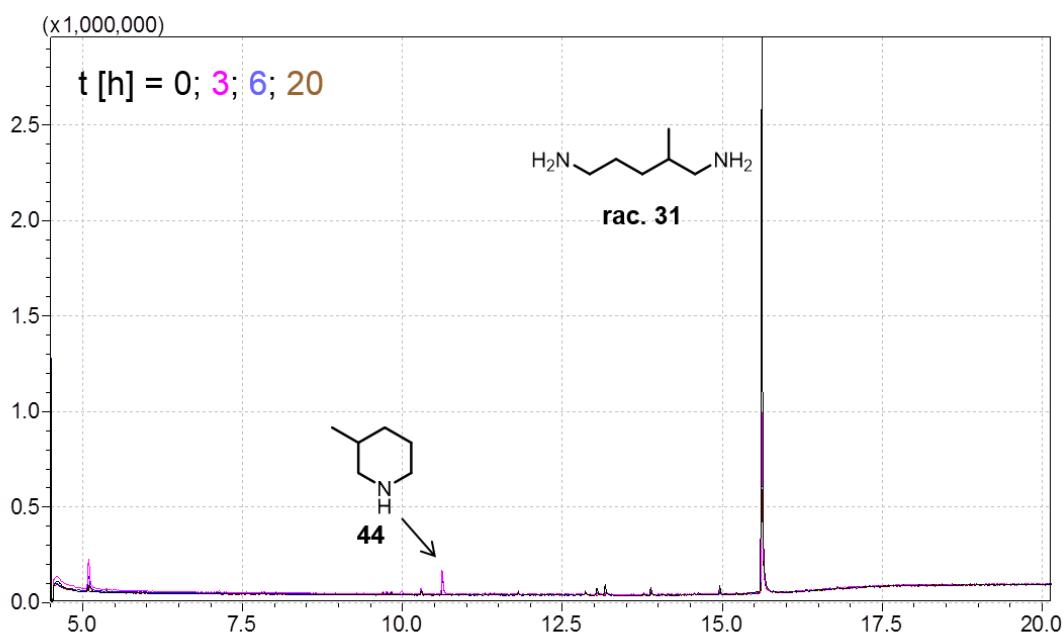
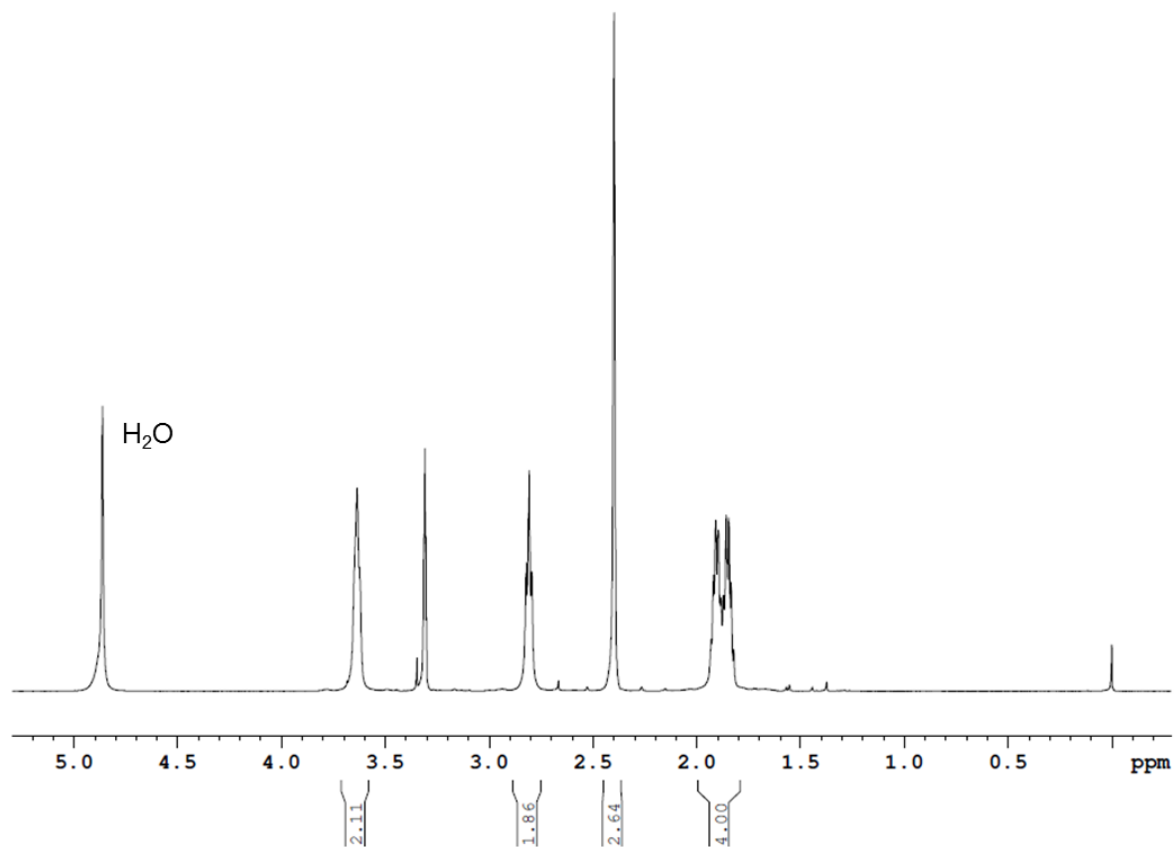


Figure S91: Whole cell biotransformation of polyamine **31** to the cyclic amine **44** with *E. coli* JW5510 expressing PuO-Re and R-IRED-St simultaneously. For the reaction time of 20 h the amount of product slightly increases. Compared to the performance of isolated enzymes the consumption of the substrate and transformation to the amine is poor.

7.12 NMR spectra

Figure S92: $^1\text{H-NMR}$ spectrum of 2-methylpiperidine (**3a**).

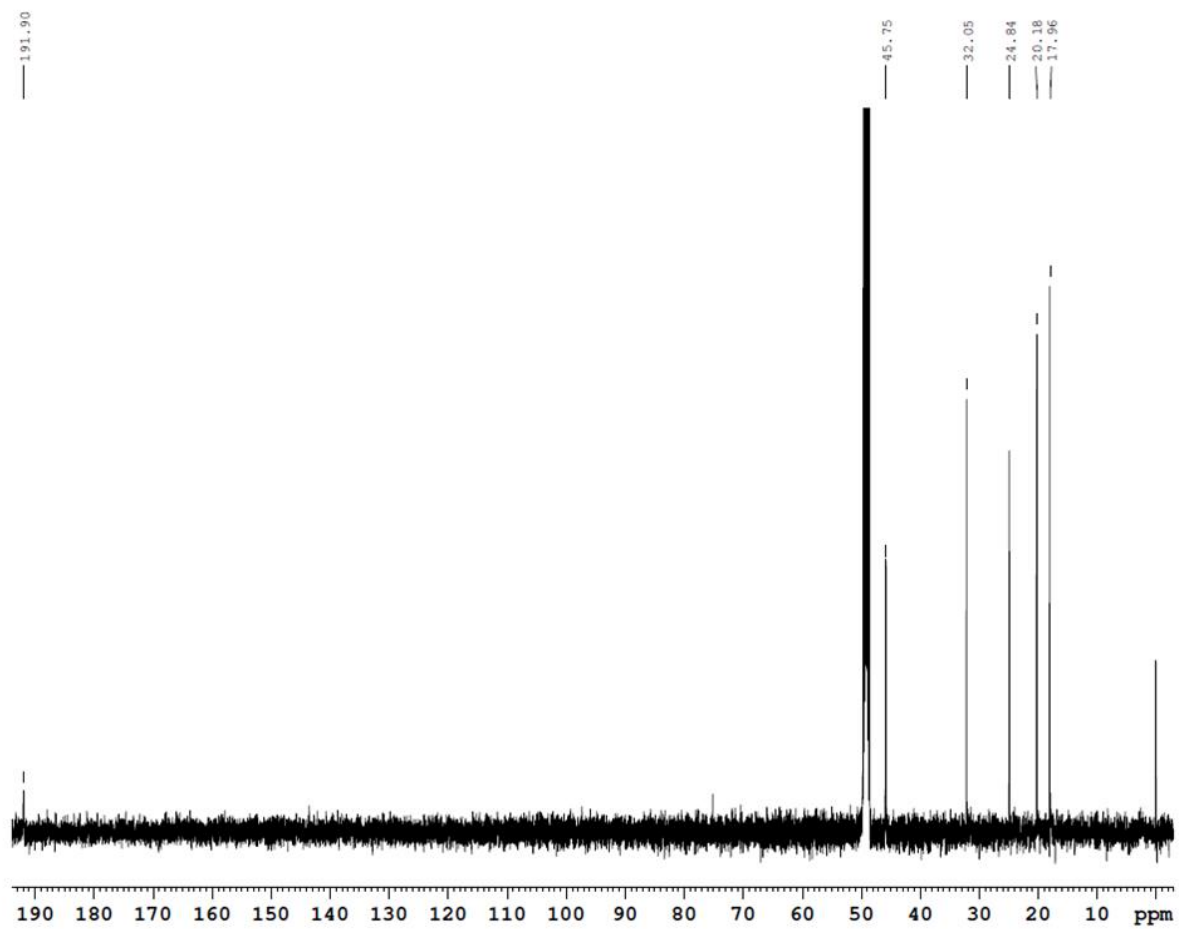
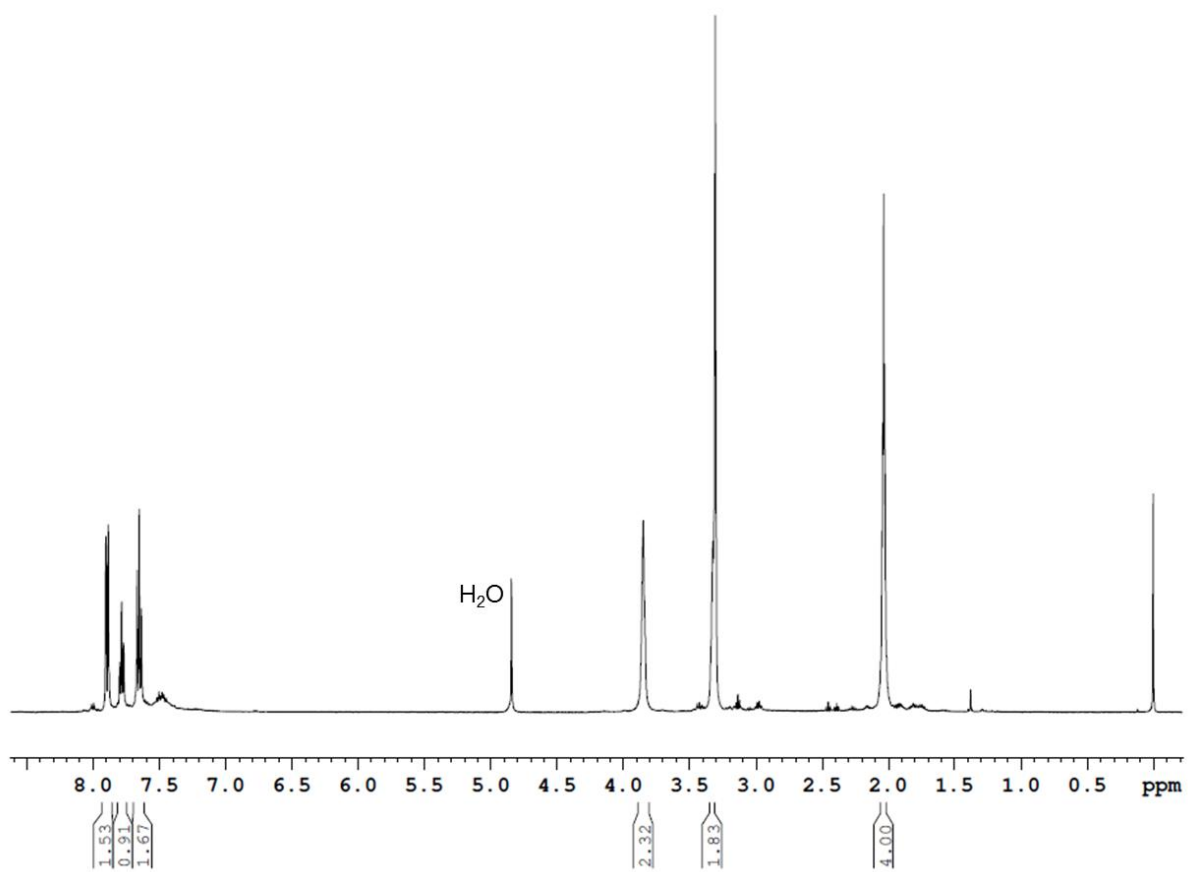


Figure S93: ^{13}C -NMR spectrum of 2-methylpiperidine (**3a**).

Figure S94: ¹H-NMR spectrum of 2-phenylpiperidine (**3b**).

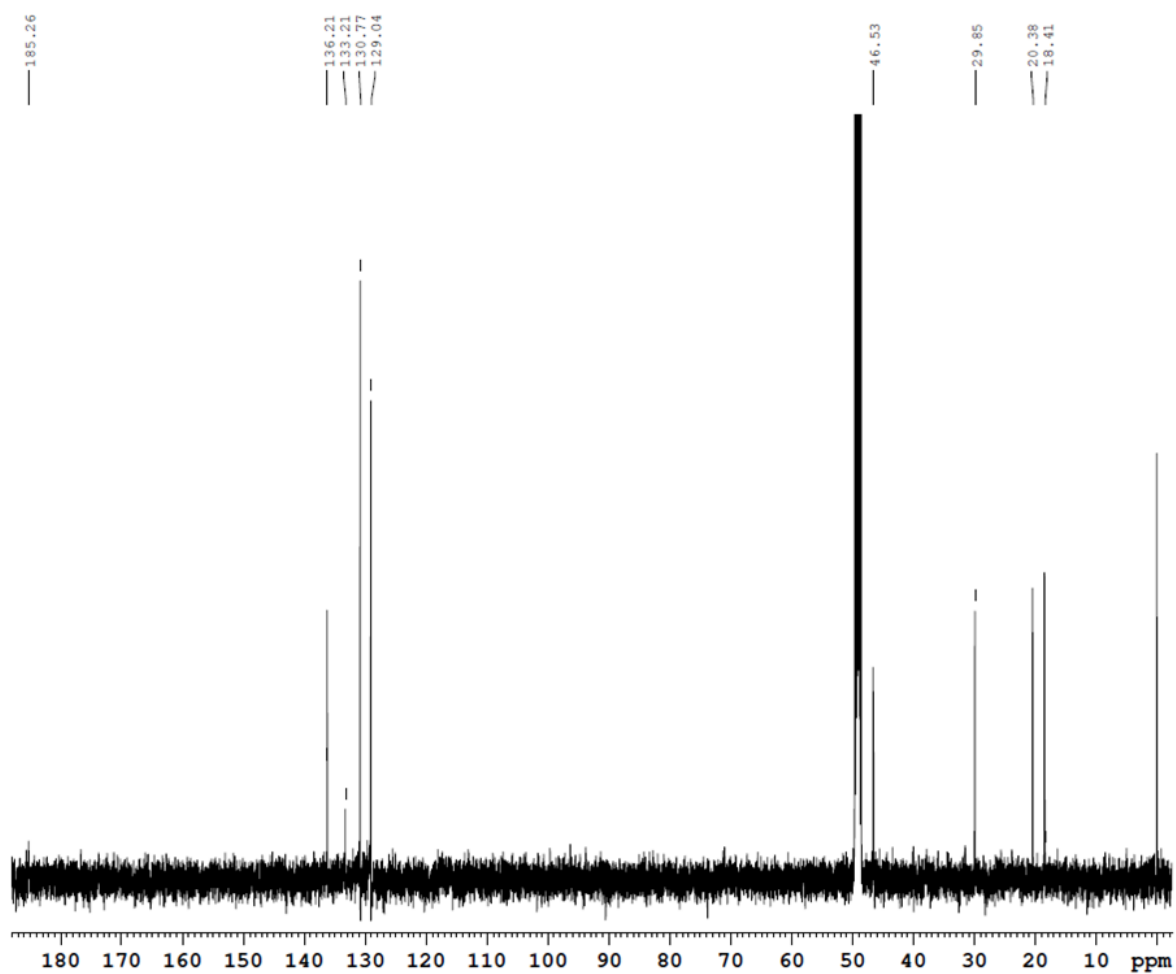


Figure S95: ^{13}C -NMR spectrum of 2-phenylpiperidine (**3b**).

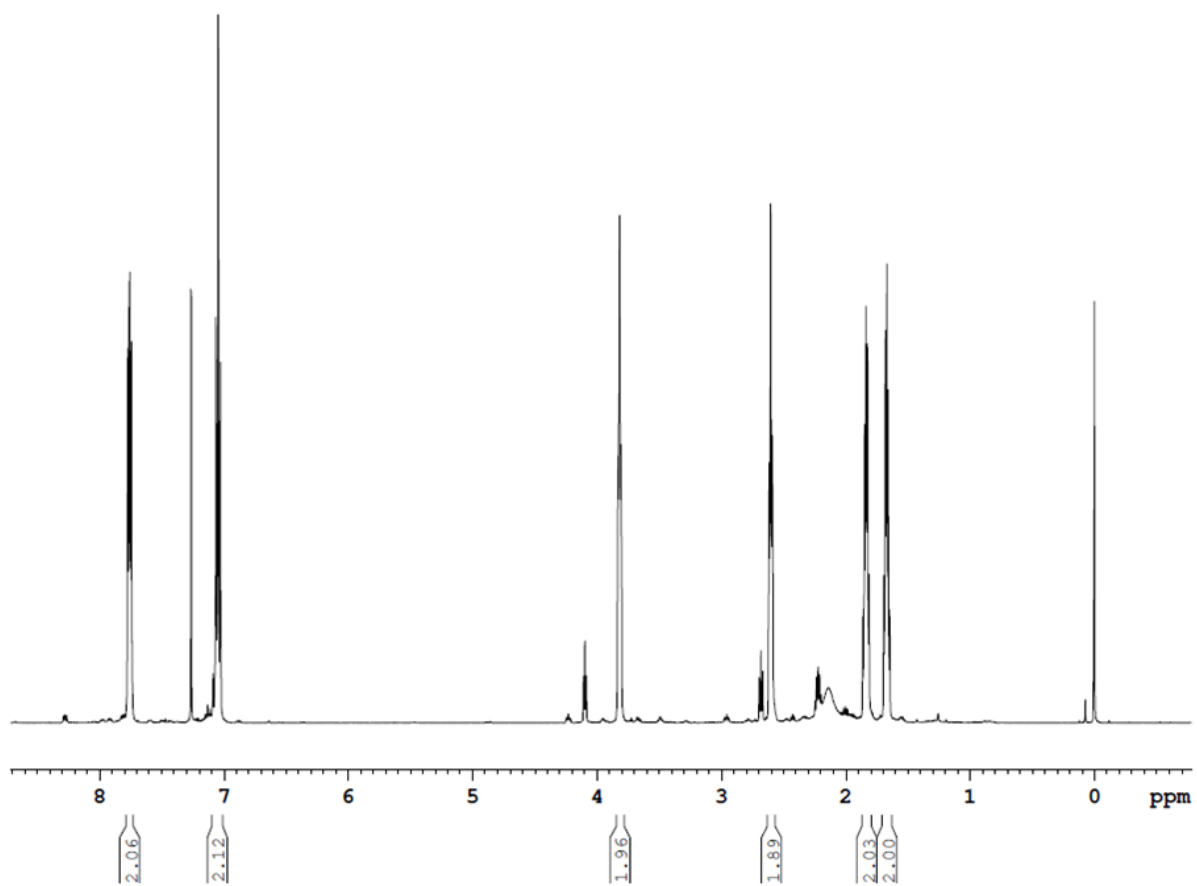


Figure S96: $^1\text{H-NMR}$ spectrum of 2-*p*-fluorophenylpiperidine (**3c**).

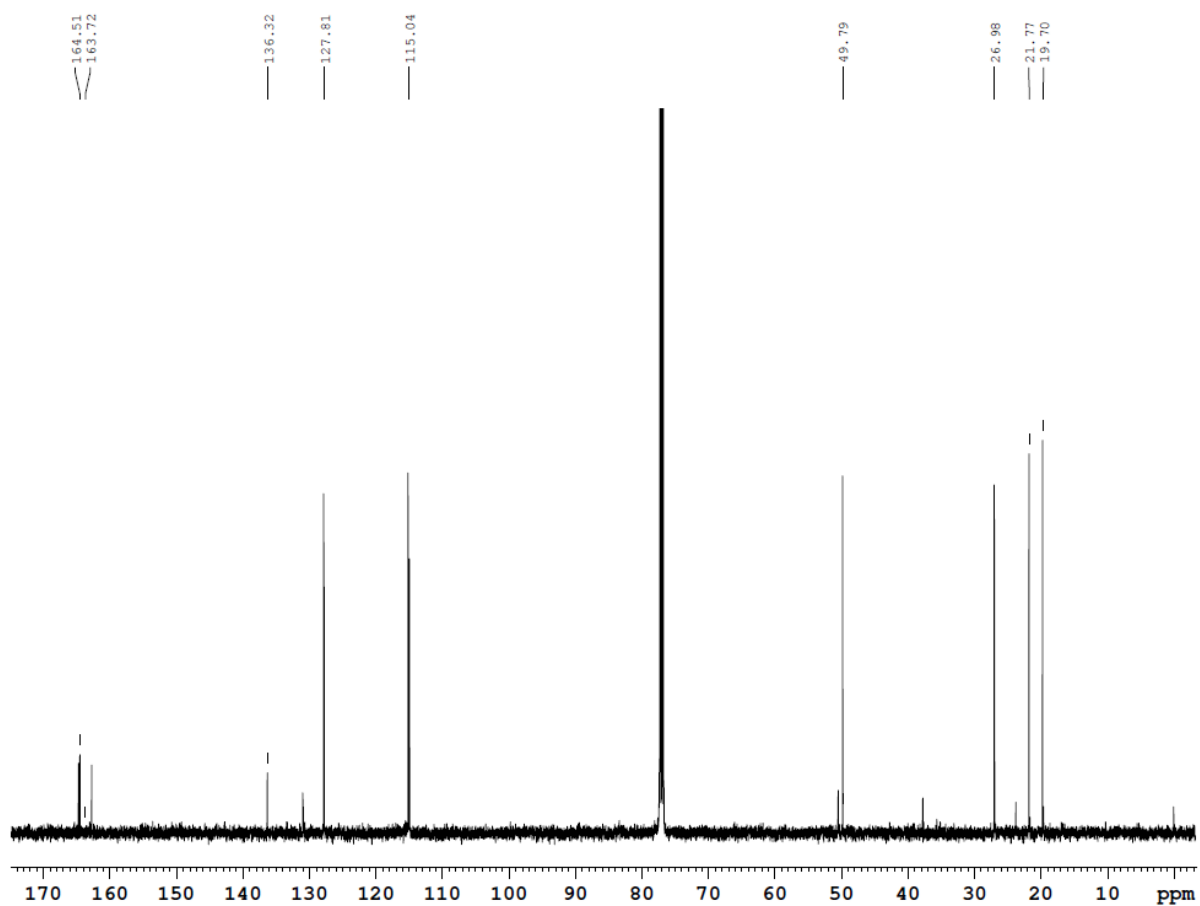


Figure S97: ^{13}C -NMR spectrum of 2-*p*-fluorophenylpiperidine (3c).

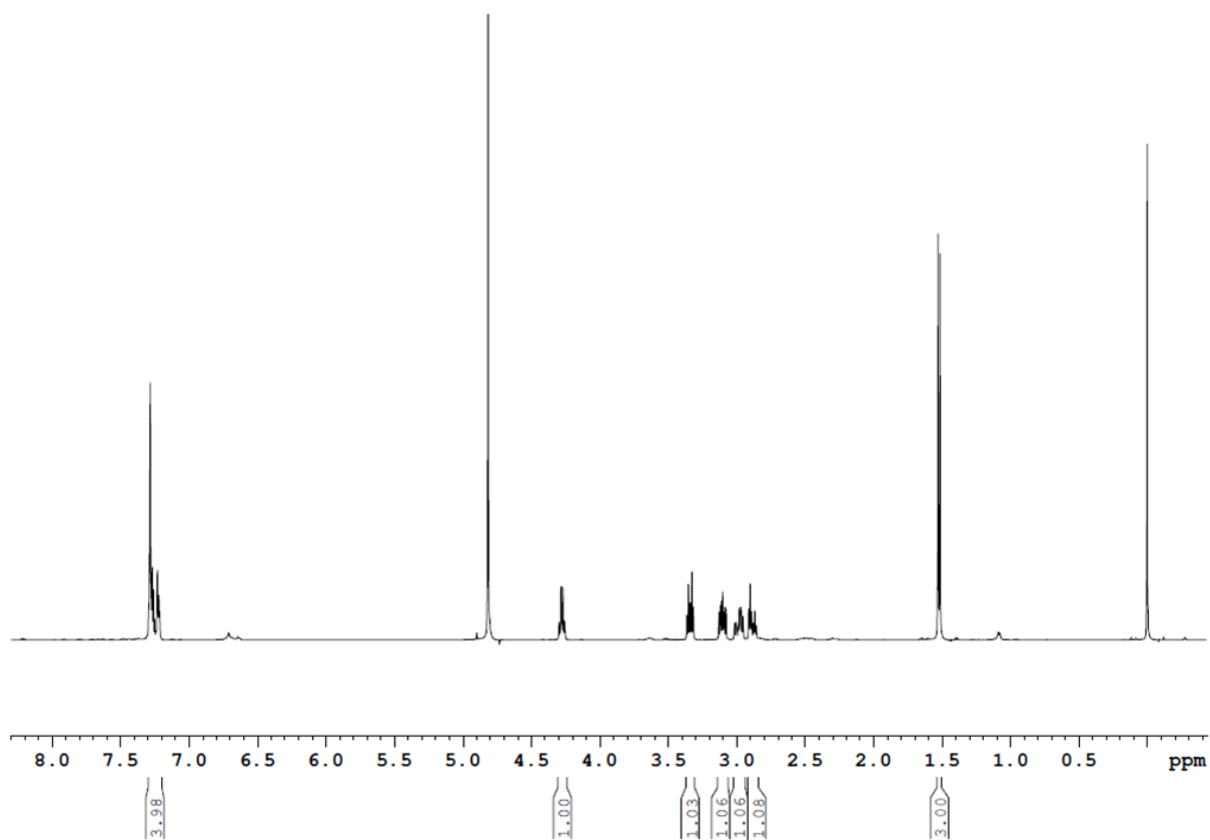


Figure S98: $^1\text{H-NMR}$ spectrum of 1-methyl-1,2,3,4-tetrahydroisoquinoline (**6b**).

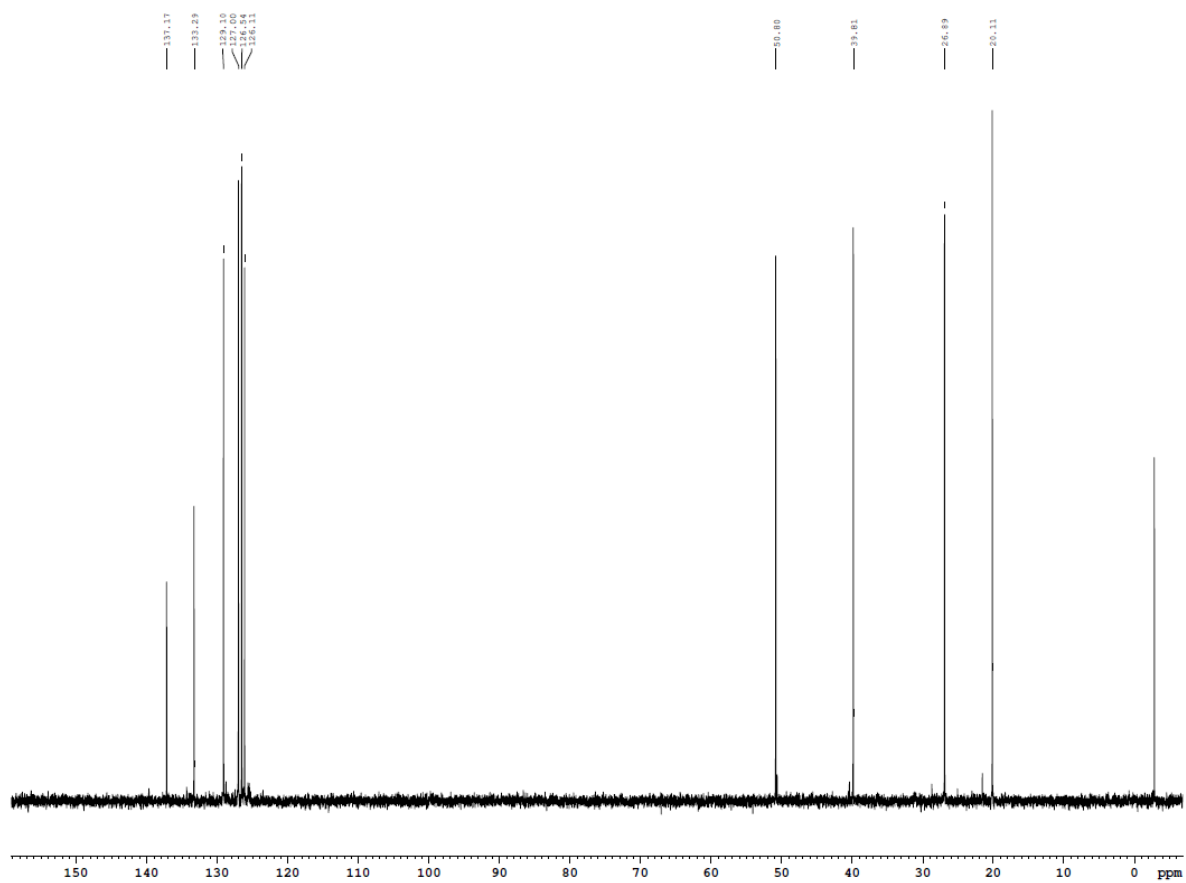


Figure S99: ^{13}C -NMR spectrum of 1-methyl-1,2,3,4-tetrahydroisoquinoline (**6b**).

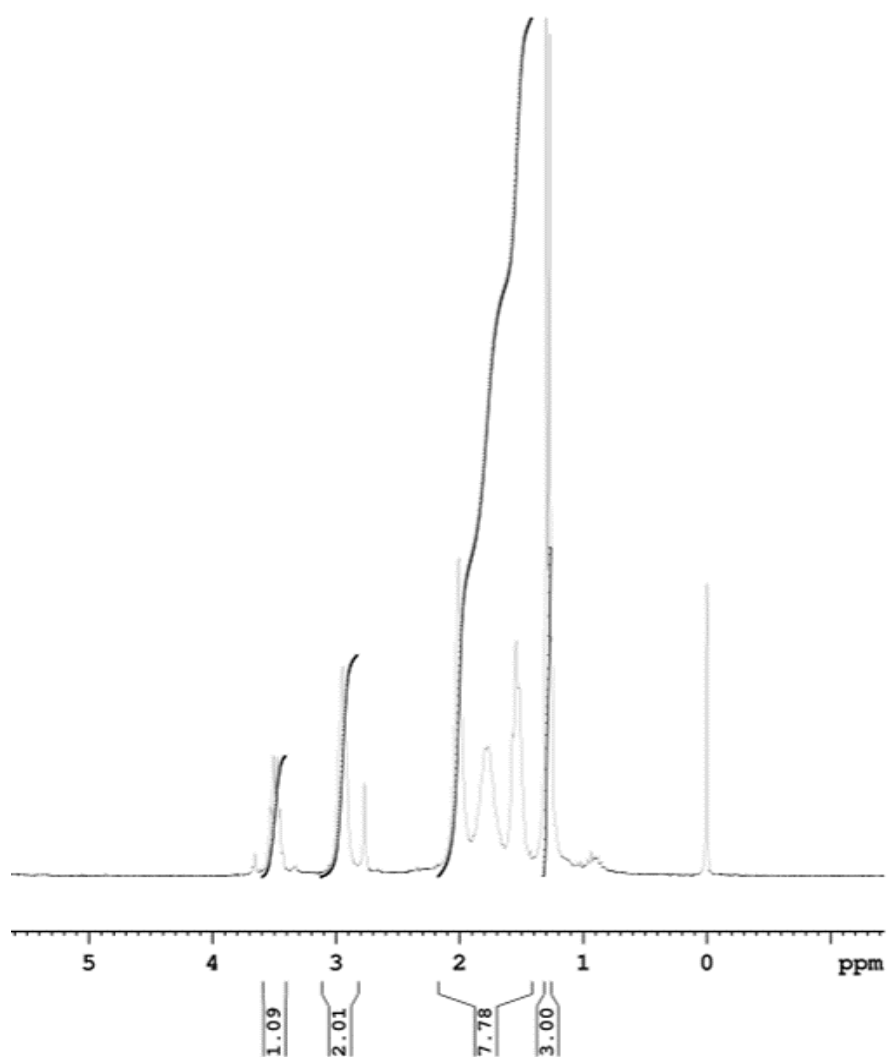


Figure S100: ¹H-NMR spectrum of 1,4-diaminopentane (**32**).

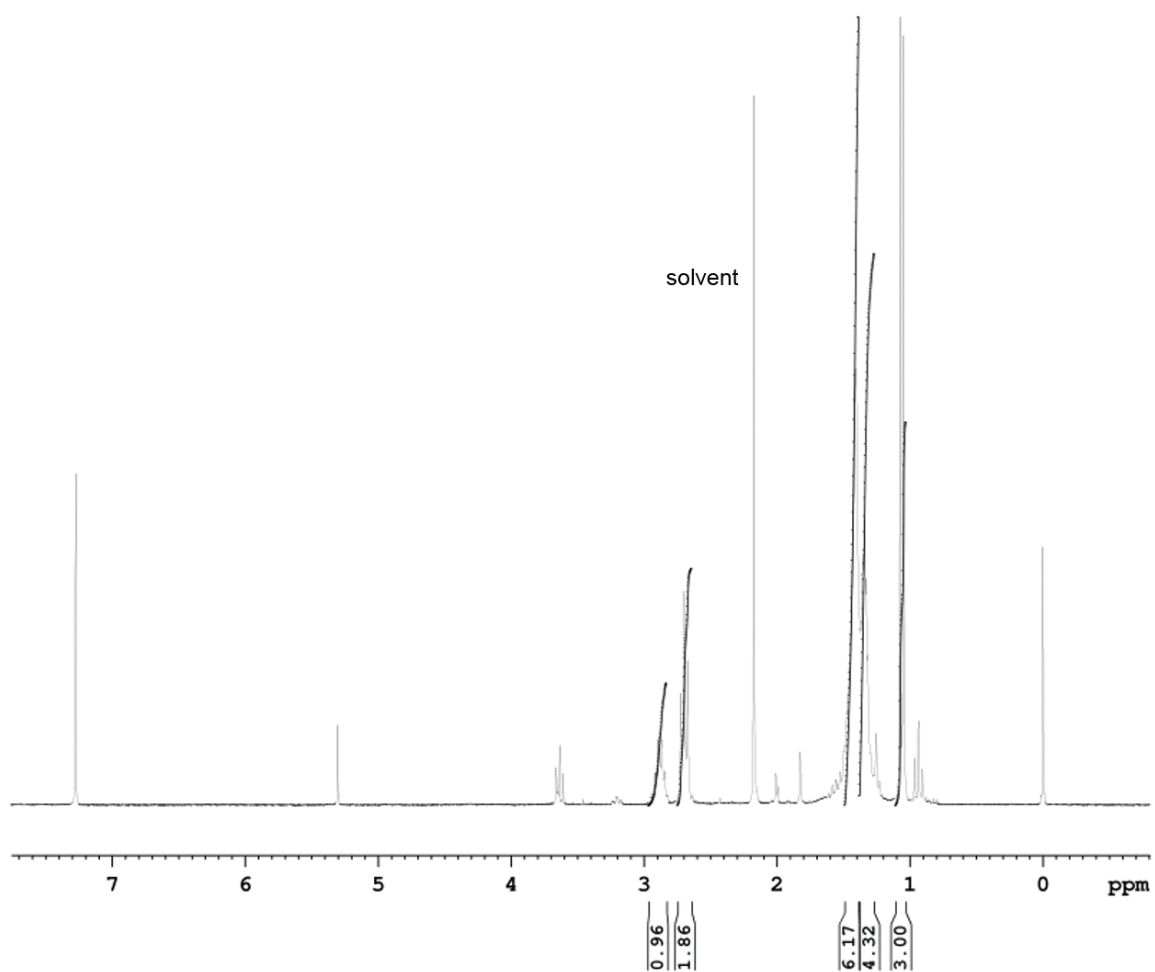


Figure S101: ¹H-NMR spectrum of 1,5-diaminohexane (**33**).

8 CURRICULUM VITAE

PERSÖNLICHE DATEN

Name Philipp Nico Scheller
Geburtsdatum und Ort 20.07.1984 in Biberach/Riß
Nationalität Deutsch

AKADEMISCHE- UND SCHULISCHE LAUFBAHN

seit 02/2012 **Promotion, Institut für Technische Biochemie, Abteilung Biokatalyse, Universität Stuttgart**
Betreuer: Prof. Dr. Bernhard Hauer

10/2005-12/2011 **Studium Technische Biologie, Universität Stuttgart**
Abschluss: Diplom Biologe t.o. (technisch orientiert)

10/2010-07/2011 **Diplomarbeit**, Institut für Technische Biochemie, Universität Stuttgart
Betreuer: Prof. Dr. Bernhard Hauer

10/2009-06/2010 **Studienarbeit**, Department of Microbiology and Immunology, University of California, San Francisco
Betreuer: Prof. Dr. Philip Coffino

9/1995-06/2004 **Wieland Gymnasium Biberach an der Riß**
Abschluss: allgemeine Hochschulreife

PRAKTISCHE ERFAHRUNG

09/2015-11/2015 **Orion Pharma, Espoo, Finnland**
Medizinische Chemie
Technologietransfer im Bereich Biokatalyse

09/2011-11/2011 **BASF SE, Ludwigshafen**
Abteilung Forschung Feinchemikalien und Biokatalyse
Praktikum im Bereich Mikrobiologie